MODERN

APPLIED

SCIENCE

Editor-in-chief
Daniel Kingst

Managing Editor
Steven Clayer

CCSE

Contents

Contents

Theoretical Analysis of Closed Rankine

Cycle Solar Pond Power Generator

Rajamohan Ganesan & Chua Han Bing

School of Engineering and Science, Curtin University Technology

Sarawak Campus, CDT 250, 98009, Miri, Sarawak, Malaysia

Tel: 6-085-443918   E-mail: rajamohan.g@curtin.edu.my

Balasundaram Mohan Kumar

Department of Mechanical Engineering, TAFE College

Lot No 5409, 70400 Seremban, Negeri Sembilan, Malaysia

Abstract

Thermal energy extraction from solar pond is theoretically studied with the use of Rankine cycle heat engine. The Rankine power cycle configuration consists of evaporator, turbine, condenser, feed pump and R-134a which is used as the working fluid. A solar pond is considered as the heat source for the evaporator. Fresh water circulates through an internal heat exchanger, located in the lower convective zone of the pond, and transfers its thermal energy to evaporator. The heat that is absorbed increases the temperature of a working fluid and causes the working fluid to vaporize. When the working fluid has taken enough potential energy, the fluid vaporizes and begins to rise, thereby converting some of the potential energy to kinetic energy. The vapor flows under high pressure to the turbine and thereby expanding through the turbine from a higher pressure to a lower pressure. Useful work can be extracted from this expansion process. The turbine is placed in between the evaporator and condenser section of the cycle. The water is acting as heat sink for the condenser. An attempt is made to analyze the thermodynamic aspects of the cycle and the net works generated by the system are elaborated. The report presents the analysis of an alternative method of thermal energy extraction from solar energy thermal resource with the use of solar pond.

Keywords: Solar Pond, Refrigerant, Rankine cycle and Thermal Energy Extraction

1. Introduction

To meet the increasing world demand for energy, the use of fossil fuel to produce power has become wide spread. Unfortunately fossil fuels are non renewable energy sources, and they pollute the environment and are considered as the largest source of emissions of carbon dioxide, which is largely blamed for the global warming and climate changes. This trend can be reduced by the construction of power plants using renewable energy sources (Zekai, 2004). There are many forms of renewable energy sources available, and this paper will focus on thermal energy extraction from solar pond that is theoretically studied with the use of Rankine cycle heat engine.

A solar pond is simply a pool of water which collects and stores solar energy. It contains layers of salt solutions with increasing concentration (and therefore density) to a certain depth, below which the solution has a uniform high salt concentration. When solar radiation (sunlight) is absorbed, the density gradient prevents heat in the lower layers from moving upwards by convection and leaving the pond. This means that the temperature at the bottom of the pond will rise to over 90 °C while the temperature at the top of the pond is usually around 30 °C. The heat trapped in the salty bottom layer can be used for many different purposes, such as the heating of buildings or industrial hot water or to drive a turbine for generating electricity (Wikipedia, 2007).

There are many advantages of using solar based power plants (Wu, 1998), and a few benefits are noted such as, heat energy is provided without burning fuel thus reducing pollution, conventional energy resources are conserved, there are no costs associated with fuel, the low operating temperatures and pressure reduces the component costs and it has a 24 hour a day potential.   The report presents the theoretical analysis of an attractive method of thermal energy extraction from solar pond that is theoretically studied with the use of Rankine cycle heat engine.

2. Rankine cycle solar pond power generator

A solar thermal energy extraction from solar pond closed power cycle is schematically shown in figure1. In this system heat is transferred from solar pond to the working fluids refrigerant in an evaporator. The heat transfer mechanism that drives a closed Rankine power cycle is the recirculation of a working fluid through a cycle of evaporation, vapor

transfer, condensation, and liquid return (Akbarzadeh, 2001).   Fresh water circulates through an internal heat exchanger, located in the lower convective zone of the pond, and transfers its thermal energy to evaporator. The power cycle gets the energy from absorbing the heat from the solar pond. The heat that is absorbed increases the temperature of a working fluid inside of the evaporator tubes and causes the working fluid to evaporate at an elevated pressure (Rai, 2002).
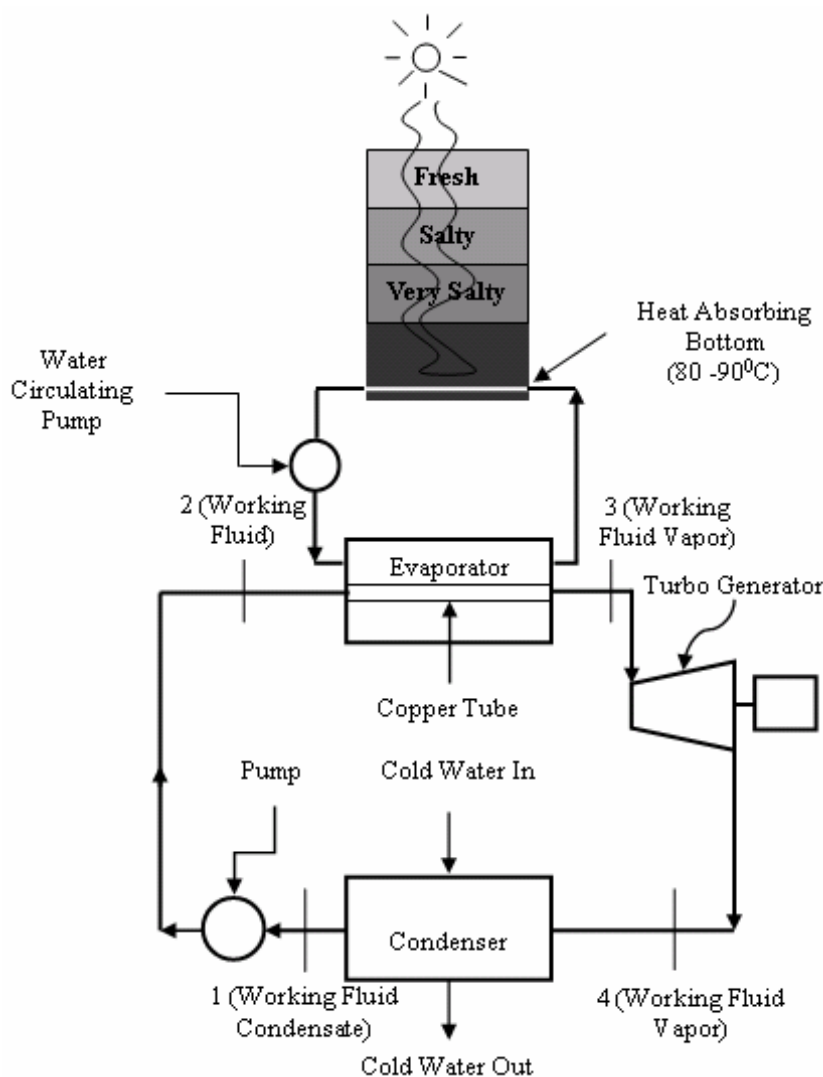
Figure 1. Schematic diagram of Rankine cycle solar pond power generator

The less dense vapor then rises. As the vapor is rising, it is expanding from a higher pressure to a lower pressure. Useful work can be extracted from this expansion process. As the working fluid flows from the evaporator to the condenser in the vapor phase, the kinetic energy of the working fluid is increased (Patrick, 1998). When a turbine and generator are incorporated into the high velocity vapor stream, electric power can be extracted. When the vapor passes through the turbine it loses the kinetic energy and the pressure and temperature of the vapor decreases. The vapor at state 4 is then sent to the second heat exchanger (condenser) where heat is transferred from the vapor to cold water and thus, the working fluids returns to a saturated liquid at state 2 back to the first heat exchanger where the process is repeated (Wu, 1198).

3. Solar pond as a heat source for the Rankine cycle solar pond power generator

Solar ponds present an economical way to obtain large amounts of low grade heat. Solar ponds utilize the natural properties of salt water to collect and store the heat energy. The most common type of solar pond is the salt gradient pond, which has the three different layers of salt concentration. Sunlight passes through the water with the majority of the sun light being absorbed by lower salt layers of water and the heat absorbing lining (Mehmet, 2006). This heats the lower layers of the pond. The concentrations of the salt layers are created such that the bottom layer of very salty water is denser than the second layer, even when heated to near boiling temperatures. Likewise, the middle layer of salty water is designed to be denser than the fresh water on top. This inhibits the convection of heat throughout the pond. The

heat is extracted from the bottom layer of the pond, which is the saltiest and reaches the highest temperatures (Rai, 2002).

4. Selection of heat source and heat sink

A reasonable temperature for a solar pond is to reach heat up to 90^0C. A reasonable temperature for the ambient temperature of the air is 20^0C. For this reason, a heat sink temperature of 20^0C is assumed. Since not all the heat would be transferred from the heat sink and heat source to the Rankine cycle, the assumed evaporator temperature in the cycle is 80^oC and the condenser temperature of our Rankine cycle is 22^0C.

5. Working fluid for the Rankine cycle solar pond power generator

The working fluid for a phase-change cycle like the one found in a Rankine cycle power plant has the following desirable characteristics. Critical temperature well above the highest temperature that can be used in the cycle. This makes it possible to vaporize the working fluid and thus adds a considerable amount of heat to it at the maximum temperature. Neither very high nor very low saturation pressures at the maximum and minimum temperatures of the cycle (Ganic, 1980 & Johnson, 1983). In this investigation, R-134a is used as working fluid because of its superior high thermal efficiency, conductivity and ozone-friendly nature.

6. Analysis of closed Rankine cycle solar pond power generator

The system analyzed here is a 10 kW power plant, which assumes warm water entering temperature of 85^0C and exiting temperature of 75^0C, cold water entering temperature of 20^0C and exiting temperature of 24^0C, the specific state points 1, 2, 3 and 4 at temperatures of 22^0C, 22^0C, 80^0C and 80^0C, respectively. Also temperature differences across both heat exchangers are modeled as isobaric (both hot and cold side). In addition, the two heat exchangers are assumed to have an overall coefficient (U) of 1 kW/m^{2}K [2].
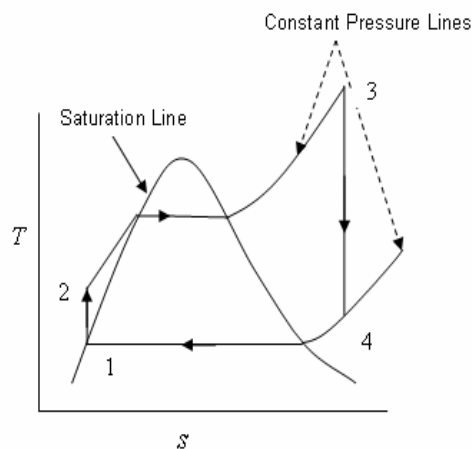
Figure 2. Ideal Rankine cycle on a temperature entropy diagram

The cycle is assumed to be an idealized Rankine cycle. The figure 2 shows the different steps of the Rankine cycle according to Nguyen et al. (Nguyen, 1994). The first process (From 1-2) consists of adiabatic compression of the liquid. During the second process (From 2-3) heat is added isobarically to convert the liquid to a vapor. The third process (From 3-4) consists of adiabatic expansion of the vapor to lower pressure. During the fourth process (From 4-1) there is isobaric heat rejection that condenses the vapor back to a liquid. The above four processes are repeated over and over again to produce the Rankine cycle.

Figure 1 shows a simplified flow diagram of the closed cycle plant. Where, h is the enthalpy at the indicated state point. It follows that the heat-added plus the pump-work is equal to the heat-rejected plus the turbine work. From the state point enthalpies, the   heat transferred to the working fluid in the boiler, the   heat transferred from the working fluid in the condenser, work generated by the turbine, work generated by the pump, net work generated by the heat engine, thermodynamic cycle efficiency, mass flow rate of the refrigerant, boiler and condenser heat transfer rate, mass flow rate of warm and cold water,   boiler and condenser surface area and   specific power output of the closed Rankine cycle plant can be calculated from the equations (1) to (17) as follows (Wu, 1998).

State 1-2

Reversible adiabatic pumping process in the pump

Pump work (kJ/kg) $W_{pump} = V_1(P_2 - P_1)$ (1)

$$W_{pump} = 0.336 \text{ kJ/kg}$$

$$W_{pump} = h_2 - h_1 \tag{2}$$
$$h_2 = 230.336 \text{ kJ/kg}$$

State 2-3

Heat supplied from evaporator at constant temperature to change state 2 into saturated R-134a at constant pressure.

Heat added (kJ/kg)
$$q_A = h_3 - h_2 \tag{3}$$
$$q_A = 198.864 \text{ kJ/kg}$$

Acknowledging the fact that is a 1 kW power plant, the mass flow rate of the working fluid (m_R) can be found via;

$$m_R = \frac{P_{out}}{W_{net}} \tag{4}$$
$$m_R = 0.180 \text{ kg/s}$$

Boiler heat transfer rate (kJ/s)

$$Q_{boil} = m_R(q_A) \tag{5}$$
$$Q_{boil} = 35.795 \text{ kJ/s}$$

Surface area of the boiler (m^2)

$$A_{boil} = \frac{Q_{boil}}{\{U_{boil}[(T_{w1} + T_{w2})/2 - (T_2 + T_3)/2\}} \tag{6}$$
$$A_{boil} = 1.234 \text{ m}^2$$

Mass flow rate of warm water (kg/s)

$$m_{warm} = \frac{Q_{boil}}{[Cp_{water}(T_{w1} - T_{W2})]} \tag{7}$$
$$m_{warm} = 0.855 \text{ kg/s}$$

Where

T_{w1} Temperature of the warm water entering the boiler (85^{0}C)

T_{w2} Temperature of the warm water exiting the boiler (75^{0}C)

State 3-4

Isentropic expansion of the vapor across the turbine, including partial condensation.

$$x_4 = \frac{s_4 - s_{f@22°C}}{s_{v@22°C}} = 0.348 \tag{8}$$

$$h_4 = h_{f@22°C} + x_4 h_{v@22°C} \tag{9}$$
$$h_4 = 373.446 \text{ kJ/kg}$$

Turbine work (kJ/kg)
$$W_{turb} = h_3 - h_4 \tag{10}$$
$$W_{turb} = 55.574 \text{ kJ/kg}$$

Cycle Network (kJ/kg)
$$W_{net} = W_{turb} - W_{pump} \tag{11}$$
$$W_{net} = 55.574 \text{ kJ/kg}$$

State 4-1

Complete condensation in the condenser at constant temperature.

Heat rejected (kJ/kg)
$$q_R = h_4 - h_1 \tag{12}$$
$$q_R = 143.446 \text{ kJ/kg}$$

Condenser heat transfer rate (kJ/s)

$$Q_{cond} = m_R(q_R) \tag{13}$$
$$Q_{cond} = 25.820 \text{ kJ/kg}$$

Surface area of the Condenser (m^2)

$$A_{cond} = \frac{Q_{cond}}{\{U_{boil}[(T_1 + T_4)/2 - (T_{c1} + T_{c2})/2\}}$$

$$A_{cond} = 0.890 \text{ m}^2 \tag{14}$$

Mass flow rate of cold water (kg/s)

$$m_{cold} = \frac{Q_{cond}}{[Cp_{water}(T_{c2} - T_{C1})]} \tag{15}$$

$$m_{cold} = 1.539 \text{ kg/s}$$

Where

T_{c1} Temperature of the cold ocean water entering the condenser (20^0C)

T_{c2} Temperature of the cold ocean water exiting the condenser (24^0C)

Thermal Efficiency (%)

$$\eta_{thermal} = \frac{W_{net}}{q_A} = \frac{[h_3 - h_4] - [h_2 - h_1]}{[h_3 - h_2]} \tag{16}$$

$$\eta_{thermal} = 27.94 \text{ %}$$

The final calculation is that of the Specific power (*P*). It is accomplished by the following equation

$$P = \frac{Q_{boil}}{(A_{boil} + A_{cond})} \tag{17}$$

$$P = 16.852 \text{ kW/m}^2$$

7. Conclusion

The analysis of thermal energy extraction from solar pond is theoretically studied with the use of closed Rankine cycle solar pond power generator. It has been concluded that the generation of maximum thermal efficiency of 27.94 % and specific power of 16.852 kW/m^2 can be achieved by using the effective closed Rankine cycle solar pond power generator. To work out minimal amount of power generation and continuous production of power from solar energy source, a closed Rankine cycle solar power generator system is an extremely attractive option. However other factors such as maintenance, operating cost and transmission, etc, were ignored in this analysis and thus may have significant impact on future power plants design. Further investigations are needed in order to test the sensitivity of the theoretical efficiency gain from solar energy heat extraction before moving to practical applications in these areas.

References

Akbarzadeh.A., Johnson.P., Nguyen.T., Mochiziki.M., Mashiko.M., Sauciuc.I., Kusaba.S., and H.Suzuki. (2001). Formulation and analysis of the heat pipe turbine for production of power from renewable sources, *Journal of applied thermal engineering*, Vol 21, PP 1551-1563, UK.

Balany.P.L (2003). *Thermal Engineering*, Khanna Publishers, India.

Ganic.E.N and J.WU (1980). On the Selection of working fluids for OTEC Power Plants, *Energy Conv & Mgmt*, Pergamon Press Ltd, V.20 ,PP.9-22.

Hazami M, Kooli S, Lazaar M, Farhat A & Belghith A 2005, Performance of a solar storage collector, Elsevier, Tunisia, 2001.

Haaf.W. (1983). Solar Chimney, Part II, Preliminary test result from the pilot plant Manzanares, *Solar energy,* Vol 2, PP 141-161.

Johnson.D.H. (1983). The Exergy of the Ocean Thermal Resource and Analysis of Second law Efficiencies of Idealized Ocean Thermal Energy Conversion Power Cycles, *Pergamon Press Ltd, Energy* Vol 12, No.12, PP 927-946.

Mehmet.K., Ibrahim.D and Marc.A.R. (2006). Performance investigation of a solar pond,   *Journal of applied thermal engineering, Elsevier Ltd,* Vol 26, PP 727-735, UK.

Nguyen.T., Johnson.P., Akbarzadeh.A., Gibson.K and Mochiziki.M. (1994). Design, Manufacture and testing of a closed cycle thermosyphon engine, *Journal of Heat Recovery System and CHP* 15 (4) 333.

Patrick.K.T., and Andrew.T. (1998). Ocean energy conversion its promises as a total resource system, *Pergamon Press Ltd*, Vol 17, PP 657-669, UK.

Rai.G.D. (2002). *Non-Conventional Energy Sources,* Khanna Publishers, India.

Wu.C and Burke.T.J. (1998). Intelligent computer aided optimization on specific power of an OTEC Rankine power plant, *Applied Thermal Engineering,* Vol 18, PP 295-300, UK.

Zekai.S. (2004). Solar Energy in progress and future research trends, Progress in Energy and Combustion Science, Vol 17, PP 367-416, *Science Direct,* UK.

Available from: <http://en.wikipedia.org/wiki/Solar_pond>.

Appendix

Table 1.Values referred from Refrigerant R-134a table (Balany, 2003).

Description	Temperature (^{0}C)	Enthalpy(kJ/kg)	Pressure (bar)
State 1	22	230.210	6.0777
State 2	22	230.336	16.000
State 3	80	429.020	16.000
State 4	80	373.446	6.013

A Novel Approach of Multiple Submodel

Integration Based on Decision Forest Construction

Limin Wang

College of Computer Science and Technology, JiLin University

Changchun 130012, China

Tel: 86-431-8517 2081   E-mail: wanglim@jlu.edu.cn

Xiaolin Li (Corresponding author)

School of Business, Nanjing University

Nanjing 210093, China

Tel: 86-431-8517 0836   E-mail: lixl_126@126.com

Yuting Mao

Information dissemination Academy of Engineering, ChangChun University of Technology

Changchun 130012, China

Tel: 86-431- 8571 6001   E-mail: valeriazuo@126.com

Abstract

An analytical general solution is derived for reasoning uncertain knowledge by multiple sub-model integration. By choosing decision rule for each specific instance, a decision forest rather than a tree will be constructed, thus all relatively independent attribute sets can be determined automatically without any human intervention. Necessary discretization for mixed-mode subset will be processed based on post-discretization strategy to minimize information loss.

Keywords: Multiple submodel integration, Decision forest, Post-discretization strategy, Conditional independence assumption

The volume of data for discovery of decision rules and recognition of patterns is growing at an exponential rate, both in the number of attributes (features) and objects (instances). One way to reduce computational complexity of knowledge discovery is dimensionality reduction, which includes projection pursuit, factor analysis, and principal components analysis. In artificial intelligence, decomposition methodology is a major tactic both for ensuring the transparent end-product and for avoiding the combinatorial explosion. And for this, the conditional independence assumption has been widely used, e.g. in Bayesian network structure learning. However, despite its popularity, the independence assumption always supposes that all attributes are discrete and continuous ones have to be discretized before learning even at the cost of information loss. Wang et al. reported that an unsteady special solution, which supposed that continuous feature subset and discrete subset are independent. This paper presents an analytical general solution to further handle mixed-mode subset based on decision forest construction to divide original feature space into several parts automatically.

Suppose instance space D with mixed-mode data has two types of attribute sets. The first k attributes are continuous and others are discrete. After pre-discretization the conditional independence assumption can be expressed as:

$$P(\bigwedge_{i=1}^{k} x_i \le X_i \le x_i + \Delta_i, \bigwedge_{j=k+1}^{n} x_j | c) = \prod_{i=1}^{k} P(x_i \le X_i \le x_i + \Delta_i | c) \prod_{j=k+1}^{n} P(x_j | c) \quad (1)$$

Where lower-case letters denote specific values taken by corresponding attributes (for instance, x_i represents the event that $X_i = x_i$). And $\triangle_i$ is arbitrary interval of the values of attribute X_i, $P(\cdot)$ refers to the probability. The following result can be formulated based on bayes theorem and differential theorem:

$$P(c|x_1, \cdots, x_n) = \prod_{i=1}^{k} p(x_i | c) \prod_{j=k+1}^{n} P(x_j | c) P(c) / \alpha \quad (2)$$

Where $\alpha = p(x_1, \Lambda, x_k | x_{k+1}, \Lambda, x_n) P(x_{k+1}, \Lambda, x_n)$ is constant irrelevant to class value. $p(\cdot)$ refers to the probability

density function. Maximum likelihood estimation is chosen to estimate probability and joint probability, and Kernel-based density estimation is chosen to estimate conditional probability density function:

$$
\begin{cases}
\hat{p}(x_i|c) = \frac{1}{mh_i}\sum_{k=1}^{l} K(\frac{x_i - x_{ik}}{h_i}) \\
\hat{P}(c) = \frac{Count(C = c)}{N} \\
\hat{P}(x_j|c) = \frac{Count(C = c, X_j = x_j)}{Count(C = c)}
\end{cases}
$$

(3)

where $x_{ik}(k=1,\Lambda,l)$ is the corresponding value of attribute X_i when $C = c$, $K(\cdot)$ is a given kernel function $K(t) = (2\pi)^{-1/2} e^{-t^2/2}$. And h_i is the corresponding kernel width, m is the number of training instances when $C = c$.

Let $\{T_1,\ldots,T_P\}$ denotes a decomposition of the attribute set A into p mutually independent subsets, each containing discrete and pre-discretized attributes or continuous input attributes. The aim of classification is to decide and choose the class that maximizes the posteriori probability, an analytical general solution based on conditional independence assumption can be obtained as follows:

$$
v_{MAP}(C) = \arg\max_{c\in C} \prod_{i=1}^{p} P(c|t_i)/P(c)^{p-1}
$$

(4)

Where t_i and $P(c|t_i)$ denote any reasonable combinations of attribute values in subset T_i and the classification accuracy of submodel constructed by t_i, respectively. t_i and $P(c|t_i)$ can be determined flexibly during the learning procedure of decision forest, which is composed of a set of decision trees. Attributes in the same tree should be dependent, while independent classification rules should be in different trees as the independent assumption suggests.

The original information entropy of class attribute C for instance space D is:

$$
H(C|D) = -\sum_{c\in C} P(c) log P(c)
$$

(5)

The information entropy of C for subspace D' which satisfied $X_i = x_i$ is:

$$
Gini = H(C|D) - H(C|D')
$$

(6)

The Gini index defined above just consider the information that each attribute value rather than specific attribute gave to class label. Since it is applicable to both continous and discrete attributes, the information loss caused by pre-discretization can be effectively avoided. The first part of Eq.(6), which describes the information entropy of class label itself, is the same to all attribute values. Thus the second part of Eq.(6) should be considered only during test selection procedure, that is to maximize the conditional information entropy. The construction procedure of decision forest can be described as follows:

Input: Training set D with n predictive attributes and N instances.

Output: Decision forest composed of n decision trees at most.

1. As to any given instance $\{x_1,\Lambda,x_n\}$, sort all attribute values according to the Gini index defined in Eq.(6) and select the one x_i which maximize the Gini index as the root node.

2. As to continuous values, the discretized interval $\triangle i$ and the scope of the next subspace are determined to minimize information loss.

3. Search for the next attribute value as the branch node in the instance subspace which satisfies Xi = xi if Xi is discrete or $x_i \leq X_i \leq x_i + \Delta_i$ if Xi is continuous, until the class label is the same or height of the decision tree is n. Then a leaf node is generated. Each path from root node to leaf node is corresponding to a classification rule, and the pre-condition is the combination of all attribute values in this path.

4. Apply the learning procedure described above recursively, after N iterations each instance can be assigned a classification rule.

5. Combine those rules which have the same root node, then subtrees or relatively independent classification rules can be determined automatically without any human intervention.

6. Prune rule sets in each subtree repeatedly until this will not help to improve classification accuracy.

7. Eliminate those rules that will result in high misclassification rate. Then decision forest with more powerful expressive ability to uncertain knowledge is constructed.

The continuous attributes in mixed-mode subset have to be discretized in step 3. According to post-discretization strategy [8], the boundary of continuous attribute *Xi* can be decided based on information gain:

$$Gain(X_i, B; S) \geq \frac{\log_2(N-1)}{N} + \frac{\Delta(X_i, B; S)}{N}$$

Where S is sorted sequence of the attribute values, N is the number of instances in set S, $\triangle(Xi,B; S) = \log_2(3^k - 2) - [k \times Ent(S) - k1 \times Ent(S_1) - k_2 \times Ent(S_2)]$, and $\{S1; S2\}$ are any given adjacent partitions. Ki is the number of class labels represented in set S_i. In order to evaluate the performance of submodel integration of decision forest, we conducted an empirical study on 12 data sets from the UCI machine learning repository to compare it with C4.5 release 8. Each data set consists of a set of classified instances described in terms of continuous or discrete attributes. Since the essence of submodel integration can be considered as partial leave-one-out validation, we also applied it to C4.5 release 8. Figure 1 summarizes the experimental results and from it, the superior generalization accuracy of submodel integration can be clear4ly seen.

References

Dunteman G.H. (1989). *Principal Components Analysis*. Sage Publications, 221-254.

Friedman J. H., & Tukey J.W. (1974). A Projection Pursuit Algorithm for Exploratory Data Analysis. *IEEE Transactions on Computers*. 23(9), pp. 881-889.

Friedman J.H. (1997). On bias, variance, 0/1 loss and the curse of dimensionality. *Data Mining and Knowledge Discovery*. 1(1): 55-77.

Kim J.O. (1978). *Factor Analysis: Statistical Methods and Practical Issues*. Sage Publications, 81-110.

Kononenko I. (1991). Seminaive Bayesian classifier. In: Proceedings of the 6th European Working Session on Learning. New York, 206-219.

Langley P., & Sage S. (1994). Oblivious decision trees and abstract cases. Working Notes of the AAAI-94 Workshop on Case-Based Reasoning. Seattle, WA: AAAI Press, 113-117.

Michie D. (1995). Problem decomposition and the learning of skills. *In: Proceedings of the 8th European Conference on Machine Learning*. London, UK, 17-31.

Silverman B. W. (1986). Density Estimation for Statistics and Data Analysis. *Monographs on Statistics and Applied Probability*. London: Chapman and Hall, 1-40.

Wang L. M., & Li, X.L. (2006). Combining decision tree and Naive Bayes for classification. *International Journal of Knowledge-Based Systems*, 19(7): 511-515.

Wang L. M., & Yuan S.M. (2004). Induction of hybrid decision tree based on post-discretization strategy. *Progress in Natural Science*, 14(6): 541-545.
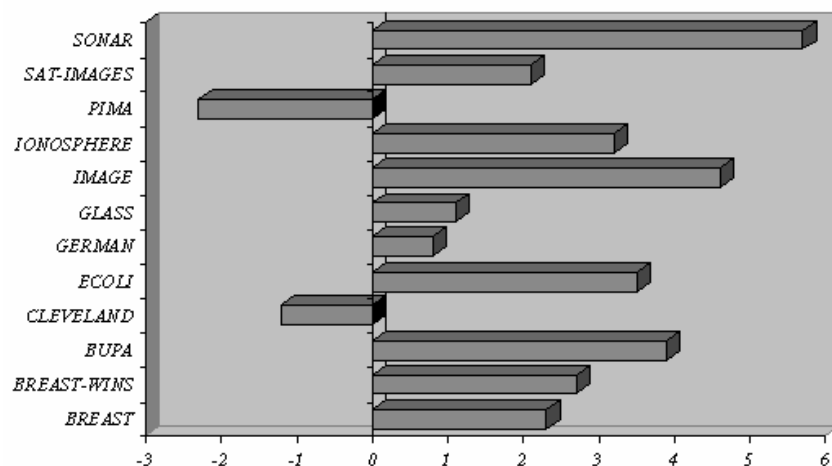
Figure 1. Comparison of classification performance % (Decision Forest-C4.5)

Peak Load Shifting Distribution by Fuzzy

Method Based on Weight Compromise Coefficient

Yang Li (Corresponding author), Jia Liu, Liqun Gao, Zhi Kong

School of Information Science and Technology, Northeastern University

3-11 Wen Hua Road, Shenyang 110004, China

E-mail: liyang@ise.neu.edu.cn

Abstract

The distribution of power supply limiting in multi-zone is discussed by means of combining analytical hierarchy process and fuzzy sets theory. From the greatest factors in power limiting distribution, guide line system and hierarchy structure are established. Also, the relative membership degree functions are determined. A novel multi-objective group decision model is suggested by introducing a compromise coefficient between subjective weight and objective weight, which can give attention to both. The model is applied to peak load shifting distribution and the result manifests this model is reasonable and applicable.

Keywords: Analytical hierarchy process, Fuzzy sets theory, Multi-objective, Group decision model

1. Introduction

Because of the fast development, Power supply crisis happened in east and centre of China frequently since 2003. In order to solve this problem, many investment and work for generate electricity capacity extending have been launched by State Grid Corporation of China around the whole country, including Three Gorges Dam. However, these cannot afford the large electricity consumption. Although some economic and political measures have been used to peak load shifting control, power limiting is still necessary for power grid security while the pinnacle coming. According to power limiting standards and safety requirements of each area, also the integrated analysis of society, economy, and environment, etc, how to distribute the finite peak power capacity over every area reasonable and get the safest grid and least loss is important. The solving of this problem is meaningful.

Peak load shifting distribution is an important task and it needs knowledge and experiment of many persons. At the same time, it is a little fuzzy. So the method of combining fuzzy sets theory with hierarchy analysis is used to discuss the multi-objective group decision of multi-zone peak load shifting, according to the systemic analysis of society, economy, resource and environment. Therefore, power limiting distribution belongs to nonlinear multi-objective group decision category.

2. Construct Peak Load Shifting Distribution Decision System

2.1 Power limiting distribution guide line system and hierarchy structure building

The reasonable time distribution of peak load shifting in multi-zone is for the sake of power capacity standard and least loss based on the grid security. In this aspect, there are many factors, which are related to range and time of power limiting, also the conditions of social economy, such as population, industry configuration, parameter of national economy and so on. Some of them can be showed in economic quantity. Such as population in power limiting area, number of electricity enterprises in power limiting area and gross product in power limiting area, etc. Furthermore, it is hard to estimate some potential indirect benefit like effect on economy, adjustment of economy structure, damage for environment. The necessity of peak load shifting control is usually appraised by economic benefit. And these always affect the distribution of power limiting time. So it has some deficiency. Thus, the guide line system and hierarchy structure (Fig 1.) should be established according to the parameters picking up from the factors affecting power supply limiting like society, economy and so on. This will be good to the reasonable distribution of power limiting time and least loss. And the law of clear conception, abundant information, easy calculation and show justice is necessary.

2.2 Building and determining relative membership degree functions of each parameter

Decision-making parameters always have four types in multi-objective decision problem. "a" is "excellent with large", "b" is "excellent with small", "c" is "fixed value" and "d" is "inter-zone".

The type of "fixed value" parameter is a kind of parameter that the excellent value is a constant. Inter-zone means that the parameter value in some fixed region is excellent. The purpose of decision parameter classification is for compare

among same parameters.

According to the difference between decision parameter types, parameter set F can be classified.

$$F = \bigcup_{i=1}^{4} F_i, \quad F_i \, I \, F_j = \Phi \, (i, j = 1, 2, 3, 4, i \neq j).$$

In this equation, F_i ($i = 1, 2, 3, 4$) is the kind of a, b, c and d respectively, and Φ is null.

Because of the difference between multi-objective dimensions, it needs to standardize the decision matrix M. And then, the eigenvalue of each decision parameter in relative state can be got. The expression of standardization is as follows.

$$a_{\max} = \max\{a_{ij} : 1 \leq i \leq n, 1 \leq j \leq r\} \tag{1}$$

$$a_{\min} = \min\{a_{ij} : 1 \leq i \leq n, 1 \leq j \leq r\} \tag{2}$$

(r_{ij} is relative membership degree of parameter j in zone i, *max* and *min* is the symbol for taking maximum and minimum respectively, α_{ij} is the objective value of parameter j(r in all) in zone i(n in all) and have character of fuzzy by effect of value and statistical error.)

For type a,

$$r_{ij} = \frac{a_{ij} - a_{\min}}{a_{\max} - a_{\min}} \quad (1 \leq i \leq n, 1 \leq j \leq r, f_k \in F_1) \tag{3}$$

For type b,

$$r_{ij} = \frac{a_{\max} - a_{ij}}{a_{\max} - a_{\min}} \quad (1 \leq i \leq n, 1 \leq j \leq r, f_k \in F_2) \tag{4}$$

For type c,

$$r_{ij} = \begin{cases} 1.0, & a_{ij} = a^0 \\ 1.0 - \dfrac{|a_{ij} - a^0|}{\max\{a_{ij} - a^0\}}, & a_{ij} \neq a^0 \end{cases} \quad (1 \leq i \leq n, 1 \leq j \leq r, f_k \in F_3) \tag{5}$$

a^0 is the optimal constant of parameter f_k.

For type d,

$$r_{ij} = \begin{cases} 1.0 - \dfrac{|b_1 - a_{ij}|}{\max\{b_1 - a_{ij}, a_{ij} - b_2\}}, & a_{ij} < b_1 \\ 1.0, & b_1 \leq a_{ij} \leq b_2 \\ 1.0 - \dfrac{|a_{ij} - b_2|}{\max\{b_1 - a_{ij}, a_{ij} - b_2\}}, & a_{ij} > b_2 \end{cases} \quad (1 \leq i \leq n, 1 \leq j \leq r, f_k \in F_4) \tag{6}$$

$[b_1, b_2]$ is the optimal region value of parameter f_k.

The decision eigenvalue matrix can be taken from the equations above.

From Fig. 1, the experts get that the Power limiting region whose population are more, electro-enterprise are more, the total value of produce are more, economic loss of Power limiting are more, proportion of using electricity peak are more, the average temperature is more, the proportion of ice air condition are less, the distributed proportion of Power Limiting distribution for Peak Load Shifting are more.

Thus, these factors are all "b", except the scale of reconcilable peak enterprises and ice air condition are "a".

3. Parameter Relative Weight Value Calculation

As a multi-objective decision method for combination of quality and quantity, hierarchy analysis has been applied extensively. But there are few examples about how to solve the group decision problem with hierarchy analysis method. In this paper, weighted geometry average group vector sort method based on different expert knowledge structure, has been used to deal with the hobby of some experts in multi-zone peak load shifting controlling time distribution and the problem of group hobby from knowledge structure.

3.1 The choice of expert group

The time of peak load shifting is mainly affected by the factors in Figure 1. Thus, the composition of expert group is always peak load shifting control expert and electric power programming expert, etc. Also including electric utility manage expert, grid economy expert and grid security expert, who are accomplished in operation, theory and scientific research respectively. Obviously, the reasonable decision weight of each expert for each factor in Figure 1 is different.

3.2 The weight vector calculation of judging matrix for each expert

In case of the number of expert is s and the number of reasonable peak load shifting control distribution factor or parameter is n,

$$P = \{P_1, P_2, \text{L } P_n\} \tag{7}$$

The important degree should be judged by every expert though all effecting factors. If V is the important degree judged matrix for factors building by expert *i*,

$$V = \begin{pmatrix} v_{11} & \text{K} & v_{1n} \\ \text{M} & \text{O} & \text{M} \\ v_{s1} & \text{L} & v_{sn} \end{pmatrix} \tag{8}$$

V follows AHP method. And the weight vector of factors judged by expert *i* can be taken according to the judged matrix.

Normalized the judged matrix V, V' can be taken.

$$V' = \begin{pmatrix} v'_{11} & \text{K} & v'_{1n} \\ \text{M} & \text{O} & \text{M} \\ v'_{s1} & \text{L} & v_{sn} \end{pmatrix} \tag{9}$$

$$v'_{ij} = \frac{v_{ij}}{\sum_{k=1}^{n} v_{ik}} , i = 1, 2, \text{L L }, s \tag{10}$$

3.3 The synthesis of expert weight vector

In the decision group, there are two methods for weight vectors synthesis of every decision-maker generally: one is synthesis of judged matrix; the other is synthesis of weight vector. Weight vector synthesize mainly use arithmetic weighted average synthesis. In this model, the relative important degree of each element has been considered and imported into the formula in the form of weight value. And this makes the appraising process reasonable. However, the weight determined in this way completely ignores the subjective information of decision-maker like knowledge, experience and hobby. Thus, it cannot afford needing of objective situations. So, a novel method for completing the parameter weight decision of multi-objective decision problem has been brought forward in this paper as follows.

Suppose, some experts is appraising the peak load shifting control distribution parameters. The number of experts is *s*, and the distribution is n. the determinate weight vector can be taken with the method above.

$$v^{(l)} = (v_{l1}, v_{l2}, v_{l3}, \text{L } v_{ln})^T \tag{11}$$

$$\sum_{k=1}^{n} v_{lk} = 1 (0 \le v_{lk} \le 1) \ (k=1,2,...n; \quad l=1,2,...s) \tag{12}$$

In case of weight of *each* decision-maker D_l is λ_l ,

$$\sum_{k=1}^{s} \lambda_l = 1 (0 \le \lambda_l \le 1) \ (l=1,2,...s) \tag{13}$$

And then, $\omega = (\omega_1, \omega_2, \text{L } \omega_n)^T$ is the unknown weight vector. Normalized ω_k, we can get

$$\omega_k = \frac{\sum_{i=1}^{s} \lambda_l v_{lk}}{\sum_{k=1}^{n} \sum_{l=1}^{s} \lambda_l v_{lk}} \tag{14}$$

The weight of decision-maker is usually determined by the appraisement between them. That's the subjective weight δ_l($l = 1, 2, ..., s$). But in fact, the weight of decision-maker is not always coincident with the subjective weight. So it is necessary to fix δ_l according to the problem and result of decision practically.

y_{lu} can be defined as the distance of $\omega^{(l)}$ and $\omega^{(u)}$ ($l, u = 1, 2, ..., s$).

$$y_{lu} = y(\omega^{(l)}, \omega^{(u)}) = \sqrt{\sum_{k=1}^{n} (\omega_{lk} - \omega_{uk})^2} \tag{15}$$

So it is easy to see that $0 \le y(\omega^{(l)}, \omega^{(u)}) \le 1$. Smaller the $y(\omega^{(l)}, \omega^{(u)})$ is, closer the distance is.

Supposing $e_l = \sum_{k=1}^{s} y_{lk}$ ($k = 1, 2, ..., s$),

e_l manifests the close degree between $\omega^{(l)}$ of decision-maker D_l and others. And if e_l is smaller, $\omega^{(l)}$ will be closer with the other weight vectors. Thus, we can use (16) as the objective weight of decision-maker D_l.

$$\beta_l = \frac{1/e_l}{\sum_{l=1}^{s} (1/e_l)} \quad l = 1, 2, ..., s \tag{16}$$

It is easy to see that β_l indicates the different degree of target weight decision between decision-maker D_l and the others. Thus the final weight of decision-maker l can be determined by

$$\lambda_l = \mu\delta_l + (1-\mu)\beta_l, \quad l = 1, 2, ..., s \quad 0 \le \mu \le 1 \tag{17}$$

It indicates the different degree for the subjective weight and objective weight.

4. Optimized Distribution Decision Calculation of Multi-objective Power Limiting Time Distribution

For the hierarchy model structure in Figure 1, the fuzzy synthesized decision model of multi-objective power limiting time distribution in multi-zone is established as follows.

$$Z = R \circ W = \begin{pmatrix} r_{11} & K & r_{1n} \\ M & O & M \\ r_{m1} & L & r_{mn} \end{pmatrix} \circ \begin{pmatrix} \omega_1 \\ M \\ \omega_n \end{pmatrix} \tag{18}$$

In the equation above, R is the relative membership degree matrix, r_{ij} means the relative membership degree of the parameter j in zone i of m, W is the parameter weight vector determined by group decision theory, ω_j is the weight of parameter j of n under group decision, Z is the scale vector of zone power limiting time distribution. "$\circ$" is the fuzzy arithmetic operators. The scale of power limiting distribution of each region can be taken according to equation (18).

5. Research of Examples

According to the data from the charge department of Liaoning province, a peak load shifting distribution in six regions is planned to operate in summer of 2005. The social economy of six regions is shown in Table 1. The loss is in Table 2.

If there are three decision-maker who participate in the decision of peak load shifting controlling distribution, the result can be got using the model above. (The calculation process is omit)

(1) Parameter absolute weight vector of decision-maker one is V_1'

$V_1' = \{0.0428, 0.0231, 0.0877, 0.0104, 0.297, 0.083, 0.241, 0.1363, 0.0485, 0.0302\}$

(2) Parameter absolute weight vector of decision-maker two is V_2'

$V_2' = \{0.0368, 0.0368, 0.1049, 0.0085, 0.098, 0.148, 0.286, 0.1573, 0.0779, 0.0458\}$

(3) Parameter absolute weight vector of decision-maker three is V_3'

$V_3' = \{0.1801, 0.0483, 0.1849, 0.0217, 0.079, 0.1273, 0.2134, 0.0583, 0.0544, 0.03263\}$

(4) According to equation (15),

$\quad y_{12} = 0.2189, y_{13} = 0.2923, y_{23} = 0.2094$

$\quad e_1 = y_{12} + y_{13} = 0.5112 \quad\quad e_2 = y_{12} + y_{23} = 0.4283$

$\quad e_3 = y_{13} + y_{23} = 0.5017$

(5) According to equation (16),

$\quad \beta_1 = 0.311, \beta_2 = 0.372, \beta_3 = 0.317$

(6) According to equation (17), suppose $\delta_1 = \delta_2 = \delta_3 = 1/3$ and $\mu = 0.5$,

$\quad \lambda_1 = \mu\delta_1 + (1-\mu)\beta_1 = 0.167 + 0.156 = 0.323$

$\quad \lambda_2 = \mu\delta_2 + (1-\mu)\beta_2 = 0.166 + 0.186 = 0.352$

$\quad \lambda_3 = \mu\delta_3 + (1-\mu)\beta_3 = 0.167 + 0.158 = 0.325$

$W = \lambda_1 \omega_1 + \lambda_2 \omega_2 + \lambda_3 \omega_3$ and normalize it.

= {0.0853, 0.0361, 0.1253, 0.0134, 0.1561, 0.1203, 0.2479, 0.1183, 0.0608, 0.0365}

(7)According to equation (18), the calculation scale of peak load shifting controlling distribution in each region is as follows:

Z_1=7.38% , Z_2=23.86% , Z_3=1.19% , Z_4=26.19% , Z_5=19.3% , Z_6=22.08%

See Figure 2 and Figure 3.

6. Conclusion

According to the diagram (Table 1, Table 2) of peak load shifting period distribution above, it can be seen:

The change of final power supply limiting distribution scale is basically coincident with the decision parameter type defined above, going with the change of social economic parameter and power limiting direct loss. Consequently, it is feasible and will afford the need of power limiting distribution.

Anyway, power limiting distribution is a complicated multi-objective group decision problem. The period distribution decision is related to technology, economy and power limiting standard, also electricity grid security and society stabilization. So the research about distribution will be more complex. In this paper, the power limiting distribution parameter system and hierarchy structure are establish, according to the main factors affecting power supply limiting time distribution. A large system multi-objective group decision model and method based on the combination of hierarchy analysis and fuzzy synthesized appraisement. And from a practical example, the result manifests good. But the research about the social appraisement, national economy appraisement, environment effect appraisement and power limiting uncertainty of peak load shifting controlling distribution should be enhanced from now on.

References

Chiclana F, Herrera F & Herrera Viedma E. (1998). Integrating three representation models in fuzzy multipurpose decision making based on fuzzy preference relations. *Fuzzy Sets and Systems*, 9, 33-48

Delgado M, Herrera F Herrera Viedma E. (1998).Combining numerical and linguistic information in group decision making. *Information Sciences*, 10, 177-194

H.C.Huang, R.C.Wang & J.G. Hsieh. (2002). A new artificial intelligent peak power load forecaster based on non-fixed neural networks. *Electr.Power Energy Syst*, 24, 245-250

Herrera F & Herrera Viedma E. (2000). Linguistic decision analysis: steps for solving decision problems under linguistic information. *Fuzzy Sets and Systems*, 11, 67-82

Herrera F & Herrera Viedma E. (2000). Choice functions and mechanisms for Linguistic preference relation. *European Journal of Operational Research*, 20, 223-239

J. Ma, Z.P. Fan & L.H. Huang. (1999). A subjective and objective integrated approach to determine attributes weights. *European Journal of Operational Research*, 12, 397-404

Marmol AM, Puerto J & Fernanndez FR. (1998). The use of partial information on weights in multi-attribute decision problem. *Journal of Multi-attribute Decision Analysis*, 7, 322-329

M. Krunic, K.I. Slavisa & N. Rajakovic. (2000). An improved neural network application for short term load forecasting in power systems. *Electr. Mach. Power Syst*, 28, 703-721

M.R.G. Al-Shakrchi & M.M. Ghulaim. (2000). Short term load forecasting for Baghdad electricity region. *Electr. Mach. Power Syst*, 28, 355–371

Noel Bryson & Ayodele Mobolurin. (1999). An action learning evaluation procedure for multiple criteria decision making problems. *European Journal of Operational Research*, 6, 379-386,

Shamsuddin Ahmed. (2005). Seasonal models of peak electric load demand. *Technological Forecasting and Social Change*, 72, 609-622

Table 1. The Parameter of Social Economy

regions	Population(10000)	Electricity consumption number	Electricity capacity(Mkw)	Reconcilable peak scale (%)	Product gross(1000rmb)
1	56.42	308	47.28	17.83	476.52
2	23.18	106	21.53	52.12	180.63
3	89.13	416	62.52	41.63	725.20
4	10.67	89	18.62	71.63	97.65
5	36.21	218	32.15	31.25	207.26
6	43.56	229	29.56	52.06	168.88

Table 2. The Economic Loss of Power Limiting

region	Power limiting capacity(Mkw)	Economic loss of power limiting(1000rmb)	Electricity consumption peak scale(%)	Average temperature	Ice air condition scale(%)
1	41.07	28.71	67.12	32.5	25.6
2	16.52	8.28	40.06	31.2	30.1
3	55.73	34.62	62.56	32.7	25.7
4	17.64	9.43	36.11	29.8	35.2
5	27.35	10.52	50.12	30.6	22.6
6	23.06	9.31	54.58	33.3	21.7
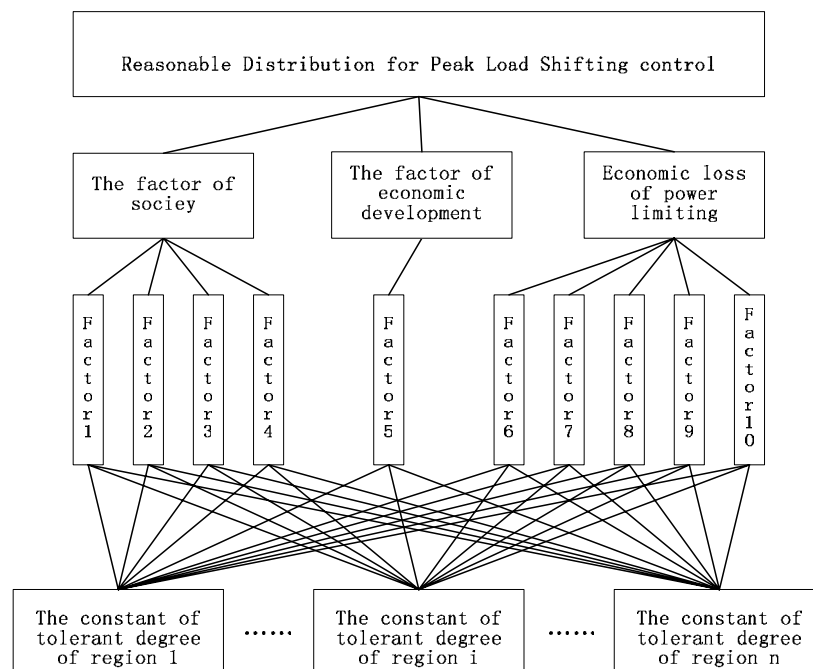
Figure 1. Decision system of Peak Load Shifting Power Limiting Distribution

Note: factor1-The population of region, factor2- The quantity of electro-enterprise, factor3-The capacity of using power, factor4-The proportion of electro-enterprise that can be power-off, factor5-The total value of produce, factor6-The capacity of power limiting, factor7-The economic loss of power liming, factor8-The proportion of peak for using power, factor9-The average temperature, factor10-The proportion of ice air condition
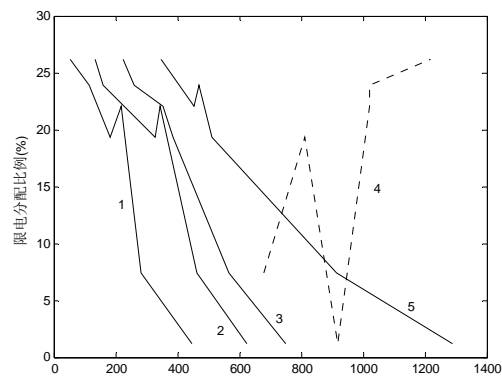
Figure 2. corresponding curve schematic diagram of social economic indicator and

Power Limiting Distribution in every region

Population-1

The quantity of electro-enterprise-2

The capacity of using electricity-3

The proportion of moving-peak enterprise-4

The total value of produce-5
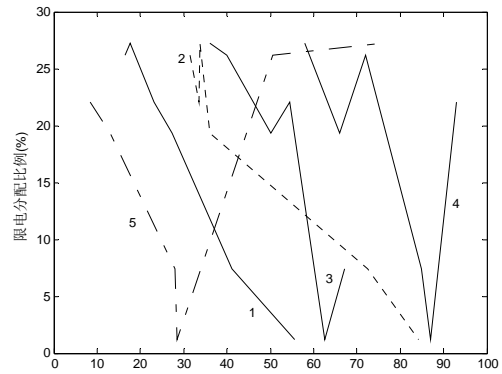
Figure 3. Corresponding curve schematic diagram of the economic loss indicator of

Power limiting and Power limiting Distribution proportion

Limited capacity-1

The economic loss of Power limiting-2

Proportion of using electricity peak-3

Average temperature-4

The proportion of ice air condition-5

Utilization of Design for Modularity

Approach to Identify Product Platform

A. B. Abdullah, A. R. Kamaruddin, Z. M. Ripin

School of Mechanical Engineering, Universiti Sains Malaysia

Engineering Campus, 14300, SPS, Pulau Pinang, MALAYSIA.

E-mail: matbaha_74@hotmail.com

Abstract

The aim of this paper is to propose a methodology to identify platform from a product variants based on modularity approach. The modules are identified by utilizing two well-established approaches. Two case studies of two types of consumer products have been carried to clarify the methodology .i.e. product which can be categorized from different family and same family. The result shows that the platform can be identified systematically.

Keywords: Modularity approach, Platform, Product family

1. Introduction

Companies are striving to produce products at low cost at shorter time. One of the best and preferred approaches is design for modularity approach. There are a lot of advantages and one of the main focus is the capability to formulate the common part that can be shared among the product variants namely product platform. The application of product platform has been suggested as a key component of a well-targeted development strategy for companies that aim better utilization from limited resources. Manufacturers and customers sometimes do not realize that most of the product in the market shares common parts or assemblies, namely platform. Platform architecture is a set of selection and configuration choices shared among products (Gonzalez-Zugasti, Baker and Otto, 2000, pp. 61-72). Product platform can be formulated as a general optimization problem in which the advantages of designing a common base must be balanced against the constraints of the individual product variants and of the whole family. Zugasti et al., (Gonzalez-Zugasti, J., Otto and Baker, 2000, pp. 61–72) defines product platform as a set of shared functionality across multiple products from similar or different family. Each different product supported by the platform is called a variant, while a set of all variants derived from a platform formed a product family. Product platform can be classified into four based on product brand and family (Abdullah and Ripin, 2003, pp. 333-345);

(a) Products from same brand and family

(b) Products from same brand but different family

(c) Products from different brand and family

(d) Products from different brand but same family

There are several approaches used in platform development, whether during, before or after product is designed. Some of the examples in developing platform are Sudjianto and Otto (Sudjianto and Otto, 2001) from multiple brand product using brand architecting rules for product modularization, i.e. dominant theme of product functions and aesthetic forms, brand signature and platform rules. Zugasti et al. (Gonzalez-Zugasti, Baker and Otto, 2000, pp. 61-72) used models of several spacecraft to identify possible subsystem that could be made common to all or some of the missions. Similarly Ripin and Abdullah (Ripin and Abdullah, 2001, pp. 190-199) developed modular UAV based on the multi-mission requirements optimization. The advantages of product platform are that by using proven modules that are known to operate effectively at their designated sub-tasks can minimize design risk. Further, reuse of previously designed modules can bring saving at least in part, the cost of redeveloping those sub-system. Product platform also could reduce design risk and also deduct time and cost to market (Martin and Ishii, 2002, pp. 213–235).

The concept of product platforms and design variants has been successfully applied to wide range of product especially consumer and industrial product. For example Sony used three platforms to support hundreds of different personal portable stereo product in its Walkman family and as shown in Figure 1 seven variants are developed i.e. cordless delta sander, cordless reciprocating saw, cordless jig saw, cordless circular saw, cordless hedge trimmer and cordless grass trimmer by using common main housing and battery mounter. Lately several names from automotive company such as

Volkswagen also takes the advantages of platforming and components commonality by sharing between its four major brands such as VW, Audi, Skoda and Seat (Bremner, 1999, pp. 30-38). (See Figure 1)

This paper emphasis on development of methodology to identify platform from variants of product based on modularity approach. The methodology involves three steps; product variant listing, module identification and platform identification. Two cases are present from same and different product family.

2. Methodology

This approach starts by listing of variants from product family. Then products are decomposed into the lowest level of components for better understanding of the physical configuration of the product. Then modularization takes place, where two established modular approaches are utilized in determining the modules and finally platforms identification. The idea of platform development can be generally visualized as shown in Figure 2. For example there are three variants that have three modules each. Module 1 from variant A consist of components 1, 2 and 3, while module 1 from variant B consist of components 1, 2 and 4 and finally for variant C consist of components 1, 2 and 3. As a result after applying algorithm in Figure 3, platform that consists of components 1, 2 and 3 can be developed. This is similar to module 2 and 3. (See Figure 2)

Based on that idea, an algorithm is developed to systematically identify the platform. Consider a variant of products with i number of models, $V = \{1......i\}$ and C_{Vi} is list of components in the variant i. After the module identification methods have been applied, there are p_i numbers of modules in each variant. The interaction between modules or similarity between modules in terms of components consisting in the modules of variant i and $i+1$ is consider as platform i, $m_{1V1} = m_{1Vi}$, the process is continue till there are no more platform can be identify. The algorithm can be formulated as follow;

Step 1: List down the variants, V_i ($i = 1, 2, \ldots n$)

Where n = number of variants

Step 2: List down the components in each variants, $C_{Vi} = \{\quad\}$

Step 3: Applying the conventional module identifications methods.

Step 4: Set $j = 1$ ($j = 1, 2 \ldots p$)

Where p = number of modules

IF, $m_{1V1} = m_{1Vi}$,

m_{1Vi} = {Components in module 1 of Variants i}

THEN, $P_1 = \{m_1\}$

P_1 = Platform 1, m_1 = {Similar components in the module from the variants}

ELSE, rearrange the module

END IF.

Step 5: Set $j = p +1$ and m_{p+1} GO TO step 4

Step 6: IF, $m_{p+1V1} \cap m_{p+1Vi} = \{m_r\}$

m_{p+1Vi} = {Components in module p of variants i}

m_r = {Components in module p of variants 1 that intersect with components in module p of variants i}

THEN $P_q = m_r = \{m_{p+1V1} \cap m_{p+1Vi}\}$

IF, $m_{p+1V1} \cup m_{p+1Vi}$

THEN $P_q = m_r = \{m_{p+1V1} \cup m_{p+1Vi}\}$

IF, $m_{p+1V1} \neq m_{p+1Vi}$

THEN $P_q = \varnothing$

END IF

Step 7: Delete all modules associated with Platform, P_p from the module, GO TO step 4

Step 8: IF $M_A = \varnothing$, STOP

An approach developed by Huang and Kusiak (Huang and Kusiak, 1998, pp. 66-77) and Stone et al, (Stone, Wood and Crawford, 2000, pp. 215-31) are applied in identifying modules. This approach is then extended to be complying for a list of variants in the family. After the platform is developed, the necessary action need to be done in order to fulfill shared requirements. Finally the potential candidate is further proceeding for redesign.

3．Implementation

3.1 Product from Different Family

In this case study, 3 types of consumer product have been used. Products from different family can be described as product which is physically having no similarity (Dobrescu and Reich, 2003, pp. 791-806). The selected products are flour mixer, blender and juice extractor as shown in Figure 3. Figure 4 show the physical decomposition and Figure 5 list the components in the products. (See Figure 3, Figure 4 and Figure 5)

Next step is to examine flow and functional chains for each of the products to construct the function structure. Modules containing in the mixer, blender and juice extractor can easily be identified after the function structure has been fully built using dominant flow, branching flow and conversion-transmission rule methods developed by Stone et al. (2000). In order to identify platform, the algorithm is applied As a result, from Table 1 four platforms can be developed;

(1) Transmit electricity module

(2) Transmit rotation module

(3) Actuating module

(4) Convert electricity module

The platforms are represented in shaded blocks. From the identified platforms, it can be concluded that the motor and switch modules are the most potential module that can be platformed. (See Table 1)

3.2 Products from Same Family

For the products from same family, also three products have been selected i.e. the table fan, wall fan and stand fan. Here products from same family can be explained as a list of products, which have some similarity either in terms of functionality or physical configuration. The steps taken are similar to the previous case study, where it begins with decomposition of the product to identify all components in the products. The decomposition can be demonstrated in the form of hierarchy structure. There are five sub-system and mechanism of fan as decomposed in the Figure 6, with total of 22 components for all three variants of fan family as listed in the Figure 7. Here switch panel and motor assembly are considered as a single component. (See Figure 6 and Figure 7)

As are result after applying the module identification approach developed by Huang and Kusiak (1998), 5 modules are identified as shown in Table 2. (See Table 2)

The algorithm is applied to identify the platform and as a result five platforms are identified as summarized in Table 3. For platform A, B and C there is clear decision in platform selection, where all three variants own the same components. But for platform D, conflict occurs where for module δ, components 20 and 22 contain in variants 3 only, not in the other variants, whereas component 14 only in variant 2 and not the other variant. But by considering the physical structure of the components, only components 12 and 13 can be combined to become a platform. The components not in the platform could be the specials features where dissimilar comes in. (See Table 3)

4. Discussion

This paper has presented the methodology to identify platform from the group of product variants from same and different family. Two conventional module identification methods are applied. The paper is not intent to compared between the approaches, but want to prove that the developed algorithm is able to easily identify platform even the approach used is different. The extended algorithm is proposed in order to ensure that the identified platform own features that can be shared among the variants. In the algorithm, the platform is developed based on the similarity of the module identified among the product variants in terms of functionality and physical configurations of the components. From the case studies, out for each fan family and products from different family shown that there are several potential platforms but with a minor modification needed to accommodate components sharing among product variants.

5. Conclusion and future works

This paper has looked into main objectives, which is developed product platform by using modular approach. After the modules are identified, an extended approach has been developed to form platform. From the case studies indicate that the platform form several variants of same family and different family can be identifying systematically. This approach also can be further extended to other module or parts in order to increase the commonality of the product.

Acknowledgement

References

Abdullah, A. B. and Ripin, Z. M. (2003). Modularization to Support Product Platform for Redesign, 19th Int. Conf.   On CAD/CAM, Robotics and Factories of the Future 2003 Vol. I: 333-345.

Bremner, R. (1999). Cutting Edge Platform, Financial Times Automotive World, 30-38.

Dobrescu, G. and Reich, Y. (2003). Progressive sharing of modules among product variants, *Computer-Aided Design*. 35(9), 791-806.

Gonzalez-Zugasti J., Baker J. and Otto K. (2000). A Method for Architecting Product Platform with an Application to Interplanetary Mission Design, *Research in Engineering Design.* 12, 61-72.

Gonzalez-Zugasti, J. P., Otto, K. N. and Baker, J.D. (2000). A method for architecting product platforms, *Research in Engineering Design.* 12(2), 61–72.

Huang, C. and Kusiak, A. (1998). Modularity in Design of Products and Systems, *IEEE Trans. On System Man and Cyber-Part A: Systems and Humans.* 28(1), 66-77.

Martin, M.V. and Ishii, K. (2002). Design for variety: developing standardized and modularized product platform architectures, *Research in Engineering Design* 13, 213–235.

Ripin, Z. M. and Abdullah, A. B. (2001). A Design Study on Modular Platform of Unmanned Aerial Vehicle, National Conf. on Aerodynamic and Related Topics Penang, 190-199.

Stone R. B, Wood, K. L. and Crawford, R. H. (2000). A Heuristics Method for Identifying Modules for Products Architectures. *Design Studies*. 21(1), 215-31.

Sudjianto, A. and Otto, K. (2001). Modularization to Support Multiple Brand Platforms, ASME DTM, Pittsburgh, PA.

www.allproducts.com.tw/prc/toomly/p05.html

Table 1. Platform identified from the approach.

Product Family	Module		
	Dominant flow	*Branching flow*	*Conversion-Trans*
Mixer	1. Hand Interface	1.Coupling/ decoupling	1. Convert electricity to rotation
	2. Coupling	2. Decoupling	
	3. Mounting	3. Actuating	
	4. Mixture Containment		
	5.Transmit rotation		
	6. Transmit electricity		
Blender	1. Soft food containment	1. Soft food containment	1. Convert electricity to rotation
	2. Hard food containment	2. Hard food containment	
	3. Coupling	3. Weight Transmission	
	4. Transmit electricity	4. Actuating	
	5. Transmit rotation	5. Food removing	
Juice Extractor	1. Transmit electricity	1. Actuating	1. Convert electricity to rotation
	2. Fruit Guide	2. Fruit Guide	
	3. Transmit rotation		
	4. Waste storing		
	5. Juice storing		

Table 2. Module identified from the algorithm

Module	Variant 1	Variant 2	Variant 3
ά	1, 2, 3, 8	1, 2, 3, 8	1, 2, 3, 8
β	4, 5, 6, 7	4, 5, 6, 7	4, 5, 6, 7
γ	9,11	9, 10, 11	9, 11
δ	12, 13	12, 13, 14	12, 13, 20, 22
ε	14	-	14
λ	-	17, 18, 19, 20	-

Table 3. Platform identified from the approach

Platform	Variant 1	Variant 2	Variant 3
A	1, 2, 3, 8	1, 2, 3, 8	1, 2, 3, 8
B	4, 5, 6, 7	4, 5, 6, 7	4, 5, 6, 7
C	9, 11	9, 11	9, 11
D	14	14	14
E	12, 13	12, 13	12, 13

Figure 1. A series of products variants that share battery and main housing
(www.allproducts.com.tw/prc/toomly/p05.html)

| Module 1: CA1, CA2 and CA3 |
| Module 1: CB1, CB2 and CB4 |
| Module 1: CC1, CC2 and CC3 |

PLATFORM →

Platform 1: C1, C2 and C3

| Module 2: CA5, CA6 and CA7 |
| Module 2: CB5, CB6 and CB7 |
| Module 2: CC4, CC5 and CC7 |

PLATFORM →

Platform 2: C5, C6 and C7

→ **REDESIGN**

| MODULE 3: CA4, CA6 and CA10 |
| MODULE 3: CB3 AND CB10 |
| MODULE 3: CC6 AND CC10 |

PLATFORM →

Platform 3: C6 and C10
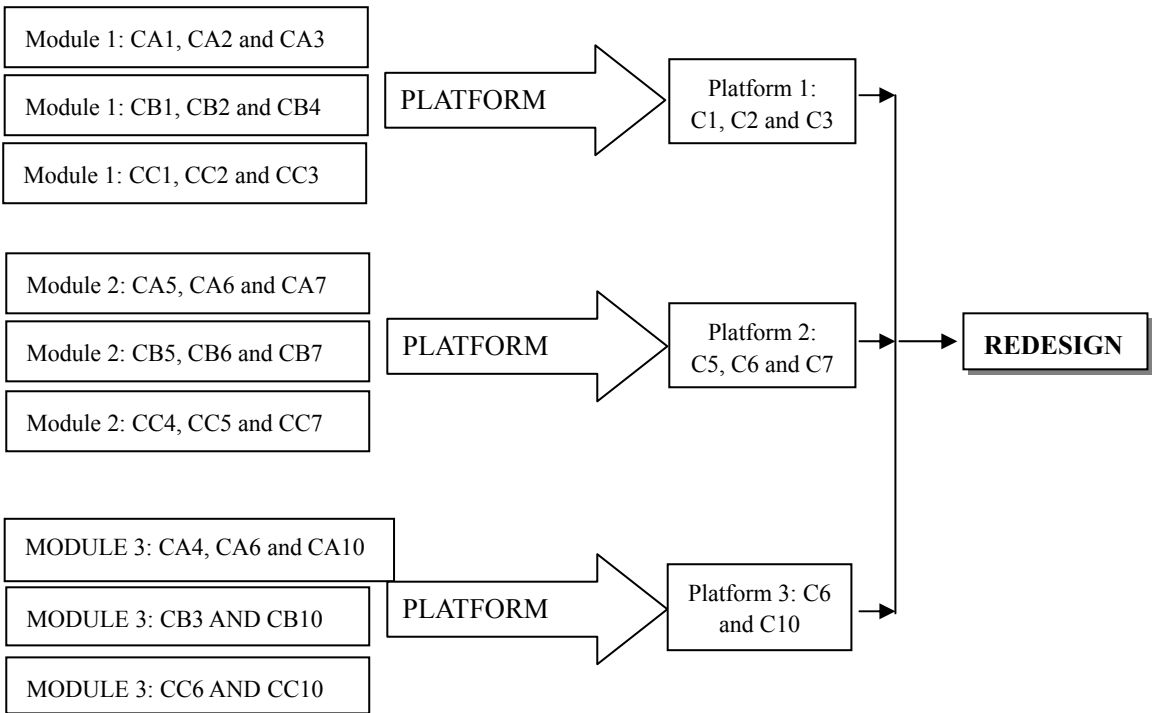
Figure 2. A generalize platform identification flow process

(a) (b) (c)
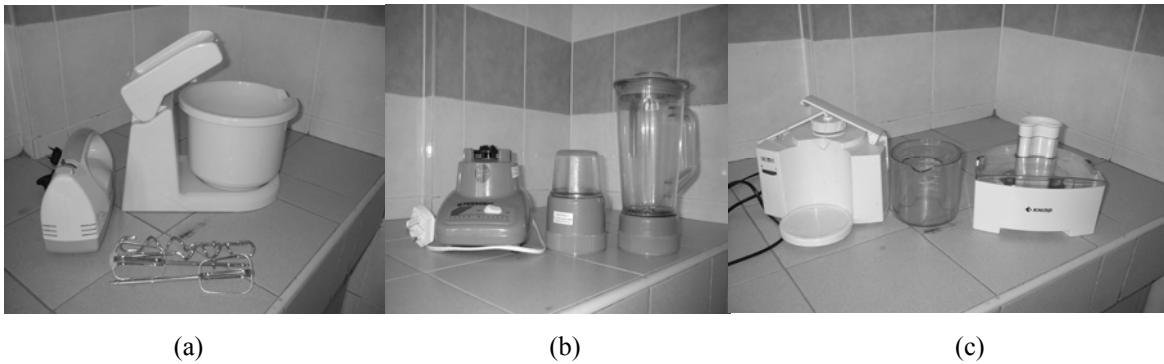
Figure 3. Customer products from different family
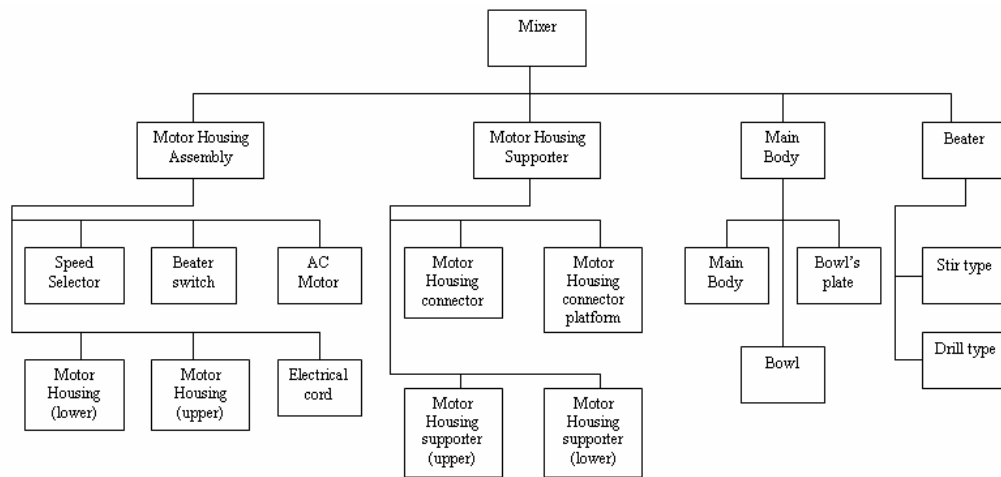
(a)
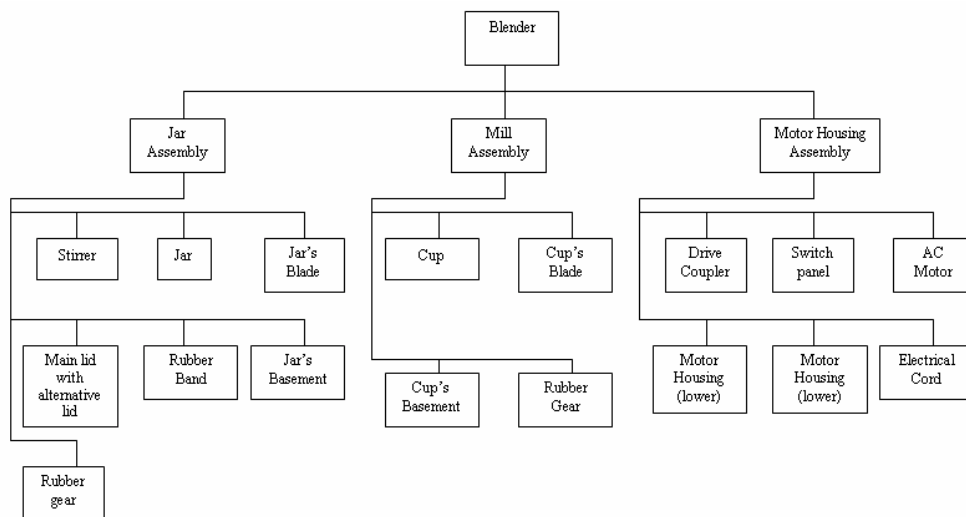
(b)
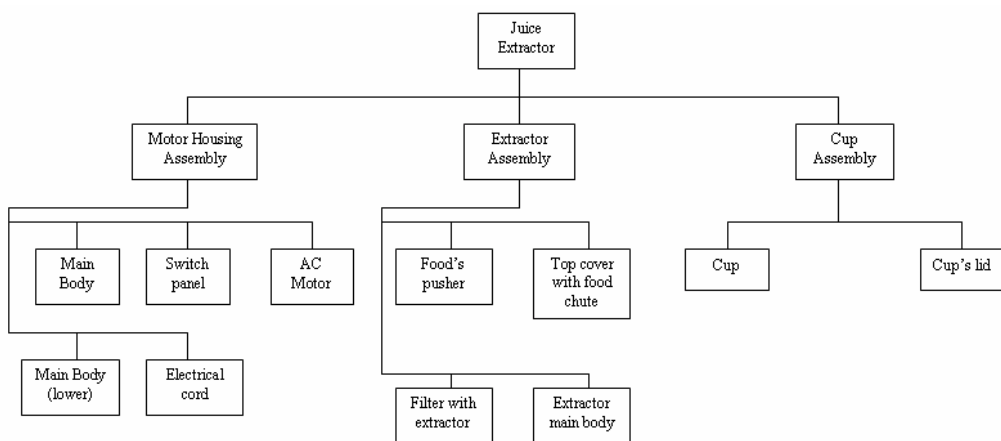
(c)

Figure 4. Physical decomposition of product (a) mixer, (b) blender and (c) juice extractor
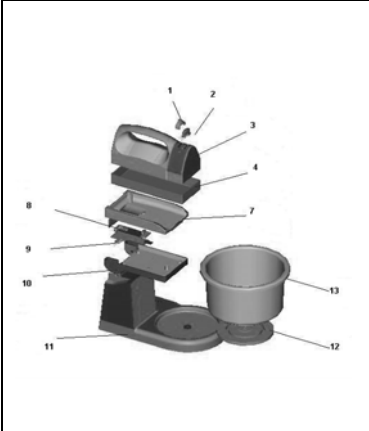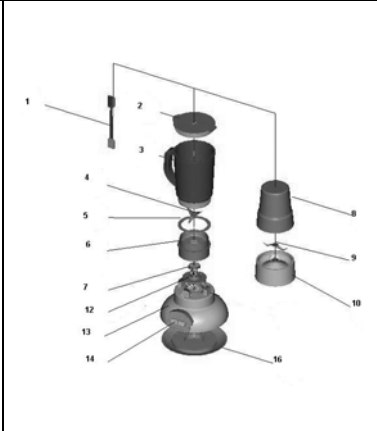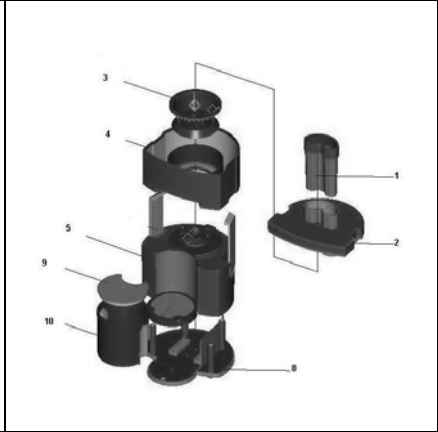
#	(a)	#	(b)	#	(c)
1	Speed Selector	1	Stirrer	1	Pusher
2	Beater Switch	2	Main lid with alternative lid	2	Top cover with food chute
3	Motor Housing(upper)	3	Jar	3	Filter with extractor
4	Motor Housing(lower)	4	Blade	4	Extractor Main Body
5	AC Motor	5	Rubber Band	5	Main Body
6	Electrical cord	6	basement	6	Switch panel
7	Motor Housing Supporter (upper case)	7	Rubber Gear	7	AC Motor
8	Motor Housing Connector	8	Cup	8	Main Body (lower casing)
9	Motor Housing connector (platform)	9	Blade	9	Electrical cord
10	Motor Housing Supporter (lower case)	10	Basement	10	Cup
11	Main Body	11	Rubber Gear	11	Lid
12	Plate	12	Drive Coupler		
13	Bowl	13	Motor housing (upper case)		
14	Stir type	14	Switch panel		
15	Drill type	15	AC Motor		
		16	Motor Housing (lower case)		
		17	Electrical cord		

Figure 5. Part listing of (a) mixer, (b) blender and (c) juice extractor
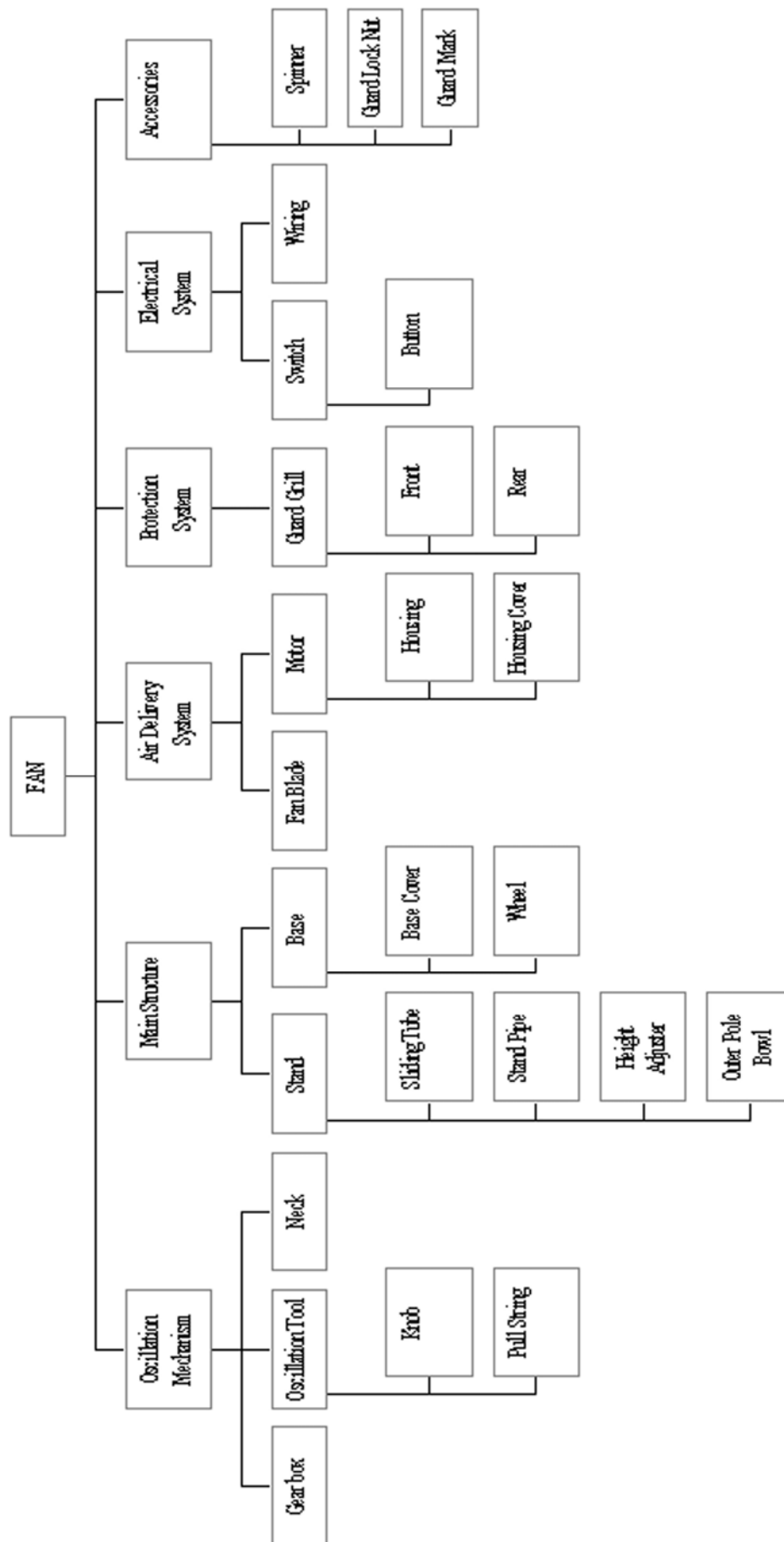
Figure 6. Physical decomposition of table fan
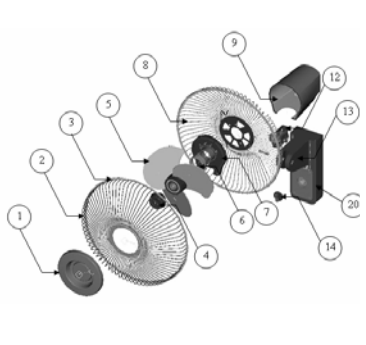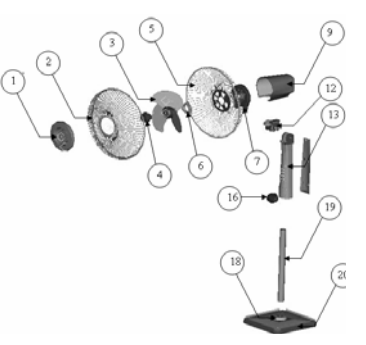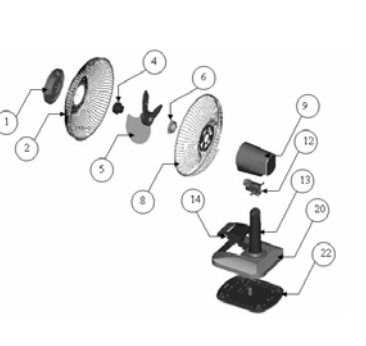
1	Guard Mark	1	Guard Mark	1	Guard Mark
2	Front Guard	2	Front Guard	2	Front Guard
3	Guard Ring	3	Guard Ring	3	Guard Ring
4	Spinner	4	Spinner	4	Spinner
5	Fan Blade	5	Fan Blade	5	Fan Blade
6	Guard Lock Nut	6	Guard Lock Nut	6	Guard Lock Nut
7	Housing Cover	7	Housing Cover	7	Housing Cover
8	Rear Guard	8	Rear Guard	8	Rear Guard
9	Motor Housing	9	Motor Housing	9	Motor Housing
		10	Oscillation Knob	10	Oscillation Knob
11	Motor	11	Motor	11	Motor
12	Neck	12	Neck	12	Neck
13	Stand	13	Stand	13	Stand
14	Switch Panel	14	Switch Panel	14	Switch Panel
15	Pull String	16	Height Adjuster	20	Base
		17	Sliding Tube	22	Base Cover
		18	Outer Pole Bowl		
		19	Stand Pipe		
		20	Base		
		21	Wheel		

Figure 7. Part listing of product (a) wall fan, (b) stand fan and (c) table fan

A Recurrent Neural Network for

Solving Convex Quadratic Program

Caihong Shan (Corresponding author)

Department of Mathematics, Yanshan University

438, He Bei street, Qinghuangdao 066004, China

E-mail: caihongshan2006@126.com

Huaiqin Wu

Department of Mathematics, Yanshan University

438, He Bei street, Qinghuangdao 066004, China

E-mail: huaiqinwu@ysu.edu.cn

Abstract

In this paper, we present a recurrent neural network for solving convex quadratic programming problems, in the theoretical aspect, we prove that the proposed neural network can converge globally to the solution set of the problem when the matrix involved in the problem is positive semi-definite and can converge exponentially to a unique solution when the matrix is positive definite. Illustrative examples further show the good performance of the proposed neural network.

Keywords: Recurrent neural network, Convex quadratic program, Convergence

1. Introduction and model formulation

In this paper, we are concerned with the following quadratic optimization program:

$$\text{minimize} \quad \frac{1}{2}x^T A x + c^T x$$
$$\text{subject to} \quad Dx \leq b, \ x \geq 0 \tag{1}$$

and its dual

$$\text{maximize} \quad -b^T y - \frac{1}{2}x^T A x$$
$$\text{subject to} \quad -D^T y - Ax \leq c, \ y \geq 0 \tag{2}$$

where $A \in R^{n \times n}$ is symmetric and positive semi-definite, $D \in R^{m \times n}, b \in R^m$, and $c \in R^n$. It is well known that quadratic optimization problems arise in a wide variety of scientific and engineering applications including regression analysis, image and signal progressing, parameter estimation, filter design, robot control, etc. In many real-time applications these optimization problems have a time-varying nature, they have to be solved in real time. The main advantage of neural network approach to optimization is that the nature of the dynamic solution procedure is inherently parallel and distributed. Therefore, the neural network approach can solve optimization problems in running time at the orders of magnitude much faster than the most popular optimization algorithms executed on general-purpose digital computers. At present, there are several neural network approaches for solving quadratic programming problem. Next, we describe the proposed neural network.

By the duality theorem of convex programming, (x^*, y^*) is an optimal solution to Eq.(1) and (2), respectively, if and only if (x^*, y^*) satisfies the Karush-Kuhn-Tucker conditions

$$u = c + A^T x + D^T y \geq 0, \quad x \geq 0, \quad x^T u = 0$$
$$v = b - Dx \geq 0, \quad y \geq 0, \quad y^T v = 0 \tag{3}$$

We see that the above Eq. (3) may be transformed into the linear projection equation of the following form

$$u = P_\Omega[u - Mu - q] \tag{4}$$

Where $\Omega = \{u = (x, y) \in R^{n+m} \mid u \geq 0\}$, $M = \begin{bmatrix} A & D^T \\ -D & 0 \end{bmatrix}$, $q = \begin{bmatrix} c \\ b \end{bmatrix}$, notice that the matrix M is positive semi-definite

because $u^T M u = x^T A x \geq 0$ .and P_Ω is a projection operator which is defined by $P_\Omega(u) = [P_\Omega(u_1), P_\Omega(u_2), ..., P_\Omega(u_{n+m})]^T$

and for $i = 1, 2, K, n + m$, $P_\Omega(u_i) = \begin{cases} d_i & u_i < d_i \\ u_i & d_i \leq u_i \leq h_i \\ h_i & u_i > h_i \end{cases}$

In particular, if $h_i = +\infty$ and $d_i = 0$, then $P_\Omega(u_i) = (u_i)^+ = \max\{0, u_i\}$.

We can see that the optimal solutions of (1) and its dual (2) can be obtained by solving the project equation (4).

We propose a neural network for solving (1) and (4), whose dynamical equation is defined as follow:

$$\frac{du}{dt} = (I + M^T)(P_\Omega(u - Mu - q) - u) \tag{5}$$

Theorem 1. If $u^* = (x^*, y^*) \in R^{n+m}$, is an equilibrium point of the proposed neural network, then x^*, y^* is optimal solution to Eq.(1) and Eq.(2), respectively. On the other hand, if x^*, y^* is optimal solution to Eq.(1) and Eq.(2), then $((x^*)^T, (y^*)^T)^T$ is an equilibrium point of the proposed neural network.

2. Preliminaries

This section, we introduce the related definitions and lemmas for later discussion.

Definition 1. If $g : \Omega_1 \in R^l \to R$, then any nonempty set of the form

$L(r) = \{u \in \Omega_1 \mid g(u) \leq r\}, \quad r \in R$,

is said to be a level set of g.

Definition 2. A system is said to have globally exponential convergence rate with degree η at u^* if every trajectory staring at any initial point $u(t_0) \in R^l$ satisfies the condition

$\| u - u^* \| \leq c_0 \| u(t_0) - u^* \| \exp(-\eta(t - t_0)) \quad \forall t \geq t_0$

where c_0 and η are positive constants independent of the initial points.

Lemma 1 (Gronwall). Let u and v be real-valued non-negative continuous functions with domain $\{t \mid t \geq t_0\}$, let

$a(t) = a_0(\mid t - t_0 \mid)$ where a_0 is a monotone increasing function. If for $t \geq t_0$ $u(t) \leq a(t) + \int_{t_0}^t u(s)v(s)ds$, then

$u(t) \leq a(t) \exp\left\{\int_{t_0}^t v(s)ds\right\}$.

Lemma 2: let Ω be a closed convex set. Then

$(v - P_\Omega(v))^T (P_\Omega(v) - u) \geq 0 \qquad \forall v \in R^n \quad \forall u \in \Omega$

and

$\| P_\Omega(u) - P_\Omega(v) \| \leq \| u - v \| \qquad \forall u, v \in R^n$

Lemma 3. let $g : \Omega_1 \in R^l \to R$, where Ω_1 is unbounded. Then for all level sets of g are bounded if and only if

$\lim_{k \to \infty} g(u^k) = +\infty$ whenever $u^k \subset D$ and $\lim_{k \to \infty} \| u^k \| = +\infty$.

With the lemma 1 and 2, we can give the existence and uniqueness of the solution to Eq. (5).

Theorem 2. For each $u_0 \in R^{n+m}$ there exists a unique continuous solution $u(t)$ for (5) with $u(t_0) = u_0$ over $[t_0, \infty)$.

Proof. Let $T(u) = (I + M^T)(P_\Omega(u - Mu - q) - u)$ .then $T(u)$ is Lipschitz continuous in R^{n+m} since for any

$u, v \in R^{n+m}$

$$\| T(u) - T(v) \| \le \| I + M^T \| (\| P_\Omega(u - Mu - q) - P_\Omega(v - Mv - q) \| + \| u - v \|)$$

$$\le \| I + M^T \| (2 \| u - v \| + \| M \| \| u - v \|)$$

$$\le \| I + M^T \| (2 + \| M \|) \| u - v \|$$

Thus for any $u_0 \in R^{n+m}$, there exists a unique and continuous solution $u(t)$ of Eq. (5), defined in $t_0 \le t < T$, with the initial condition $u(t_0) = u_0$. Let $[t_0, T)$ be its maximal interval of existence, we next show that $T = \infty$. From lemma 2, it follows

$$\| T(u) \| = \| I + M^T \| \| P_\Omega(u - Mu - q) - u \|$$

$$\le \| I + M^T \| (\| Mu + q \| + \| P_\Omega(u) - P_\Omega(u^*) \| + \| P_\Omega(u^*) - u \|)$$

$$\le \| I + M^T \| ((2 + \| M \|) \| u \| + \| q \| + \| u^* \| + \| P(u^*) \|)$$

then

$$\| u(t) \| \le \| u_0 \| + \int_{t_0}^{t} \| T(u(s)) \| \, ds$$

$$\le (\| u_0 \| + k_1(t - t_0)) + k_2 \int_{t_0}^{t} \| u(s) \| \, ds$$

where $k_1 = \| I + M^T \| (\| q \| + \| u^* \| + \| P_\Omega(u^*) \|)$ and $k_2 = \| I + M^T \| (2 + \| M \|)$. Therefore, using Lemma 1 we have

$\| u(t) \| \le (\| u_0 \| + k_1(t - t_0)) e^{k_2(t - t_0)}, \quad t \in [t_0, T)$.

Hence the solution $u(t)$ is bounded on $[t_0, T)$. So $T = \infty$.

3. Convergence result

In the present section, under the assumption that $\Omega^* \ne \Phi$. We prove the convergence of the proposed neural network.

Theorem 3. Let M is positive semi-definite, then the neural network (5) is stable in the sense of Lyapunov and globally convergences to the solution subset of the problem (4).

Proof. First, definite

$F(u) = (I + M^T)(P_\Omega(u - Mu - q) - u)$.

Clearly, $F(u) = 0$ if and only if u is a solution to problem (4). Thus the equilibrium point of the system in Eq.(5) correspond to solutions to problem (4) because $I + M^T$ is non-singular. Next, by theorem 2 we see that there exists a unique and continuous solution $u(t)$ with any initial point $u_0 \in R^{n+m}$ for system (5).

Now let u_0 be any initial point taken in Ω, and let $u(t) = u(t, t_0; u_0)$ be the solution of the initial value problem associated with (3). We then consider the following Lyapunov function

$$V(u) = \frac{1}{2} \| u - u^* \|_2^2, \quad u \in R^{n+m},$$

where $u^* \in \Omega^*$. Clearly, $\lim_{k \to \infty} V(u^k) = +\infty$ whenever the sequence $\{u^k\} \subset \Omega$ and $\lim_{k \to \infty} \| u^k \| = +\infty$. Thus by Lemma 3 we see that all the level sets of V are bounded. On the other hand, using the technique of the proof from the literature, by the properties of the projection operator we have for all $u \in R^{n+m}$ and all $y \in \Omega$

$[y - P_\Omega(u - Mu - q)]^T [Mu + q - u + P_\Omega(u - Mu - q)] \ge 0$.

Since u^* is a solution of the problem (4), for all $y \in \Omega$

$\{y - u^*\}^T \{Mu^* + q\} \ge 0$

Taking $y = u^*$ in the first inequality and taking $y = P_\Omega(u - Mu - q)$ in the second inequality and then adding the two resulting inequalities yields

$\{u^* - P_\Omega(u - Mu - q)\}^T \{M(u - u^*) - u + P_\Omega(u - Mu - q)\} \ge 0$

Then

$(u^* - u)^T M(u - u^*) + (u - u^*)(I + M^T)(u - P_\Omega(u - Mu - q)) \ge \| u - P_\Omega(u - Mu - q) \|_2^2$

Since is M positive semi-definite, it follows that

$(u - u^*)^T (I + M^T)(u - P_\Omega(u - Mu - q)) \ge \| u - P_\Omega(u - Mu - q) \|_2^2$

Therefore, we have

$$\frac{d}{dt}V(u) = \frac{dV}{du}\frac{du}{dt}$$

$$= (u - u^*)^T (I + M^T)(P_\Omega(u - Mu - q) - u)$$

$$\leq -\|u - P_\Omega(u - Mu - q)\|_2^2 \leq 0$$

Thus $V(u)$ is a global Lyapunov function for the system in (5) and the system (5) is stable in the sense of Lyapunov. Since $\{u(t)\,|\,t \geq t_0\} \subset \Omega_0$ where $\Omega_0 = \{u \in \Omega\,|\,V(u) \leq V(u_0)\}$ and the function $V(u)$ is continuously differentiable on the bounded and closed set Ω_0, it follows from Lasalle's invariance principal that trajectories $u(t)$ will converge to E, the largest invariant subset of the following set:

$$E = \left\{ u \in \Omega_0 \mid \frac{dV}{dt} = 0 \right\}$$

It is easy to see that $du/dt = 0$ if and only if $dV/dt = 0$. It follows that

$$E = \left\{ u \in \Omega_0 \mid \frac{dV}{dt} = 0 \right\} = \Omega_0 \cap \Omega^*$$

Which is a nonempty, convex, and invariant set containing in the solution set Ω^*. So

$$\lim_{t \to \infty} dis(u(t), E) = 0 \cdot$$

Therefore, the proposed neural network converges globally to the solution set of the problem (4).

Remark 1. If A is positive definite then M is positive definite, too. Thus, form the proof of theorem 3 we can get the neural network (5) is globally exponentially convergent.

Since

$$(u^* - u)^T M(u - u^*) + (u - u^*)(I + M^T)(u - P_\Omega(u - Mu - q)) \geq \|u - P_\Omega(u - Mu - q)\|_2^2$$

We have

$$(u^* - u)^T M(u - u^*) + (u - u^*)(I + M^T)(u - P_\Omega(u - Mu - q)) \geq 0$$

by Schwarz inequality we obtain

$$\|I + M^T\|\,\|u - P_\Omega(u - Mu - q)\| \geq \mu\,\|u - u^*\|$$

where $\mu = \lambda_{\min}\left(\dfrac{M^T + M}{2}\right)$, thus

$$\|u - P_\Omega(u - Mu - q)\| \geq \frac{\mu}{\|I + M^T\|}\|u - u^*\|$$

So

$$\frac{d}{dt}V(u) \leq -\|u - P_\Omega(u - Mu - q)\|^2$$

$$\leq -\frac{\mu^2}{\|I + M^T\|^2}\|u - u^*\|^2$$

$$\leq -\frac{2\mu^2}{\|I + M^T\|^2}V(u)$$

Thus

$$V(u) \leq V(u_0)e^{-2\delta(t - t_0)}$$

where $\delta = \dfrac{\mu^2}{\|I + M^T\|^2} > 0$, and hence

$$\|u(t) - u^*\| \leq \|u_0 - u^*\|\,e^{-\delta(t - t_0)}$$

Therefore, the proposed neural network is globally exponentially converges to the solution subset of the problem (4) if M is positive definite.

4. Simulation example

In order to demonstrate the effectiveness and efficiency of the proposed neural network, in this section, we discuss the simulation results through an example. The simulation is conduct on Matlab, the ordinary differential equation solver

engaged is ode45s.

Example 1. Consider the convex quadratic program

$$\text{minimize} \quad \frac{1}{2}x^T A x + c^T x$$
$$\text{subject to} \quad Dx \le \text{b}, \text{x} \ge 0$$

and its dual

$$\text{maximize} \quad -\text{b}^T y - \frac{1}{2}x^T A x$$
$$\text{subject to} \quad -D^T y - A x \le \text{c}, \text{y} \ge 0$$

where

$$D = \begin{bmatrix} 5/12 & -1 \\ 5/2 & 1 \\ -1 & 0 \\ 0 & 1 \end{bmatrix}, \quad A = \begin{bmatrix} 2 & 1 \\ 1 & 2 \end{bmatrix}, \quad b = \begin{bmatrix} 35/12 \\ 35/2 \\ 5 \\ 5 \end{bmatrix}, \quad c = \begin{bmatrix} -30 \\ -30 \end{bmatrix}.$$

Its exact solution is $(5,5)^T$. we use the system (5) to solve the above problem. All simulation result show that the solution trajectory always converges to the unique point $u^* = (5.000, 5.000, 0, 6.000, 0, 9.000)^T$ which corresponds to the optimal solution $(5,5)^T$ and its dual solution $(0,6,0,9)^T$. Let the starting point be $(2,4,0,0,0,0)^T$ and $(5,6,1,0,3,0)^T$ respectively. Figure 1 (a) and (b) show the transient behavior of the neural network for those starting point, respectively.
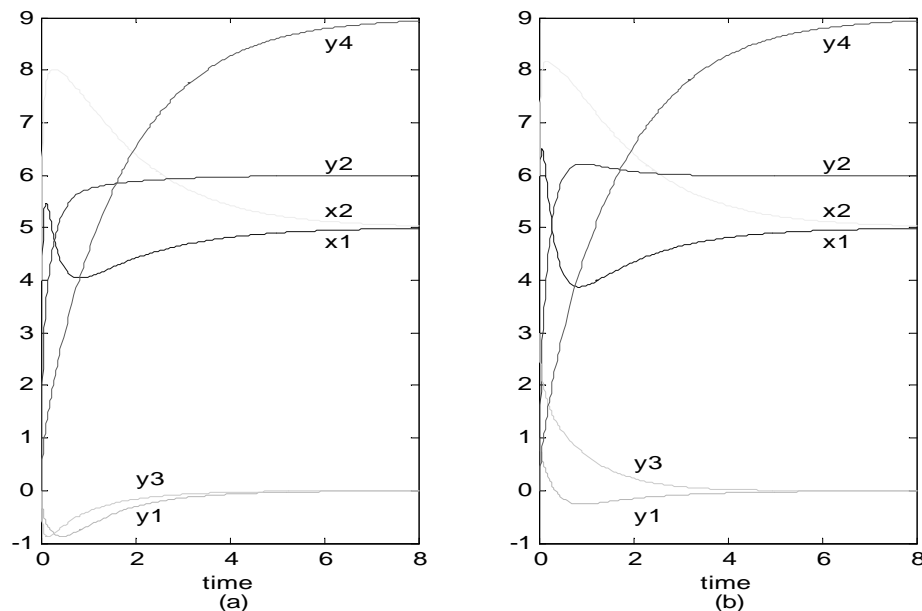
Figure 1. Transient behavior of the neural network (5) in example 1

(a) the initial point $(2,4,0,0,0,0)^T$; (b) the initial point $(5,6,1,0,3,0)^T$

5. Conclusion

In this paper, we have presented a recurrent neural network for solving convex quadratic programming problems, in the theoretical aspect, we have proved that the proposed neural network can converge globally to the solution set of the problem when the matrix involved in the problem is positive semi-definite and can converge exponentially to a unique solution when the matrix is positive definite. Illustrative examples further show the good performance of the proposed neural network.

References

Tao, Q., Cao, J. D., & Sun, D. M. (2001). A simple and high performance neural network for quadratic programming problems. *Appl. Math. Comput*. 124, 251-260.

Xia, Y. S. & Wang, G. (2005). An improved network for convex quadratic optimization with application to real-time beamforming. *Neurocomputing*, 64, 359-374

Xia, Y. S. & Wang, J. (2000). A recurrent neural network for solving linear projection equations. *Neural Networks*. 13, 337-350.

Xia, Y. S., Feng, G., & Wang, J. (2004). A recurrent neural network with exponential convergence for solving convex quadratic program and related linear piecewise equation. *Neural Networks*. 17, 1003-1015.

Xia, Y.S. (1996). A new neural network for solving linear and quadratic programming problems. *IEEE Transactions on Neural Networks*. 7,1544-1547.

Xue, X. P., & B, W. (2007). A project neural network for solving degenerate convex quadratic program. *Neurocomputing*. 70, 2449-2459.

Electric Power Customer Positioning Model Based on Decision Tree

Yingchun Guo

Department of Economics and Management, North China Electric Power University, Baoding 071003, China

College of Mathematics & Computer Science, Hebei University, Baoding 071002, China

E-mail: guoyc@hbu.edu.cn

Dongxiao Niu

Department of Economics and Management, North China Electric Power University, Baoding 071003, China

Abstract

The electric power consumer positioning analysis is a very important aspect of the electric power consumer relationship management, and the decision tree is a usual tool to implement classification analysis. Based on the segmentation of electric power consumers, this article mainly discusses how to construct the decision tree of electric power consumer positioning by ID3 algorithm, introduce this concrete operation process, and accordingly offers technical supports for the electric power marketing department to better hold consumer characters and implement individual services.

Keywords: Electric power consumer relationship management, Electric power consumer positioning, Decision tree, ID3 algorithm

1. Introduction

For electric power companies, consumer positioning analysis and developing potential consumers are very important. We divide electric power consumers into four classes, i.e. important consumer, risk consumer, developmental consumer and common consumer, and different classified consumers need different marketing strategies. For example, those important consumers with good credits will acquire more and better services, but for those risk consumers with bad credits, we should adopt certain risk prevention measures. Then when a new consumer occurs, we should judge the consumer's possible class according to his special behavior characters and adopt sales strategy with strong pertinences to obtain maximum benefits. But how can we predict the new consumer's possible class objectively, exactly and quickly? One scientific and quick method is to apply decision tree, mine consumer data in virtue of computer and make objective positioning analysis for the consumer.

In classification analysis, the decision tree model is one of the most popular models because it can expediently show the mining results by means of figure (tree structure) and suit decision-making for the management department of the enterprise. In this article, we will discuss how to apply the ID3 algorithm to construct the decision tree of electric power consumer positioning and introduce this concrete operation process.

2. The basic construction process of decision tree

The decision tree is a data structure similar to flow chart and every interior node denotes an attribution test. Every branch denotes a test output and every leaf node denotes class or class distribution.

The operation process of decision tree is seen in Figure 1.

(1) The system collects consumer information from various nodes in the interior network, settles and integrates data information, and forms the consumer information resources with uniform structure.

(2) Pretreat data resources and eliminate attributions independent of decisions, approximate numerical value attribution and deal with those attributions with vacant values, and form the training set of decision tree.

(3) Train the training set, compute information increase of every attribution, select the attributions with maximum information increase as the present main attribution node, and construct a branch for every value of this attribution. Recursively implement above process to sample subsets included in this sub-node until the values of data records on the main attribution in the subset are same, or no attributions can be divided, and form the induction decision tree.

(4) Extract classification rules from obtained decision tree. Establish a rule for every approach from root to leaf and form the rule set. Display the rule set to consumers, and store feasible rules selected by consumer into the rule database.

(5) When new consumer logs in the company website, the system will analyze the new consumer's information material

by means of rules obtained from decision tree, predict which class the consumer belongs to, give the consumer a reasonable position, and accordingly offer assistants to establish individuation sales strategy for the company.

3. The ID3 algorithm to implement decision tree classification

In various decision tree classification algorithms, the most influential one is the ID3 algorithm put forward by Quinlan in 1979, which takes the descending speed of entropy as the standard to test attribution. This algorithm utilizes samples of known classes to give sequence to test attribution until all samples are classified exactly.

In the forming process of decision tree, we utilize one method of information theory, and this method can seek and offer maximum information increase at any time, i.e. it can offer the attribution with maximum entropy decrease. The entropy is denoted by character E.

To N samples, they are divided and respectively belong to class $C_i (i = 1, 2, ..., c)$, the sample number in class C_i is N_i, every sample has K attributions, and every attribution has J_k values. The construction process of decision tree can be described as follows.

(1) Compute initial entropy.

$$E(I) = \sum_{i=1}^{c} -(N_i / N) / \log_2 (N_i / N) = \sum_{i=1}^{c} -p_i \log_2 p_i$$

For the training set, the classes of all samples are known, so N samples compose the initial entropy of the system.

(2) Select one attribution as the root node of the decision tree.

First, for every attribution $A_k (k = 1, 2, ..., K)$, divide original samples into the first class sample set according to J values a_{kj} of the attribution A_k. Though the branch of a_{kj} includes n_{kj} samples, but they may not belong to single class.

Second, for n_{kj} samples of every branch, the sample number belonging to class C_i is $n_{kj}(i)$, and the following formula can compute the entropy of this branch.

$$E(I, A_k, J) = \sum_{i=1}^{c} \left[-n_{kj}(i) / n_{kj} \right] \log_2 \left[n_{kj}(i) / n_{kj} \right]$$

$$E(I, A_k) = \sum_{j=1}^{J} (n_{kj}(i) / N) \sum_{i=1}^{c} \left[-n_{kj}(i) / n_{kj} \right] \log_2 \left[n_{kj}(i) / n_{kj} \right]$$

Third, compute the entropy decrease induced by testing attribution A_k, i.e. $\Delta E(k) = E(I) - E(I, A_k)$.

Fourth, select the attribution A_{k0} which can produce maximum entropy decrease, i.e. A_{k0} should fulfill the condition that $\Delta E(k_0) > \Delta E(k), (k = 1, 2, ... K, \text{ and } k \neq k_0)$.

Fifth, the attribution A_{k0} is just the root of the decision tree.

(3) The attribution A_{k0} will produce J_{k0} leaf nodes, and based on that the sample set is divided into J_{k0} subsets. To the sample subset of every leaf node, select one attribution $A_{k\phi}$ as the down class utilizing above method in turn to make this leaf node obtain maximum entropy decrease.

(4) Continually construct the down class of the decision tree according to step (3) until all sample subsets have only one class, which indicates the entropy of the system is zero, and the construction process of the decision tree ends.

4. The decision tree model of electric power consumer positioning

4.1 Construction of decision tree

Before the decision tree is constructed, we must find out the main attribution of the decision tree. The main attribution of the decision tree is confirmed by the actual situation. The consumer positioning analysis through decision tree is mainly based on the consumer's class character, which attention is to find out consumer's class and differences through consumer's character index and action index and institute corresponding marketing strategies aiming at different consumers. So the main attribution of the consumer positioning decision tree

should be "consumer class", i.e. the consumer class through the consumer segmentation based on the consumer character. The consumer classes are divided into the important consumer (class Ⅰ), the risk consumer (class Ⅱ), the developmental consumer (class Ⅲ) and the common consumer (class Ⅳ).

Based on the collection and analysis of electric power consumer data, we select three representative attributions, consumer power consumption level, consumer credit degree and consumer potential. For the selection of data, not all data can apply the requirements, and the data required by decision tree should have no noises and absences, so data

need to be collected and disposed. The collection and disposal can not only integrate data of different departments and different marketing stations, but also can approximate data, i.e. replace initial data on the low level to the concept on the high level, in order to implement data mining. Here, we approximate actual consumer power consumption level into high, middle and low stages, approximate consumer credit degree into high, middle and low classes, and approximate consumer potential into good, middle and bad sorts.

Through actual researches on the consumer data of Jinan Electric Power Company, we select the data from 20 consumers, dispose and approximate these data, and the result is seen in Table 1.

According to above construction process of decision tree, the actual computation process can be described as follows.

(1) Compute the initial entropy value of the sample class.

$$E(I) = -\frac{6}{20}\log_2\left(\frac{6}{20}\right) - \frac{3}{20}\log_2\left(\frac{3}{20}\right) - \frac{7}{20}\log_2\left(\frac{7}{20}\right) - \frac{4}{20}\log_2\left(\frac{4}{20}\right) = 1.9261.$$

(2) Compute the information entropy of every attribution.

If taking the power consumption level as the testing attribution, so we have

$$E(I,\text{level}) = \frac{5}{20}\left[-\frac{4}{5}\log_2\left(\frac{4}{5}\right) - \frac{1}{5}\log_2\left(\frac{1}{5}\right)\right] + \frac{6}{20}\left[-\frac{2}{6}\log_2\left(\frac{2}{6}\right)\times 3\right]$$

$$+\frac{9}{20}\left[-\frac{5}{9}\log_2\left(\frac{5}{9}\right) - \frac{4}{9}\log_2\left(\frac{4}{9}\right)\right] = 1.1020.$$

If taking the credit degree as the testing attribution, so we have

$$E(I,\text{credit}) = \frac{7}{20}\left[-\frac{2}{7}\log_2\left(\frac{2}{7}\right) - \frac{1}{7}\log_2\left(\frac{1}{7}\right) - \frac{4}{7}\log_2\left(\frac{4}{7}\right)\right]\times 2$$

$$+\frac{6}{20}\left[-\frac{3}{6}\log_2\left(\frac{3}{6}\right) - \frac{1}{6}\log_2\left(\frac{1}{6}\right) - \frac{2}{6}\log_2\left(\frac{2}{6}\right)\right] = 1.4029.$$

If taking the potential as the testing attribution, so we have

$$E(I,\text{potential}) = \frac{6}{20}\left[-\frac{3}{6}\log_2\left(\frac{3}{6}\right) - \frac{1}{6}\log_2\left(\frac{1}{6}\right) - \frac{2}{6}\log_2\left(\frac{2}{6}\right)\right]$$

$$+\frac{6}{20}\left[-\frac{1}{6}\log_2\left(\frac{1}{6}\right)\times 2 - \frac{4}{6}\log_2\left(\frac{4}{6}\right)\right] + \frac{8}{20}\left[-\frac{3}{8}\log_2\left(\frac{3}{8}\right)\times 2 - \frac{1}{8}\log_2\left(\frac{1}{8}\right)\times 2\right] = 1.5377.$$

(3) Respectively compute information plus of various attribution.

$$\Delta E(\text{level}) = E(I) - E(I,\text{level}) = 1.9261 - 1.1020 = 0.8241$$

$$\Delta E(\text{credit}) = E(I) - E(I,\text{credit}) = 1.9261 - 1.4029 = 0.5232$$

$$\Delta E(\text{potential}) = E(I) - E(I,\text{potential}) = 1.9261 - 1.5377 = 0.3884$$

(4) Because the "power consumption level" has maximum information plus, so we take it as the first class attribution of the decision tree, and hereby divide this sample set into large, middle and small subsets, produce three leaf nodes, apply above method to every leaf node in turn, so the decision tree seen in Figure 2 is formed.

4.2 Rule extraction of decision tree

Establish a rule for every approach from root to leaf, form classification rule with the form of "If-Then", and compose the rule set. Form a conjunction item for the part of "If" along every pair of "attribution-value" on the confirmed approach, the leaf nodes including class prediction forms the part of "Then", and store rules into the rule base.

From Figure 2, we can confirm approximate deployment of character attribution of four sorts of consumer, and according to known information, we can approximately know these consumers' positions in four sorts from these characters. We present the information of the tree diagram by means of the form of "If-Then". For example,

(1) If the power consumption level = "high" and (the credit degree = "high" or the credit degree = "middle"), then the consumer belongs to class Ⅰ, i.e. the important consumer.

(2) If the power consumption level = "high" and the credit degree = "low", then the consumer belongs to class Ⅱ, i.e. the risk consumer.

(3) If the power consumption level = "low" and the credit degree = "high" and (the potential = "good" or the potential = "middle"), then the consumer belongs to class Ⅲ, i.e. the developmental consumer.

(4) If the power consumption level = "low" and the credit degree = "high" and the potential = "bad", then the consumer belongs to class Ⅳ, i.e. the common consumer.

4.3 Application of decision tree

When new consumer logs in the company website, the system will record the new consumer's information, analyze and position the new consumer's information material by means of rules obtained from decision tree, put in the positioning result to the decision-making personnel for the company, and accordingly offer assistants to establish individuation sales strategy for the company. For example,

(1) If the new consumer belongs to class Ⅰ, i.e. the important consumer, so this consumer is the key consumer locked by the electric marketing department, the key object that the electric marketing department adopts individuation service, because he will bring large economic benefits for the electric power company.

(2) If the new consumer belongs to class Ⅱ, i.e. the risk consumer, so the consumer is not stable, and the electric marketing department should adopt measures to prevent risks according to actual situation, such as reducing power fees return cycle or requiring offering caution money and so on.

(3) If the new consumer belongs to class Ⅲ, i.e. the developmental consumer, so this consumer is the key development object for the electric marketing department, and the electric company should follow the consumer's development process, dig potential, and timely offer individual power consumption strategy suiting for the consumer, such as implementing favor policies, advising changing power consumption period and so on.

(4) If the new consumer belongs to class Ⅳ, i.e. the common consumer. Though the consumer can not bring high economic benefits, but because this sort of consumer occupies large proportion, so the electric marketing department also should offer good client services and try to fulfill consumer's demands to enhance social benefits of the electric power company.

5. Conclusions

The electric power consumer relationship management is a sort of new management mechanism which aim is to strengthen the relation between the electric power company and consumers. The key in the research of consumer relationship management is how to utilize the data mining technology to deeply analyze consumer data, know consumer character, dig consumer potential, and offer appropriate products and services at the appropriate time. In this article, based on the collection and analysis to electric power consumer information, we put forward constructing the electric power consumer positioning decision tree by means of the ID3 algorithm, which can mine the positioning knowledge about consumers, fully realize consumers' demands of difference and levity, make the marketing strategy made by the electric power marketing department more suit for the demands of the market and change with consumers' demands, enhance service quality, and accordingly acquire higher economic and social benefits for the electric power company.

References

Berson A, Stephen S & Kurt T, interpreted by Heqi. (2001). *Construct Data Mining Application Facing CRM.* Beijing: People's Post and Telecommunication Press.

Diao, Baiqing and Zhou, Zunguo. (2004). *Consumer Relationship Management under the Environment of Electric Power Reform.* Beijing: China Electric Power Press. December, 2004.

Jiawei Han & Micheline Kamber, interpreted by Fanming and Meng, Xiaofeng. (2001). *Data Mining: Concepts and Technology.* Beijing: China Machine Press. Augest, 2001.

Kangjian, Liang, Yunrong. (2003). Application of Classification Data Mining in Financial Customer Relationship Management. *Journal of Beijing Institute of Technology (Natural Science Edition).* 23 (2). p. 207-211.

Michael J. S, Chandrasekar S & Gek W. T. (2001). Knowledge Management and Data Mining for Marketing. *Decision Support Systems.* 31(1). p. 127-137.

S.C. Hui & G. Jha. (2000). Data Mining for Customer Service Support. *Information and Management.* 38 (1). p. 1-13.

Wan, Zhihua and Xu, Zhongjian. (2004). Application of Data Mining in CRM. *Computer Engineering and Design.* 25 (12). p. 2324-2326.

Zhou, Danchen, Yin, Guofu & Long, Hongneng. (2004). Research on Application of Data Classification Technology for Knowledge Discovery in CRM. *Computer Applications and Software.* 21 (2). p. 9-11.

Table 1. Data collection of consumers

Consumer number	Level	Credit	Potential	Class
1	high	high	middle	important consumer
2	high	high	bad	important consumer
3	high	middle	middle	important consumer
4	high	middle	bad	important consumer
5	high	low	bad	risk consumer
6	middle	high	good	important consumer
7	middle	high	middle	important consumer
8	middle	middle	good	developmental consumer
9	middle	middle	middle	developmental consumer
10	middle	low	good	risk consumer
11	middle	low	middle	risk consumer
12	low	high	good	developmental consumer
13	low	high	middle	developmental consumer
14	low	high	bad	common consumer
15	low	middle	good	developmental consumer
16	low	middle	middle	developmental consumer
17	low	middle	bad	common consumer
18	low	low	good	developmental consumer
19	low	low	middle	common consumer
20	low	low	bad	common consumer

Consumer data collection

Data pretreatment

Training set

Induction decision tree

Decision tree

Extraction classification rules

Rule set

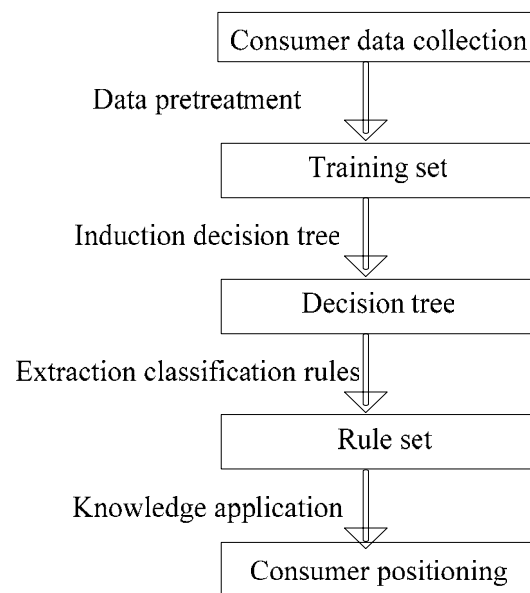Knowledge application

Consumer positioning
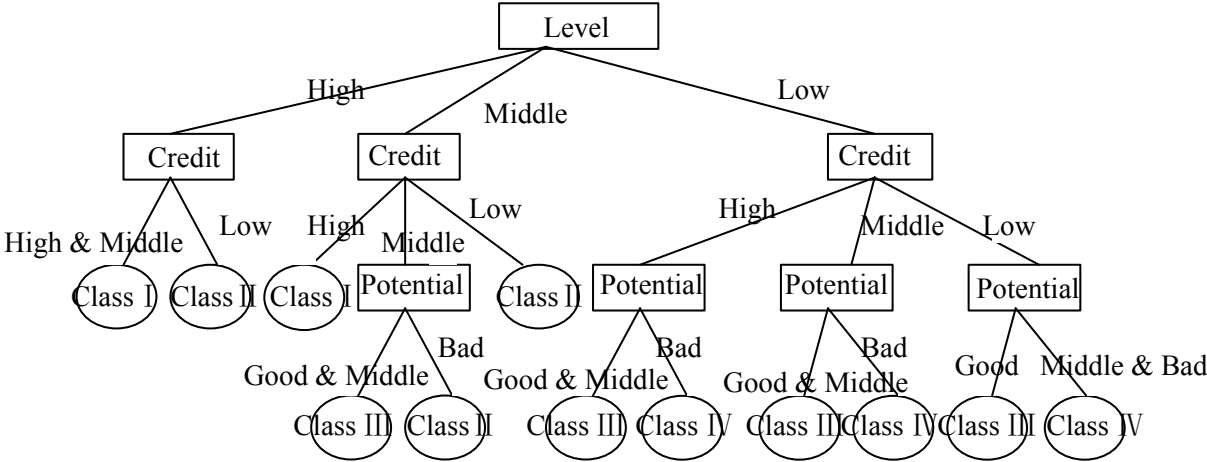
Figure 1. Forming Process of Decision Tree

Figure 2. Consumer Positioning Decision Tree

The Effect of Etchant Concentration on Surface Morphology

Of Porous GaP Produced By Laser-Induced Etching

Khalid M. Omar

School of Physics

University of Science of Malaysia

11800, Penang, Malaysia

E-mail: khalhadithi@yahoo.com

Zahid H. Khan

Department of Physics, Jamia Millia Islamia, 110025-New Delhi, India

R. K. Soni & S. C. Abbi

Department of Physics, Indian Institute of Technology, 110016-New Delhi, India

Abstract

Porous GaP have studied and fabricated by using an argon-ion laser beam of energy 2.41 eV was to recording the Raman spectra. The peak position shifts in Raman spectra was observed at 398 cm^{-1} after etching. The Raman line is broad and asymmetric in comparison to the Raman line for crystalline GaP of 402 cm^{-1}. The weak structure near 350 cm^{-1} is a forbidden TO phonon, which arises due to structural disorder in the material. The peak that appears near 378 cm^{-1} is attributed to a surface phonon mode. The surface phonon frequency depends on the nanocrystalline size, shape and dielectric constant of the surrounding medium. We have studied the surface morphology of porous layers obtained by LIE of n-type GaP (100) substrates by using a Scanning Electron Microscope (SEM). The morphology of porous GaP layers changes rapidly with laser power densities and irradiation times. As well as both the size and shape of the structure depend on the nature and concentration of etchant solution.

Keywords: RS, SEM, Porous, GaP, LIE.

1. Introduction

The room temperature Raman scattering studies of first-order mode in samples etched with different laser power densities and radiation times of the argon-ion laser. The Raman studies of the first-order mode in the CW laser etched samples and phonon confinement for one, two and three-dimensional confinement models have been described. The results are analyzed in the quantum confinement effects on the electronic structure of nanocrystals and also estimated the average size of the nanocrystals. Etching process, Raman scattering and photoluminescence of porous GaP is obtained.

Raman scattering has become an important technique for the characterization of semiconductor quantum structures. The Raman Effect is an inelastic scattering process where the sample absorbs one photon while simultaneously emitting another photon of a different frequency. The difference in the energy of the incident and scattering photon is characteristic of the lattice vibrational mode and contains important information about the semiconductor. Raman scattering is an effective tool and a suitable method and has been widely used to investigate vibrational and structural properties of nanocrystals. (Kanesmitsu, 1993, Liu, 1994 & Xia, 1995) Moreover, it is used to estimate the characteristic size of nanocrystallites via the phonon confinement. In a bulk semiconductor material, the phonon-photon interaction is limited to the Brillouin-zone center, but in the case of a finite size crystal, the presence of quantum-size nanostructures relaxes the associated selection rules so that the Raman peak depends upon nanostructure shape and size parameters. For example, the peak shape gives information about the microstructure in the complex matrix of the porous layer.

The Raman spectra for these materials were show, for the first time, to be sensitive to surface phonon modes of clean semiconductors. (Tütüncü, 1996) Two surface gap modes as well as three additional surface phonon modes have been observed in InP. The exact determination of the positions and line-widths of these microscopic gap modes opens a new field of application in studying surface bonding, anharmonicity effects and coupling to other excitations. (Hinrichs, 1994)

The confinement of electrons and holes in quantum wires of GaP in the porous layer was proposed as the origin for the blue and UV emission bands in porous GaP. For the quantum confinement structure in the porous layer, the blue and UV emission is expected to be much stronger than the orange emission from bulk GaP. (Meijerink, 1996) The optical properties of the porous GaP are different from the properties of the original single crystal. The modification of the properties of GaP could be due to an intensification of the electron-phonon interaction in the submicron to nanometer size structures of the porous layer. (Zoteev, 1996) Quantum confinement also affects the excitonic properties of indirect-gap material, which is responsible for inducing an indirect to direct conversion for the character of optical transition.

In n-GaP made porous by anodization etching, the photocurrent response within the porous layer indicates an increase in the optical path length in the porous layer. When the absorption length (penetration depth) $(1/\alpha)$ is larger than the thickness of the porous layer, significantly large electron-hole pairs are created in that region. (Erne', 1996)

2. Characterization of GaP

The laser–induced etching process is used to create GaP nanostructure. This photosynthesis method is proposed as an alternative technique for our studies, and was pioneered by (Noguchi, 1994) who used the visible –light irradiation of Si wafers immersed in an aqueous HF solution to obtain the pore formation. (Noguchi, 1993) This method offers a fundamental technique for the selective formation of optical devices. The electrochemical etching is a common technique to prepare the porous Si, porous GaP, and different other semiconductor materials. Recently, a more advantageous technique has been used to produce a porous material, that is, laser-induced etching. (Rasheed, 2001, Omar, 2001, Yamamoto, 2000 & Koker, 1999) These opto-electronic devices need strong luminescence intensity and a control of the peak position of luminescence over a range of wavelengths that depend on the size distribution of nanocrystallites. The etching was carried out at a laser power density of 12 W.cm^{-2} and 15 min irradiation time (IT). An argon-ion laser beam of energy 2.41 eV (λ = 514.5 nm) was used for recording the Raman spectra.

2.1 Laser-induced etching

Like porous silicon formation, in n-type Si, valence band holes are required at the surface of the sample and during the chemical reaction of silicon wafer initiated that the holes reach the wafer surface, thereby this wafer is known to be inert in aqueous HF acid. The porous GaP in n-type GaP, the valence band holes are also required for the dissolution reaction, (Gomez Rivas, 2002)

$$(GaP)_n + 6h^+ \rightarrow (GaP)_{n-1} + Ga(III) + P\ (III) \tag{1}$$

The charge transfer occurs at the semiconductor-electrolyte interface when a semiconductor is immersed in aqueous solution, which contains the electron acceptor species. The photo-generated holes are directly transferred to the electrolyte solution in the pores when the motion of electrons in the porous GaP, which has to be done by employing a modulated photocurrent.

The electrical current enhances the etching process in the wafer when this current flows from the backside through the electrolyte of the wafer to complete the electrical circuit. The schematic diagram of laser-induced etching process is shown as under Figure1.

It is desirable to construct the surface with different pore size distributions. The experimental conditions are very important to characterize the nature of nanocrystallites and distribution sizes during the LIE process; the morphological study images the surface and the size distribution of crystallites and it is thus an important study. We can prepare the porous materials by the laser–induced etching on different substrates.

3. The phonon confinement model

The phonon confinement model is used to evaluate the crystallite size from the frequency downshift and peak broadening of the Raman line. Among the several models proposed, (Brandt, 1992 & Prokes, 1992) the quantum confinement model (*QCM*) is based on the confinement of lattice vibrations in nanocrystallites, and the peak position and shape is directly related to the size of crystallites.

The phonon confinement model has been developed to explain the Raman spectra of microcrystalline materials and it is based upon the fact that, in an infinite crystal, only the phonon near the center of Brillouin-zone $(\vec{q} = o)$ contributes to the Raman spectrum because of momentum conversation between incident and scattered photon.

3.1 Three-dimensional confinement in porous GaP

The phonon confinement model was developed by (Richter, 1981) to explain the frequency shift and broadening of the Raman line in microcrystalline Si. The model has been used to explain Raman line shapes and to estimate microcrystallite sizes in samples of Si (Richter, 1981 & Campbell, 1986) and GaAs. (Tiong, 1984 & Brauustein, 1989) Phonons from the center of the Brillouin-zone $(\vec{q} = o)$ contribute to the Raman signal in crystalline materials. The

Raman line shape is constructed by assuming a Lorentzian line shape centered at ω(q), with the line width of the infinite crystalline material, and this is then weighted by the modified wave-vector of the phonon caused by the finite size effect. Therefore, I (ω) is a Lorentzian centered at ω(0) with a line width of Γ.

$$I(\omega) = \int \frac{|c(0,q)|^2}{[\omega - \omega(q)]^2 + \left(\Gamma/2\right)^2} d^3q \qquad (2)$$

where, $\omega(q)$ is the phonon-dispersion curve, Γ is the natural line width, and $q = 0$ for zone-center first-order Raman scattering.

The confining function that we have used is a Gaussian given by

$$|c(0,q)|^2 = \exp\left[\frac{-q^2(L_0)^2}{a^2 \cdot 4}\right] \qquad (3)$$

with q in units of $2\pi/a$, where a is a lattice constant (5.45 $A°$ for GaP) and L is in units of a.

Therefore, the three–dimensional (3D) Brillouin–zone integration in equation 2, can be approximated with a one-dimensional integration in a Brillouin-zone using an appropriately averaged dispersion curve,

$$I(\omega, L) = \int_0^1 \frac{\exp\left[-q^2(L_0)^2/a^2 \cdot 4\right] \cdot 2 \cdot \pi \cdot q}{[\omega - \omega(q)]^2 + \left(\Gamma/2\right)^2} dq \qquad (4)$$

where, $\omega(q)$ is an approximated one-dimensional phonon dispersion curve,

$$\omega(q) = A + B\cos(\pi \cdot \frac{q}{2}) \qquad (5)$$

where, A= 365.3 cm^{-1} and B= 37 cm^{-1}.

The values of ω and Γ are taken as 402 cm^{-1} and 3.3 cm^{-1} for crystalline GaP, and L_0 is the quantum confinement dimension.

The shape of this averaged curve is similar to that used in Si, diamond and GaAs phonon confinement calculations. This model is based on the optical phonons at the center of Brillouin-zone $(q = o)$, contributing to the first-order Raman at 402 cm^{-1} from the crystal GaP. The momentum conservation in nanocrystals is relaxed due to breakdown of translation symmetry and optical phonons are confined within the nanostructures and optical phonons with $(q \neq o)$ are allowed for that reason to contribute to the first-order Raman mode as in equation 4.

3.2 The crystallite size distribution in porous GaP

The choosing of the single value of L of crystallite size in equation 4, determines the peak position of Raman line from porous GaP. The confinement dimensions of nanocrystallites give the position of Raman line and have been used to match the Raman line-shape from porous Si. (Le Rendu, 2001) However, the observed broad Raman line shape is a consequence of the crystallite size distribution around a mean value L_0 as well as the confining geometry. The size distribution function that we have used is a Guassian:

$$\Phi(L) = \frac{1}{\sqrt{2 \cdot \pi}} \cdot \frac{1}{\sigma} \cdot \exp\left[\frac{-(L-L_0)}{2 \cdot \sigma^2}\right] \qquad (6)$$

where, L_0 and σ are parameters, which are called the mean and standard deviation of the crystallite size distribution. In the present work, these are taken as fitting parameters. The Gaussian functions for the crystallite size distribution in the phonon confinement model have been used to convolute equation 4 with the Gaussian of equation 6 for the total Raman intensity:

$$I(\omega, L) = \int_{L_1}^{L_2} \Phi(L) \cdot I(\omega, L) dL \qquad (7)$$

The peak position for the Raman mode is determined by L_0, which is the value of L for which $\Phi(L)$ is maximum. L_1 & L_2 are the minimum and maximum contributing nanocrystallites sizes (1 & 10 nm). A change in the mean nanocrystallite size, L_0, leads to shift in Raman peak position and variations of L_1 & L_2 values lead to changes in the Raman line shape broadening without changing the peak position.

By using equation 7, results of a calculation for the Raman line shape of GaP nanocrystallites of uniform size, $L_0 = 6$ nm and same fitting parameters, is shown in Figure 2. The spectra have peak position 400 cm⁻¹.

The particles in 3D and 2D can move around the origin of the Coulomb potential without directly touching the origin. But in 1D, it is always moving through the origin because the spatial direction of motion is restricted to one dimension. The spatial phase volume around the origin is given as $4\pi r^2 dr$, $2\pi r dr$ and $2dr$ for 3D, 2D and 1D, respectively, where spherical, circular and linear shell regions from r to r + dr are considered. One and two-dimensional structures remain as interesting alternatives for integrated opto-electronics; only three-dimensional ones can provide full control of spontaneous emission in all space directions with the ultimate perspective of three-dimensional opto-electronic. Three-dimensional structures of the order of an optical wavelength have attracted a great deal of attention because of their potential use in various applications.

The first-order Raman line shape for one, two and three-dimensional confinement in GaP with the Gaussian distribution function and an identical mean nanocrystallite size $L_0 = 3$ nm and $\sigma = 5$ nm are shown in Figure 3.

The theoretical calculation of first-order Raman line can be show in figure 4 for the three-dimensional confinement of phonons incorporating the Gaussian size distribution for different nanocrystallite sizes by using equation 7.

3.3 Raman spectra of porous GaP

The Raman spectrum of porous GaP which prepared by laser-induced etching technique (LIE) is shown in Figure 5. The Raman peak position shifts to a lower frequency of 398 cm⁻¹ after etching.

The Raman line is broad and asymmetric in comparison to the Raman line for crystalline GaP, which has a narrow and symmetric shape centered at 402 cm⁻¹. The SEM images show a lateral structure with thin pore walls consisting of spherical nanostructures.

The downward shift of the LO phonon frequency and an increase broadening is apparent. The theoretical fit to the experimental curve is obtained by using a three-dimensional quantum confinement model incorporating appropriate size distribution. A shift in the frequency of the surface mode (not shown here) depends on the state of the surface of the pores. The average size estimated from the fitting procedure is 3 nm. The broadening of Raman line is caused by the size distribution, which is dependent on etching parameters; we have observed two other weak Raman lines besides intense LO phonon line at 398 cm⁻¹.

The weak structure near 349 cm⁻¹ is a forbidden TO phonon, which arises due to structural disorder in the material. The peak at 378 cm⁻¹ is attributed to a surface phonon mode. The surface phonon frequency depends critically on the nanocrystalline size, shape and dielectric constant of the surrounding medium. We have calculated surface phonon frequency (ω_s) considering a shape using: (Hayashi, 1982)

$$\omega_s^2 / \omega_T^2 = \left[\varepsilon_0 + \varepsilon_m \left(1/L - 1\right)\right] / \left[\varepsilon_\infty + \varepsilon_m \left(1/L - 1\right)\right] \qquad (8)$$

where, ω_T is the frequency of the TO phonon,

$\varepsilon_0 = 11.01$, $\varepsilon_\infty = 9.09$ are the static and high frequency dielectric constant,

$\varepsilon_m = 1.00$, in the case of air surrounding, and

L is the depolarizing factor (0.3 for cylindrical shape, 1/3 for sphere and 0.4 for non-spherical particle shape).

The calculated value of surface phonon frequency in air for cylindrical shape is in good agreement with the observed value.

The effect of the particle shape should be taken into account to explain the observed shift of surface mode frequency with respect to the dielectric constant of the surrounding medium. (Sarua, 1999)

4. Surface morphology

Many semiconductor compounds have been investigated in the porous form. Pore formation has been reported for GaP in many electrolytes. (Belogrokhov, 1994, Tiginyanu, 1997& Zavaritskaya, 1998) A majority of this work has focused on the light emission process, blue and UV- luminescence from porous GaP. (Anedda, 1995 & Stevens-Kalceff, 2001) Through GaP has an indirect band gap structure similar to silicon, the pore structure and pore formation is significantly

different. Surface morphology of porous semiconductors, in general, is known to be very complicated and depend strongly on fabrication conditions. In this work, we study the surface morphology of porous layers obtained by laser-induced etching of n-type GaP (100) substrates. The morphology of porous gallium phosphide layers changes rapidly with laser power densities and irradiation times.

4.1 The effect of electrolyte concentration

4.1.1 The HF with Ethanol

Porous GaP layers have been prepared by laser-induced etching from n-GaP, (100) orientation having carrier concentration $3.7 \times 10^{17} cm^{-3}$. The GaP substrate was immersed in HF acid 40% diluted by ethanol 50% and irradiated by an argon-ion laser (λ=514.5 nm) under different irradiation times and with a fixed power density of 12 W.cm^{-2}. The etching process was carried out for 5, 10 and 15 min.

It can be seen from the SEM micrographs that the surface morphology and pore structure of the etched GaP samples are quite different from sample etched with concentrated HF electrolyte. Figure 6 (a) shows the morphology of porous GaP sample that was irradiated for 5 min. The pore morphology is random with no sign of any preferential etching. There are coarse features in the micrometer range and, on top of them, fine features with size in the range below 250 nm. It appears that the photochemical etching produces a bimodal effect in the crystal size distribution with coarse structure supporting the fine nanometer size structure. (Oskam, 1997, Ottow, 1996 & Schuurmans, 1999)

With an increase in the irradiation time, the pores grow selectively along a preferred crystallographic direction. On increasing the etching time to 10 min, Figure 6 (b), the pore structure is more oriented, while for 15 min irradiation time, Figure 6 (c), the orientation probably change from (100) to (111) direction, under same etching conditions. The structures are more uniform and the pore dimension is around 150-200 nm. The pore diameter is same throughout.

4.1.2 The HF without Ethanol

For the laser power density of 12 W.cm^{-2}, a well-defined wire like pore structure is formed even for 5 min. irradiation time due to the large density of hole supplied at the semiconductor-electrolyte interface. The long wires running parallel to (111) direction have varying sizes. Therefore, the regular structures have been synthesized for 100 nm pore dimension under these parameters as can be seen in Figure 7 (a). At longer irradiation time of 10 min., the pore structure has grown deeper with thinner pore walls. Some of the pore walls are 20-50 nm in dimension as shown in Figure 7 (b). Further increasing the irradiation time to 15 min. the pore propagates deep into the substrate and the pore walls become extremely thin, in the range of 10-50 nm as can be seen in Figure 7 (c), the large portion of the walls is also etched away and pore walls become shorter. At much higher laser power density the pore structure becomes disordered and a hole is created in the substrate.

5. Conclusion

The SEM micrographs revealed that the pores grow in the (111) direction along gallium or phosphorous planes. The chemical reaction of the hole with phosphorous is stronger than with gallium due to the high reactivity of phosphorous. A choice of suitable power density and irradiation time could be used to control both the size and shape of the structures. The technique of laser-induced etching was successfully adopted to synthesize GaP nanoparticles. Also, if the laser energy is tuned, the etched structure could be created shallow or deeper into the substrate due to the variation in the penetration depth of the laser light.

The process of laser-induced etching is initiated by first absorbing band–gap photons by the semiconducting electrode immersed in HF electrolyte. Electron-hole pairs are created in the semiconductor, which then separate to form the space charge layer on the semiconductor. In anisotropic etching, the crystallographic orientation significantly determines the density, dimensions and shapes of pores. The SEM images show a lateral structure with thin pore walls consisting of spherical nanostructures.

Surface morphology and porosity of the layers were found to be essentially independent of the electrolyte solution, increasing the concentration of the electrolyte solution mainly increases the PL peak energy due to the high rate of etching. The porosity increases slightly with the increasing concentration of the solution at same etching conditions.

Raman studies of nanocrystals provide information on the behavior of the fundamental optical and vibrational properties. Raman scattering is very sensitive to the lattice microstructure. A phonon confinement model is employed to explain the Raman shift of phonon modes of a nanocrystal and describes the size confinement effect on lattice vibration wave functions.

The Raman scattering spectra of porous GaP have a number of characteristic features. Both LO and TO phonons are always simultaneously present in the porous GaP spectra.

References

Anedda, A. Serpi, A. karavanskii, V. A. Tiginyanu, I. M. & Ichizli,V. M. (1995).   Time resolved blue and ultraviolet photoluminescence in porous GaP. *Appl. Phys. Lett,* 67, 3316

Belogrokhov, A. I. Karavanskii,V. A. Obraztsov, A. N. & Timoshenko, V. Yu. (1994). Intense photoluminescence in porous gallium phosphide. *JETP Letter*, 60, 274

Brauustein, G. Tuschel, D. Chen, S. & Lee, S. T. (1989). Raman scattering study of lattice disorder in 1-MeV Si-implanted GaAs. *J. Appl. Phys.,* 66, 3515

Brandt, M. S. Fuchs, H. D. Stutzmann, M. Weber, J. & Cardona, M. (1992). The origin of visible luminescence from "porous silicon": A new interpretation. *Solid State Commun,* 81, 307

Campbell, I. H. & Fauchet, P. M. (1986).   The effects of microcrystal size and shape on the one phonon Raman spectra of crystalline semiconductors. *Solid State Commun*, 58, 739

Erne', B. H. Vanmaekelbergh, D. & Kelly, J. J. (1996). Morphology and Strongly Enhanced Photoresponse of GaP Electrodes Made Porous by Anodic Etching.   *J. Electrochem. Soc.*, 143, 305

Gomez Rivas, J. Lagendijk, A. Tjerkstra, R. W. Vanmaekelbergh, D. & Kelly, J. J. (2002). Tunable photonic strength in porous GaP.   *Appl. Phys.* Lett., 80, 4498

Hinrichs, K. Schierhorn, A. Haier, P. Esser, N. Richter, W. & Sahm, J. (1997). Surface Phonons of InP (110) Studied by Raman Spectroscopy.   *Phys. Rev.* Lett, 79, 1094

Hayashi, S. & Kanamori, H. (1982). Raman scattering from the surface phonon mode in GaP microcrystals. *Phys. Rev.,* B 26, 7079

Koker, L. & Kolasinski, K.W. (1999). Observation and application of optical interference and diffraction effects in reflection. *J. Appl. Phys.,* 86, 1800

Kanesmitsu, Y. Uto, H. Masumuto, Y. Matsumoto T. Futagi, T. & Mimura, H. (1993). Microstructure and optical properties of free-standing porous silicon films: Size dependence of absorption spectra in Si nanometer-sized crystallites. *Phys. Rev.*, B 48, 2827

Le Rendu, P. Nguyen, T. P. Lakehal, M. Ip, J. Tiginyanu, I. M. Sarua, A. & Irmer, G. (2001).   Poly (*p*-phenylene vinylene)/porous GaP composite materials. *Optical Materials*, 17, 175

Liu, X. N. Wu, X. W. Bao, X. M. & He, Y. L. (1994). Photoluminescence from nanocrystallites embedded in hydrogenated amorphous silicon films. *Appl. Phys*. Lett, 64, 220

Meijerink, M. Bol, A. A. & Kelly, J. J. (1996). The origin of blue and ultraviolet emission from porous GaP.   *Appl. Phys*. Lett, 69, 2801

Noguchi, N. & Suemune, I. (1994). Selective formation of luminescent porous silicon by photosynthesis. J. *Appl. Phys*., 75, 4765

Noguchi, N. & Suemune, I. (1993).   Luminescent porous silicon synthesized by visible light irradiation. *Appl. Phys*. Lett, 62, 1429

Omar, K. M. Soni, R. K. Rasheed, B. G. Abbi, S. C. & Khan, Z. H. (2001). Synthesis and Optical Properties of Porous GaP. Proc. "Physics of Semiconductor Devices", Indian Institute of Technology, *New Delhi, India,* Vol. 1, 248

Oskam, G. Natarajan, A. Searson, P. C. & Ross, F. M. (1997). The formation of porous GaAs in HF solutions.   Appl. Surf. Sci., 119, 160

Ottow, S. Lehmann, V. & Foll, H. (1996). Processing of three-dimensional microstructures using macroporous n-type silicon. *J. Electrochem. Soc*.,   143, 385

Prokes, S. M. Glembocki, O. J. Bermudez, V. M. Friedersdorf, L. E. & Searson, P. C. (1992). SiH$_x$ excitation: An alternate mechanism for porous Si photoluminescence. *Phys. Rev.*, B45, 13788

Rasheed, B. G. Mavi, H. S. Shukla,A. K. Abbi, S. C. & Jain, K. P. (2001). Surface reconstruction of silicon and polysilicon by Nd: YAG laser etching: SEM, Raman and PL studies. *Mat. Sci. & Eng.,* B 79, 71

Richter, H. Wang, Z. P. & Ley, L. (1981). The one phonon Raman spectrum in microcrystalline silicon.   *Solid State Commun*, 39, 625

Sarua, A. Tiginyanu, I. M. Uraski, V. V. Irmer, G. Monecke, J. & Hartnagel, H. L. (1999). Charge carrier distribution in free-standing porous GaP membranes studied by Raman spectroscopy. *Solid State Commun,* 112, 581

Stevens-Kalceff, M. A. Tiginyanu, I. M. Langa, S. Foll, H. & Hartnagel, H. L. (2001). Correlation between morphology and cathodluminescence in porous GaP. *J. Appl. Phys.,* 89, 2560

Schuurmans, F. J. P. Vanmaekelbregh, D. Vande Lagenaat, J. &   Lagendijk, A. (1999). Strongly Photonic Macroporous Gallium Phosphide Networks. *Science*, 284, 141

Tütüncü, H. M. & Srivastava, G. P. (1996).   Surface phonons on InP (110) with the adiabatic bond-charge model. *Phys.*

Rev. B 53, 15675

Tiong, K. K. Amirtharaj, P. M. Pollack, F. H. & Aspnes, D. E. (1984). Effects of As[+] ion implantation on the Raman spectra of GaAs: "Spatial correlation" interpretation. *Appl. Phys. Lett*, 44, 122

Tiginyanu, I. M. Irmer, G. Monecke, J. & Hartnagel, H. L. (1997). Micro-Raman-Scattering study of surface-related phonon modes in porous GaP. *Phys. Rev.*, B 55, 6739

Yamamoto, N. Sumiya, A. & Takai, H. (2000). Electroluminescence (EL) from photo-chemically etched silicon. *Mat. Sci. & Eng.* B, 69-70, 205

Xia, H. He, H. L. Wang, L. C. Zhang, W. Liu, X. N. Zhang, X. K. & Feng, D. (1995). Phonon mode study of Si nanocrystals using micro-Raman spectroscopy. *J. Appl. Phys*. 78, 6705

Zoteev, A. V. Kashkarov, P. K. Obraztov, A. N. & Timoshenko, V. Yu. (1996). Electrochemical formation and optical properties of porous gallium phosphide. *Semiconductors*, 30, 775

Zavaritskaya, T. N. Kvit, A. V. Mel'nik, N. N. & Karavanskii, V. A. (1998). Amorphous, Glassy, and Porous Semiconductors. *Semiconductors*, 32, 213

Table 1. Fitting parameters of Figure 5, L_0 (mean value), L_1 and L_2 are minimal and maximum contributing nanocrystallite in equation 7.

Excitation photon energy (eV)	L_0 (nm)	L_1 (nm)	L_2 (nm)	σ (nm)	FWHM (cm^{-1})	Raman peak position (cm^{-1})
2.41	3	1	10	5	6.5	398

Table 2. Surface phonon frequency in air calculated by using equation 8.

Surface phonon peak (cm^{-1})	TO phonon peak (cm^{-1})	Dielectric constant			Depolarizing Factor L
		ε_0	ε_∞	ε_m	
378	349	11.01	9.09	1.00	0.3
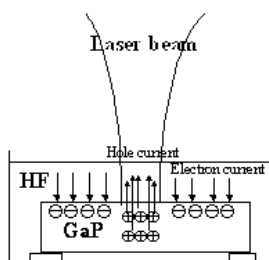
Figure 1. Schematic diagram of Laser-induced etching process
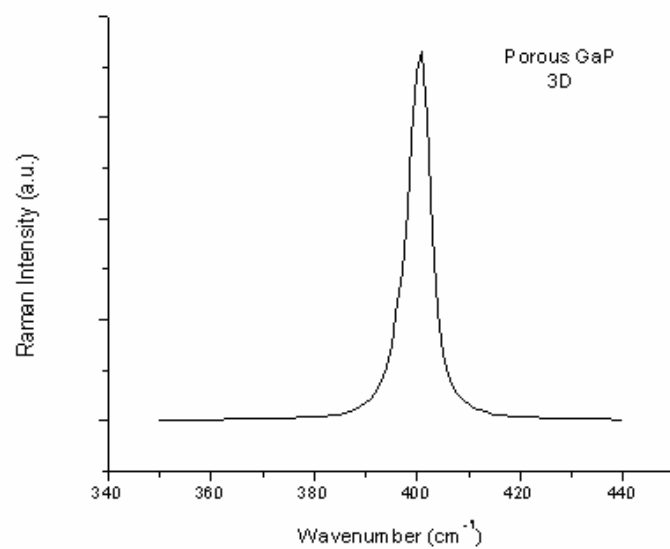
Figure 2. Effect of the nanocrystallites size distribution.
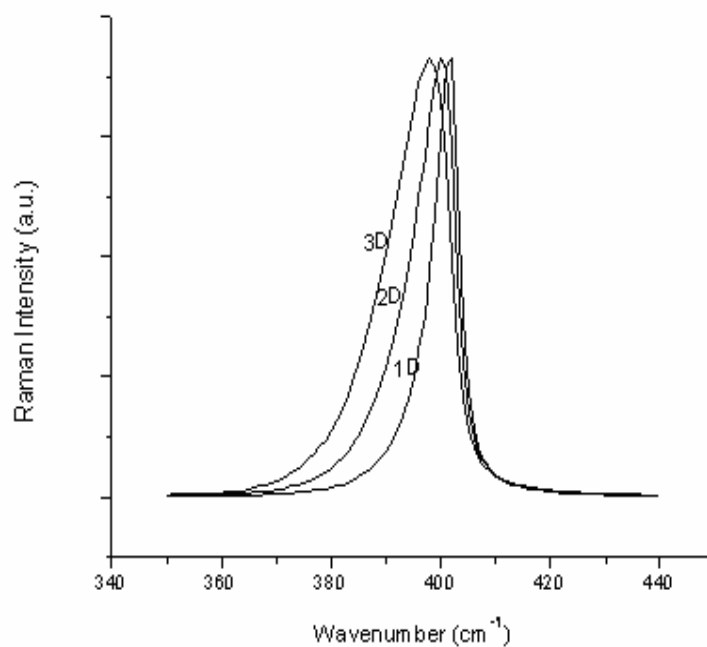
Figure 3. One, two and three-dimensional confinement model for porous GaP
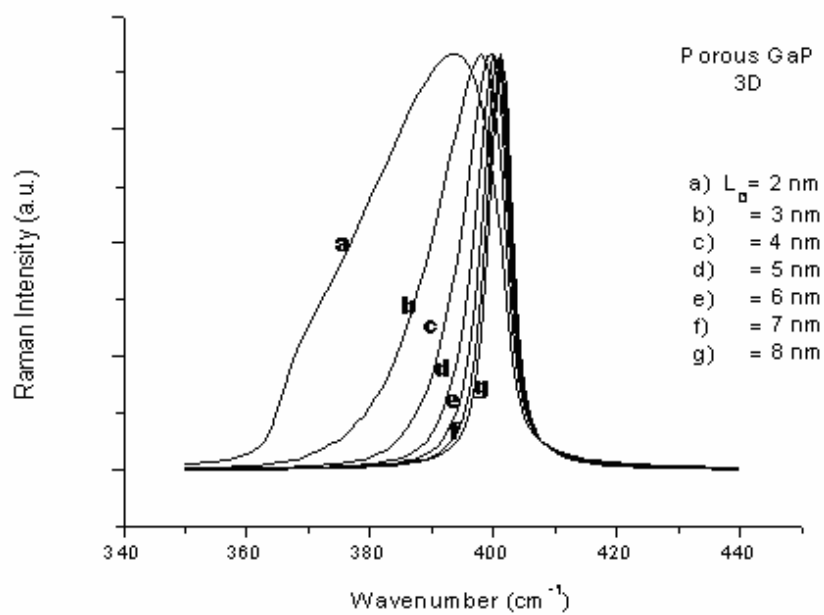
Figure 4. Size-dependent LO-phonon Raman line shape in GaP. Three-dimension
Confinement geometry appropriate for sphere has been used.
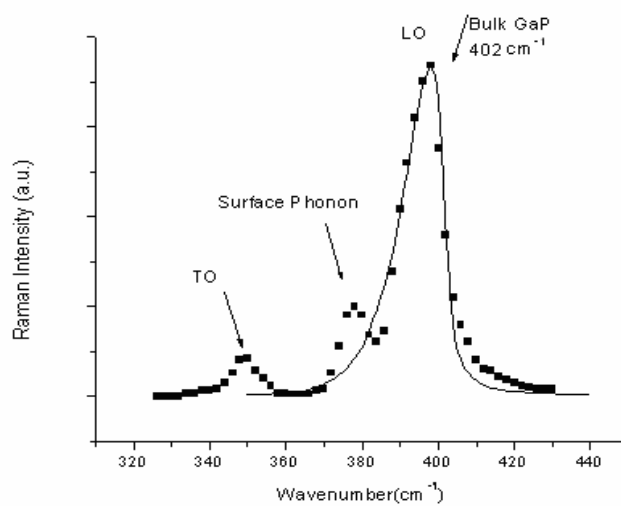
Figure 5. Raman spectra of GaP nanostructure prepared by LIE
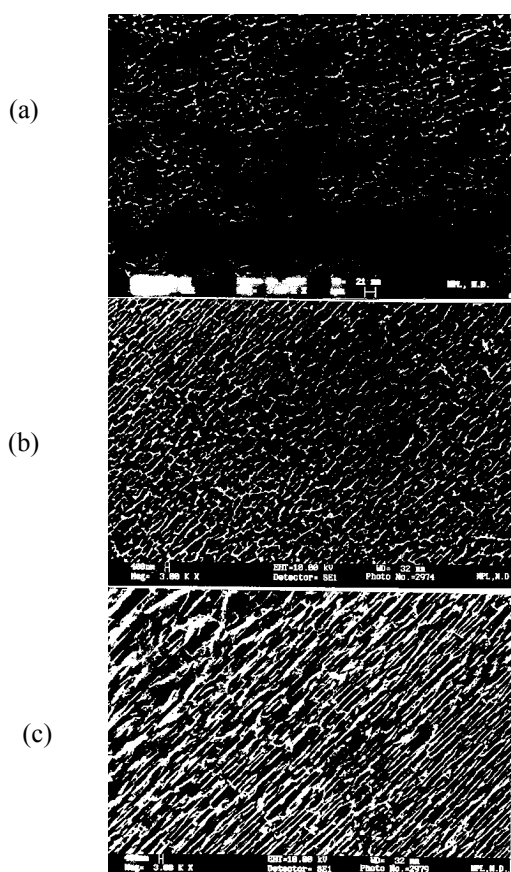
Figure 6. SEM images of porous GaP produced by
LIE at 12 W.cm^{-2} for (a) 5 min, (b) 10 min, and
(c) 15 min. with HF +Ethanol as electrolyte
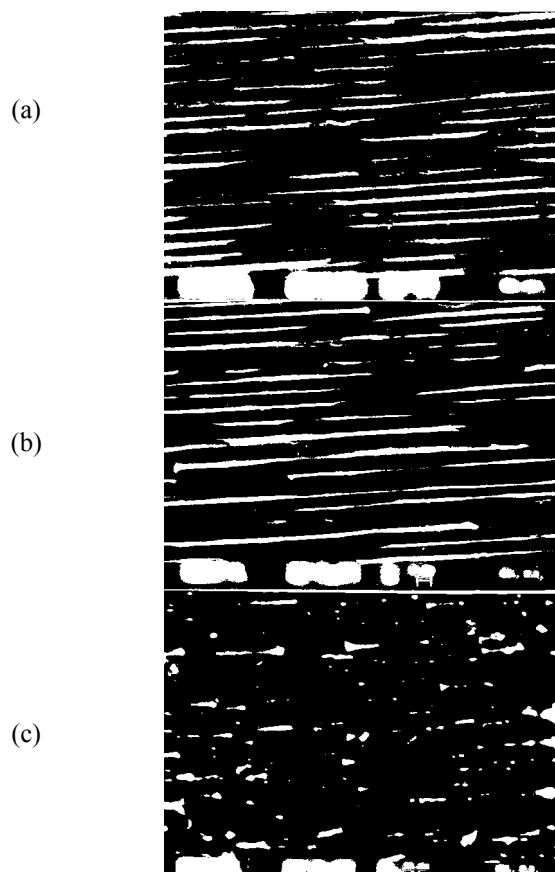
Figure 7. SEM images of porous GaP produced by
LIE at 12 W.cm^{-2} for(a) 5 min, (b) 10 min, and
(c) 15 min. with HF only

On the Management Based on

Characteristics of Knowledge Workers

Jinghua Wu

School of Business Management, Shandong University of Finance, Jinan 250014, China

E-mail: wujh666@sina.com

Abstract

How to manage knowledge workers effectively is an important project for most managers. Because of knowledge workers' different characteristics from common workers, the effective management for them should be based on their unique characteristics. Therefore, a systematic, comprehensive, and pertinent management strategy is necessary.

Keywords: Knowledge employee, Empower, Redesign of work, Corporate culture

Because of the information technology revolution, the world economy has been changed from the resource- dependent industry economy toward the knowledge-dependent knowledge economy. Knowledge workers, as the main carriers of knowledge, become more and more important in the economic development of future. Due to the knowledge workers' different characteristics from common workers, the traditional management way has been challenged. How to manage knowledge workers effectively has become an important issue for many managers. Just as what was said in Peter F. Drucker's, an authority in the management field in America, Management Challenges for the 21th Century: to improve knowledge workers' productivity would become the key of management, just as one hundred years ago when to improve physical workers' productivity was the key of management (Peter F. Drucker, 2000, p16).

1. Knowledge workers and their characteristics

The "knowledge worker" concept was firstly advanced by Peter F. Drucker, a famous scholar in management field, in 50s in 20th century. It refers to people who master and use notes and concepts, and work by knowledge and information. As they create wealth, they use brains more than hands. They bring about added values for products by their innovations, analyses, estimations, integrations, and designs. Generally speaking, managers and technologists belong to the scope of knowledge workers. Comparing with traditional physical workers, knowledge workers have following characteristics.

(1) Stronger self-determination.

Comparing with workers who have to catch up with the operation of machine passively in work flow, knowledge workers are engaged in creative work, instead of simple and repetitive procedure work. Their work does not have established procedures and processes. And the job introduction and fixed work rules are meaningless for knowledge workers. Therefore, knowledge workers have more self-determination.

(2) Greater possibility of job-hopping. On one hand, because of the speeded-up reform, an enterprise's life cycle is shortened. Knowledge workers usually have longer career life than the life of the enterprise that they work for. The enterprise can not promise for a life-long employment. On the other hand, because knowledge workers possess the main production tools, namely the implicit knowledge in their brains, they are capable of accepting new tasks and new jobs. Therefore, they have greater freedom in choosing their jobs, comparing with traditional workers. They have less dependence on the enterprise relatively. In other words, once they find the present job is short of attraction or space for personal growth and development, they may turn to other enterprises and seek for new career chance. Besides, the specialties of knowledge workers and the great social demand for knowledge provide with more chances for knowledge workers changing their jobs among enterprises, regions, and even countries.

(3) Higher demand of knowledge workers. In general, knowledge workers have accepted higher education. They possess relatively higher individual qualities and specialties in certain fields. Their salaries and life have been guaranteed in a sense. Therefore, they pursue for self-esteem and realization of self-worth. They do not satisfy with common daily work. They are wild about more challengeable and creative work. And they hope for realizing their self-worth by displaying their wisdom in the process.

(4) It is hard to control and supervise the work process. Knowledge workers undertake knowledge work under uncertain environment. The work process is usually virtual. Traditional operation rules are meaningless for them. They have greater freedom and self-determination. Even their work places are far different from traditional fixed workshops or

offices. Their inspirations and innovations may happen in any time and space out of work time and space. Therefore, it is hard to control and supervise knowledge workers' work process.

(5) The complexity and uncertainty of work evaluation. On one hand, because knowledge workers are engaged in creative work, it is hard to set up an evaluation standard in advance. Besides, knowledge workers accomplish their work in form of certain ideas, innovations, technology innovations, and management innovation, which can not be measured directly. On the hand, because of modern science and technology's fast development, one person's specialty can not satisfy the complex job's need for knowledge. Many knowledge innovation and scientific research fruit have to be accomplished by team coordination. Take Microsoft for example. A large software is usually accomplished by nearly 500 programmers cooperated together. This trans-branch and organization cooperation has its advantages, which makes it impossible to separate the achievement. As a result, it is hard to evaluate individuals' performance.

2. Execute effective management strategy based on characteristics of knowledge workers

In order to achieve effective management on knowledge workers, it is necessary to constitute systematic, comprehensive, and pointed management strategy according to characteristics of knowledge workers. In specific, it includes these aspects as follow.

(1) Recognize and redefine the relationship between knowledge workers and entrepreneurs. At the industrial economy time, capitals, as the important and scarce source, determines the capital-and-employment relationship between entrepreneurs and employees. But at the knowledge economy time the traditional relationship between knowledge workers and entrepreneurs changes. Knowledge workers are not followers but partners because knowledge workers possess their own production tools, namely the knowledge stored in their brains. They are suppliers of knowledge resource. Similar to suppliers of capitals, they should have the residual claim right.

(2) Reengineer the enterprise's organization structure. Researches show that the organization structure of Chinese enterprises is too simple. 56.2 percent of enterprises adopt the unitary organization form. Even for large-scale enterprises, 54.23 percent of them adopt this kind. However, this pyramid organization structure is a kind of level management vertically, what leads to poor information communication and lower management efficiency. Horizontally, this organization form classifies branches based on specialties and responsibilities, which leads to a competitive relationship between branches. Therefore, this organization form may cause severe departmental selfishness, affecting the cooperation between branches and workers. Especially for interactive operations, different branches may tempt to escape from responsibilities. Besides, due to this leveled organization, many excellent experts and technologists focus on how to achieve further promotion instead of specialties. Practices prove that after excellent technologists became managers, the organization would confront with fatal disasters, which may lead to a great waste of talents. The principle of reforming the organization structure is to benefit the cooperation between knowledge workers and exert their potentials to a great degree. Therefore, the organization structure should be reformed toward being flatten, network, flexible, and virtual.

(3) Empowerment. The so-called empowerment means the top level empowers the low level to exert certain authority and responsibility, what makes the lower levels possess certain self-determination and freedom. An empowerment to knowledge workers has two advantages at least. Firstly, it can satisfy knowledge workers' demand for self-determination. Most knowledge workers are engaged in creative work. Too-much control may depress their creativity. Secondly, it can enhance knowledge workers' responsibilities. As empowering knowledge workers to authorities, make them shoulder relevant responsibilities. Equity of authority and responsibility is an essential principal of management. Thirdly, it can improve the quality of decision. The fast updated knowledge, together with the fact that today's managers usually do not familiarize with their followers' work, makes managers face up with such a challenge that how to manage their followers who are experts in certain fields. Empower the decision right to relevant experts. It can greatly improve the quality and efficiency of decision. The quality of decision is usually determined by the match between knowledge and decision right.

(4) Redesign of work. According to Hackman and Oldham's model, an incentive job should have five characteristics as follow: diversity of techniques, completeness of work, importance of task, self- determination, and feedback. Therefore, we can redesign the work and make it more challengeable, by which we can encourage knowledge workers. In specific, we can realize this goal by extending the scope of work, enriching the work, and the flexible work system.

To extend the scope of work is to absorb one or more relevant tasks into present job. By extending the scope of work, we can reduce the repetitiveness of short-term job, and the workers' disgusting feelings toward tedious job, adding more importance into the job. And the diversified technologies demanded by one joy will effectively encourage knowledge workers.

To enrich the work is to make knowledge workers possess a sense of achievement, acceptance, and responsibility as accomplishing a work by changing the work's contents and responsibilities' levels. As knowledge workers do not regard their present work as challengeable, managers can redeploy them to more challengeable work, which can enrich the

work and reduce the baldness of work.

Besides, because most knowledge workers are engaged in brain work, fixed work places and time are meaningless for them. Enterprises can apply a flexible work system that permits knowledge workers adjust their work time and work place to coordinate personal need and work need. In fact, today's information technologies and official businesses provides with favorable conditions for the implement of flexible work system. By network, knowledge workers can connect with enterprises, transmitting information and data, at home anytime. Correspondingly, managers can direct and supervise knowledge workers, avoiding the malfunction of management.

(5) Emphasize the construction of corporate culture. A nice corporate culture can help employees understand and accept enterprises' value trends, adding their senses of adscription. Especially for knowledge workers who change their jobs more frequent, a sense of acceptance and adscription can sustain their loyalty to enterprises.

In constructing the corporate culture, these aspects should not be neglected.

a. Encouragement instead of punishment for failures. Because there are no rules or experiences for knowledge workers' creative work, they face higher risks. If punish failures, it will depress knowledge workers' creativity.

b. Existence of informal organization. Informal organization is formed in work by members with common values or interests. In a sense, informal organization can satisfy members' need for social acceptance, psychology, and ascription, enhancing the cohesion of organization, and driving the share of knowledge. Researches show that 70 percent of knowledge workers' knowledge obtained in work place is coming from informal communication. Most ideas come into being in chatting with colleagues, friends, and clients. However, some managers mistake informal organizations as factions, and evil parties, and strike them. As a matter of fact, it blocks the source of creativity.

c. Encourage cooperation and realize knowledge sharing. Knowledge sharing is not natural. People are not willing to share their accumulated knowledge and experiences with others, especially as knowledge sharing may lead to staff reduction or threaten their superiorities in enterprises. Therefore, in constructing the corporate culture, we should encourage the knowledge sharing among workers. In an environment with knowledge sharing, if a knowledge worker can publicize and advertise his or her specialties, he can gain respect from colleagues and important position in an organization, which are valuable return for his or her deeds. Knowledge sharing among workers can reduce or avoid the learning costs in organizations. If everyone has to learn others' knowledge, the advantages of specialization will disappear.

d. Emphasize training. At the fast-changing times, what knowledge workers pursue is not merely a job but a lifetime career. Tampoe, a knowledge management expert, think that, after lots of researches, the first four incentive factors for knowledge workers are personal growth (33.74%), work self-determination (30.51%), work achievement (26.69%), and money (7.07%). In order to satisfy workers' demand for constant growth, enterprises have to emphasize trainings, providing more training opportunities for employees.

References

Charles Despres. (2004). *Knowledge horizons: the Present and Promise of knowledge management*. Beijing: Posts & Telecom Press.

Frances Horibe. (2000). *Managing Knowledge Workers*. Beijing: China Machine Publishing House.

Peter F. Drucker. (2000). *Management Challenges for the 21th Century*. Beijing: SDX Joint Publishing Company.

Jianming, Li. (2004). Difficulties and suggestions for China's corporate management in 21th century. *China Enterprise News*. 16th, March.

Simulation Research of Brushless Direct Current

Motor Speed System Based on Neuro-PID Position Controller

Xiang Li

Institute of Computer Technology & Automatization, Tianjin Polytechnic University

Tianjin 300160, China

E-mail: tjudx@126.com

Abstract

A new speed control strategy is presented for high performance control of a Brushless Direct Current Motor (BLDCM). A self-tuning Neuro-PID controller is developed for speed control. The PID gains are tuned automatically by the neural network in an on-line way. In recent years, the re-searches on the control of electrical machines based on Neuro-PID Position Controller are increased. It offers inherent advantages over conventional PID controller for BLDCM, Such as reduction of the effects of motor parameter variations, improvement of controller time response and improvement of drive robustness. The BLDCM drive system was simulated by using MATLAB 7.0/Simulink software package. The performance of the proposed method is compared with the conventional PID methods. At the result, the control based on self-tuning Neuro-PID control has better performance than the conventional PID controller.

Keywords: BLDCM, Neuro-PID, Self-tunning, Speed servo system

1. Introduction

Recent advances in power semiconductor devices, microprocessor, converter design technology and control theory have enabled ac servo drives to satisfy the high performance requirements in many industrial application. Current-regulated Brushless Direct Current Motor (BLDCM) are used in many applications that require rapid torque response and high-performance operation such as robotics, vehicle propulsion, heat pumps, actuators, computer numerically machine tools and ship propulsion.

The control performance of the BLDCM servo drive is still influenced by uncertain-ties, which usually are composed of unpredictable plant parameter variations, external load disturbance, and unmodeled and nonlinear dynamics of the plant. In the past decade, many modern control theories, such as nonlinear control, variable structure system control, adaptive control, optimal control, and the robust control have been developed for the BLDCM drive to deal with uncertainties. In the application of such techniques, development of mathematical models is a prior necessity. However, such mathematical modelling which is largely based on the assumption of linearization of system might not reflect the true physical properties of the system.

The complex mathematical models which do reflect precise input-output physically relation of the system can be build, but the sensivity of parameters should be low in order to make the control system useful. And, if some changes in the plant occur, the model must be re-build and the new control law must be determined. Therefore, these control theory is difficult to apply for real world problem.

The purpose of this paper is to develop a self tuning Neuro-PID position control drive system for BLDCM. The analysis, design and simulation of the purposed controller are described. Good and robust control performance, both in command tracking and the load regulating characteristics of the rotor position, is achieved.

2. System Description and Machine Model

The Fig shows the total configuration of a field-oriented Permanent Magnet Synchronous Motor drive system investigated in this work. The system consists of a BLDCM and load, a hysteresis current controlled voltage source inverters, a field-orientation mechanism and a coordinate translator, a position control loop and a self-tuning Neuro-PID speed controller. The torque in BLDCM's is usually controlled by controlling armature current. In high-performance drives, pulse-width modulated (PWM) inverters are used to provide effective current control. Various techniques and control algorithm of current control of PWM inverters have been studied and reported in the literature. In one of these control schemes called hysteresis on-off current control, the motor currents are compared to their reference currents and the switching instants for the inverter power switches are determined using hysteresis control strategy. In this work, the hysteresis control strategy is used for current control of PWM inverter and the reference currents are produced by

self-tuning PID-neuro controller.

2.1 Introduction of the Model of Brushless Direct Current Motor

The machine model is developed for the simulation work. At the developed machine model, magnetic saturation is neglected, all parameters of the motor are not assumed to be constant and dependent operation condition. All harmonic torques resulting from supply harmonics and operation temperature are neglected. The inverter is assumed to be ideal and the machine has damper windings. The machine model is shown Figure 2.

The BLDCM used in this drive is three-phase, wye-connected stator windings, six pole, 2500W, 5.75A and 5000 r/min type. The stator windings are identical, sinusoidal distributed and displaced 120°.

2.2 The Mathematical Model BLDCM

The voltage equations of the wye-connected permanent magnet synchronous machine, which is shown Figure 2, are given by,

$$V_{as} = r_s i_{as} + L_{ss}\frac{di_{as}}{dt} + \omega_r \lambda_m Cos(\theta_r)$$

$$V_{bs} = r_s i_{bs} + L_{ss}\frac{di_{bs}}{dt} + \omega_r \lambda_m Cos(\theta_r - \frac{2\pi}{3}) \qquad \text{Eq.(1)}$$

$$V_{cs} = r_s i_{cs} + L_{ss}\frac{di_{cs}}{dt} + \omega_r \lambda_m Cos(\theta_r + \frac{2\pi}{3})$$

Where r_s, L_{ss}, θ_r, ω_r, and λ_m denote the stator resistance, stator self inductance, the position of the rotor, angular shaft speed and the flux linkage due to permanent magnet, respectively. The voltage equation of the BLDCM is established using reference frame theory to express the variables in the rotor reference frame.

This transform is:

$$f^r qdo = K_s^r f_{abcs} \qquad \text{Eq. (2)}$$

Where f may represent voltage, current or flux linkage. K_s^r, which is matrix, are as follows,

$$K_s^r = \begin{pmatrix} Cos(\theta_r) & Cos(\theta_r - \frac{2\pi}{3}) & Cos(\theta_r + \frac{2\pi}{3}) \\ Sin(\theta_r) & Sin(\theta_r - \frac{2\pi}{3}) & Sin(\theta_r + \frac{2\pi}{3}) \\ \frac{1}{2} & \frac{1}{2} & \frac{1}{2} \end{pmatrix} \qquad \text{Eq.(3)}$$

The voltage equations of BLDCM are transformed from abc variable to qdo variable using Eq.(3). A circuit model of a BLDCM, which is used predicting its transient behaviour, can be obtained using either of two equivalent circuits representation of BLDCM.

3. Design of the Self-tuning PID-Neuro Controller

This approach direct applications for many traditional control techniques which include adaptive control methods. Many adaptive control methods have a number of parameters or user defined polynomials that are needed to be selected or tuned in prior. These are usually by trial and error. By integrating a neural network into the control scheme, it can than tune the these parameters in on-line way. Thus this self-tuning neuro-control strategy has possible application in many traditional control approaches. The neural network is used to tune the parameters of the PID controller. The neural network is minimized error function by adjusting the PID gain, such as, KP, KI, KD. There are many artificial neural network architectures that have been proposed. One of these architecture is the feed-forward neural network (FFNN). A typical multi input, multi output two layer FNN structure is illustrated in Figure 3.

4. Simulation of the Drive System

The dynamic performance of the BLDCM drive is evaluated by using computer simulation. The control system is shown in Figure 4.

The MATLAB 7.0/Simulink software package was used to analyze the position con-troller. The simulation was run

three different times for each specified reference trajectory. The first run was to demonstrate position response with nominal machine parameters. PID and Neuro-PID position controller responses are shown in Fig.5. The a–position response with only PID controller, b- position response with neuro-PID controller, c-electrical torque with Neuro-PID controller d- phase current of PMSM with Neuro-PID controller.The load torque is increased to 5 Nm at 0.3s.

The electrical time constant is increased to 1.5 times the nominal value for PID and neuro-PID controllers. The simulation results are shown in Figure 6.

5. Conclusion

A robust BLDCM drive system, which is based on self-tuning PID neuro-control structure , has been presented in this paper. A PI position controller was described first. Next self-tuning Neuro-PID speed controller is designed with three layer and three output neural network. The Neural Network is tuned PID gains on-line. Then, the self-tuning Neuro-PID controller was on line designed to match the time domain reference tracking specification under the parameter variation. In this work, the mathematical basis of the proposed controller was derived and the drive system simulated. The simulation result showed that this self-tuning Neuro-PID control strategy effectively achieved the desired dynamic performance of BLDCM.

References

Jiao, Zuqin. (2006). *The speed servo system of BLDCM based on improved BP neural network PID controller.* 23 (2). p. 112-114.

Liang, Yu. (2007). Simulation Research of DC Adjusting Speed System Based on Neuron PID. *Coal Mine Machinery.* 28(6).p.53-55.

Pan, Xiao. (2007). The Application of PID Controller Based on Neural Network in main steam system of Once-through boiler. *Control & Automation.* 23 (6). p. 34-36.
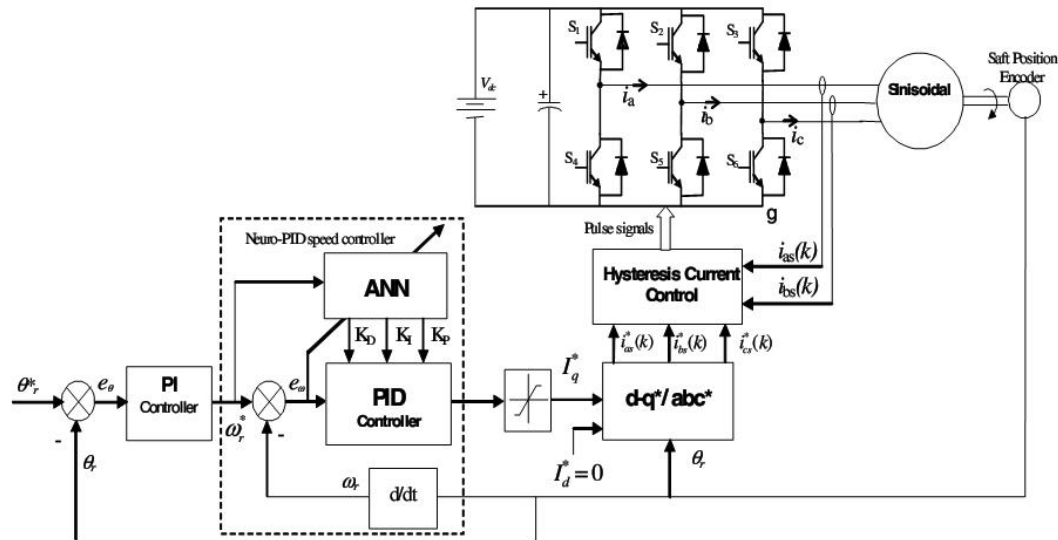
Figure 1. The block diagram of proposed BLDCM motor drive system

(a)   (b)
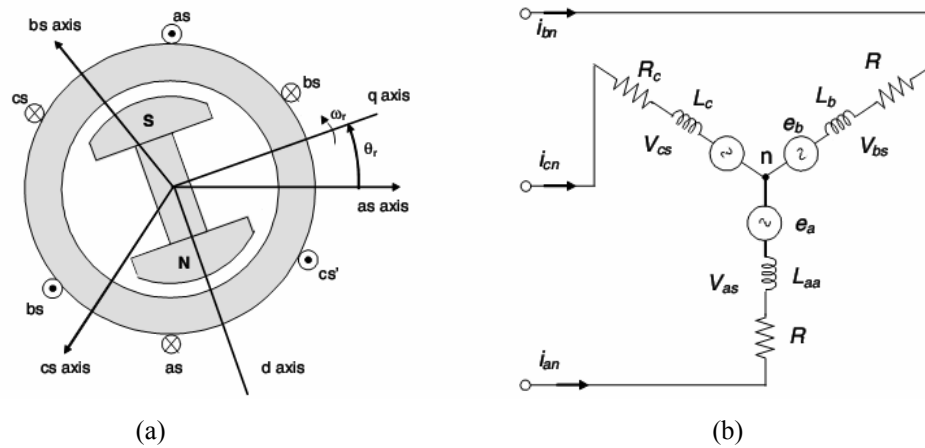
Figure 2. Model of Brushless Direct Current Motor
(a) A BLDCM, (b) the stator windings of the machine
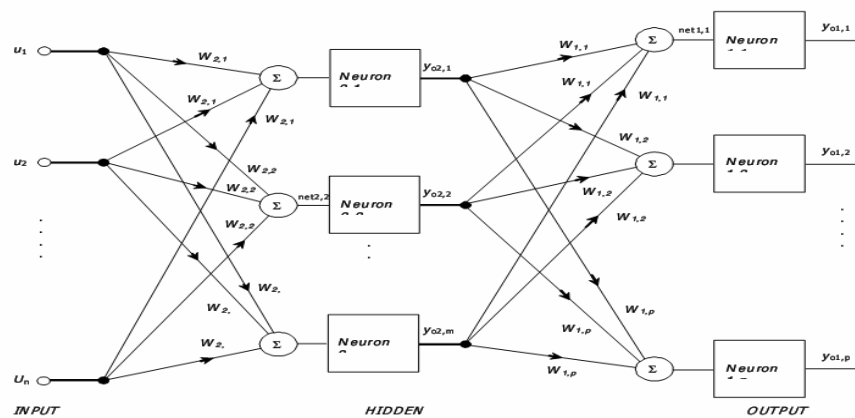
Figure 3. Topology of multi input ,multi output 2 layer feed-forward neural network
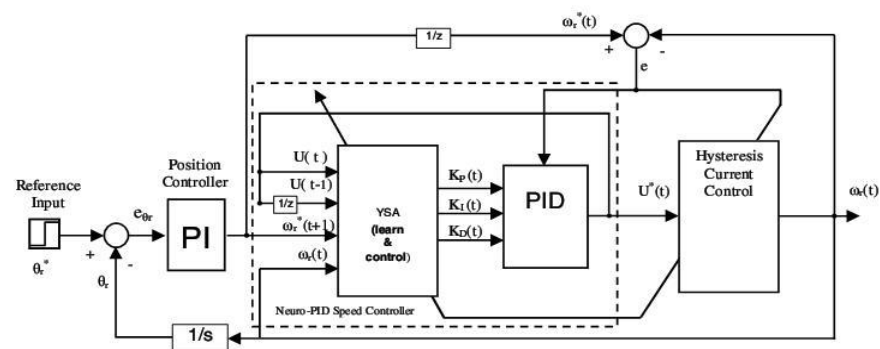
Figure 4. The block diagram of the self tuning neuro-PID control system
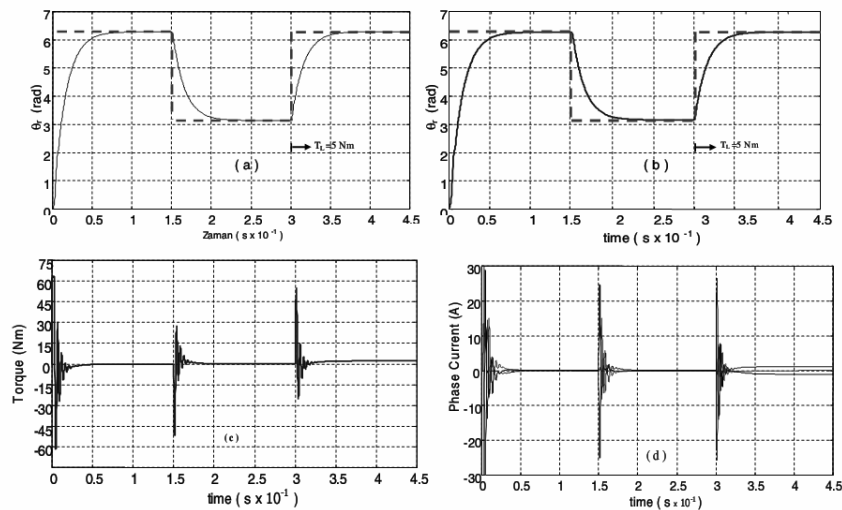
Figure 5. The simulation results with nominal parameters.
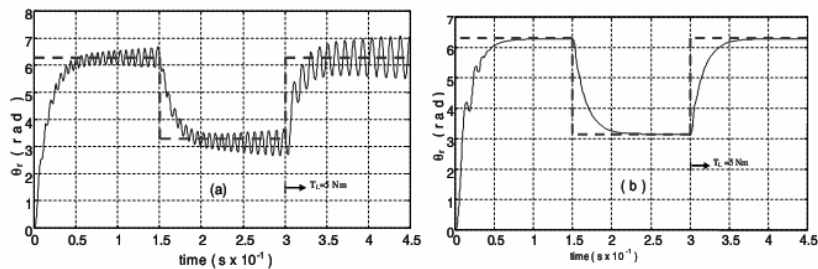
Figure 6. Simulation results with variation, a- PID, b- proposed Neuro-PID control

Vibration Suppression Techniques in Feedback

Control Loop of a Flexible Robot Manipulator

Mohd Ashraf Ahmad (Corresponding author)

Faculty of Electrical and Electronics Engineering, Universiti Malaysia Pahang,

Karung Berkunci 12, 25000, Kuantan, Pahang, Malaysia

Tel: 6013-926 4212   E-mail: ash_usc@hotmail.com

Zaharuddin Mohamed

Faculty of Electrical Engineering, Universiti Teknologi Malaysia,

81310 UTM Skudai, Johor, Malaysia

Tel: 607-553 5247   E-mail: zahar@fke.utm.my

Abstract

This paper presents the use of angular position control approaches for a flexible robot manipulator with disturbances effect in the dynamic system. Delayed Feedback Signal (DFS), Linear Quadratic Regulator (LQR) and Proportional-Derivative (PD) controller are the techniques used in this investigation to actively control the vibrations of flexible structure. A constrained planar single-link flexible manipulator is considered and the dynamic model of the system is derived using the assumed mode method. A complete analysis of simulation results for each technique is presented in time domain and frequency domain respectively. Performances of the controller are examined in terms of vibration suppression and disturbances cancellation. Finally, a comparative assessment of the impact of each controller on the system performance is presented and discussed.

Keywords: Flexible manipulator, Vibration control, Delayed feedback signal, Linear quadratic regulator, PD controller.

1. Introduction

Flexible robot manipulators exhibit several advantages over the rigid link manipulators as they require less material, are lighter in weight, have higher manipulation speed, lower power consumption, require smaller actuators, are more manoeuvrable and transportable, have less overall cost and higher payload to robot weight ratio (Martins et al., 2003). However, the control of flexible manipulators to maintain accurate positioning is a challenging problem. A flexible manipulator is a distributed parameter system and has infinitely many degrees of freedom. Moreover, the dynamics are highly non-linear and complex. Problems arise due to precise positioning requirements, system flexibility leading to vibration, the difficulty in obtaining accurate model of the system and non-minimum phase characteristics of the system (Yurkovich, 1992). To attain end-point positional accuracy, a control mechanism that accounts for both the rigid body and flexural motions of the system is required. If the advantages associated with lightness are not to be sacrificed, precise models and efficient control strategies for flexible manipulators have to be developed.

The requirement of precise position control of flexible manipulators implies that residual vibration of the system should be zero or near zero. Over the years, investigations have been carried out to devise efficient approaches to reduce the vibration of flexible manipulators. The considered vibration control schemes can be divided into two main categories: feed-forward control and feedback control techniques. Feed-forward techniques for vibration suppression involve developing the control input through consideration of the physical and vibrational properties of the system, so that system vibrations at dominant response modes are reduced. This method does not require additional sensors or actuators and does not account for changes in the system once the input is developed. On the other hand, feedback-control techniques use measurement and estimations of the system states to reduce vibration. Feedback controllers can be designed to be robust to parameter uncertainty.

In general, control of flexible manipulators can be made easier by locating every sensor exactly at the location of the actuator, as collocation of sensors and actuators guarantees stable servo control (Gevarter, 1970). In the case of flexible manipulator systems, the end-point position is controlled by obtaining the parameters at the hub and end-point of the manipulator and using the measurements as a basis for applying control torque at the hub. Thus, the feedback control can be divided into collocated and non-collocated control. By applying control torque based on non-collocated sensors, the problem of non-minimum phase and of achieving stability is of concern. Several approaches utilising closed-loop

control strategies have been reported for control of flexible manipulators. These include linear state feedback control (Cannon and Schmitz, 1984; Hasting and Book, 1987), adaptive control (Feliu et al., 1990; Yang et al., 1992), robust control techniques based on H-infinity (Moser, 1993) and variable structure control (Moallem et al., 1998) and intelligent control based on neural networks (Gutierrez et al., 1998) and fuzzy logic control schemes (Moudgal et al., 1994).

Another method of controlling flexible structures is based on time delay control (TDC). In the TDC method, time delay is used to estimates the effects of unknown dynamics and unpredictable disturbances (Youcef and Ito, 1990a; Youcef and Bobbett, 1992a). The TDC introduces delay terms in the closed-loop of the system in order to cancel the unwanted dynamics. In (Youcef and Wu, 1992b), time delay has been used to achieve an input/output linearization of a class of nonlinear systems with a special application to the position control of a single-link flexible arm. In general, time delays occur in real systems in several forms. Transport delays and acoustic feedback are considered the main sources. The stability of systems with delay has been dealt with extensively in the literature (Youcef and Reddy, 1990b; Malek and Jamshidi, 1987; Kharitonov, 1979). Recently, a generalized approach to investigate the stability of time delay systems has been presented in (Olgac and Sipahi, 2001). This approach resembles the Routh-Hurwitz technique for linear systems and can be used to select the time delay parameters that lead to a stable closed-loop system. More recently, TDC has been used in the control of aerodynamic systems. In (Ramesh and Narayanan, 2001), a time-delayed feedback to control the chaotic motions in a two-dimensional airfoil was used and, a similar technique to stabilize the motion of helicopter rotor blades was used in (Krodkiewski and Faragher, 2000) except that the time delay in this case was selected to be the period of the motion to be stabilized. A method for determining the stability switches for time delayed dynamic systems with unknown parameters has been presented in (Wang and Hu, 2000; Jnifene, 2007). In the present paper, the time delay has been introduced to generate the control signal and the delay time is considered as the design parameter.

This paper presents investigations of angular position control approach in order to eliminate the effect of disturbances applied to the single-link flexible robot manipulator. A simulation environment is developed within Simulink and Matlab for evaluation of the control strategies. In this work, the dynamic model of the flexible manipulator is derived using the assumed mode method (AMM). To demonstrate the effectiveness of the proposed control strategy, the disturbances effect is applied at the tip of the flexible link. This is then extended to develop a feedback control strategy for vibration reduction and disturbances rejection. Three feedback control strategies which are DFS, LQR and PD controller are developed in this simulation work. Performances of each controller are examined in terms of vibration suppression and disturbances rejection. Finally, a comparative assessment of the impact of each controller on the system performance is presented and discussed.

2. The Flexible Manipulator System

The single-link flexible manipulator system considered in this work is shown in Figure 1, where X_oOY_o and XOY represent the stationary and moving coordinates frames respectively, τ represents the applied torque at the hub. E, I, ρ, A, I_h and m_p represent the Young modulus, area moment of inertia, mass density per unit volume, cross-sectional area, hub inertia and payload mass of the manipulator respectively. In this work, the motion of the manipulator is confined to X_oOY_o plane. Transverse shear and rotary inertia effects are neglected, since the manipulator is long and slender. Thus, the Bernoulli-Euler beam theory is allowed to be used to model the elastic behaviour of the manipulator. The manipulator is assumed to be stiff in vertical bending and torsion, allowing it to vibrate dominantly in the horizontal direction and thus, the gravity effects are neglected. Moreover, the manipulator is considered to have a constant cross-section and uniform material properties throughout. In this study, an aluminium type flexible manipulator of dimensions $900 \times 19.008 \times 3.2004$ mm³, $E = 71 \times 10^9$ N/m², $I = 5.1924 \times 10^{11}$ m⁴ , $\rho = 2710$ kg/m³ and $I_h = 5.8598 \times 10^{-4}$ kgm² is considered.

3. Modelling of the Flexible Manipulator

This section provides a brief description on the modelling of the flexible robot manipulator system, as a basis of a simulation environment for development and assessment of the control techniques. The AMM with two modal displacements is considered in characterising the dynamic behaviour of the manipulator incorporating structural damping and hub inertia. Further detailed of the description and derivation of the dynamic model of the system can be found in (Subudhi et al., 2002). The dynamic model is validated with an actual experimental rig to study the performance of the model in (Martin et al., 2003).

Considering revolute joints and motion of the manipulator on a two-dimensional plane, the kinetic energy of the system can thus be formulated as

$$T = \frac{1}{2}(I_H + I_b)\dot{\theta}^2 + \frac{1}{2}\rho\int_0^L (\dot{x}^2 + 2\dot{x}\dot{\theta})dx \tag{1}$$

where I_b is the beam rotation inertia about the origin O_0 as if it were rigid. The potential energy of the beam can be

formulated as

$$U = \frac{1}{2}\int_0^L EI\left(\frac{\partial^2 v}{\partial x^2}\right)^2 dx \tag{2}$$

This expression states the internal energy due to the elastic deformation of the link as it bends. The potential energy due to gravity is not accounted for since only motion in the plane perpendicular to the gravitational field is considered.

To obtain a closed-form dynamic model of the manipulator, the energy expressions in (1) and (2) are used to formulate the Lagrangian $L = T - U$. Assembling the mass and stiffness matrices and utilizing the Euler-Lagrange equation of motion, the dynamic equation of motion of the flexible manipulator system can be obtained as

$$M \ddot{Q}(t) + D \dot{Q}(t) + KQ(t) = F(t) \tag{3}$$

where *M, D* and *K* are global mass, damping and stiffness matrices of the manipulator respectively. The damping matrix is obtained by assuming the manipulator exhibit the characteristic of Rayleigh damping. *F(t)* is a vector of external forces and *Q(t)* is a modal displacement vector given as

$$Q(t) = [\theta \quad q_1 \quad q_2 \quad ... \quad q_n]^T = [\theta \quad q^T]^T \tag{4}$$

$$F(t) = [\tau \quad 0 \quad 0 \quad ... \quad 0]^T \tag{5}$$

Here, q_n is the modal amplitude of the *i* th clamped-free mode considered in the AMM procedure and *n* represents the total number of assumed modes. The model of the uncontrolled system can be represented in a state-space form as

$$\dot{x} = Ax + Bu$$
$$y = Cx \tag{6}$$

with the vector $x = [\theta \quad \dot{\theta} \quad q_1 \quad q_2 \quad \dot{q}_1 \quad \dot{q}_2]^T$ and the matrices A and B are given by

$$\mathbf{A} = \left[\begin{array}{c|c} 0_{3\times3} & I_{3\times3} \\ \hline -M^{-1}K & -M^{-1}D \end{array}\right], \quad \mathbf{B} = \left[\begin{array}{c} 0_{3\times1} \\ M^{-1} \end{array}\right]$$

$$\mathbf{C} = [I_{1\times3} \mid 0_{1\times3}], \qquad \mathbf{D} = [0] \tag{7}$$

4. Controller Design

In this section, three feedback control strategies (DFS, LQR and PD controller) are proposed and described in detail. The main objective of the feedback controller in this study is to maintain the angular position of flexible manipulator while suppressing the vibration due to disturbances effect. All the feedback control strategies are incorporated in the closed-loop system in order to eliminate the effect of disturbances.

4.1 DFS Controller

In this section, the control signal is calculated based on the delayed position feedback approach described in Equation (8) and illustrated by the block diagram shown in Figure 2.

$$u(t) = k(y(t) - y(t - \tau)) \tag{8}$$

Substituting Equation (8) into Equation (6) and taking the Laplace transform gives

$$sIx(s) = Ax(s) - kBC(1 - e^{-s\tau})x(s) \tag{9}$$

The stability of the system given in Equation (9) depends on the roots of the characteristic equation

$$\Delta(s, \tau) = |sI - A + kBC(1 - e^{-s\tau})| = 0 \tag{10}$$

Equation (10) is transcendental and results in an infinite number of characteristic roots (Olgac and Sipahi, 2001). Several approaches dealing with solving retarded differential equations have been widely explored. In this study, the

approach described in (Ramesh and Narayanan, 2001) will be used on determining the critical values of the time delay τ that result in characteristic roots of crossing the imaginary axes. This approach suggests that Equation (10) can be written in the form

$$\Delta(s,\tau) = P(s) + Q(s)e^{-s\tau} \tag{11}$$

P(s) and *Q(s)* are polynomials in *s* with real coefficients and deg(*P(s)*)=n>deg(*Q(s)*) where *n* is the order of the system. In order to find the critical time delay τ that leads to marginal stability, the characteristic equation is evaluated at *s=jω*. Separating the polynomials *P(s)* and *Q(s)* into real and imaginary parts and replacing $e^{j\omega\tau}$ by *cos(ωτ)-jsin(ωτ)*, Equation (11) can be written as

$$\Delta(j\omega,\tau) = P_R(\omega) + jP_I(\omega) + (Q_R(\omega) + jQ_I(\omega))(\cos(\omega\tau) - j\sin(\omega\tau)) \tag{12}$$

The characteristic equation $\Delta(s,\tau) = 0$ has roots on the imaginary axis for some values of $\tau \geq 0$ if Equation (12) has positive real roots. A solution of $\Delta(j\omega,\tau) = 0$ exists if the magnitude $|\Delta(j\omega,\tau)| = 0$. Taking the square of the magnitude of $\Delta(j\omega,\tau)$ and setting it to zero lead to the following equation

$$P_R{}^2 + P_I{}^2 - (Q_R{}^2 + Q_I{}^2) = 0 \tag{13}$$

By setting the real and imaginary parts of Equation (13) to zero, the equation is rearranged as below

$$\begin{bmatrix} Q_R & Q_I \\ Q_I & -Q_R \end{bmatrix} \begin{bmatrix} \cos\beta \\ \sin\beta \end{bmatrix} = \begin{bmatrix} -P_R \\ -P_I \end{bmatrix}, \tag{14}$$

where $\beta=\omega\tau$.

Solving for sin β and cos β gives

$$\sin(\beta) = \frac{(-P_R Q_I + P_I Q_R)}{(Q_R{}^2 + Q_I{}^2)} \text{ and } \cos(\beta) = \frac{(-P_R Q_R - P_I Q_I)}{(Q_R{}^2 + Q_I{}^2)}$$

The critical values of time delay can be determined as follows: if a positive root of Equation (13) exists, the corresponding time delay τ can be found by

$$\tau_k = \frac{\beta}{\omega} + \frac{2k\pi}{\omega} \tag{15}$$

where $\beta \in [0\ 2\pi]$. At these time delays, the root loci of the closed-loop system are crossing the imaginary axis of the s-plane. This crossing can be from stable to unstable or from unstable to stable. In order to investigate the above method further, the time-delayed feedback controller is applied to the single-link flexible manipulator. Practically, the control signal for the DFS controller requires only one position sensor and uses only the current output of this sensor and the output τ second in past. There is only two control parameter: *k* and τ that needs to be set. Using the stability analysis described in (Wang and Hu, 2000), the gain and time-delayed of the system is set at *k=55* and $\tau=0.005$. The control signal of DFS controller can be written as below

$$u_{DFS}(t) = -55(\theta(t) - \theta(t - 0.005))$$

4.2 LQR Controller

A more common approach in the control of manipulator systems involves the utilization LQR design [31]. Such an approach is adopted at this stage of the investigation here. In order to design the LQR controller a linear state-space model of the flexible manipulator was obtained by linearising the equations of motion of the system. For a LTI system in Equation (6), the technique involves choosing a control law $u = \psi(x)$ which stabilizes the origin (i.e., regulates x to zero) while minimizing the quadratic cost function

$$J = \int_0^\infty x(t)^T Qx(t) + u(t)^T Ru(t)dt \tag{16}$$

where $Q = Q^T \geq 0$ and $R = R^T > 0$. The term "linear-quadratic" refers to the linear system dynamics and the quadratic cost function.

The matrices Q and R are called the state and control penalty matrices, respectively. If the components of Q are chosen large relative to those of R, then deviations of x from zero will be penalized heavily relative to deviations of u from zero. On the other hand, if the components of R are large relative to those of Q, then control effort will be more costly and the state will not converge to zero as quickly.

A famous and somewhat surprising result due to Kalman is that the control law which minimizes J always takes the form $u = \psi(x) = -Kx$. The optimal regulator for a Linear Time Invariant (LTI) system with respect to the quadratic cost function above is always a linear control law. With this observation in mind, the closed-loop system takes the form

$$\dot{x} = (A - BK)x \tag{17}$$

and the cost function J takes the form

$$J = \int_0^\infty x(t)^T (Q + K^T R K)x(t)dt \tag{18}$$

Assuming that the closed-loop system is internally stable, which is a fundamental requirement for any feedback controller, the following theorem allows the computation value of the cost function for a given control gain matrix *K*.

In order to implement the LQR controller, all the state variables need to be available either through direct measurement or through estimation. The block diagram of LQR controller is illustrated in Figure 3. For the single-link flexible manipulator described by the state-space model given by Equation (6) and with *M, K*, and *D* matrices calculated earlier, the LQR gain matrix for

$$Q = 10 \begin{bmatrix} I_{3\times3} & 0_{3\times3} \\ 0_{3\times3} & 0_{3\times3} \end{bmatrix} \qquad \text{and} \qquad R = 1$$

was calculated using Matlab and was found to be

$$K_{LQR} = \begin{bmatrix} 3.1623 & 2.1991 & 8.1477 & 0.4476 & 0.5333 & 5.1509 \end{bmatrix}$$

The control signal for the LQR is calculated as

$$u_{LQR} = -3.1623\theta - 2.1991\dot{\theta} - 8.1477q_1 - 0.4476q_2 - 0.5333\dot{q}_1 - 5.1509\dot{q}_2$$

4.3 PD Controller

To demonstrate the performance of the PD controller in dealing with vibration and disturbances, a PD feedback of collocated sensor signals is adopted for control the angular position of the flexible manipulator. A block diagram of the PD controller is shown in Figure 4, where K_P and K_D are the proportional and derivative gains respectively, θ and $\dot{\theta}$ represent hub angle and hub velocity, respectively. Essentially the task of this controller is to position the flexible arm to the specified angle of demand. The hub angle and hub velocity signals are fed back and used to control the hub angle of the manipulator.

To design the PD controller, a linear state-space model of the flexible manipulator was obtained by linearising the equations of motion of the system. The control signal $u(s)$ in Figure 4 can be written as

$$u_{PD}(s) = -[K_P\theta(s) + K_D\dot{\theta}(s)]$$

where *s* is the Laplace variable. In this study, the Ziegler-Nichols approach is utilized to design the PD controller. Analyses the tuning process of the proportional and derivative gains using Ziegler-Nichols technique shows that the optimum response of PD controller is achieved by setting $K_P = 1.2$ and $K_D = 0.8$.

5. Simulation Results

In this section, the proposed control schemes are implemented and tested within the simulation environment of the flexible manipulator and the corresponding results are presented. The control strategies were designed by undertaking a computer simulation using the fourth-order Runge-Kutta integration method at a sampling frequency of 1 kHz. Three system responses namely the angular position, hub-angular velocity, and modal displacement are obtained. Moreover, the power spectral density (PSD) of the modal displacement is evaluated to investigate the dynamic behaviour of the system in frequency domain. Two criteria are used to evaluate the performances of the control strategies:

(1) Level of vibration reduction at the natural frequencies. This is accomplished by comparing the responses of the controller with the response to the open loop system.

(2) Disturbance cancellation. The capability of the controller to achieved steady state conditions at zero angular position.

In all simulations, the initial condition $x_o = [0 \ \ 0 \ \ 1 \times 10^{-3} \ \ 0 \ \ 1 \times 10^{-5} \ \ 0]^T$ was used. This initial condition is considered as the disturbances applied to the flexible manipulator system. The first two modes of vibration of the system are considered, as these dominate the dynamic of the system.

Figure 5 shows the open loop response of the free end of the flexible arm which consist of angular position, modal displacement, angular velocity and PSD results. These results were considered as the system response with disturbances effect and will be used to evaluate the performance of feedback control strategies. It is noted that, in open loop configuration, the steady-state angular position for the flexible manipulator system was achieved at 0.014 radian within the settling times of 1 s. The angular velocity response shows the maximum oscillation between -4 and 6 rad/sec, whereas the modal displacement oscillate between ±0.03 m. Resonance frequencies of the system were obtained by transforming the time-domain representation of the system responses into frequency domain using power spectral analysis. The vibration frequencies of the flexible manipulator system under disturbances effect were obtained as 16 and 55 Hz for the first two modes as demonstrated in Figure 5.

The system responses of the flexible manipulator with the DFS controller are shown in Figure 6. It shows that, with the gain and time delay of 55 and 0.005s respectively, the effect of the disturbances has been successfully eliminated. This is evidenced in angular position response whereas the flexible manipulator system maintained its steady-state conditions at zero radian in a very fast response. It is noted that the vibration in the angular position, angular velocity and modal displacement responses were reduced as compared to the open loop response. This can be clearly demonstrated in frequency domain results as the magnitudes of the PSD at the natural frequencies were significantly reduced.

Figure 7 shows the response of the closed loop system using the LQR controller. The angular position result demonstrates that, the LQR controller can handle the effect of disturbances in the system by optimizing the feedback gain in order to achieve zero radian steady state conditions. It is noted that the overall system vibrations were significantly reduced with the LQR controller even though the level of vibration reduction was less than the case with the DFS controller. It is noted that, the magnitude reduction of the PSD only effect the first mode of the natural frequencies as demonstrated in Figure 7.

The closed loop system responses of the flexible manipulator under PD controller are shown in Figure 8. The angular position, angular velocity and modal displacement response shows a similar pattern as the case of LQR and DFS controller. The results also demonstrated that the conventional PD controller can eliminate the effect of disturbances in the system. It is noted that, the overall time response results exhibits small magnitude of oscillation as compared to the LQR and DFS controller. Besides, the vibration in the angular position, angular velocity and modal displacement responses in overall were reduced as compared to the open loop response. The PSD result shows that the magnitudes of vibration were significantly reduced especially for the first mode of vibration.

By comparing the results of DFS, LQR and PD controller, it is noted that higher performance in the reduction of vibration of the system is achieved with the DFS control strategies. This is observed and compared to the LQR and PD controller at the first two modes of vibration. For comparative assessment, the levels of vibration reduction with the modal displacement using DFS, LQR and PD controller are shown with the bar graphs in Figure 9. The result shows that highest level of vibration reduction is achieved with the DFS controller, followed by PD and LQR controller. Therefore, it can be concluded that overall the delayed feedback signal (DFS) provide better performance in vibration reduction as compared to the both PD and LQR controller. Moreover, the vibration of the system settles within 0.25 s for DFS, LQR and PD controller, which is fourfold improvement as compared to the open loop response. This is evidenced in the angular position, hub-angular velocity, and modal displacement responses for each controller respectively.

6. Conclusion

Investigations into vibration suppression of a flexible robot manipulator with disturbances effect using the DFS, LQR and PD controller have been presented. Performances of the controller are examined in terms of vibration suppression and disturbances cancellation. The results demonstrated that the effect of the disturbances in the system can successfully be handled by DFS, LQR and PD controller. A significant reduction in the system vibration has been achieved with the DFS controller as compared to the LQR and PD controller. The result reveals that the proposed controllers provide a high speed system response in cater the disturbances effect to the flexible manipulator system.

References

Cannon, R.H. and Schmitz, E. (1984). Initial experiment on the end-point control of a flexible one-link robot.

International Journal of Robotics Research. 3(3), 62-75.

Feliu, V., Rattan, K.S. and Brown, H.B. (1990). Adaptive control of a single-link flexible manipulator. *IEEE Control Systems Magazine*. 10(2), 29 –33.

Gevarter, W.B. (1970). Basic relations for control of flexible vehicles. *AIAA Journal*. 8(4), 666-672.

Gutierrez, L.B., Lewis, P.L. and Lowe, J.A. (1998). Implementation of a neural network tracking controller for a single flexible link: comparison with PD and PID controllers. *IEEE Transactions on Industrial Electronics*. 45(3), 307-318.

Hasting, G.G. and Book, W.J. (1987). A linear dynamic model for flexible robot manipulators. *IEEE Control Systems Magazine*. 7, 61-64.

Jnifene, A. (2007). Active vibration control of flexible structures using delayed position feedback. *Systems & Control Letters,* 56(3), 215-222.

Krodokiewski, J.M. and Faragher, J.S. (2000). Stabilization of motion of helicopter rotor blades using delayed feedback-modelling, computer simulation and experimental verification. *J. Sound Vibration*. 234 (4), 591-610.

Malek-Zavarei, M. and Jamshidi, M. (1987). Time Delay Systems: Analysis, Optimization, and Applications. *North-Holland Systems and Control Series*. vol. 9.

Martins, J.M., Mohamed, Z., Tokhi, M.O., Sá da Costa, J. and Botto, M.A. (2003). Approaches for dynamic modelling of flexible manipulator systems. *IEE Proceedings-Control Theory and Application*. 150(4), 401-411.

Moallem, M., Khorasani, K. and Patel, R.V. (1998). Inversion-based sliding control of a flexible-link manipulator. *International Journal of Control*. 71(3), 477-490.

Moser, A.N. (1993). Designing controllers for flexible structures with H-infinity/μ-synthesis. *IEEE Control Systems Magazine*. 13 (2), 79-89.

Moudgal, V.G., Passino, K.M. and Yurkovich, S. (1994). Rule-based control for a flexible-link robot. *IEEE Transactions on Control Systems Technology*. 2(4), 392-405.

Olgac, N. and Sipahi, R. (2001). A new practical stability analysis method for the time delayed LTI systems. *Third IFAC Workshop on TIME DELAY SYSTEMS (TDS 2001)*. Santa Fe, NM.

Ogata, K. (1997). *Modern Control Engineering*. Prentice-Hall International, Upper Saddle River, NJ.

Ramesh, M. and Narayanan, S. (2001). Controlling chaotic motions in a two dimensional airfoil using time-delayed feedback. *J. Sound Vibration*. 239 (5), 1037-1049.

Subudhi, B. and Morris, A.S. (2002). Dynamic modelling, simulation and control of a manipulator with flexible links and joints. *Robotics and Autonomous Systems*. 41, 257-270.

V.L. Kharitonov. (1979). Asymptotic stability of an equilibrium position of a family of systems of linear differential equations. *Differential Equations* 14, 1483-1485.

Wang, Z.H., Hu, H.Y. (2000). Stability switches of time-delayed dynamic systems with unknown parameters. *J. Sound Vibration*. 233(2), 215-233.

Yang, T.-C., Yang, J.C.S. and Kudva, P. (1992). Load-adaptive control of a single-link flexible manipulator system. *IEEE Transactions on Systems, Man and Cybernetics*. 22(1), 85-91.

Yurkovich. S. (1992). Flexibility effects on performance and control. In: *Robot Control* (Eds.: M.W. Spong, F.L. Lewis and C.T. Abdallah, IEEE Press), Part 8, pp. 321-323.

Youcef-Toumi, K. and Ito, O. (1990a). A time delay controller for systems with unknown dynamics. *J. Dyn. Syst. Meas. Control*. 112, 133-142.

Youcef-Toumi, K. and Reddy, S. (1990b). Stability analysis of time delay control with application to high speed magnetic bearings. *ASME Winter Annual Meeting*.

Youcef-Toumi, K. and Bobbett, J. (1992a). Stability of uncertain linear systems with time delay. *J. Dyn. Syst. Meas. Control*. 113, 558-567.

Youcef-Toumi, K. and Wu, S.-T. (1992b). Input/output linearization using time delay control. *J. Dyn. Syst. Meas. Control*. 114, 10-19.
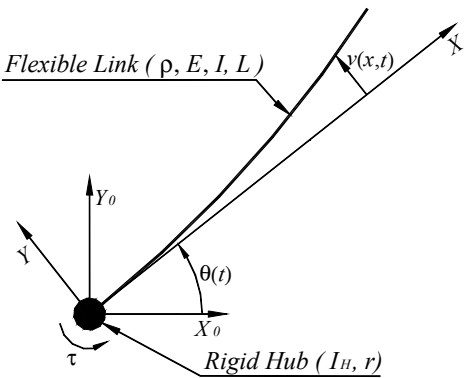
Figure 1. Description of the flexible manipulator system.
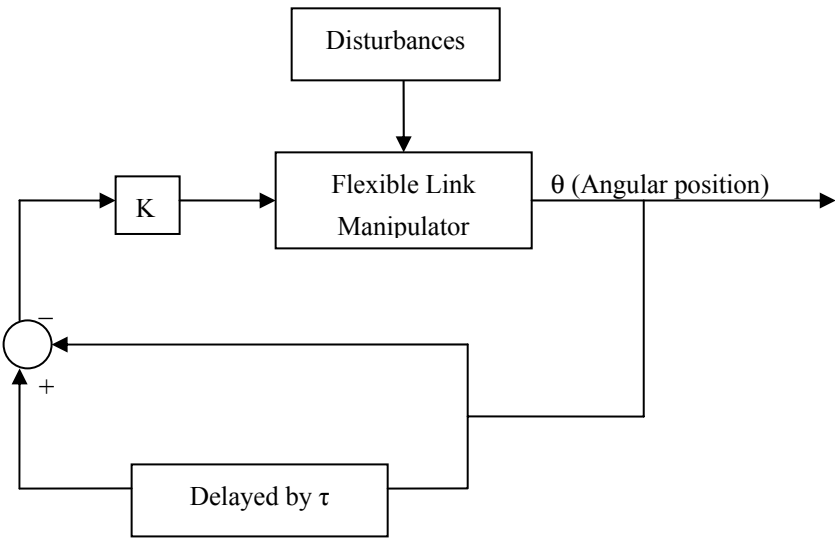
Figure 2. The delayed feedback signal (DFS) controller structure.
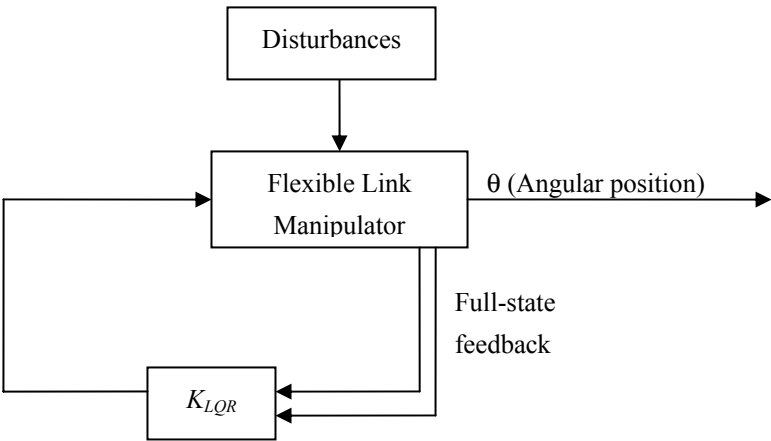
Figure 3. The linear quadratic regulator (LQR) controller structure.
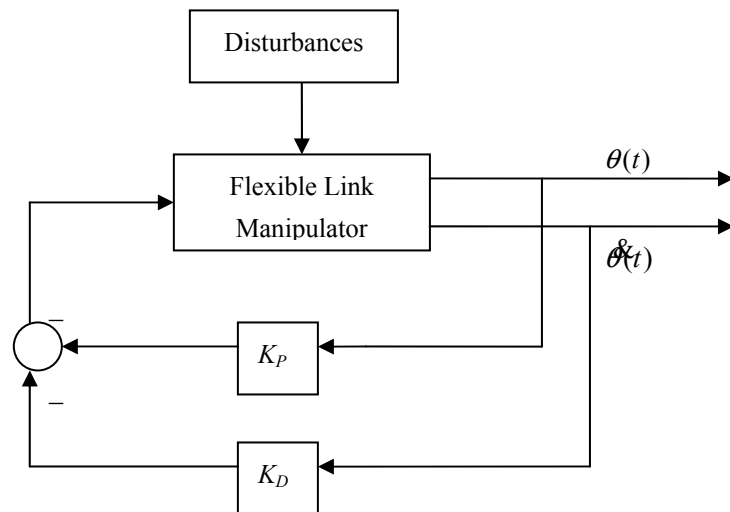
Figure 4. The proportional-derivative (PD) controller structure.
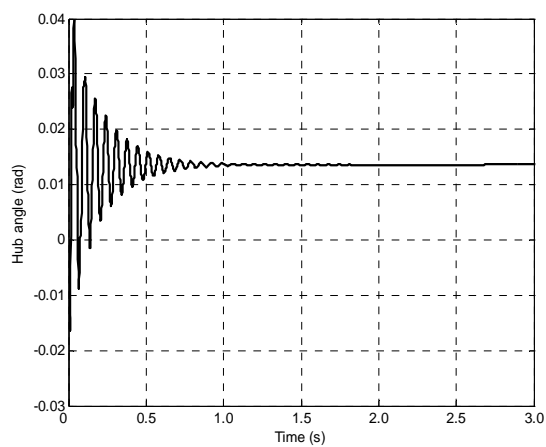
(a) Angular position.
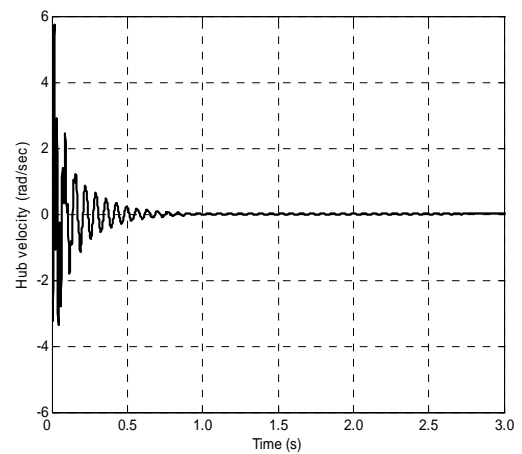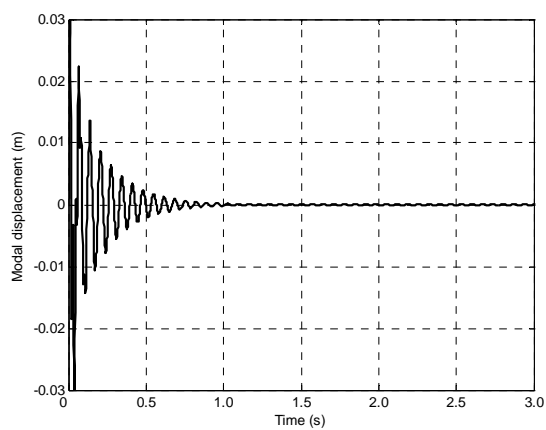
(b) Angular velocity.

(c) Modal displacement.
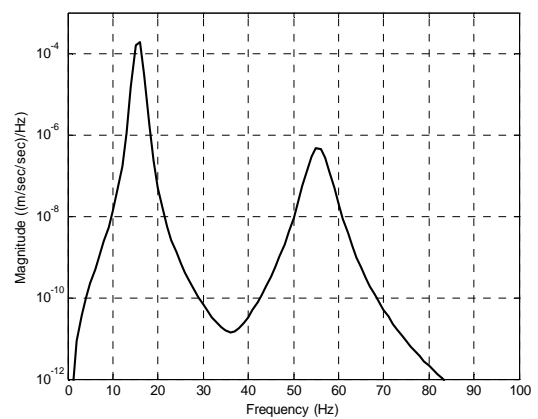
(d) PSD of modal displacement.

Figure 5. Open loop response of the flexible manipulator.
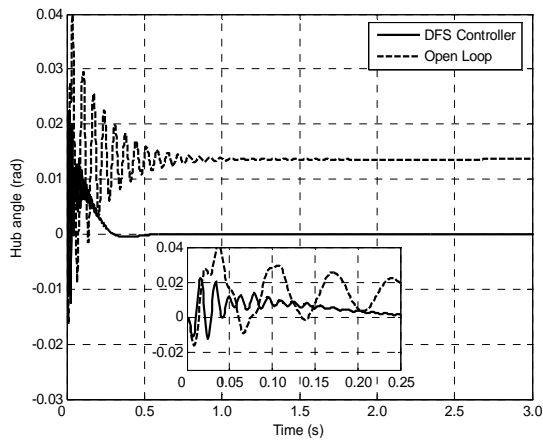
(a) Angular position.   (b) Angular velocity.
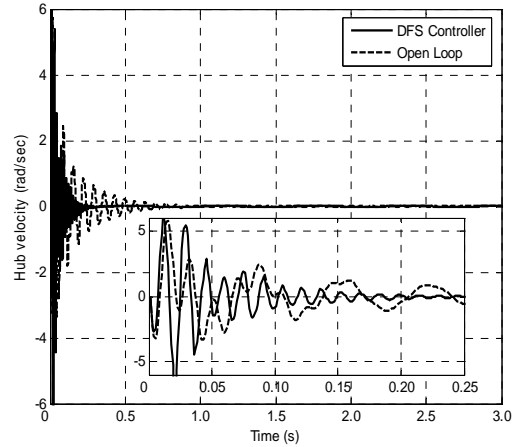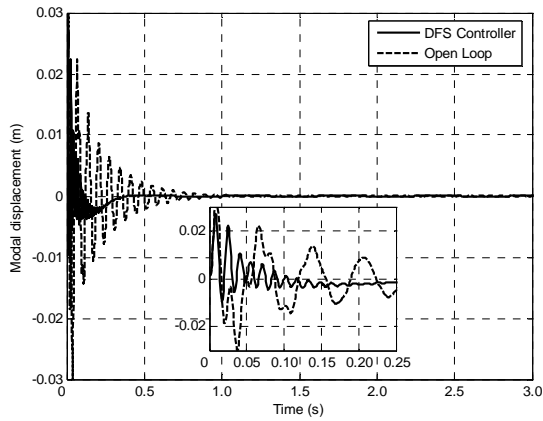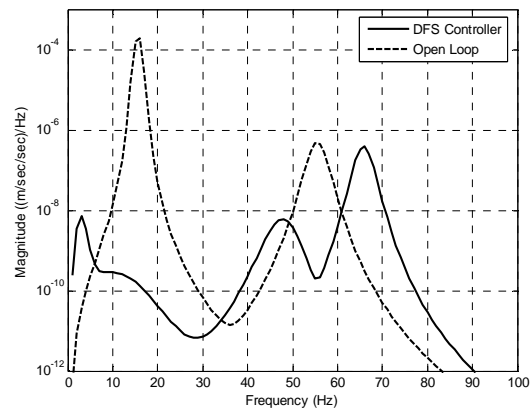
(c) Modal displacement.   (d) PSD of modal displacement.

Figure 6. Response of the flexible manipulator with DFS Controller.
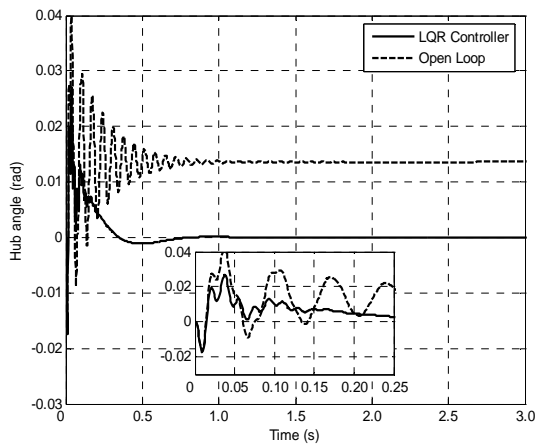
(a) Angular position.   (b) Angular velocity.
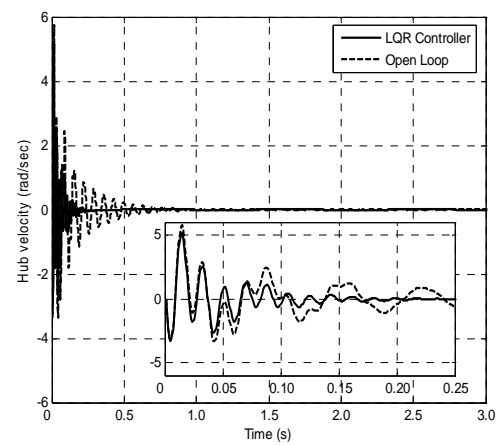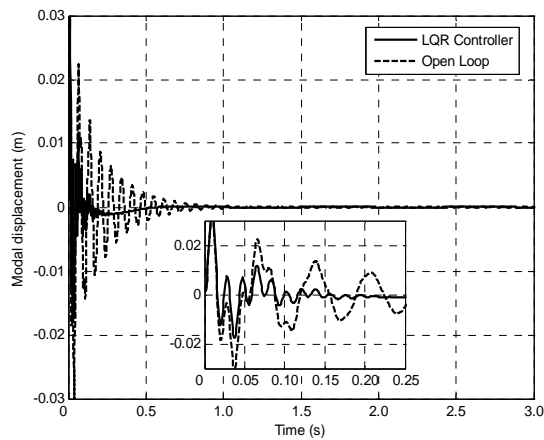
(c) Modal displacement.
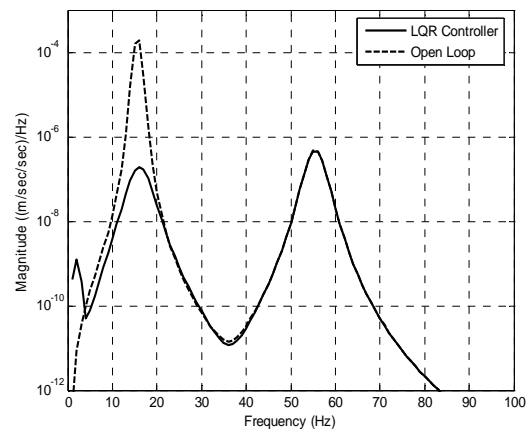
(d) PSD of modal displacement.

Figure 7. Response of the flexible manipulator with LQR Controller.
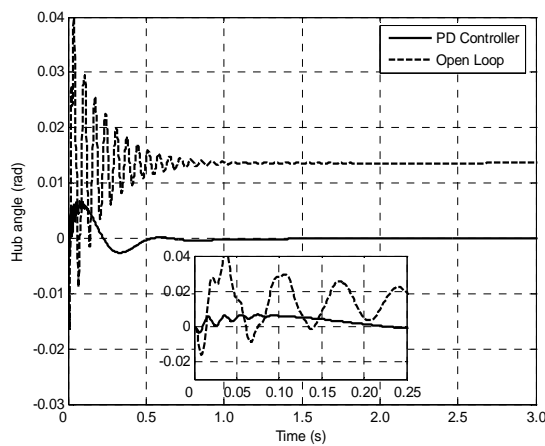
(a) Angular position.
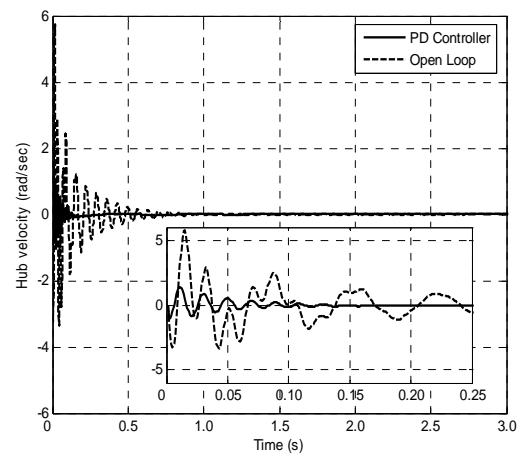
(b) Angular velocity.
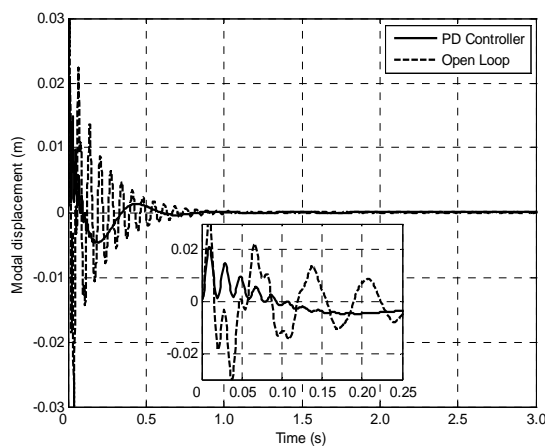
(c) Modal displacement.
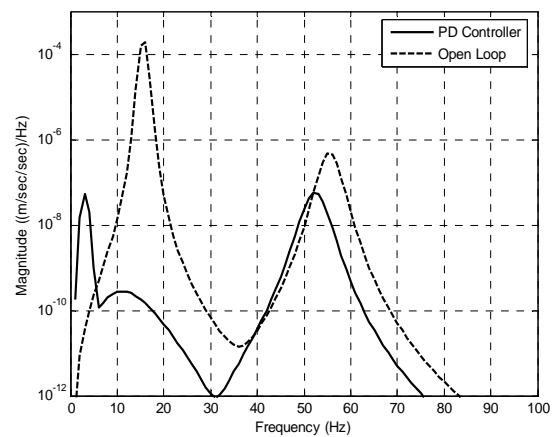
(d) PSD of modal displacement.

Figure 8. Response of the flexible manipulator with PD Controller.
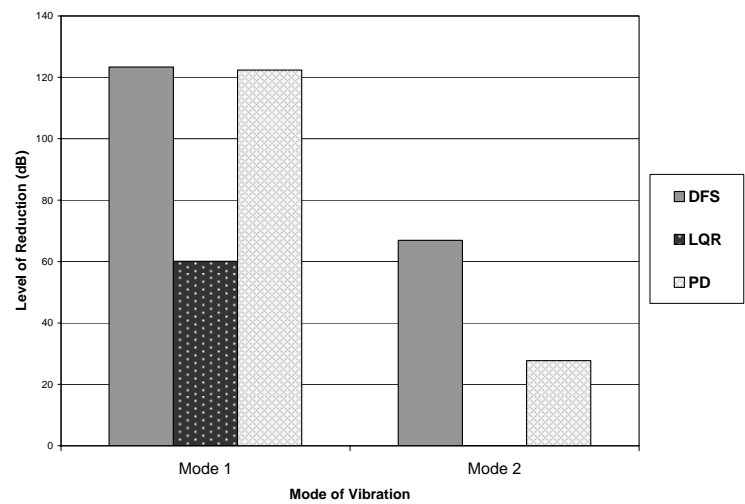
Figure 9. Level of vibration reduction using DFS, LQR and PD controller.

The ε-Core of a n-person Stochastic Cooperative Game

Zuofeng Gao

College of Science, Yanshan University, Qinhuangdao 066004, China

Hongxin Bai (Corresponding author)

College of Science, Yanshan University, Qinhuangdao 066004, China

Department of math and computer, Baoding College, Baoding 071051, China

E-mail: baihongxin1@126.com

Suting Zhang, Yongbo Yu, Chunyan Han, Hua Zhang

College of Science, Yanshan University, Qinhuangdao 066004, China

Abstract

In this paper, based on the core of the stochastic cooperative game (Oviedo, 2000, pp. 519-524), We define the $\varepsilon-$core of the stochastic cooperative game. Thus, we recuperate the defect in theory that the core is empty usual. And we introduce some characters and properties about the kind ε-core.

Keywords: Stochastic game, n-person stochastic cooperative game, Core, ε-core

Introduction

It is well known, there is difficult that the core of cooperative game, as a solution of the game because of the core of the game is empty usual. The core of the stochastic cooperative game which Suijs et al. developed in 1995. In order to solve the problem, this paper import the concept of ε-core and discuss the properties of the ε-core.

1. Basic definitions

The stochastic cooperative game which Suijs introduced denoted by $\Gamma = \left(N, \{X_S\}_{S \subset N}, (f_i)_{i \in N}\right)$, N is the set of players, X_S is the payoff function of the coalitions S, and every stochastic payoff has finite expectation.

We denote the stochastic payoff has X_S of S as $(d^S, r^S) \in R^S \times R^S$, and for all of i in S it satisfies $\sum_{i \in S} d_i \leq 0$, $\sum_{i \in S} r_i = 1, r_i \geq 0$. According to (d^S, r^S) the stochastic payoff of player i in S is equal to $d_i + r_i X_S$, and denoted by $(d^S, r^S)_i$. It is noted that $(d^S, r^S)_i$ is a stochastic variable. The set of all the payoff of S, we denoted by $Z(S)$, and the set all of the individually rational payoff S we denote by $IR(S)$. So

$$IR(S) = \left\{ (d^S, r^S) \in Z(S) \,\middle|\, \forall i \in S : d_i + r_i X_S \, f_i \, X_{\{i\}} \right\}.$$

Let $(d^N, r^N), (\tilde{d}^N, \tilde{r}^N) \in Z(N)$ are two stochastic payoff. If exist is a coalition S, for all of $i \in S$, we have $\tilde{d}_i + \tilde{r}_i X_S \, f_i \, d_i + r_i X_S$, and $\sum_{i \in S} (d^N, r^N)_i \leq X_S$ then we call $(\tilde{d}^N, \tilde{r}^N)$

dominate (d^N, r^N) with respect to S, and denoted by $(\tilde{d}^N, \tilde{r}^N) \, f_S \, (d^N, r^N)$.

We define the core of stochastic cooperative game Γ as the sets of payoffs which are undominated, and denoted by $core(\Gamma)$. i.e.

$$core(\Gamma) = \left\{ (d^N, r^N) \,\middle|\, \begin{array}{l} (d^N, r^N) \in IR(N), \text{there are no exist S} \\ \text{and } (\tilde{d}^N, \tilde{r}^N) \in Z(N), \text{satisfy}: (\tilde{d}^N, \tilde{r}^N) \, f_S \, (d^N, r^N) \end{array} \right\}$$

2. The ε core of a repeater n-person stochastic cooperative game

Definition 1   Let $\Gamma = \left(N, \{X_S\}_{S \subset N}, (f_i)_{i \in N}\right)$ be a n-person stochastic cooperative game, $\varepsilon \in R$, we denote the ε-core of Γ by

$$C_{\varepsilon}(\Gamma) = \left\{ (d^N, r^N) \in IR(N) \left| \begin{array}{l} \left| \sum\limits_{i \in S} (d^{\%}, p^{\%})_i - \sum\limits_{i \in S} (d^N, r^N)_i \right| \leq \varepsilon, \\ \forall S \subseteq N, \forall i \in N, \forall (d^{\%}, p^{\%}) \in Z(S), \sum\limits_{i \in S} (d, r)_i = X_N \end{array} \right. \right\}$$

When $\varepsilon = 0, C_{\varepsilon}(\Gamma) = C(\Gamma), C(\Gamma)$ is the 0-core of Γ. When ε is sufficient min, $C_{\varepsilon}(\Gamma) = \phi$;

When ε sufficient enough, $C_{\varepsilon}(\Gamma) \neq \phi$. Let $\varepsilon_0 = \inf \{ \varepsilon | C_{\varepsilon}(\Gamma) \neq \phi \}$, then we call $C_{\varepsilon}(\Gamma)$ is the least core of Γ and denoted by $LC(\Gamma)$.

It is noted that when the ε -core is not empty, the elements of the ε -core are not always stochastic payoffs of the stochastic cooperative game.

3. Result

Theorem 1. Let $(\Gamma^t)_{t=0}^m = \left(H, (\{X_S\}_{S \subset N}^t)_{t=0}^m \right)$ be a repeater n -person stochastic

cooperative game,if $\varepsilon < \varepsilon'$,then $C_{\varepsilon}((\Gamma^t)_{t=0}^m) \subset C_{\varepsilon'}((\Gamma^t)_{t=0}^m)$.

Proof. Let $(d^N, r^N) \in C_{\varepsilon}(\Gamma)$,be a stochastic payoff, for $\forall S \subseteq N$, $\forall (d^{\%}, p^{\%}) \in Z(S)$, $\forall i \in N$,

$$\sum\limits_{i \in S} (d^{\%}, p^{\%})_i - \sum\limits_{i \in S} (d^N, r^N)_i \leq \varepsilon$$

and $\varepsilon < \varepsilon'$, so

$$\sum\limits_{i \in S} (d^{\%}, p^{\%})_i - \sum\limits_{i \in S} (d^N, r^N)_i \leq \varepsilon$$

Then the stochastic payoff $(d^N, r^N) \in C_{\varepsilon'}(\Gamma)$,i.e. $C_{\varepsilon}((\Gamma^t)_{t=0}^m) \subset C_{\varepsilon'}((\Gamma^t)_{t=0}^m)$.

Theorem 2. Let $\Gamma = \left(N, \{X_S\}_{S \subset N}, (f_i)_{i \in N} \right)$ and $\Gamma' = \left(N, \{X'_S\}_{S \subset N}, (f_i)_{i \in N} \right)$ be two n -person stochastic cooperative game, there exist ε and ε',satisfy:

$C_{\varepsilon}(\Gamma) = C_{\varepsilon'}(\Gamma') \neq \phi$,then $\forall \delta > 0$, $C_{\varepsilon - \delta}(\Gamma) = C_{\varepsilon' - \delta}(\Gamma')$.

Proof.   First, we make proof $C_{\varepsilon - \delta}(\Gamma) \subseteq C_{\varepsilon' - \delta}(\Gamma')$. Let $(d^N, r^N) \in C_{\varepsilon}(\Gamma)$ be a stochastic payoff , and $(d^N, r^N) \in C_{\varepsilon}(\Gamma)$,

It is known

$C_{\varepsilon}(\Gamma) = C_{\varepsilon'}(\Gamma')$,

i.e. for $\forall S \subseteq N, \forall (d^{\%}, p^{\%}) \in Z(S), \forall (d^{\%}, p^{\%}) \in Z'(S), \forall i \in N$,

we have

$$\sum\limits_{i \in S} (d^{\%}, p^{\%})_i - \sum\limits_{i \in S} (d^N, r^N)_i \leq \varepsilon \tag{1}$$

$$\sum\limits_{i \in S} (d^{\%N}, p^{\%N})_i - \sum\limits_{i \in S} (d^N, r^N)_i \leq \varepsilon' \tag{2}$$

For $(d^N, r^N) \in C_{\varepsilon - \delta}(\Gamma)$, we have

$$\sum\limits_{i \in S} (d^{\%}, p^{\%})_i - \sum\limits_{i \in S} (d^N, r^N)_i \leq \varepsilon - \delta$$

$$\sum\limits_{i \in S} (d^{\%}, p^{\%})_i - \left(\sum\limits_{i \in S} (d^N, r^N)_i - \delta \right) \leq \varepsilon$$

From (1) and (2):

$$\sum\limits_{i \in S} (d^{\%N}, p^{\%N})_i - \left(\sum\limits_{i \in S} (d^N, r^N)_i - \delta \right) \leq \varepsilon$$

i.e. $\sum\limits_{i \in S} (d^{\%N}, p^{\%N})_i - \sum\limits_{i \in S} (d^N, r^N)_i \leq \varepsilon - \delta$

i.e. $(d^N, r^N) \in C_{\varepsilon' - \delta}(\Gamma')$, so $C_{\varepsilon - \delta}(\Gamma) \subseteq C_{\varepsilon' - \delta}(\Gamma')$.

Similarly

$C_{\varepsilon'-\delta}(\Gamma') \subseteq C_{\varepsilon-\delta}(\Gamma)$,

So

$C_{\varepsilon-\delta}(\Gamma) = C_{\varepsilon'-\delta}(\Gamma') \cdot$

Theorem 3. Let $\Gamma = \left(N, \{X_S\}_{S \subset N}, (f_i)_{i \in N}\right)$ and $\Gamma' = \left(N, \{X'_S\}_{S \subset N}, (f_i)_{i \in N}\right)$ be two n-person stochastic cooperative game, there are ε and ε', satisfy: $C_\varepsilon(\Gamma) = C_{\varepsilon'}(\Gamma') \neq \phi$, then for $\forall \delta > 0$, we have $LC(\Gamma) = LC(\Gamma') \cdot$

Proof. According to theorem 2, because of the randomlity of δ, so

$LC\left(\left(\Gamma^t\right)_{t=0}^m\right) = LC\left(\left(\Gamma'^t\right)_{t=0}^m\right) \cdot$

References

Gao, Z.F. (2007).The core of n-person repeated stochastic cooperative game. *Applied mathematics transaction of senior.* 22 (1), 1-8.

Gao, Z.F. (2006).Game theory and the economy. *China forestry*, (Chapter 4).

Liu, D.M. (1995).*Game theory and its application, defence-related science and of technology university,* (Chapter 4).

Oviedo J. (2000).The core of a repeated n-person cooperative game.European *Journal of Operational Research.* 127, 519-524.

Suijs J, Borm P, & De Waegenaere A et al.(1999). Cooperative game with stochastic payoffs. *European Journal of Operational Research*. 113, 193-205.

Suijs J, & Borm P. (1999). Stochastic cooperative game: superadditivity, convexity, and certainty equivalents.*Game and Economic Behavior*. 27, 331-345.

Suijs J, De Waegenaere A, & Borm P. (1998).*Stochastic cooperative game in insurance: Mathematics & Economics.* 22, 209-228.

Xie, Z.(2004).Game theory, *Publishing company of defence-related science and of technology university* (Chapter 6).

Empirical Researches on Corporate Governance of

China Commercial Banks Based on Panel Data

Zhongming Ding & Zhiqiang Hu

Anhui University of Finance & Economics, Bengbu 233041, China

Tel: 86-552-3171 666   E-mail: dingzm2006@sina.com

Abstract

This article empirically analyzes the relation between the corporate governance mechanism of China commercial banks and their performances based on the unbalanced panel data selected from 36 annual report samples in 12 Chinese commercial banks during 2003 to 2006, and the results indicate that the improvement of corporate governance of China commercial banks is the essential approach to enhance performances of commercial banks.

Keywords: Commercial bank, Corporate Governance, Empirical research, Panel data

1. Introduction

When the interim that China joined WTO was ended at the end of 2006, the era of comprehensive competition between China commercial banks and foreign capital banks has come. Facing more and more intense competition, only China commercial banks deepen system reform and perfect corporate governance of banks, they can really actualize sustainable developments.

Four China state-owned commercial banks except Agricultural Bank of China, Bank of China, China Construction Bank and Industrial and Commercial Bank of China all have come into the market. Shenzhen Development Bank, Shanghai Pudong Development Bank, China Minsheng Bank, Huaxia Bank, China Merchants Bank, Bank of Communications, Industrial Bank and CITIC Industrial Bank in Chinese national shareholding commercial banks all have come into the market. The forthgoers in urban commercial banks such as Nanjing Bank and Ningbo Bank have come into the market just before, and other urban commercial banks are also implementing finance recombination and introducing into strategic investors like a raging fire, gradually advancing shareholding reform, and in several years for the future, China commercial banks will come into the market cosmically. As viewed from the form, various shareholding commercial banks especially listed banks all form integrated corporate governance structure including shareholders conference, board of directors, board of supervisors, and management layer, but as viewed from the essential, it needs to further study how to father China commercial banks. Therefore, at the crises that China commercial banks implement shareholding reform and come into the market, it has especially important practical meanings to study the corporate governance of commercial banks.

2. Theoretical analysis

The problem of corporate governance can cast back to Smith Adam's "the wealth of the nations (1976)", but because of era limitation, the author didn't deeply expatiate this problem. After 156 years, Berle A. and Means (1932) really put forward modern corporate governance, i.e. to separate ownership from managerial authority induced the actions that managers departed from stockholder's benefits. After that, because the corporate governance of enterprise became increasingly serious, scholars such as Johnson and Maclean (1976), Phlip L. Cochran and Steven L. Wartick (1988), Michael Hart (1995) and Andrei Shleifer and Robert Vishny (1997) begun to deeply study this problem from different views.

Comparing with general corporate governance, the researches to bank corporate governance are comparatively late. From 1980 to 1997, serious problems occurred in three fourths of IMF member banks, and especially the Asian Financial Crisis in 1997 induced people's attention to the self corporate governance of commercial banks. In September 1999, Basel Committee issued the guide document of "Enhancing Corporate Governance for Banks" aiming at the corporate governance of commercial banks, which emphasized that the importance of corporate governance in the bank management and finance supervision, and the prologue to study corporate governance of commercial bank had been undrawn.

The corporate governance mainly solves the agent problem and the benefit eroded problem of big holding stockholders

to middle and small stockholders produced after the separation of owner and manager. It mainly has two sorts of solution, and one is the interior governance mechanism including shareholding structure, board of directors, board of supervisors and encouragement of senior managers, and the other one is the exterior governance mechanism including law system, market environment and so on. But the interior frangibility of commercial banks limits the function of the exterior governance mechanism (Cai, 2003, p.208), so this article mainly studies the corporate governance of commercial banks from the interior governance mechanism.

2.1 Shareholding structure and bank performance

The shareholding structure is the most important part of corporate governance of banks, and the researches on this domain are generally centralized in the contents such as the equity concentration ratio, shareholder character and the reasons that different types shareholding structure form, but these researches finally come down to the influences of shareholding structure to bank performance. To the influences of shareholding structure to bank performance, there still has not an accordant conclusion. Shleifer and Vishny (1986) thought the equity concentration ratio had positive correlation relation with bank performance (Shleifer, 1986), but Burkart, Gromb and Panunzi thought the equity concentration ratio had negative influences to bank performance (Burkart, 1997, p.693-728), and Cao, Tingqiu (2004) took 19 annual reports from 11 commercial banks during 2001-2003 as references, took return on assets (ROA) and return on equity (ROE) of banks as performance indexes, and found the shareholding structure of banks had no influences on bank performances (Cao, 2004, p.35-40), and Weihua and Liu, Jinyan (2005), Zhu, Jianwu (2005) and Sun, Yuejing (2006) all got the conclusions that the equity concentration ratio had negative correlation relation with bank performance.

2.2 Board of directors and bank performance

As the double status of stockholder agent and manager client, the board of directors decides its core status in the corporate governance of banks, which takes the decision-making rights and supervisory rights to banks. The researches on this aspect are mainly centralized in the influences of independent characters, behavior characters and encouragement character of board of directors to bank performance. Cao, Tingqiu (2004) thought the size of board of directors had positive influences to bank performance (Cao, 2004, p.35-40), Weihua and Liu, Jinyan (2005) found that the size of exterior directors had positive correlation relation with bank performance through research (Wei, 2005, p.77-82), and Zhu, Jianwu (2005) got the conclusion that the proportion of executive directors had positive correlation relation with bank performance (Zhu, 2007, p.33-40), in addition, both Zhu, Jianwu (2005) and Sun, Yuejing (2006) thought the factors such as the size of board of directors and meeting times and so on had no influences to bank performance. These opposite opinions may be related with different selected bank performance indexes and sample zones, All Cao, Tingqiu, Weihua and Liu, Jinyan, Sun, Yuejing adopted ROA and ROE as bank performances, but Zhu, Jianwu selected EVA return ratio as bank performance.

2.3 Board of supervisors and bank performance

Because the Britain and US mode doesn't weaken the board of supervisors and its functions, so there are few researches on the board of supervisors. Theoretically, the board of supervisors with big size could find problems existed in banks and implement effective supervision because it has more persons with different professional knowledge backgrounds, and more meetings of the board of supervisors indicate it exerts strong actions and isn't the form department of bank any more, which should actively influence bank performance. But in fact, the practices educed different conclusions. Zhu, Jianwu's researches found that the size of board of supervisors and meeting times had no influences to bank performance, and Sun, Yuejing (2006) also got the same conclusion (Sun, 2006, p.29-34).

2.4 Senior managers' salary and bank performance

Because the salary of senior manager can harmonize the agent friction between owner and manager, so it is regarded as one of most important corporate governance mechanisms (Shleifer, 1986). Through encouraging managers with professional bank management knowledge, the salary of senior manager makes their actions accord with stockholders' benefits, their aims accord with stockholders' aims to reduce agent costs and enhance bank performance. Ang, Lauterbach and Schreiber (2000) studied 166 US banks during 1993 to 1996 year, and they found that the salary structure of commercial bank CEO had large differences with CEO of other industries, and the salary of commercial bank CEO was not only higher, but the salary structure embodied more obvious encouragement effects (Ang, Lauterbach, 2000).

3. Design of researches

3.1 Research variables and sample data

3.1.1 Bank performance variables

Because the traditional single earning capacity index may induces accountant's operation and its preconditions are not mature, so in this article, we select accountant comprehensive index (IOAP) to measure the level of bank performance.

According to the particularity of commercial bank, when we consider the productiveness of commercial bank, we bring

into security and fluidity of bank index, select ROE, ROA, earnings per share (EPS), average return (AR), assets utilization (FU) as the earning capacity index of bank, choose loan-to deposit ratio (CD) and assets liquidity ratios (LD) as the fluidity index, use non performing loan (NPL), interest return ratio (LH), capital adequacy ratio (CAR), loan proportion of single largest client (OP) and loan proportion of ten largest clients (SP) to reflect bank security, and the definitions of   various original indexes are seen in Table 1.

We utilize the analysis technology of main component through the software SPSS to integrate information indicated by above indexes into a single index, accountant comprehensive index (IOAP), and this index fully reflect three characters of commercial banks including productiveness, fluidity and security. The practical operation process includes three steps. First, implement "unitization" processing to above 12 indexes respectively. Second, choose five main components through main component analysis which can explain 85% variance changes together. Third, compute the weighted average of those five main components by taking eigenvalue as the weight and obtain annual observation values of every bank.

3.1.2 Bank corporate governance variables

According to the research frame of corporate governance of commercial bank, this article implements empirical analysis to the influences of bank performance from four aspects including shareholding structure, board of directors, board of supervisors and the salary encouragement of senior manager.

(1) Shareholding structure. Adopt the stockholding proportion of the first largest stockholder (SI) and the stock-controlling proportion of the first largest stockholder (HC) to reflect the control power of the first largest stockholder to the bank, and if the value of HC is bigger than 1, so it indicates that the first stockholder in that bank has absolute control power. Use the sum of stockholding proportions from the second to the tenth largest stockholder (CST) to measure the concentration degree of shareholding structure of commercial bank and these stockholders' balance power, and use the virtual variable whether state-owned stock-controlling to measure the government's potential influences to the bank corporate governance mechanism.

(2) Board of directors. The governance of board of directors is embodied mainly through the independent character, action character and encouragement character of board of directors. So we select independent director proportion (IDP) and the virtual variable which reflects duty status of board chairman (deputy) and bank president to represent the independence of the board of directors, use the members of board of directors (SIZE) to represent the size of the board of directors, and use the annual meeting times of the board of directors (N) to represent the action character of the board of directors. We use the quantity of directors who don't draw salaries (NPA) to reflect the situation of bank exterior governance, because these directors generally are appointed by governmental department or holding stockholders, who have few contacts with the operation of the corporation, and the characters of exterior.

(3) Board of supervisors. The members of the board of supervisors (TP) represent the size of the board of supervisors, and the annual meeting times of the board of supervisors (JC) represent the action characters that the board of supervisors operates its functions.

(4) Salary of senior manager. Because the senior managers of China commercial banks possess few stock ownerships and the information is not clear, so we select one third of the salary gross of three senior managers who have the highest salaries (PAY) to measure the encouragement character of corporate governance of commercial banks.

3.1.3 Control variables

The bank scale reflects the capacities that bank obtain resources and implement investment opportunities, so we select the bank scale (TB) as the control variable. The specific variable definitions are seen in Table 2.

3.1.4 Sample data

The unclear information of commercial bank and the relative research data which are difficult to obtain are the main obstacles to implement empirical researches. To China, this problem is more notable, and because of the influences of system transform and total environment, the data issuances of China commercial bank are fewer than state-owned banks of developed countries. But in recent years, the annual reports continually issued by various commercial banks make the actuality of the information issuance change apparently and offer opportunities for relative researches. Based on that, this article takes the collected annual reports of China commercial banks as the data resources to empirically analysis the corporate governance and governance performance of China commercial banks. Considering that the commercial banks selected should have enough representations, so this article chooses sample data from three layers. The first layer is the solely state-owned commercial banks, and we select two years' data from 2005 to 2006 of Bank of China, China Construction Bank and Industrial and Commercial Bank of China which have comparatively abundant information issuances. The second layer is the shareholding commercial banks, and we select four years' data from 2003 to 2006 of China Merchants Bank, Huaxia Bank, China Minsheng Bank, Shenzhen Development Bank, Shanghai Pudong Development Bank and CITIC Industrial Bank, and two years' data from 2005 to 2006 of Bank of Communications. The third layer is the urban commercial banks, and we select two years' data from 2005 to 2006 of Nanjin Bank and Ningbo Bank just listed. We select 36 groups of sample data together to compose unbalanced panel data. The annual

reports of banks are obtained from the web of "http://www.cninfo.com.cn/" and the public web of various banks.

3.2 Descriptive statistical analysis

3.2.1 Corporate governance characters of state-owned commercial banks

We implement descriptive statistical analysis to the first layer in commercial banks, i.e. the corporate governance of state-owned commercial banks, and the results are seen in Table 3.

From Table 3, we can see the establishment and governance of corporate governance mechanism after the stockholding transform of state-owned commercial banks.

First, as viewed from shareholding structure, the mean of the first largest stockholder's holding proportion achieves more than 50% and the mean of the stock holding achieves 1.88, and the mean of the second largest to the tenth largest stockholders' holding proportion is 40.12%. Absolute stock holding of the country indicates the equity of state-owned commercial banks after stockholding transform is still centralized in the country, and though the second largest to the tenth largest stockholders have certain restrictions to the first largest stockholder, but under the absolute state-own stock holding condition, other stockholders are difficult to their restriction functions to the first largest stockholder.

Second, as viewed from the board of directors, the mean of the size of board of directors is 15.88 persons, the mean of proportion of independent directors is 25.81%, in 87.5% of banks, the board chairman and president are the same person, and the annual meeting times of board of directors is 8.6. From that, we can see that board of directors of China commercial banks has larger size and fewer independent directors.

Third, as viewed from the board of supervisors, the mean of members of the board of supervisor is 6.6, the annual meeting times are 4.5, and we can see that the board of supervisors has small size and weak action power.

Fourth, as viewed from the salary of senior manager, the average salary of the three senior managers who have the highest salaries is 1.1989 million Yuan.

3.2.2 Corporate governance characters of shareholding commercial banks

The corporate governance mechanism of shareholding commercial banks is comparatively perfect in China commercial banks. And we can obtain comparatively better corporate governance characters of commercial banks through descriptive statistical analysis to corporate governance variables of sample banks during 2003 to 2006. The results are seen in Table 4.

From Table 4, we can see following four aspects.

(1) Shareholding structure. The mean of the first largest stockholder's holding proportion is 15.26% and the mean of the stock holding achieves 0.899, and the mean of the second largest to the tenth largest stockholders' holding proportion is 32.74%. 70.83% of banks are held by the country. It indicates that the shareholding structure of China shareholding commercial banks is relatively centralized, the first largest stockholders has no absolute control power, the second to the tenth largest stockholders have strong balance function to the first largest stockholder, but most equities are centralized in the country.

(2) Board of directors. The mean of the size of board of directors is 16 persons, the mean of proportion of independent directors is 33%, only in 87.5% of banks, the board chairman and the president are the same person, and the annual meeting times of board of directors is 9.5. From that, we can see that board of directors of China commercial banks has larger size and fewer independent directors, but the leading structure has strong independence and the board of directors has strong action power.

(3) Board of supervisors. The mean of members of the board of supervisor is 8.63, the annual meeting times are 5, and we can see that the board of supervisors has comparatively reasonable size, but it has fewer annual meeting times and weak action power.

(4) Salary of senior manager. The average salary of the three senior managers who have the highest salaries is 1.248 million Yuan, but the maximum of 4.7167 million Yuan and the minimum of 0.2492 million Yuan have a large difference.

3.3 Multiple regression analysis

3.3.1 Research method and model enactment

The panel data is the data collection with two-dimensional structure which takes time list extend along space direction and takes section data extend along time direction. It can not only reflect the rules of various individual data in certain term, but also can describe the rule of every individual with the changes of time, and reflect mutual advantages of time list and section data.

The basic form of panel data model is:

$y_{it} = \alpha_{it} + x'_{it}\beta_{it} + \mu_{it}$, i=1, 2 …, n, t= 1, 2…, T.   (1)

Where, y_{it} is the attributive variable, x_{it} is the $K \times 1$ directional explanation variable with, T is the sum of observation terms of every section member. Parameter α_{it} represents the constant of the model, β_{it} is the coefficient vector corresponding to the regression vector x_{it}. Random errors μ_{it} are independent mutually and fulfill the hypothesis of zero mean and equal variance. On the member section, this model includes n section member equations together, and on the time section, this model includes T time section equations together.

In the model described in equation (1), the free degree (nT) is far smaller than the number of parameter ($nT(K+1)$, which is the number of parameter describing the distribution μ_{it}), which makes the model can not be estimated. To actualize the estimation of the model, we suppose that the parameter fulfill the coherence of time, i.e. the parameter values don't change with the difference of time. Therefore, the model can be simplified as:

$$y_{it} = \alpha_i + x_{it}^{'}\beta_i + \mu_{it} \tag{2}$$

Where, parameter α_i and β_i are the constants in the individual term, which values are influenced by different section units. According to different restriction requirements of intercept α_i and coefficient vector β_i, we can divide the panel data model described in equation (2) into three sorts including invariable coefficient model without individual influences, i.e. the mixed estimation model, invariable coefficient model with individual influences, and the variable coefficient model with individual influences. If the coefficient α_i is the definite variable, i.e. the omitted factors in the model have fixed influences to the individual differences, so the model is the fixed effect model, and if the coefficient α_i is the random variable, i.e. the omitted factors in the model have random influences to the individual differences, so this model is the random effect model (Gao, 2006, p.302-326).

This article studies the influences of corporate governance mechanism to bank performance, implements analysis by the samples themselves, doesn't deduce the individual differences of the collectivity by the samples, so the random effect model can be eliminated, and we adopt the test method of covariance to consider selecting the mixed estimation model or the fixed effect model.

H_0: To different section model, intercepts are same, i.e. we should establish the mixed estimation model.

H_1: To different section model, intercepts are different, i.e. we should establish the fixed estimation model.

The statistic F can be defined as:

$$F = \frac{(SSEr - SSEu)/(T+K-2)}{SSEu/(NT-T-K)} \sim F_\alpha(T-1,\ NT-T-K) \tag{3}$$

Where, $SSEr$ and $SSEu$ respectively represent the sum squared resid of the mixed estimation model and the individual fixed effect model, T is the time and K is the explanation variable.

Through the software of Eview5.1, we can obtain $SSEr$ =1.735, $SSEu$ =0.0783, T =4, K =13, and F =26.93 and we can get corresponding critical value through F distribution table:

$F_{0.05}(3,16)$ =3.24.

Because $F > 3.24$, so we reject the former hypothesis and should establish individual fixed effect model:

$$IOAP_{it} = b_0 + b_1 \times SI_{it} + b_2 \times HC_{it} + b_3 \times CST_{it} + b_4 \times DG_{it} + b_5 \times SIZE_{it}$$

$$+ b_6 \times IDP_{it} + b_7 \times NP_{it} + b_8 \times NPA_{it} + b_9 \times TP_{it} + b_{10} \times DN_{it} + b_{11} \times JN_{it} + b_{12} \times PAY_{it}$$

$$+ b_{13} \times TB_{it} + \varepsilon_{it} \tag{4}$$

Where, b_0 is the constant, b_j (j =1, 2, 3…) is the regression parameter of corresponding explanation variable, ε_{it} is the random error, i =1, 2…,12, which includes all samples from 12 banks, t represents four years' time from 2003 to 2006, SI_{it} is the first largest stockholder's holding proportion of the i th bank in the year of t, HC_{it} is the first largest stockholder's stock controlling proportion of the i th bank in the year of t, in this way, TB_{it} is the size of the i th bank in the year of t.

3.3.2 Regression result and analysis

Because of different perfect degrees of corporate governance mechanism of various commercial banks and great differences among bank scales, i.e. so-called cross section heteroscedasticity, so in the model estimation, we adopt the generalized least square method modified by section unit heteroscedasticity and the estimation software Eviews5.1.

The parameter estimation results and statistical test results of the model are seen in Table 5.

From the results of regression, both the value of R^2 and the value of R^2 after modification are higher and achieve above 99%, the value of F also achieves 1% of notable level, the value of D.W is reasonable, which indicates that the matching degree of the model is higher and the total of independent variable has strong explained powers for attributive variables. Especially the equation re-estimated after eliminating the corresponding explanation variables of statistical non-notable parameter estimation has better statistical effect, and every independent variable is notable on 1% of the level. The analysis of the regression results includes following four aspects.

(1) Shareholding structure. The first largest stockholder's holding proportion has positive correlation relation with bank performance on 1% of the notable level, which indicates that the equity concentration is propitious to correct stockholders' actions of "pick-up" and the rise of the first largest stockholder's holding proportion has positive influences to enhance bank performance. The first largest stockholder's controlling proportion has negative correlation relation with bank performance, but the statistical test is not notable, and the reason may be that the first largest stockholder's controlling proportion is higher, it has stronger control power to banks, which makes the first largest stockholder not only may erode other stockholders' benefits, but also has enthusiasms to try to enhance the management level of bank, and both functions would balance out, so the first largest stockholder has not obvious function to bank performance. The sum of the second to the tenth largest stockholder's holding proportion presents positive correlation relation with bank performance on 5% of the notable level, which indicates the second to the tenth largest stockholders of China commercial banks have equity balance function to the first largest stockholder and reduce the first largest stockholder's "tunneling effect" to bank performance. State-owned equity has notable positive correlation relation with bank performance, which may be the selected samples after 2003, and at that time, the banks reform has begun, and the state-owned shareholding banks can get great policy and capital supports of the government, accordingly the bank performance is enhanced to a certain extent.

(2) The governance of board of directors. The size of board of directors presents negative correlation level with bank performance on 1% of the notable level, which indicates huge size of board of directors may induce low efficiency of board of directors, accordingly influence the enhancement of bank performance. The independent director proportion (IDP) has notable negative correction relation with bank performance, which indicates the independent directors of China commercial banks have not exerted their own supervisory functions. The combination of both duties presents negative correlation relation with bank performance, but statistical test is not notable, which may be China commercial banks generally request both duties of board chairman and bank president are separated, so the differences among samples are not big and counteract functions to bank performance. The meeting times of board of directors present positive correction relation with bank performance, but the statistical test is not notable, which indicates the meeting of board of directors may stay on the form, can not exert its supervisory functions of manager and bank development strategy, can not enhance bank performance. The number of directors who don't draw salaries in the bank presents positive correlation relation with bank performance, but the statistical test is not notable, and these directors basically belong to exterior directors of the bank and come from main stockholder corporations of the bank, and theoretically they can exert supervisory functions to bank managers, but in practice the operation is difficult, because they represent different stockholders' corporate benefits and induce different opinions and influence bank decisions in the board of directors.

(3) The governance of board of supervisors. The size of board of supervisors presents positive correlation relation with bank performance on 1% of the notable level, which indicates that the number increase of board of supervisors increases the board of supervisors' ability and efficacy to supervise bank managers. The meeting times of board of supervisor present positive correlation relation with bank performance on !% of the notable level, which indicates that the board of supervisors in the bank is exerting its function, begins to supervise senior manager, harmonize board of directors and promote the developments of banks.

(4) The salary of senior manager. The average salary of senior manager presents positive correlation relation with bank performance, but the statistical test is not notable, which indicates the salary policy of China commercial banks has not exerted its function, and the encourage mechanism is absent. The reasons may come from two aspects. First, at present, most senior managers' salaries of China commercial banks have not related with bank performance, so the senior managers' higher salaries don't represent higher performance of banks. Second, the senior managers' salaries have not been related with their contributions to the future developments of banks, there are no long-term encouragements, and the real enhancements of bank performance are influenced.

4. Conclusions

This article selects 36 groups of sample data from 12 banks to compose unbalanced panel data and implements empirical analysis to the influences of corporate governance mechanism of China commercial banks to bank performance. The part empirical results include three following aspects.

First, sample data selected in this article are comparatively few, which reflect that the information issuance mechanism of China commercial banks is not perfect and needs further strengthen the transparence of China commercial banks.

Second, through descriptive statistical analysis, we find that whether former state-own commercial banks just listed or

shareholding commercial banks with comparatively perfect corporate governance all have many problems in the corporate governance mechanism. For example, the size of board of directors is too huge, the proportion of independent director is too low, the action power of board of supervisors is not strong, the encouragement mechanism is not perfect, and especially the problem that state-owned equity is too huge. The corporate governance of commercial banks is "similar in shape not in spirit", so it needs to be further optimized.

Third, through multiple regression analysis, we find the bank performance is intensely related with structure variables of corporate governance, especially those invariables which reflect equity structure such as the holding proportion of the first largest stockholder, the sum of holding proportion of the second to the tenth largest stockholder, whether state-owned holding equity and so on, and the size of board of directors and the independent director proportion which reflect the governance of board of directors, and the size of board of supervisors and the annual meeting times of board of supervisors which reflect the governance of board of supervisors. The results indicate the improvement of bank corporate governance is the essential approach to enhance the values of banks.

References

Ang, Lauterbach & Schreiber. (2000). Pay at the Executive Suite: How do U.S. Banks Compensate their Top Management teams? *Unpublished paper of Florida State University.*

A. Shleifer & R. Vishny. (1997). A Survey of Corporate Governance. *Journal of Finance.* No.52. p.737-783.

Burkart M., D. Gromb & F. Panunzi. (1997). Large Shareholders, Monitoring and the Value of the Firm. *Quarterly Journal of Economics.* No.112. p.693-728.

Cai, Esheng, et al. (2003). *Corporate Governance and Control of Banks.* Beijing: Economic Science Press. p.208.

Cao, Tingqiu. (2004). Governance of Shareholding Commercial Banks: the Empirical Analysis Based on Annual Report. *Reform.* No.6. p.35-40.

Gao, Tiemei. (2006). *Econometrical Analysis Method and Modeling: Application and Examples of Eviews.* Beijing: Tsinghua University Press. p.302-326.

Shleifer, Andrei & Robert W. Vishny. (1986). Large Shareholders and Corporate Control. *Journal of Political Economy.* No.9.

Sun, Yuejing. (2006). An Empirical Study on Relationship of Corporate Governance. *Research on Financial and Economic Issues.* No.3. p.29-34.

Weihua & Liu, Jinyan. (2005). Management Mechanism within Commercial Bank and Its Influence on the Performance of the Bank. *NaiKai Journal.* No.1. p.77-82.

Zhu, Jianwu, et al. (2007). An International Comparative Analysis of Small and Medium Banks' Performance. *Finance & Economics.* No.1. p.33-40.

Table 1. Definitions of original indexes

Index	AB. of index	Explanation of index
Earning Capacity	ROE	The ratio of retained profits and stockholder's share
	EPS	The ratio of net assets and ordinary stock gross at the end of the report term
	ROA	The ratio of net income and total assets
	AR	The ratio of total profits and employee quantity
	FU	The ratio of taking and average total assets
Fluidity	CD	The ratio of various loan gross at the end of the report term and deposit gross
	LD	The ratio of floating assets and floating debts
Security	NPL	The proportion of bad loans to total loans
	LH	The ratio of interests received at the end of term to total interests
	CAR	The proportion of net capitals to total capitals
	OP	The ratio of loan balances for same loan client to total capitals
	SP	The ratio of loan amount for ten largest clients to total capitals

Table 2. Definitions of various variables

Variable	Variable name	Explanation of variable name
IOAP	Accountant comprehensive index	The bank performance reflected by comprehensively considering productiveness, fluidity and risk
SI	Stockholding proportion of the first largest stockholder	The stockholding proportion of the first largest stockholder to total stocks
HC	Stock-controlling proportion of the first largest stockholder	The stockholding proportion of the first largest stockholder to the stockholding difference between the first largest stockholder with five former largest stockholders
CST	Stockholding concentration	The sum of stockholding proportions from the second to the tenth largest stockholder
Dg	Whether state-owned stock-controlling	Virtual variable, state-owned stock-controlling is 1, or else is 0
SIZE	The size of board of directors	The member quantity of board of directors in the report term
IDP	Independent directors proportion	The proportion of independent directors all directors
NP	Combination of two duties	Virtual variable, suppose that the bank president and (deputy) board chairman are one person, so the variable is 1, or else is 0
DN	Annual meeting of board of directors	The meeting times convened by board of directors in the same year (including communication meeting)
NPA	Directors who don't draw salaries from bank	The quantity of directors who don't draw salaries in the report term
TP	The size of board of supervisors	The member quantity of supervisors in the report term
JN	Meeting times of board of supervisors	The meeting times convened by board of directors in the report term
PAY	Average salaries of senior managers	One third of the salary gross of three senior managers who have the highest salaries
TB	The size of bank	The natural logarithm of total back assets at the end of the year

Table 3. Corporate governance variable statistics of state-owned commercial banks

Item	Mean	Median	Maximum	Minimum	Std. Dev.
SI	0.503325	0.5575	0.8315	0.2178	0.223
HC	1.88145	1.7226	4.9347	0.5347	1.525
CST	0.4012	0.4096	0.604	0.1685	0.1304
DG	1	1	1	1	0
SIZE	15.875	16	19	13	1.959
IDP	0.2581	0.2566	0.3125	0.2143	0.0299
NP	0.875	1	1	0	0.3535
NPA	6.625	6.5	8	6	0.744
TP	6.625	6	9	4	2.133
DN	8.625	9.5	12	3	3.622
JN	4.5	5	6	2	1.414
PAY	119.886	121.57	152.71	86.2	22.528

Table 4. Corporate governance variable statistics of stockholding commercial banks

Item	Mean	Median	Maximum	Minimum	Std. Dev.
SI	0.1526	0.1603	0.34	0.0598	0.0779
HC	0.899	0.591	2.548	0.2935	0.7648
CST	0.3274	0.3197	0.4895	0.088	0.1218
DG	0.7083	1	1	0	0.4643
SIZE	16.083	17	19	13	2.1653
IDP	0.3304	0.353	0.4117	0	0.083
NP	0.1667	0	1	0	0.3807
NPA	6.375	7	10	0	3.36
TP	8.625	9	11	7	1.096
DN	9.542	9	15	5	3.31
JN	5	4.5	13	2	2.246
PAY	124.8	83.31	471.67	24.92	108.79

Table 5. Multiple regression statistics

Explained variable (IAOP)			
Explanation variable		Equation (4)	Equation (5)
Stockholding structure	SI	1.903235* (3.805123)	1.476062* (18.65169)
	HC	-0.069879 (-1.537004)	--
	CST	0.736499** (2.736304)	0.574852* (9.101275)
	DG	0.534787* (7.244697)	0.712878* (9.028681)
Governance of board of directors	SIZE	-0.092372* (-6.098518)	-0.092908* (-32.75789)
	IDP	-0.726868* (-7.780650)	-0.625409* (-5.917374)
	NP	-0.014542 (-0.393882)	--
	NPA	0.013877 (1.629651)	--
	DN	0.001757 (0.279774)	--
Board of supervisors	TP	0.052169* (3.510236)	0.050185* (13.30411)
	JN	0.049715* (3.221976)	0.059679* (11.77652)
Salaries of senior managers	PAY	5.24E-05 (0.447106)	--
Control variable	TB	0.950638* (9.254706)	0.926314* (10571.35)
R^2		0.997696	0.999983
Adj. R^2		0.992670	0.999962
Statistic F		198.4873*	48410.70*
Value of D.W		2.25	2.14

Notice: Those values in the bracket are the T statistics of various variables, "*" denotes the notable level of 1%, "**" denotes the prominence level of 5%, and the equation (5) is obtained from equation (4) which is eliminated corresponding explanation variables of non-notable parameter evaluations.

Bed Expansion Characteristics of

Liquid-Solid Fluidized Bed with Internals

E. Ramaswamy

Department of Chemical Engineering

Coimbatore Institute of Technology

Coimbatoe-641014

India

C.Srinivasakannan

Monash University Malaysia

2-Jalan University

Bandar Sunway

46150 Petaling Jaya

Selangor

Malaysia

N.Balasubramaniam (Corresponding author)

Department of Chemical Engineering

A.C.Tech. Campus

Anna University-Chennai

Chennai-600 025

India

Tel: 91-44-2220 3501   E-mail: nbsbala@annauniv.edu

Abstract

It is attempted in the present investigation to study the influence of internals in the riser of liquid-solid fluidized bed. Experiments on bed expansion characteristics in liquid-solid fluidized bed have been carried out in a conventional liquid-solid fluidized bed and in a fluidized bed having string plates of spheres and twisted tapes as internals covering wide range in operating conditions. It has been observed in the present investigation that an increase in particle diameter, density and twist ratio is found to decrease the bed voidage and an increase in the pitch of the string increases the bed voidage. Further it has been observed that the bed voidage is higher in fluidized bed without internals when compared to fluidized bed with internals for a given operating conditions. A model based on slip velocity has been developed for predicting bed voidage and observed that more than 92% of the experimental data match with the model predictions within 10% error.

Keywords: Liquid-solid fluidized bed, Internals, Bed expansion, Slip velocity

1. Introduction

Fluidized beds find extensive applications in chemical process industries as they provide large interfacial area, high degree of mixing, and temperature uniformity. In particular, liquid-solid fluidized beds are increasingly used in chemical processes such as fermentation, biological wastewater treatment, flue gas desulfurization, ore reduction etc. Although fluidization can be achieved either by liquid or gas as fluidizing medium, gas fluidized beds have gained more importance in scientific community due to its far more applications. This is in spite of the fact that   possible uses of liquid fluidisation in the mining industry   were suggested as early as in 16th century   as a means of separating solids of   different sizes.   Since the emergence of biosciences in the recent years and the adaptability of liquid fluidized bed for various applications, the importance of solid-liquid fluidized bed is receiving greater attention among scientists and researches (Yang & Renken, 1998, pp. 537–544).

In recent years, the applications of liquid–solid fluidized beds are being extended for hydrometallurgy, food technology, biochemical processing, water treatment, etc (Narvaez, Orio, Aznar & Corella, 1996, pp. 2110–2120. Olivares, Aznar, Caballero, Gil, Frances & Corella, 1997, pp. 5220– 5226. Narvaez, Orio, Aznar & Corella, 1996, pp.2110–2120). Scientific research concerns with reference to the hydrodynamic structure of liquid-particles, the equilibrium forces for fluid-particle interactions and heat or mass transfer properties in fluidized beds. Fluidization quality is closely related to the intrinsic properties of particles, e.g. particle density, particle size and size distribution, and also their surface characteristics. The expansion characteristic of solid particles in a liquid-solid fluidized bed is a function of superficial liquid velocity. A quantitative relationship linking the bed expansion with these parameters is necessary for a fundamental understanding of fluidization behavior and subsequent applications (Richardson & Jeronimo, 1979, pp. 1419–1422. Kmiec, 1982, pp.133–136).

The bed expansion characteristic is an important parameter in the design of fluidized beds. Extensive work has been reported on bed expansion characteristics in liquid-solid fluidized bed. A comprehensive work attempted by Renzo Di Felice (Renzo, 1995, pp. 1220-1225) identified four different types of bed expansion behavior with gradual transition from one to another occurring as the physical conditions are changed. Suitable predictive bed expansion equations for each of the region were presented. Although the use of internals to reduce axial mixing and enhance the conversion in liquid phase is well known, studies relating to bed expansion characteristics in liquid-solid fluidized bed with internals are very scarce. It is attempted to study bed expansion characteristics of liquid-solid fluidized beds with internals such as twisted tapes and string of spheres in the present study. A theoretical work is attempted to predict the bed expansion characteristics, based on slip velocity.

2. Experimental

The schematic representation of experimental set-up shown in Figure 1, consist of a glass column of 75mm internal diameter and height of 750mm. The column has three sections: calming section (7) at the bottom, test section (8) in the middle and disengaging section (9) at the top of the column. Glass beads and sand particles of different sizes were used as solids particles. The fluidizing particles are supported by a wire mesh having 1.5mm perforation fitted at the bottom column. PVC solids spears of 25mm and 50mm diameters were fixed on a 3mm rod were used as internals. The spheres pitch has been varied from one column diameter to 3-column diameter to check the effect of the pitch on bed hydrodynamics. Similarly the diameter of twisted tapes were 25mm, and the twist ratio varied from 3.22 to 14.44. The liquid from the storage tank was pumped through a control valve (4) and the flow rate was measured by a rotameter (3) connected on the line. The liquid enters the through calming section (7) and leaves through disengaging section (9). The disengaging section has the provision for addition of particles into the test section. The column pressure drop has been estimated using a U tube manometer connected via pressure tappings (6). The height of solids in the column was measured with respect to change in flow rate of the liquid and bed voidage. The bed voidage can be estimated using the fluidization equation,

$$\Delta P = \frac{W}{A} = L(1-\varepsilon)(\rho_S - \rho_l) \tag{1}$$

Experiments were carried out covering a wide range in operating conditions and the results are presented in the Figures 2-7. The minimum fluidization velocity for the solids materials has been estimated using Wen and Yu (Wen and Yu, 1962, pp.100) equation, i.e.

$$U_{mf} = \frac{\mu_g}{d_p \rho_g} \sqrt{(33.7)^2 + 0.0408 \frac{d_p^3 \rho_g (\rho_s - \rho_g) g}{\mu_g^2}} - 33.7 \tag{2}$$

The minimum fluidization velocity has also been estimated experimentally. It has been observed that the experimental prediction match with the prediction using equation (2) within ± 5% error. The Figure 2 shows the variation of bed voidage with liquid velocity. It can be seen from figure 2 that the bed voidage increases with an increase in liquid velocity. The rate of increase of bed voidage is high at the beginning and gradually reduced to marginal with liquid rate. It can also be ascertained from the figure that the voidage decreases with increasing solid particle size. These observations are in qualitative agreement with the observations reported in literature (Handley, Doraisamy, Butcher and Franklin, 1966, pp. 260-273). Similar observation has been recorded for the system having twisted taps as internals [Figure 3].

Experiments were carried out with sand and glass beads of same size, to study the effect of particle density on bed voidage and the observations are given is given in Figure 4. It can be ascertained from Figure 4 that an increase in the particle density decreases the bed voidage. An increase in bed voidage with decrease in particle size and density is well understood in conventional fluidization and the present observations are in qualitative agreement the reported literature.

An increase in particle density leads to an increase in the particle Archimedes number, i.e. the gravitational forces resulting in reduction in bed voidage.

The Figures 5 & 6 show the effect of pitch of sphere pitch and twist ratio on bed voidage. It can be ascertained from the figures that the bed voidage increases with an increase in the pitch of the spheres as well as the twist ratios of twisted tapes. An increase in twist ratio reduces the number of twists in the bed while with an increase in the pitch of

the spheres reduces the number of spheres in the bed resulting in an increase in the bed voidage. This can be explained that the presence of internals reduces the bed voidage due to i) hindrance effect on free upward flow of fluidizing particle ii) formation of eddies. The liquid move along the internals resulting in the localization of solids in eddies. This is evident from the higher bed voidage in fluidized bed without internals as compared to fluidized bed with internals under similar fluidization conditions.

3. Slip Velocity

Solids concentration in a liquid-solid fluidized bed may be considered to depend upon the relative velocity particle characteristics (Richardsonand Zaki, 1954, pp. 35-53) i.e.

$$\varepsilon = f\,(U_s, d_p, \rho_s) \tag{3}$$

where Us is the slip velocity between the phases, which is defined as the relative velocity difference between the phases, i.e.

$$U_s = \frac{U_c}{\varepsilon} \pm \frac{U_d}{1-\varepsilon} \tag{4}$$

where U_c and U_d refer the true velocity of continuous and dispersed phases respectively. when U_c is zero U_d tends to zero. The positive sign refers to counter current operation while negative sign represents concurrent operation. Slip velocity defined as above represents free fall velocity of a single particle in an infinite medium. However in a medium of finite particle population, it differs from the free fall velocity due to the presence of other particles. Several empirical models and correlations have been proposed to predict the relative velocity between the phases. Barnea & Mizrahi (Barnea & Mizrahi., 1973, pp. 171) considered in detail for creeping flow, the hindrance effects in sedimentation and fluidization and classified them into, pseudo hydrostatic effect, momentum transfer effect and wall hindrance effect. Taking into account all these effects the authors proposed the following equation for fluidization of liquid drops,

$$\frac{U_s}{U_t} = \frac{\varepsilon}{\left(\left[1+(1-\varepsilon)^{\frac{1}{3}}\right]\exp\frac{5(1-\varepsilon)}{3\varepsilon}\right)} \tag{5}$$

U_s/U_t is the ratio of true fall velocity of a particle in medium of particle population, to the free fall velocity of a particle in an infinite medium. 'ε' in the numerator arises from choosing the mixture density for buoyancy effect, the pre-exponential term in denominator accounts for hindrance effect due to the presence of other particles, the exponential term is the correction due to the momentum transfer effect. Since the momentum transfer and hindrance effects are introduced in terms of particle holdup, the above equation may be modified and written as,

$$\frac{U_s}{U_t} = \frac{\varepsilon^n}{\left(1+(1-\varepsilon)^{1/3}\right)^m} \tag{6}$$

n is equal to 1 for creeping flow and 2/3 for intermediate flow range of Reynolds number. The experimental data of the present study corresponds to the intermediate range of Reynolds number ($1 < Re_t < 1000$). Substituting the single particle rise velocities in infinite medium for intermediate region the corresponding equation for slip velocity is,

$$U_s = \left[\frac{4gd_p\Delta\rho}{3k\rho_l^{0.5}\mu^{0.5}}\right]^{2/3}\left[\frac{\varepsilon^{2/3}}{\left(1+(1-\varepsilon)^{1/3}\right)^{2m/3}}\right] \tag{7}$$

Where k=10 for specified Reynolds number range.

The index m accounts for particle-particle, particle-wall effects. The value of m is has been evaluated using experimental data for the specified Reynolds number range covered in the present investigation by minimizing the error as given in following equation:

$$\sqrt{\frac{\sum\left(U_{S\,\exp} - U_{S\,pred}\right)^2}{n-1}} \tag{8}$$

The value of m for liquid solid fluidized bed with as internals in the present study has been observed to be 1.4. The particle terminal velocity and drag co-efficient can be estimated using the following equations (Wen & Yu, 1966, pp. 610):

Terminal velocity

$$U_t = \frac{g(\rho_s - \rho_g)d_p^{\,2}}{18\mu_g} \qquad \text{for Re} < 0.4 \tag{9}$$

$$U_t = \left[\frac{4}{225} \frac{(\rho_s - \rho_g)^2 g^2}{\rho_g \mu_g} \right]^{1/3} d_p \qquad \text{for } 0.4 < \text{Re} < 500 \tag{10}$$

$$U_t = \left[\frac{3.1(\rho_s - \rho_g)gd_p}{\rho_g} \right]^{1/2} \qquad \text{for } 500 < \text{Re} \tag{11}$$

and

$$C_D \text{Re}^2 = \frac{4gd_p^{\,3}\rho_g(\rho_s - \rho_g)}{3\mu_g^{\,2}} \tag{12}$$

The slip velocity estimated using the above analysis has been compared with the experimental observations [Figure 7]. It can be ascertained from the figure 7 that the predicted slip velocity using the present slip velocity model math satisfactorily with the experimental observations.

4. Conclusion

Experiments were carried out on bed expansion in a liquid solid fluidized bed with internals. It has been observed from the present investigation that the bed voidage increases with an increase in the internals pitch/twist ration and decreases with an increase in diameter of the string. The bed voidage is higher in fluidized bed with internals than the conventional fluidized bed under same operating conditions. A slip velocity model has been proposed is developed and compared with the experimental data due to the present study.

References

A. Olivares, M.P. Aznar, M.A. Caballero, J. Gil, E. Frances & J. Corella. (1997). Biomass gasification: produced gas upgrading by in-bed use of dolo-mite, *Ind. Eng. Chem. Res*. 36, 5220– 5226.

Barnea, E., Mizrahi., J. (1973). Generalised approved to the dynamics of particulate system: Part 1: General correlation for fluidization and sedimentation in solid multi-particle system. *Chem. Engg*. Jl., 5, 171.

Handley, D., Doraisamy, A., Butcher, K. L. & Franklin, N. L. (1966). A study of the fluid and particle mechanics in liquid-fluidised beds. *Trans. Instn Chem. Engrs 44,* 260-273.

I Narvaez, A. Orio, M.P. Aznar & J. Corella. (1996). Biomass gasification with air in an atmospheric bubbling fluidized bed. Effect of six operational variables on the quality of the produced raw gas, Ind. Eng. Chem. Res. 35, 2110–2120.

I. Narvaez, A. Orio, M.P. Aznar & J. Corella. (1996). Biomass gasification with air in an atmospheric bubbling fluidized bed. Effect of six operational variables on the quality of the produced raw gas, *Ind. Eng. Chem. Res*. 35. 2110–2120.

J. Yang & A. Renken. (1998). Intensification of mass transfer in liquid fluidized beds with inert particles, *Chem. Eng. Process*. 37, 537–544.

J.F. Richardson & M.A. Jeronimo. (1979). Velocity–voidage relations for sedimentation and fluidisation, *Chem. Eng. Sci*. 34 1419–1422.

Kmiec. (1982). Equilibrium of forces in a fluidized bed—experimental verification, *J. Chem. Eng*. 23, 133–136.

Renzo Di Felice. (1995). Hydrodynamics of liquid fluidization. *Chem. Eng. Sci.*, 50, 1220-1225.

Richardson, J. F. & Zaki, W. N. (1954). Sedimentation and fluidisation. Part I. *Trans. lnstn Chem. Engrs* 32, 35-53.

Wen, C.Y. & Yu, *Y.H*. (1962). Mechanics of fluidization. *AIChE Symp. Ser*. 62, 100.

Wen, C.Y., Yu, Y-H, (1966). A generalized method for predicting the minimum fluidization velocity. *AIChEJ*, 12, 610

Table 1. Nomenclature

A	Cross sectional Area of the column, m^2
C_D	Drag Coefficient
ID	Internal Diameter, m
d_p	Particle diameter, m
D	Column diameter, m
G	Acceleration due to gravity, m/s^2
L	Bed height, m
PT	Pitch
TR	Twist ratio
U_c	Velocity of continuous phase, m/s
U_d	Velocity of dispersed phase, m/s
U_t	Terminal settling velocity, m/s
U_s	Slip Velocity, m/s
U	Superficial liquid velocity, m/s
W	Weight of solids in the bed, kg
ΔP	Pressure drop, kg/m^2
ρ_l	Density of the liquid, kg/m^3
$\Delta \rho$	Density difference, kg/m^3
ρ_s	Density of solid, kg/m^3
μ	Viscosity of liquid, kg/m s
ε	Voidage, dimensionless
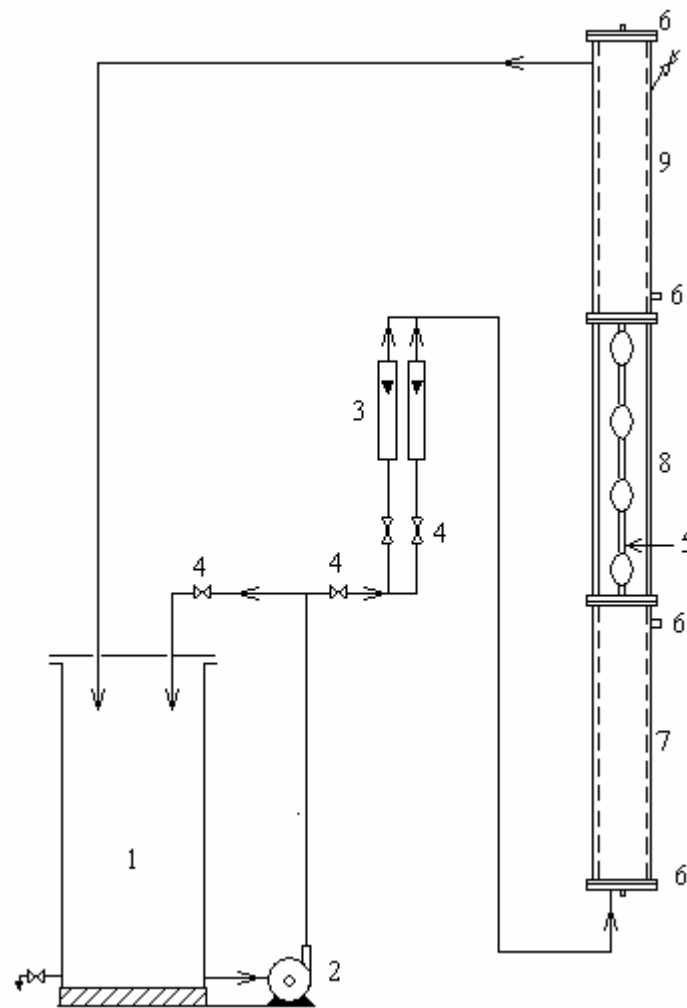
Figure 1. Schematic diagram of the experimental set up

Note. 1: Storage tank; 2: Centrifugal pump; 3: Flow meter; 4: Control valves; 5: Internals; 6: pressure tapings; 7: Calming section; 8: Test Section, 9: Disengaging section
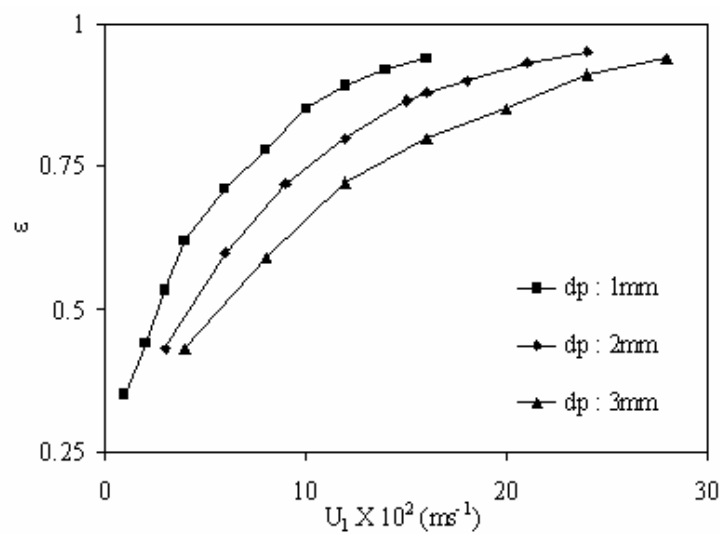
(a)
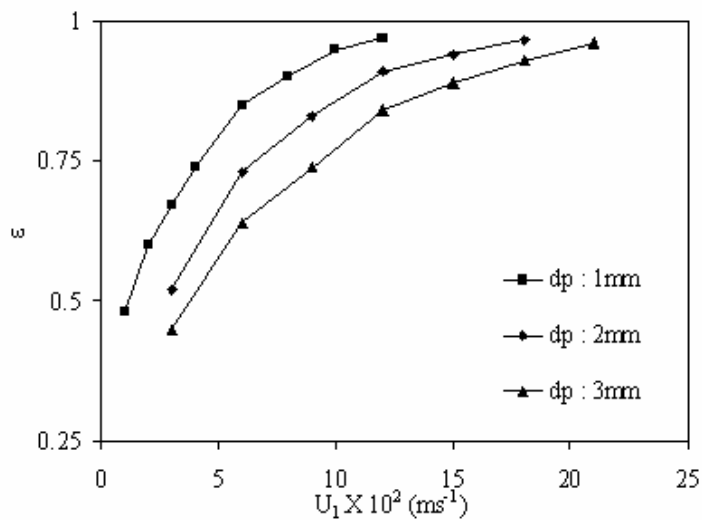
(b)

Figure 2. Variation of bed voidage with liquid flow rate.
Material: Sand; Internal: Sphere; Pitch: (a): 1D; (b): 2D
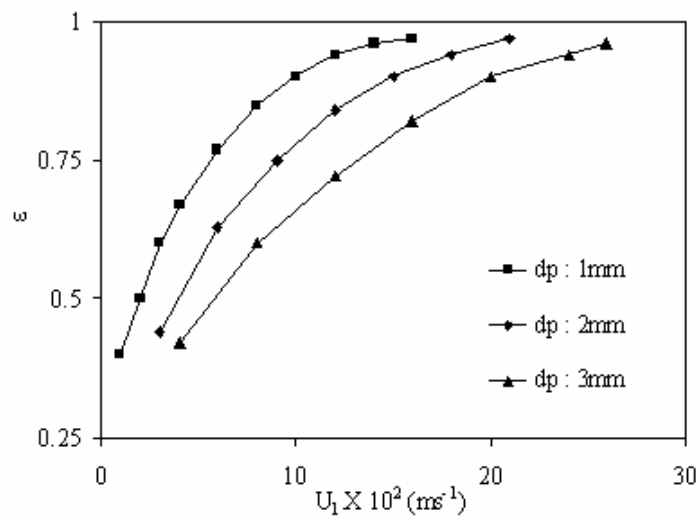
Figure 3. Variation of bed voidage with liquid flow rate.
Material: Glass beads; Internal: Twisted tapes; TR: 3.22
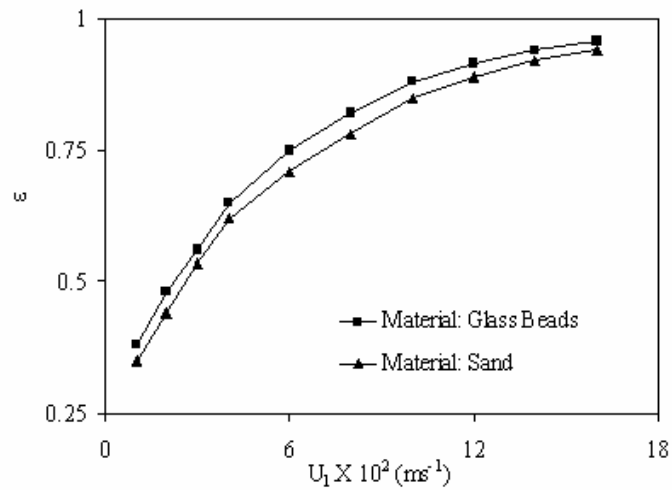
Figure 4.   Effect of particle Density on bed voidage: Internal: Sphere: PT: 1D
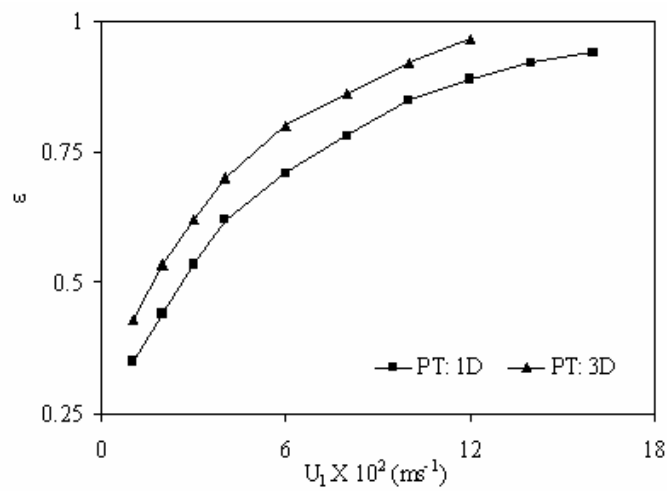
Figure 5. Effect of pitch diameter on the bed voidage. Internal: Sphere; Material: Sand
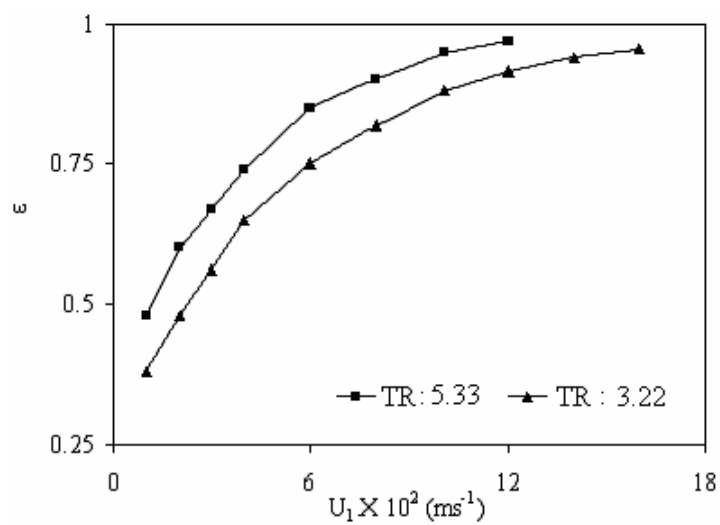
Figure 6. Effect of internal twist ratio on bed voidage. Internal: Twisted tapes; Material: Glass beads
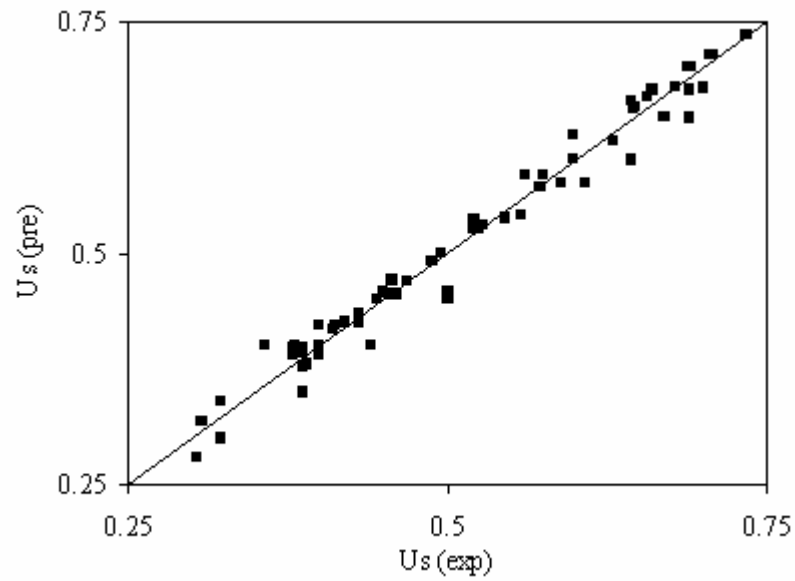
(a)
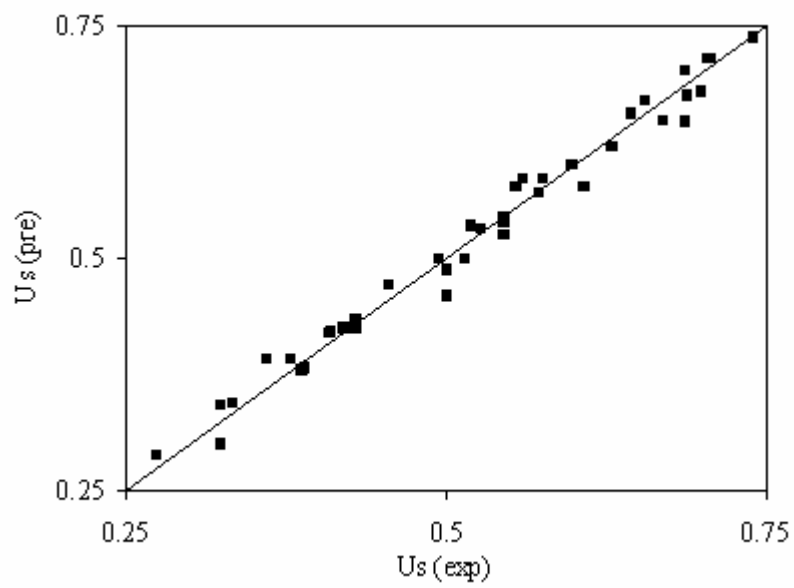
(b)

Figure 7. Comparison of calculated slip velocity with experimental observation
(a) Conventional Liquid-Solid fluidized bed, (b) Liquid-Solid Fluidized bed with internals.

Analysis of DDR3 SDRAM Standard Technology

Jianghong Cui, Wencheng Guo, Jingli Yang

Department of Computer Technology and Automatization, Tianjin Polytechnic University, Tianjin 300160, China

E-mail: cckarlen@sina.com

Abstract

With requirements of high data transmission efficiency, as the new SDRAM standard, DDR3 has gradually entered into our views. This article will analyze main functions of DDR3 and mainly compare DDR3 with DDR2.

Keywords: DDR3, ODT

1. Introduction

After long-term waiting, EMS memory standard organization JEDEC claimed that drafting, development and publication of DDR3 standard had been completely ended and this standard had normally been the industry standard. The data transmission efficiency of present DDR2 can achieve 800MHz, and its core work frequency has achieved 200MHz, so it is more and more difficult to realized higher data transmission efficiency through continually enhancing the core work frequency. And because the developments of market and technology require continual enhancements of data transmission efficiency, so DDR3 is the production to big extents when the market faces this sort of corner.

2. Basic functions of DDR3

DDR3 has no subversive designs, and it is ameliorated on the bases of DDR2. DDR3 adopts lower voltage of 1.5V according with the standard of JEDEC SSTL-1.5, and because it adopts the prefetch design of 8bit, comparing with DDR2 core with the prefetch design of 4bit, the work frequency of DDR3 is half reduced. For example, when the exterior data transmission efficiency is 800Mb, the work frequency of DDR3 is only 100MHz and DDR2 is 200MHz, so DDR3 can realize higher data transmission efficiency. Table 1 shows explanations of various DDR3 signals.

3. Similarities and differences between DDR3 and DDR2

Comparing with DDR2, DDR3 has been adjusted in many aspects such as encapsulation, work voltage, ODT, heat sensor, output control, the quantity of bank and so on. The detailed ameliorations are introduced as follows.

3.1 Low voltage and low power

On the base that the work voltage of DDR2 is 1.8V, the work voltage of DDR3 is reduced to 1.5V, 16% of original voltage, which will compensate power increase brought by enhancement of work frequency. And DDR3 adopts new technique and makes its kernel size smaller than original one, which will also bring the effect of power decrease. Some relative data forecast DDR3 will save 30% of power than present DDR2. Balancing bandwidth and power consumption, comparing with present DDR2-800, the power consumptions of DDR3-800, 1066 and 1333 are respectively 0.27 times, 0.83 times and 0.95 times, and the DDR3-800 not only possesses wider bandwidth, but also has less power consumption. The reference voltage signal VREF which is very important for the work of EMS memory system is divided into two signals. The reference voltage which can order, control and address signal is VREFCA, and VREFDQ services for data signals. This design can be similarly thought in one same reference voltage surface, instantaneous currents brought by large of signals are reduced, and accordingly the signal-to-noise class of system data bus can be effectively enhanced.

The tolerable degree of voltage signals to the uprush area and undershoot area is reduced comparing with DDR2, for example, classical VDD and VDDQ voltage of DDR3 is 1.5V±0.75V, and the maximal uprush and undershoot peak value of address/order/control/data/clock signals is ±0.4V. Considering various factors such as DDR3 grain topological structure, actual situation of layerout trace, equivalent resistance, PCB material, the quality requirement to signal is higher than DDR2. In addition, we can rewrite ODT Register of DDR3 EMS memory controller to restrain the uprush and undershoot on the data and address lines. The definitions of the uprush area and the undershoot area for voltage signal are seen in Figure 1.

3.2 Increase the quantity of logic bank

DDR2 has designs of 4 Banks and 8 Banks, which aim is to face future demands for large capability CMOS chip. But the initiative logical Bank has eight ones, which aim is to offer technological repertory for the CMOS chip possesses 16 logical Banks, thus DDR3 can start from higher capability.

3.3 Encapsulation

The biggest breakthrough of DDR2 technology is actually not the ability of double transmission to DDR thought by

users, but it can acquire higher frequency enhancement and break through the limitation of 400MHz of standard DDR under lower heat and power consumption. The DDR EMS memory usually adopts encapsulation of TSOP chip, and this encapsulation form can work on 200MHz well, and when the frequency is higher, its overlong pins will produce high impedance and parasitical capacitance, which will influence its stability and the difficulty of frequency enhancement. DDR2 adopts the encapsulation form of FBGA which can offer better electric performance and heat elimination (but when the form of the positive and negative chip is adopted, FBGA can not adopt ICT test, so the new problem of test occurs.) and make grains more stably work and offer good guarantees for the developments of future frequency. DDR3 inherits the encapsulation advantage of DDR2, and it adopts new technology small than 0.1 μm, which makes kennel size smaller than original one, saves power consumption, reduces encapsulation heat and possesses better electric performance.

Because DDR3 increases some functions, so it increases some pins and improves pin distribution and signal reference. The 8bit chip adopts 86 ball FBGA encapsulation (because the encapsulation forms of Micron and Samsung are different, this article takes Micron as the example.), and 16bit chip adopts 96 ball FBGA encapsulation, and DDR2 has the encapsulation standard of 60/84 ball FBGA. DDR3 must adopt the green encapsulation without lead and accord with the standard of RoHs. In addition, the pin distribution of DDR3 encapsulation is symmetrical, which can enhance pin use rate and have more power pin distribution comparing with DDR2.

3.4 New function of "Reset"

"Reset" is an important new function of DDR3, and DDR3 specially prepares a pin for that. This pin makes the initialization processing of DDR3 become simple. When the order of "Reset" is effective, DDR3 memory will stop all operations and switch to least activity status to save electric power. In the process of "Reset", DDR3 memory will close most interior functions, all data receivers and transmitters will be closed, all interior program sets will be reset, DLL (Delay Locked Loop) and clock circuit will stop working and ignore any changes on the data but, which can reduce power consumption for DDR3.

3.5 New function of "ZQ adjustment"

DDR2 uses OCD to enhance the signal integrality through reducing the incline of DQ-DQS and enhance signal quality through controlling voltage. OCD realizes the function through adjusting the values of pull-up resistance and pull-down resistance. But DDR3 increases one ZQ pin which joints one low tolerance reference resistance of 240 ohm. This pin can automatically test on-resistance of data output driver and end resistance of ODT through an order set and On-Die Calibration Engine (ODCE). When the system sends this order, it will use corresponding clock cycle (512 clock cycles are used after electricity and initialization, 256 clock cycles are used after exiting self-refresh operation, 64 clock cycles are used under other conditions.) to readjust on-resistance and ODT resistance for actualizing better matching, which is more precise comparing with DDR2 which uses voltage and current thresholds to confirm the value of RTT. The on-resistance adjustment principle of output driver is seen in Figure 2, where, the enabling pull-up resistance $RON_{PU} = (VDDQ-V_{OUT})/|I_{OUT}|$, and the enabling pull-down resistance $RON_{PU} = (VDDQ-V_{OUT})/|I_{OUT}|$.

3.6 Burst Length, BL

The Burst Length (BL) of DDR3 is fixed at 8, and the prefetch operation is also 8bit. Relative to DDR2 and early DDR structure, the BL in common use for the system is 4, and DDR3 increases a 4bit Burst Chop pattern, i.e. a read-write operation with BL=4 and a write operation with BL=4 compose a data Burst Length with BL=8, and this burst pattern can be controlled by A12 address line. And any burst interrupt operation will not be supported in DDR3, and more flexible burst transmission control will be used.

3.7 Timing

Just like that the delay cycle of DDR2 would be increased when it is transformed from DDR, the CL cycle of DDR3 will be also enhanced comparing with DDR2. The CL range of DDR2 is usually in 2 to 5, and this range of DDR3 is in 5 to 11, and the design of additional delay (AL) changes. The AL range of DDR2 is in 0 to 4, and the AL of DDR3 has three forms which respectively are 0, CL-1 and CL-2. In addition, DDR3 also increase a timing parameter, CWD, which is confirmed by concrete work frequency.

3.8 Refresh of timing characteristic

The CL cycle of DDR3 is enhanced comparing with DDR2, the CL range of DDR2 is usually in 2 to 5, this range of DDR3 is in 5 to 11, and the design of additional delay (AL) changes. The AL range of DDR2 is in 0 to 4, and the AL of DDR3 has three forms which respectively are 0, CL-1 and CL-2. In addition, DDR3 also increase a timing parameter, CWD, which is confirmed by concrete work frequency. The CAS delay time of the memory has close relations with access time. The so-called CAS time is the response time of lengthways address pulse of the memory. The CAS delay time is one of important signs to measure the memories supporting different standards under certain frequency. According to these data, we likely find that the CAS time of DDR3 is worse than DDR2's, but through referring concrete delay parameter time, we find that the CAS time of DDR3 presents downtrend, i.e. the CL time of DDR3 is shorter than DDR2's. For example, the CL/RCD/RP values of DDR2-533 are respectively 4-4-4, so the CL time is 15ns,

and the CL/RCD/RP values of DDR3-1066 are respectively 7-7-7, so the CL time is reduced to 13.125ns, and if the CL/RCD/RP values of DDR3-1600 are respectively 9-9-9, so the CL time can be reduced to 11.25ns.

3.9 Design of automatic refresh

To ensure that the saved data can not be lost, DRAM must implement refresh at a certain time, and DDR3 can not be exceptional too. But for saving maximal electric power, DDR3 adopts a sort of new automatic self-refresh (ASR) design. When ASR begins, the refresh frequency is controlled by a temperature sensor inside DRAM chip, and because the refresh frequency is high, the power consumption will increase and the temperature will increase with it. And the temperature sensor can try to reduce refresh frequency and work temperature and ensure the data can not be lost at the same time. The ASR of DDR3 is a selectable design, and not all DDR3 memories in the market can support this function, so there is an additional function, self-refresh temperature (SRT). Through pattern register, two temperature ranges can be selected, and one is common temperature range (for example 0 centigrade degrees to 85 centigrade degrees), and the other is extended temperature range, for example, the highest temperature can achieve 95 centigrade degrees. To these sorts of temperature ranges set in the DRAM, DRAM will implement refresh operation with constant frequency and current.

4. Conclusions

This article emphasize the new characters and advantages of DDR3 comparing with DDR2. In the day that DDR2 is extensively applied, people expect it can quit the historical stage as soon as possible and continue to lead the step of SDRAM family. In the road map published by Intel at present, the series chips of Bearlake-X will integrate DDR3 memory controller, and with the support of CPU manufacturers, various chip groups and network processors supporting DDR3 will also occur continually. Therefore, we have enough reasons to believe the age of DDR3 will come soon.

References

JEDEC. (2007). *DDR3 SDRAM Standard.* June 2007.

MICRON. (2007). *MT41J512M4/MT41J256M8JE.*

Table 1. Explanations of various DDR3 signals

Signals	Type	Explanation
CK/CK#	I	Difference clock signal: all addresses and control input signals are sampled on the ascending border of CK and the descending border of CK#.
CKE	I	Clock enabling signal: high efficiency, the high voltage must be kept in the process of read-write.
CS#	I	Interrupt signal: when many DDR3 grains exist in the system, this signal can be one part of control orders through signal selection.
ODT	I	Interior end: the interior terminal resistance of DDR3 can effectively restrain the reflected noises in the transmission path and improve the integrality of the signal.
RAS#/CAS#/WE#	I	Order input signal: when the signal is effective, the order is thought it has been inputted.
DM/(DMU)/(DML)	I	Data input sign: in the write operation process, the data input is thought that the sampling is high.
BA0-BA2	I	Block address input: deciding which block is activated, read-written, pretreated.
A0-A15	I	Address line: providing row and list addresses for various operations.
A10/AP	I	Pretreatment: sampling read-write order cycle A10 to decide whether implementing automatic pretreatment after read-write operation.
A12/BC#	I	Burst break: sampling read-write order cycle and deciding whether burst break exists.
RESET#	I	Reset signal: low efficiency, CMOS voltage.
DQ	I/O	Data input and output: bidirectional data signals.
DQU/DQL/DQS/DQS#/DQSU/DQSU#/DQSL/DQSL#	I/O	DQS/DQS #: referring edge intersection of CK/CK#.
TDQS/TDQS#	O	Terminal data check: it only is used in grain X8, and can realize the function similar to the terminal resistance of DQS/DQS# through pattern register enabling.
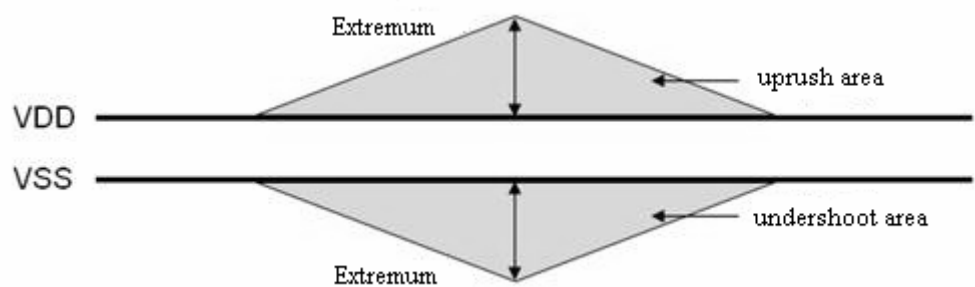
Figure 1. Definitions of the Uprush Area and the Undershoot Area for Voltage Signal
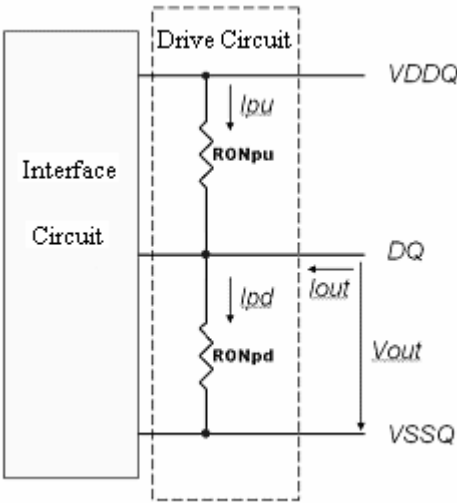
Figure 2. Output Drive Circuit

The Stable Set and Weak Stable Set

For n-person Repeated Fuzzy Cooperative Games

Zuofeng Gao

Department of Science, Yanshan University, Qinhuangdao 066004, China

Suting Zhang (Corresponding author)

Department of Science, Yanshan University, Qinhuangdao 066004, China

E-mail: zhangsuting2002@yahoo.com.cn

Hongxin Bai

Department of Science, Yanshan University, Qinhuangdao 066004, China

Chunyan Han

Department of Science, Yanshan University, Qinhuangdao 066004, China

Sheng Zhao

Department of Science, Yanshan University, Qinhuangdao 066004, China

Abstract

In this paper,based on the fuzzy games,we define the imputation sequences of the n-person repeated games,and the domination,weak domination for the imputation sequences.Further,based on this theory,we define the core ,the weak core,the stable set,and the weak stable set of the n-person repeated fuzzy cooperative games.At last,some properties of the stable set and the weak stable set are given.

Keywords: Fuzzy game, Repeated cooperative game, Core, Weak core, Stable set, Weak stable set

Introduction

In the former literature about the cooperative game, how to allocate the total benefit among the the players have been studied widely.In 1974, Aubin, JP introduced Fuzzy games, and combine cooperative game with fuzzy coalition for the first time (Aubin, 1981, PP. 1-13). And in 1999, Jorge Oviedo developed the n-person repeated cooperative game, the core of this game was discussed in his paper.And based on the these theory, we develoepde n-person Repeated fuzzy cooperative games.Further,we define the weak core,the stable set and the weak stable set for n-person Repeated fuzzy cooperative games.Thus,we extend the study for the solution of Repedted fuzzy games.

1. Basic definitions

Definition1. Let $N := \{1,2,...,n\}$ be the set whose elements are called players.$[0,1]^n = [0,1] \times [0,1] \times ... \times [0,1]$, v is a fuction on $[0,1]^n$,and $v : [0,1]^n \to R$,satisfy: $v(\Phi) = 0$,where $\Phi = (0,0,...0)$,then we call v is a characteristic function on $[0,1]^n$,and call $([0,1]^n, v)$ is a fuzzy cooperative game with player set N .We call v fuzzy game in short.

We dnote by FG^N the set of Fuzzy Games.And $d = (d_1, d_2, ... d_n) \in [0,1]^n$ is a fuzzy coalition.The i th coordinate is called the participation degree of player i to fuzzy coalition d .And denote F^N all the possible fuzzy coalitions.

We denote $e^i \in R^n$ the i th coordinate is 1, and 0 otherwise.And we denote

$$e^N = \sum_{i \in N} e^i , \sup pd = \{i \in N : d_i > 0\}$$

We repedte the fuzzy game v m times(m may be ∞),and we denote (d, v_t, t) the fuzzy cooperative game of players in t th period,we call it the stage game of the n-person repeated fuzzy game.In order to make the stage-game and the repedted-game characteristic function to be measured in the same unities,we use a discount factor δ^t, $\delta \in (0,1)$,and we call $1 - \delta$ the normalization factor.The imputation vector of the fuzzy coopertive game (d, v_t, t) shulde satisfy the follwing :

$$(1) \sum_{i=1}^{n} x_i^{\ t} = v_t(e^N) = (1-\delta)\delta^t v(e^N)$$

$$(2) d_i x_i^{\ t} \ge v_t(d \mid i) = (1-\delta)\delta^t v(d \mid i)$$

So we denote the core of the fuzzy cooperative game as

$$c(v_t) = \{x \in R^n : \sum_{i \in N} x_i = v_t(e^N), \sum_{i \in N} d_i x_i \ge v_t(d), \forall d \in [0,1]^n \}$$

Let $d^t \in [0,1]^n$ ia a fuzzy coalition when v at time t. Then let $(d^0, d^1, ... d^t)$ be the coalition sequences when t from 0 to t. We denote $H^t = (L(u))^t$ the all possible coalitions when t th stage. where $L(u)$ is all the possible fuzzy coalitions. We denote H the set of all the coalition sequences.

Definition 2. Let $\theta = (d^0, d^1, ... d^m) = (d^t)_{t=0}^m \in H$ is a coalition sequence, then $w(\theta)$ is called the characteristic function of repeated fuzzy cooperative games, if it satisfies:

$$w(\theta) = (1-\delta) \sum_{t=0}^m \delta^t v(d^t), \text{ and } w(\tilde{\theta}) = 0, \text{where } \tilde{\theta} = (0,0,...0)$$

Definition 3. Let H be the set of coalition sequence, and w is the characteristic function of repeated fuzzy cooperative games. We denote (H, w) as repeated fuzzy cooperative game.

2. The core and the weak core for the n-person repeated fuzzy cooperative game

Definitin 4. An imputation sequence or payoff allocation sequence $x = (x^0, x^1, ...)$ for the repeated fuzzy cooperative game is a sequence of the stage game's imputation or payoff allocations.

Definition 5. Let (H, w) be a repeated fuzzy game, x, y are imputation sequences, $\theta = (d^0, d^1, ... d^m)$ is a coalition sequence if it satisfies:

$$(1) \sum_{t=0}^m d_i^{\ t} x_i^{\ t} > \sum_{t=0}^m d_i^{\ t} y_i^{\ t} \qquad \qquad \forall i \in \underset{k}{Y} \sup pd^k$$

$$(2) \sum_{i \in \underset{k}{Y} \sup pd^k} d_i^{\ t} x_i^{\ t} \le (1-\delta)\delta^t v(d^t)$$

Then we call x dominates y through $\theta (x \underset{\theta}{\phi} y)$

Definition 6. Let $x = (x^0, x^1, ... x^m)$ is a imputation sequence of (H, w). where x^t is the imputation of t th stage game. then we define the core of the repeated fuzzy cooperative game as:

$$c(w) = \{x \in I(w) \mid \sum_{t=0}^m \sum_{i \in \underset{k}{Y} \sup pd^k} d_i^{\ t} x_i^{\ t} \ge (1-\delta)\sum_{t=0}^m \delta^t v(d^t), \sum_{i \in N} x_i^{\ t} = v_t(e^N) = (1-\delta)\delta^t v(e^N)\}$$

Definition 7. Let x, y be two imputations of the repeated fuzzy cooperative game. θ is a coalition sequence, if it satisfies

$$(1) \sum_{i \in \underset{k}{Y} \sup pd^k} \sum_{t=0}^m d_i^{\ t} x_i^{\ t} > \sum_{i \in \underset{k}{Y} \sup pd^k} \sum_{t=0}^m d_i^{\ t} y_i^{\ t} > \qquad \forall i \in \underset{k}{Y} \sup pd^k$$

$$(2) \sum_{i \in \underset{k}{Y} \sup pd^k} d_i^{\ t} x_i^{\ t} \le (1-\delta)\delta^t v(d^t), \qquad \qquad t \in [0,1,...m]$$

Then we call x dominate y weakly through θ, we denote by $x \overset{w}{\underset{\theta}{\phi}} y$.

Definition 8. All of the set of imputation sequences for repeated fuzzy cooperative game, if they are not dominated, then we call them the weak core of the repeated fuzzy cooperative game. And we denote by $\tilde{c}(w)$, i.e.

$$\tilde{c}(w) = \{x \mid x \in I(w), \text{ there exist no } \theta \text{ and } y \in I(w), \text{satisfy: } y \overset{w}{\underset{\theta}{\phi}} x\}$$

3. The stable set and the weak stable set for n-person repeated fuzzy cooperative games

Definition 9. Let L be the set of some imputation sequences of repeated fuzzy game (H, w), i.e. $L \subset I(w)$, we call

L the stable set of (H, w), if it satisfies

(1) $\forall x = (x^0, x^1, \ldots x^m)$, $y = (y^0, y^1, \ldots y^m) \in I(w)$, there is no domination relationship between x and y (inner stability)

(2) $\forall \ x' \in I(w) \setminus L$, there exist a coalition sequence θ and an imputation sequence $x \in L$, satisfy: $x \underset{\theta}{\phi} x'$ (outer stability)

Definition 10. Let $\tilde{L}$ are the set of some imputation sequences of repeated fuzzy cooperative game, i.e. $\tilde{L} \subseteq I(w)$, we call $\tilde{L}$ the weak stable set of (H, w) if it satisfis:

$\forall x, y \in I(w)$, there is no weak dominationship between x and y .(inner stability)

$\tilde{x} \in I(w) \setminus \tilde{L}$, there is a coalition sequences θ and an imputation sequences $y \in \tilde{L}$, satisfy: $y \overset{w}{\underset{\theta}{\phi}} \tilde{x}$.(outer stability)

4. The properties of the stable set for n-person repeated fuzzy cooperative game

Theorem 1. To the same n-person repeated fuzzy cooperative game, $\tilde{c}(w) \subseteq c(w)$.

Proof. $\forall \tilde{x} \in \tilde{c}(w)$, we know from the definition of the weak core that there exist no coalition sequence θ and imputation sequence $\tilde{y}$, satisfy: $\tilde{y} \overset{w}{\underset{\theta}{\phi}} x$ .If $\tilde{x} \notin c(w)$, then there exist a coalition θ and an imputation sequence y, and $y \underset{\theta}{\phi} \tilde{x}$, i.e. for all $i \in \underset{k}{Y} s^k$, we have

$$\sum_{t=0}^{m} y_i^t > \sum_{t=0}^{m} \tilde{x}_i^t$$

To the inequlity above, for all $i \in \underset{k}{Y} s^k$, we make sum to each side respectively. So we have

$$\sum_{i \in Y \sup pd^k} \sum_{t=0}^{m} y_i^t > \sum_{i \in Y \sup pd^k} \sum_{t=0}^{m} \tilde{x}_i^t \text{, i.e. } y \overset{w}{\underset{\theta}{\phi}} \tilde{x} \text{,it is contradict. So } \tilde{x} \in c(w) \text{,then } \tilde{c}(w) \subseteq c(w).$$

Theorem 2. If the stable set of the n-person repeated fuzzy cooperative game $L \neq \Phi$, then $c(w) \subset L$

Proof. When $c(w) = \Phi$, clearly we have $c(w) \subset L$.

When $c(w) \neq \Phi$, $\forall x \in c(w)$, if $x \notin L$, then there exist coalition sequence θ and imputation sequence $y \in L$, satisfy: $y \underset{\theta}{\phi} x$, so $x \notin c(w)$. It is contradict. So, $c(w) \subset L$.

Theorem 3. For all $t(0 \leq t \leq m)$, if $x \in I(w)$, and it satisfies $x \in c(w)$, then $x \in \tilde{c}(w)$.

Proof. If $x \notin \tilde{c}(w)$, then there exist a coalition θ and an imputation sequence $\tilde{x} \in I(w)$, and

It sastifies
$$\sum_{i \in Y \sup pd^k} \sum_{t=0}^{m} d_i^t \tilde{x}_i^t > \sum_{i \in Y \sup pd^k} \sum_{t=0}^{m} d_i^t x_i^t \tag{5}$$

And
$$\sum_{i \in Y \sup pd^k} \sum_{t=0}^{m} d_i^t \tilde{x}_i^t \leq (1-\delta)\delta^t v(d^t), 0 \leq t \leq m, \tag{6}$$

To (6), we make sum in both sides respecr to t, and we have

$$\sum_{t=0}^{m} \sum_{i \in Y \sup pd^k} d_i^t \tilde{x}_i^t \leq \sum_{t=0}^{m} (1-\delta)\delta^t v(d^t) \tag{7}$$

Further becauce for all of the t $(0 \leq t \leq m)$, $x \in c(w)$, so, for all of the t $(0 \leq t \leq m)$, we have

$$\sum_{i \in Y \sup pd^k} d_i^t x_i^t \geq (1-\delta)\delta^t v(d^t)$$

We make sum in both sides respect to t, and we have

$$\sum_{t=0}^{m}\sum_{i\in \mathrm{Y}\sup_{k} pd^{k}} d_{i}^{t} x_{i}^{t} \geq \sum_{t=0}^{m}(1-\delta)\delta^{t} v(d^{t}) \tag{8}$$

compare (7)and (8),we have

$$\sum_{i\in \mathrm{Y}\sup_{k} pd^{k}}\sum_{t=0}^{m} d_{i}^{t} \tilde{x}_{i}^{t} \leq \sum_{i\in \mathrm{Y}\sup_{k} pd^{k}}\sum_{t=0}^{m} d_{i}^{t} x_{i}^{t}$$

This is contradict with (5). then $x\in \tilde{c}(w)$.

References

Aubin, J. P. (1981). Cooperative fuzzy games. Mathematics of Operations Research. (6):1-13.

Gao, H.W. (1998). The discussion to the weak stable sets of the cooperative games. Transaction of qingdao university. (11): (1-5).

Gao, Z.F, Wang,Y & Zhang, X.D. (2004). The fuzzy stable set of the convex fuzzy game. Operational and administer research. 13(1)59-62.

Jorge, Oviedo. (2000). The core a repeated n-person cooperative game. european Journal of Operational Research. (127):519-524.

Rodica, & Branzei, et.al.. (2003). Convex fuzzy games and participation monotonic allocation. Fuzzy set and systems. (139):267-281.

Tijs, S & Branzei, R. (2004). On cores and stable sets for fuzzy games. Fuzzy sets and systems. (146):285-296.

Optimal Workload Allocation in a Network of

Computers with Single Class Job

Rahela Rahim

Faculty of Quantitative Sciences

University Utara Malaysia, 06010, Sintok, Kedah, Malaysia

Tel: 604-928405   E-mail: rahela@uum.edu.my

Ku Ruhana Ku-Mahamud

Faculty of Information Technology

University Utara Malaysia

Tel: 604-9283118   E-mail: ruhana@uum.edu.my

Abstract

Queueing models for multiple queue with multiple server are used to model workload allocation problems in a network of computers. The problem of determining optimal allocation of workload with single class jobs to a parallel of computers using optimization technique is presented. The generalized exponential (GE) distributional model has been used to represent general inter arrival and service time distributions as various jobs have various traffic characteristic. A close-loop expression is derived from a non-linear optimization problem based on a queueing theory objective function to obtain an optimal value for jobs arrival. The analysis of the recomputation has been done and has shown improvement.

Keywords: Workload allocation, Multi server queueing system, Optimization, Generalized Exponential distribution.

1. Introduction

In a distributed computer system, task generated by a user or a group of users can be allocated over a number of available computers. This situation is opposed to a system which a single computer provide its capacity for all users, or systems in which each user is provided with its own local processor, usually with very limited capacity. An operational aspect of such a distributed system is the availability of workload balancing policy. Such policy balances the workload over the available computers, aiming to optimize performance measures for the system. Most traffic allocation problems in the literature have been tackled by assuming that all jobs are identical or single class (Chow & Kohler, 1979; Ni & Hwang, 1981; Tantawi & Towsley, 1985; Ross & Yao, 1991; Chombe & Boxma, 1995, Tavana & Rappaport, 1997; Wolf & Yu, 2001). This assumption is normally done when the diversity of jobs is not of importance.

In this paper, we stress on the quantitative measures of workload allocation to a network of computers. Based on this, we show that by using quantitative modeling, arrival to a network of computers can be reallocated to get the optimal performance measure. We focus on the issue of job allocation in a network of computers where different computers have different job processing time. The optimization criterion studied here is to minimize the expected job response time in the systems to which jobs are allocated. Jobs arrive at a scheduler that allocates jobs to the computers according to a calculated arrival rate computed using Lagrange multiplier theorem. The paper is organized as follows: system model is described and the proposed GE optimization model of workload allocation is presented in section 2.0 and 2.1, followed by the computational results in section 2.2.

2. Optimal Workload Allocation in a Network of Computers with General Exponential (GE) Arrival and Service time Distribution

In this section, we consider workload allocation problems for static allocation protocol for the model of a single GE stream of jobs offered to a fixed number of computers. The allocation protocol which has been studied is static in the sense that only the total incoming traffic and information about basic characteristic, like arrival rate and service times are used. The objective of the network of computer systems studied here is to maximize user perceived performance, which is a function of the amount of time the user spends waiting for a file to download from a server. In this context, download refers to the actions from the time the user requests a file from a computer to the time the file or an error message is delivered to the user's terminal. The shorter the download time, the higher the user's perceived performance.

Most of the previous studies on workload allocation used exponential distribution for inter arrival and service time. The reason is that network traffic has long been assumed to have exponential behavior. However this situation is not always true since the number of network users is unpredictable. Furthermore mean queue length derived from exponential distribution does not factor in variation in the inter arrival and service time. Clearly, the more information is available for making decision, the better the workload allocation can be. So our proposed models include variation parameters in inter arrival and service time that we found lack in previous models. In this model, requests arrive at the system according to a GE process. They are numbered in the order that they arrive at the system. Once a request has entered the system, it does not leave until it completes service. The metric of interest is mean response time, the user spends on the system an amount relative to the download time upon the server's completion of the user's request. Here, the transit time required to send the result of the request back to user's interface has been ignored, and the response time is assumed to be achieved instantaneously upon the file's departure from the server or computer.

Criterion of Optimality

For a given total network traffic φ, find the optimal traffic workload λ_i, i = 1, 2,...,N so that the expected response time incurred on any system is minimized.

2.1   Mathematical Model Description

We will first present a mathematical description of the related workload allocation problems. Jobs arrive at a routing point according to a GE process with rate φ. At the instance of arrival, each job has to be assigned to one of N servers in parallel. The service rate μ_i that is assigned to server i has GE distribution as well. All service times are independent. Any job that is not fully processed, branches with certain probability and returns back to the scheduler for further processing. Otherwise the job is complete and exits the system. Let π denote an allocation policy and p_i, i = 1,…, N, be the fraction of the jobs that is routed to computer i under policy π. In our workload allocation problem, the aim is to minimize

$$\sum_{i=1}^{N} D_i W_i(\pi)$$

$W_i(\pi)$ denote the mean response time of a job assigned to computer i under allocation policy π. D_i is the cost associated with waiting one time unit at queue i. The objective function can have various interpretations, by varying D_i. Little's Law shows that the objective is to minimize the mean number of jobs in the queues. Instead of $W_i(\pi)$, we use $L_i(\pi)$, the mean queue length of queue i. The objective is to minimize a weighted sum of the mean queue length in the system. To obtain the assignment probabilities $p_i* = \dfrac{\lambda_i*}{\phi}$ which minimize this function, the following Mathematical Programming

problem has to be solved

$$\text{P1} \quad \text{Min} \quad \sum_{i=1}^{N} L_i = \sum_{i=1}^{N} D_i \left(\frac{\frac{\lambda_i}{\mu_i}}{1 - \frac{\lambda_i}{\mu_i}} \right) \left(\frac{\lambda_i}{\mu_i} \left(\frac{C_{si}^2 - 1}{2} \right) + \frac{C_{ai}^2 + 1}{2} \right) \tag{2.1}$$

$$\text{s.t} \quad \sum_{i=1}^{N} \lambda_i = \phi \tag{2.2}$$

$$0 \le \lambda_i \le \mu_i, \quad i = 1, \text{K}, N. \tag{2.3}$$

$$\lambda_i \ge 0 \tag{2.4}$$

$$\mu_i \ge 0 \tag{2.5}$$

The term L_i is strictly convex functions in λ_i and it can also be verified that the problem has a feasible solution provided that $\sum_{i=1}^{N} \mu_i > \phi$ that is the arrival rate does not exceed the total service capacity. Before analyzing the model, it is important to understand the meaning of the model parameters. Network Traffic (λ_i) is the average number of file request received by the computer each second. Service rate (μ_i) is the average rate the computer can serve. Obviously, this value will vary widely from one request to another.

Problem P1 allows an analytical solution. Using Lagrange multiplier theorem we obtain δ the Lagrange multiplier with the following first order Kuhn-Tucker constraints:

$$\frac{d}{d\lambda_i}\left\{D_i\left(\frac{\frac{\lambda_i}{\mu_i}}{1-\frac{\lambda}{\mu_i}}\right)\left(\lambda_i\left(\frac{C_{si}^2-1}{2}\right)+\frac{C_{ai}^2+1}{2}\right)\right\}=\delta \qquad i=1,\mathrm{K},N. \tag{2.6}$$

$$\sum_{i=1}^{N}\lambda_i-\phi=0 \tag{2.7}$$

From (2.6) we find the unique optimal values $\lambda_i{}^*$ as follows:

$$\lambda_i{}^*=\mu_i\left(1-\left(\frac{C_{si}^2+C_{ai}^2}{C_{si}^2-1+2\mu_i\delta}+\right)^{1/2}\right), \tag{2.8}$$

Lagrange multiplier, δ is derived by solving the constraint equation below

$$\sum_{i=1}^{N}\mu_i\left(1-\left(\frac{C_{si}^2+C_{ai}^2}{C_{si}^2-1+2\mu_i\delta}+\right)^{1/2}\right)=\phi \tag{2.9}$$

The computation has been developed in the MathCAD version 7 professional.

2.2 Computational result

In this section, numerical results are presented to assess the credibility of the GE distribution used. Two configurations will be shown. For the first configuration, service rate of the tasks are assumed to be $\mu_1=3,\mu_2=4,\ C_{a1}=0.5,C_{a2}=0.3,C_{s1}=0.2,C_{s2}=0.4$. The improvement of the performance measures is presented in Figure 2.1 and 2.3. To verify the results, we use simulation and the comparative results are presented in Figure 2.2 and 2.4. Further analysis of sample cases for N = 2, 3, 4, 5 and 6 computers are computed and the analysis shows that a larger range for the service rates results in greater percentage improvements of the aggregate objectives. For example, a two computer system with $\mu_1=2$, $\mu_2=1$ and $\rho=0.9$ results in a 1.75 per cent improvement in mean queue length compared with 11. 6 per cent improvement for a six computer system with μ_i, i = 1, 2, …, N. The results of the analysis for such queueing systems are summarized in Figure 2.5.

3. Conclusions

The proposed solution mechanism focuses on the workload allocation of single class jobs through the use of optimal GE arrival rate in the workload allocation scheme. The key idea of optimizing the workload allocation scheme is to send a disproportionately fraction of workload to the computers with known capacities. GE component processes are expected to be more regular that a Poisson process, in the sense of having variation parameters.

We have described models that consider the workload allocation decision for the single class job case. The problem of workload allocation in an open network of queues is formulated as a non-linear optimization problem. The problems of maximizing system's mean queue length and mean response time for a given total arrival rate, and a specified arrival and service variation, are found to have the optimality condition. These optimality conditions are used to prove that, for queueing networks with unbalanced configuration of computer capacity, the optimal allocation of workload is unbalanced. A larger per computer share of workload goes to a larger capacity of computers. The unbalanced allocation result is related to efficiencies gained from computer pooling systems, we show that, holding utilization per computer constant, increasing the number of computers in the network reduces the average number in queue.

References

Allen, A. O. (1990). *Probability, Statistics and Queueing Theory with Computer Science Applications*, 2nd ed. San Diego: Academic Press.

Bell, S. L. & Williams, R. J. (1999). Dynamic scheduling of a system with two parallel servers: Asymptotic optimality of a continuous review threshold policy in heavy Trac. *In Proceedings of the 38th Conference on Decision and Control*, Pheonix, Arizona, 1743-1748.

Boxma, O. J. (1995). Static Optimization of Queueing Systems, *CWI Report*. BS-R 9302.

Chombe, M. B. & Boxma, O. J. (1995). Optimization of Static Traffic Allocation Policies, *Theoretical Computer Science*, 125, 17-43.

Chandy, K. M., Herzog, U. & Woo, L. (1975). Parametric Analysis of Queueing Networks, *IBM J. Research and Development,* 19(1), 36-42.

De Jongh, J. F. C. M. (2002). *Share Scheduling in Distributed System*, PhD Thesis University of Technische, Netherland.

Gelenbe, E & Mitrani, I. (1980). *Analysis and Synthesis of Computer Systems*, London: Academic Press.

Gunther, N. J. (2000). *The Practical Performance Analyst*, McGraw Hill.

Harrison, P. G. & Patel, N. M. (1992) *Performance Modeling of Communication Networks and Computer Architecture*, Addison Wesley.

Hsiao, M. T. & Lazar A. A. (1990). Optimal Flow Control of Multiclass Queueing Networks with Partial Information, *IEEE Transaction on Automatic Control*, 35(7) 855-860.

Hsiao, M. T. & Lazar, A. A. (1991). Optimal Decentralized Flow Control of Markovian Queueing Networks with multiple Controllers, *Performance Evaluation*, 13(3), 181-204.

Ross, K. W. & Yao, D. D. (1991). Optimal Load Balancing and Scheduling in a Distributed Computer System, *Journal of the ACM* , 38(3), 679-690.

Klienrock, L. (1975). *Queueing Systems Volume 1: Theory*, John Wiley Inc.

Kobayashi, H. (1974). Application of the Diffusion Approximation to Queueing Networks I: Equilibrium Queue Distribution*, J. of the Association for Computing Machinery*, 21(2), 316-328.

Koole, G. (1999). On the Static Assignment to parallel Servers, *IEEE Transaction on Automatic Control*, 44, 1588-1592.

Kouvatsos, D. D. (1986). A Maximum Entrophy Queue Length Distribution for A G/G/1 Finite Capacity Queue, *Journal of ACM*, 224-236.

Kouvatsos, D. D. & Othman, A. T. (1989). Optimal Flow Control of a G/G/1 Queue*,   International J. of Systems Science*, 20(2), 251-265.

Kouvatsos, D. D. & Othman, A. T. (1986). Optimal Flow Control of a G/G/C Finite Capacity Queue, *J. Operational Research Society*, 40(7), 659-670.

Kouvatsos, D. D. & Othman, A. T. (1989). Optimal Flow Control of end to end   Packet Switched Network with Random Routing, *IEEE Proceeding*, 136(2), 90-100.

Ku Mahamud, K. R. (1993). *Analysis and Decentralized Optimal Flow Control of Heterogeneous Computer Communication Network Models*, PhD thesis, Universiti Pertanian   Malaysia.

Lazar, A. A. (1981). Optimal Control of an M/M/1 Queue, *In Proc. 19th Allerton Conf. On Communication, Control and Computing*, 279-289.

Lazar, A. A. (1982). Centralized Optimal Control of a Jacksonian Network, *In Proceedings of the Sixteenth Conference on Information Science and Systems*, 316-324.

Lazar, A. A. (1983). The Throughput Time Delay Function of an M/M/1 Queue, *IEEE Transaction on Information Theory*, 6, 1001-1007.

Lazar, A. A. (1984). Optimal Control of an M/M/m Queue, *Journal of the Association for Computing Machinery*, 86-98.

Lin, W. & Kumar, A. (1984). Optimal Control of a Queueing System with Two Heterogeneous Servers, *IEEE Trans Automatic Control*, 29(8), 696-703.

Liu, J. B. (1999). A Multilevel Load Balancing Algorithm in a Distributed System, *Proceedings of the 19th annual conference on Computer Science*, 35-142.

Menasce, D. A. and Almeida, V. A. F. (2000). *Scaling for E-Business*, Prentice Hall.

Ni, L. M., & Hwang, K. (1985). Optimal Load Balancing in a multiple Processor System with Many Job Classes. *IEEE Trans. Software Engineering*, 491-496.

Smith, C. U. & Williams, L. G. (2001). *Performance Solutions, A Practical Guide to Creating Responsive, Scalable Software*, Pearson Education.

Table 2.1 Results for the classical and proposed approaches of a dual GE/GE/1 with $Ca_1^2 = 0.5$, $Ca_2^2 = 0.3$ $Cs_1^2 = 0.2$, $Cs_2^2 = 0.4$ and $\mu_1 = 3$, $\mu_2 = 4$.

Classical		Proposed		Classical		Proposed	
λ_1	λ_2	λ_3	λ_4	L	W	L	W
1.6	2.1	1.578	2.122	1.158	0.313	1.153	0.312
1.8	2.4	1.776	2.424	1.47	0.35	1.465	0.349
2.0	2.7	1.981	2.719	1.896	0.403	1.891	0.402
2.2	2.9	2.15	2.95	2.396	0.47	2.377	0.466
2.4	3.2	2.367	3.233	3.36	0.6	3.342	0.597
2.6	3.4	2.544	3.456	4.86	0.81	4.775	0.796

Table 2.1 provides numerical results after recomputation of arrival rate and the improvement in performance measures of mean queue length and waiting time for the stated parameters.

Table 2.2. Results for the classical and proposed approaches of a dual GE/GE/1 with $Ca_1^2 = 0.1$, $Ca_2^2 = 0.2$ $Cs_1^2 = 0.4$, $Cs_2^2 = 0.3$ and $\mu_1 = 3$, $\mu_2 = 4$.

Classical		Proposed		Classical		Proposed	
λ_1	λ_2	λ_3	λ_4	L	W	L	W
1.6	2.1	1.465	2.235	0.906	0.245	0.897	0.212
1.8	2.4	1.698	2.502	1.14	0.27	1.132	0.253
2.0	2.7	1.931	2.769	1.455	0.31	1.449	0.298
2.2	2.9	2.117	2.983	1.82	0.357	1.805	0.342
2.4	3.2	2.35	3.25	2.52	0.45	2.507	0.446
2.6	3.4	2.536	3.464	3.599	0.6	3.539	0.598

Table 2.2 provides numerical results after recomputation of arrival rate and the improvement in performance measures of mean queue length and waiting time for the stated parameters.
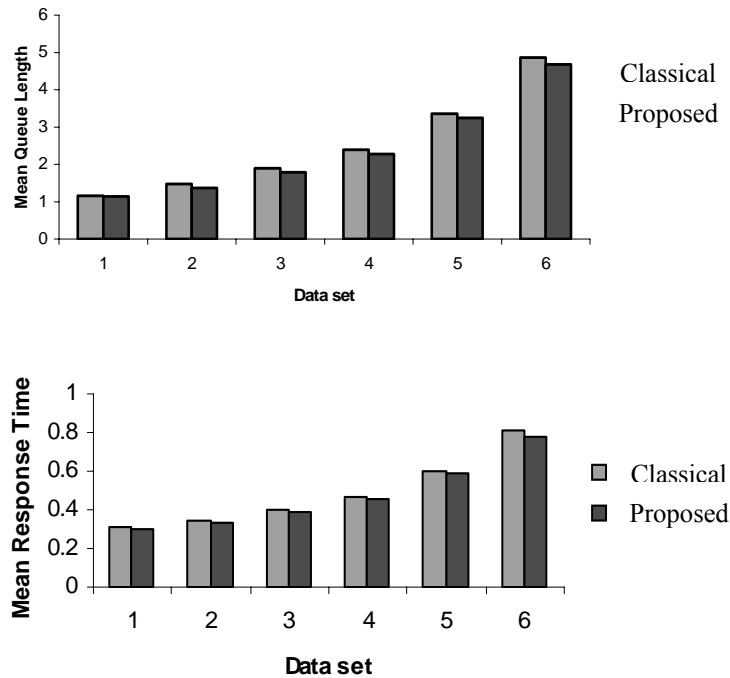
Figure 2.1. Performance improvement of a dual GE/GE/1 with

$Ca_1^2 = 0.5$, $Ca_2^2 = 0.3$, $Cs_1^2 = 0.2$, $Cs_2^2 = 0.4$ and $\mu_1 = 3$, $\mu_2 = 4$.

Figure 2.1 shows the improvement of the two computers system's mean response time using dataset in Table 2.1.
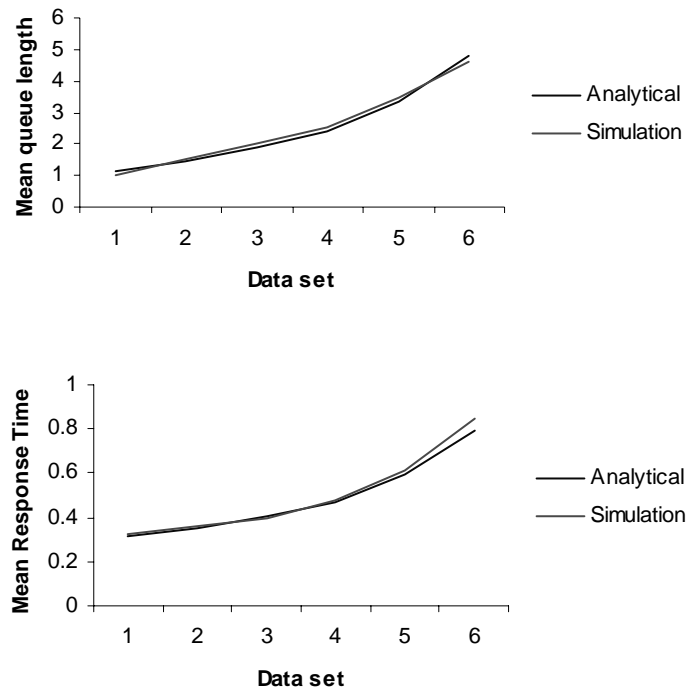
Figure 2.2. Analytical versus simulation result for a a dual GE/GE/1 with
$Ca_1^2 = 0.5$, $Ca_2^2 = 0.3$, $Cs_1^2 = 0.2$, $Cs_2^2 = 0.4$ and $\mu_1 = 3$, $\mu_2 = 4$

Figure 2.2 shows verification of the results with simulation using the stated parameters.
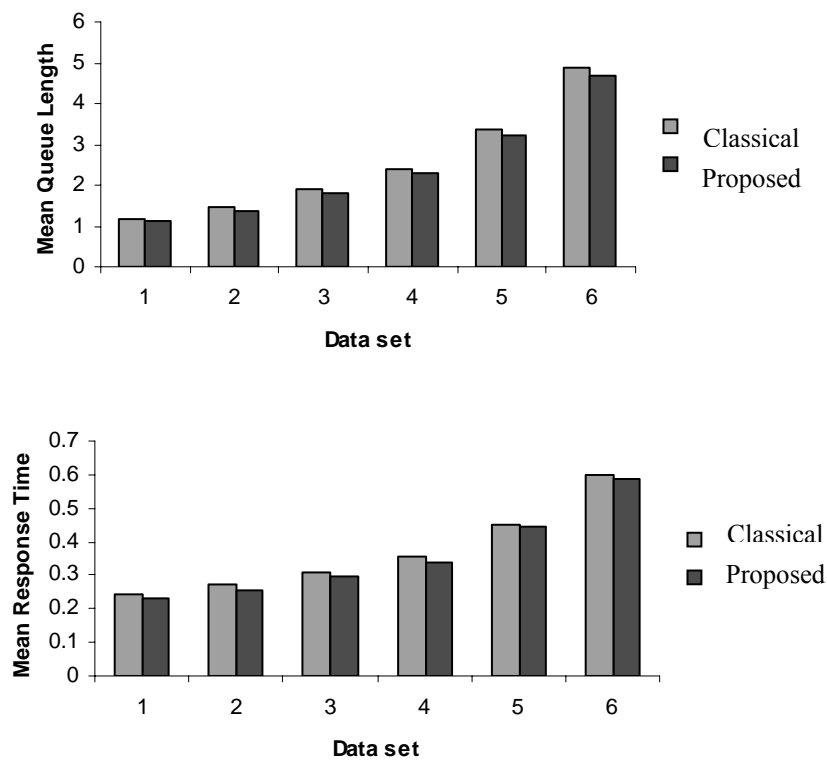
Figure 2.3. Performance improvement of a dual GE/GE/1 with
$Ca_1^2 = 0.1$, $Ca_2^2 = 0.2$, $Cs_1^2 = 0.4$, $Cs_2^2 = 0.3$ and $\mu_1 = 3$, $\mu_2 = 4$.

Figure 2.3 shows the improvement of the two computers system's mean response time using dataset in Table 2.2.
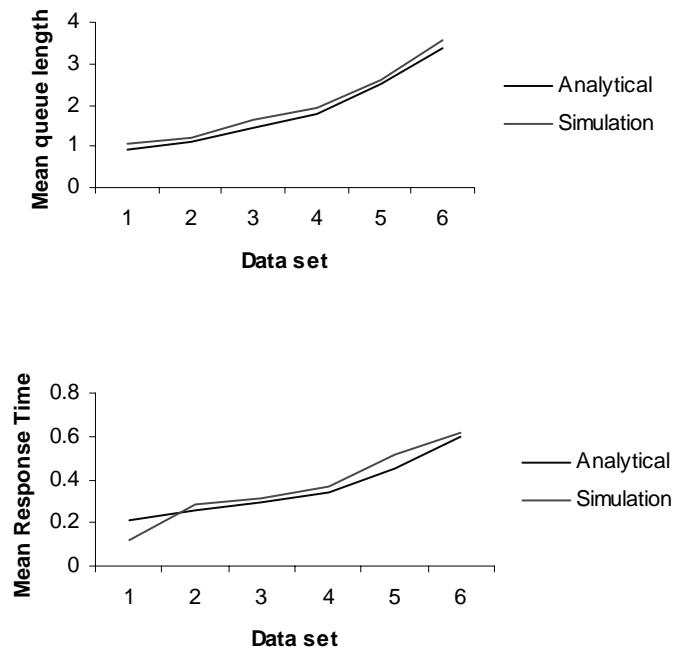
Figure 2.4. Performance improvement of a dual GE/GE/1 with
$Ca_1^2 = 0.1$, $Ca_2^2 = 0.2$ $Cs_1^2 = 0.4$, $Cs_2^2 = 0.3$ and $\mu_1 = 3$, $\mu_2 = 4$.

Figure 2.4 shows the verification of the results with simulation using the stated parameters.
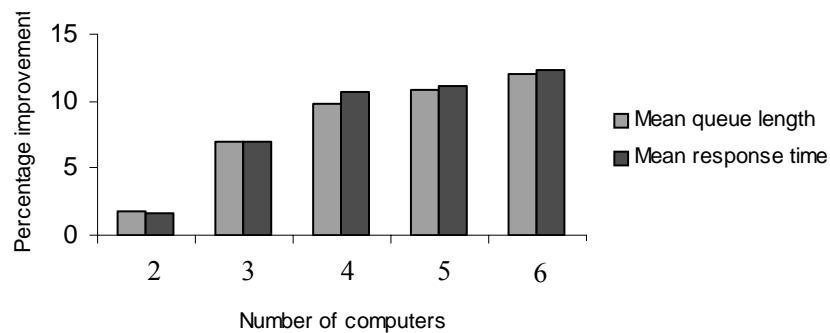
Figure 2.5. Performance improvement for a sample number of computers where $\rho = 0.9$.

Figure 2.5 shows the results of the analysis for sample cases for $N = 2, 3, 4, 5$ and 6 computers. The analysis shows that a larger range for the service rates results in greater percentage improvements of the aggregate objectives.

Research on Establishment of Accounting

System for Safety Resources

Enzhu Li

School of Management, China University of Mining & Technology, Xuzhou 221116, China

School of Accounting, Shandong University of Finance, Ji'nan 250014, China

E-mail: lez11513@163.com

Abstract

With the method of theoretical analysis, this thesis, combining the new managerial policies of economic resources invested to areas of safety production, the current severe actual situation of safety production, the negative social influences and the heavy economic losses of the accidents in production, demonstrates the necessity of establishing the accounting system for safety resources systematically. Meanwhile, the main features of the proposed new accounting system of the safety resources are analyzed and the connotations of this accounting system are also given by this paper. The main viewpoint of the author includes that accounting system for safety resources is used in all units with possible accidents in production and for reflecting and controlling the resources provided in preventing accidents and the entire process of estimating and compensating the losses caused by the accidents in production. On the basis of the connotations of this accounting system, the main functions of the new accounting system are also explained by the paper. The purpose of the author is to promote the innovation of accounting system of safety resources.

Keywords: Resource, Safety, System, Accounting, Accident

1. Introduction

Safety production is an important component of sustainable development, and is the symbol of social civilization and progress. The need on safety guarantee in production and life is one of the basic needs of human. The relationship between human and nature, economy and society, safety and production should be taken into consideration in economic development so as to create a safe, harmonious and civilized productive and living environment. This paper briefly discussed the establishment of accounting system for safety resources.

2. The necessity of establishing accounting system for safety resources

According to the basic rule of science development, social practice is not only the origin of accounting system for safety resources, but also the basis for the formation, development and improvement of accounting system for safety resources. People's basic need on safety guarantee in production and life is the reason for the putting forward of establishing accounting system for safety resources. The necessity of establishing accounting system for safety resources can be explained from the following aspects.

2.1 The establishment of accounting system for safety resources is the inevitable result of social development

With the development of society and economy, and the progress of science and technology, the traditional managerial function of financial accounting has evolved to some extent, specifically, the function of accounting management is gradually expanded, accounting management is providing service for more and more objects, and the accounting business is carried out in more and more fields. So it is necessary to study the problems in theory and practice of accounting from different angles, different levels and different orientations. Accordingly, there are new changes in accounting science, which will make it develop roundly and face up to new research object and research field. Accounting science will be enriched and improved and will bring up new branches after the struggle of theoretical and practical workers. Productive activity is the fundamental power of social development, safety production and the equilibrium of economic benefit and social benefit should be strengthened in order to guarantee the normal running of productive activity. The all-around control of safety production should be strengthened in order to realize the unification of economic benefit and social benefit. Under the guidance of management theory, accounting theory and safety economy theory, systematically studying the safety in production and corresponding configuration, management and accounting of safety resources, as well as the relating information disclosure rule will be a new subject in accounting science.

2.2 The establishment of accounting system for safety resources is the inevitable result of sustainable development

Sustainable development can be traced back to the bankruptcy of traditional development concept. In sustainable development, not only economic growth, but also resource, environment, social progress and the all-round development of human are the indexes to evaluate development. In 1984, Yining Lai, a famous Chinese economist, put forward a theory that a perfect economic growth should includes the effective growth and reasonable configuration of material resource, human resource and capital resource (Lai, 1984). In 1992, the World Commission on Environment and Development (WCED) defined the sustainable development; briefly speaking, sustainable development means the development that meets the needs of the present without compromising the ability of future generations to meet their own needs. Human is the subject of social existence and development, and human's need includes various aspects. Maslow, the famous psychologist put forward that individual needs can be included in the levels of human needs, the basic need of human is physiological need, i.e. the need for clothing, food, housing and transportation, then it is the safety need, social needs, esteem needs, and self actualization needs. Maslow's "Hierarchy of Needs" reflects the diversified value system, and these values can not be reduced to single value. Similarly to all the things, safety production is a process, and the process includes different phases and specific development objectives, in addition, the content and emphasis of safety production will be different in different countries, areas and at different stages.

2.3 The establishment of accounting system for safety production is the inevitable demand of high-frequency accident in production

In recent years, data from international organizations indicate that production accident has become a world problem. In 1999, Kofi A. Annan, the former Secretary General of United Nations, pointed out at the World Occupational Safety and Health Conference held in Brazil that the economic loss caused by casualty accidents and occupational disease accounts for 4% of world GDP (Zhang, 2005). In 2003, International Labor Organization estimated that the number of people who died from serious production accidents in the world is 355 thousand (ILO, 2005). Production accident causes great harm to Chinese economy and sustainable development, including the following aspects:

2.3.1 Serious personal injury and economic loss

In recent years, over 100 thousand people died from variant accidents and occupational diseases, and 700 thousand people are injured by them, the economic loss estimated is 80 to 120 billion Yuan (Zhang, 2006). State Administration of Work Safety publicized on line in the beginning of 2007 that, from Juanary 1st, 2006 to December 24th, 2006, there were 95 large accidents, in which over 10 people died, and a total of 1562 people died (State Administration of Work Safety, 2006). Production Accidents caused damage to life and health of present generations and future generations, and seriously endangered the human resource of China.

2.3.2 Shortage of human resource in relating industries

With the improvement of living standard in China, people's demand on safety production is becoming higher and higher. Chinese basic policy of family planning will be influenced if the situation of high-frequency production accidents and occupational damage is not controlled, because only child will be the main labor force in 21st century, several families and individuals will be influenced if a young man is injured in accident. Accordingly, it will be difficult for some high risk industries to hire workers and technicians, if the situation goes on, the development of some industries will be influenced.

2.3.3 The export of products meets "green barrier"

After China' entry into WTO, China should abide by the rules of international health and safety management system, enterprise should have safety production conditions and the product should measure up to the safety standard. China is becoming a "world factory", if the situation of safety production becomes "green barrier", Chinese foreign trade and global image of China will be directly influenced.

2.4 The establishment of accounting system for safety resources is needed by the enlargement of safety investment scale

In the era of knowledge economy, people depend on safety intensely and demand on safety urgently. The personal casualty and great economic loss caused by production accidents make human pay more attention to the economic meaning of safety. When attaching importance to the meaning of life and health, social benefit and economic loss should be paid attention to, so investment in safety resources should be increased. In order to establish long-term effective mechanism of safety production in high dangerous trades, strengthen financial management of the invested safety resources, and stick up for the interest of enterprise, employees and social public, in accordance with law and decision of State Council, Chinese Ministry of Finance and State Administration of Work Safety established Provisional Measures on Financial Management of Safety Production Expenses in High Dangerous Industries and Enterprises, which prescribed that enterprise should establish management system for safety production expenses. Safety production expenses is the capital specially used to improve on the conditions of safety production of enterprise, the capital should be set aside according to the standard and be listed in the cost of enterprise. The measure has come into effect since

January 1st, 2007; it is no doubt that enterprises will greatly increase the investment of various safety resources, accordingly the management and accounting of the large amount of investment will bring new challenge to accounting science.

3. The connotation and orientation of accounting system for safety resources

3.1 The connotation of accounting system for safety resources

Accounting system for safety resources is a management system to reflect and control the process and results of safety resources investment and estimation and compensation of loss in accident using multiple units, and the main unit is money. The main function of accounting system for safety resources is to provide accurate, timely and effective information for the users of safety accounting information. The information about input and usage of safety resources as well as the situation of production accident, loss compensation will help users to make corresponding decisions, which will be propitious to the improvement of economic benefit and social benefit of the whole process of production.

3.2 The orientation of accounting system for safety resources

The problems relating to accounting of safety production are usually discussed from the aspects of labor rights and social responsibility macroscopically or microcosmically.

Corporate social responsibility means that, in market economy, corporate should not only pursuit profit for the stockholders, but also think about the interests of people who will influence or will be influenced by the behavior of corporate. The interest of employee is the most direct and most important content of corporate social responsibility. Corporate social responsibility is not a new concept, it is put forward in 1920s, at that time, the expansion of capital brought about a series of contradictions, such as rich and poor differentiation, labor problem, labor and capital conflict (Liu, 1999), but no special study was carried out in the accounting of safety resources. Safety is a common problem of human, and is a practical problem corporate or industry has to face up to. So it is necessary to carry out study on the accounting of safety resources microscopically and to carry out study on the allocation of safety resources macroscopically. The orientation of accounting system for safety resources should be studied from the following angles.

3.2.1 Study on the influence of macro-economic factors on safety

Macro-economic factors include economic system, economic structure and economic development and so on; the influence of macro-economic factors on safety, and the relationship between macro-economic factors and human safety activity should be studied; the relationship between safety investment growth rate and the development speed of social economy should be probed into theoretically.

3.2.2 Study on the influence of production accident on social economy

Probe into the influence of loss in accident on social economy and find out the rule at different stages, in different areas, industries, departments, and in different technological level and productivity level. Probe into the theory and method to analyze and evaluate the accident and loss, find out scientific and accurate theory and method according to the characteristics of loss, so as to provide support for grasping the rule of the influence of production accident on social economy.

3.2.3 Study on the effect of safety activity

The contribution of safety to the human and society should be probed into scientifically, accurately and roundly, in other words, the rule of interests brought by safety should be studied. The interests brought by the realization of safety to individuals, corporate, the nation and the whole society will be of great significance for the establishment and programming of policy for investment in safety, and will be the necessary step to evaluate safety benefit scientifically.

3.2.4 Study on the benefit rule of safety activity

The benefit of safety has relationship with the benefit of production, but there are differences between the two concepts. The benefit of safety includes not only economic benefit, but also the social benefit of non value factors including health, stability, happiness etc. Hence it is difficult to evaluate the benefit of safety. Therefore, the rule of safety benefit, such as long-term effectiveness, complexity, should be studied carefully, the comprehensive benefit of safety should be revealed thoroughly so as to provide scientific evidence for evaluating and controlling the safe economic activity

3.2.5 Study on the financial management of safety resources

The method to argue about the feasibility of safety economy project, the investment policy of safety economy, the audit system for safety economy, the statistical method of loss and compensation in accident should be probed into with the purpose of using the limited appropriation reasonably and bringing the manpower, financial resource, and material resource invested into safety into play.

4. Conclusion

The established accounting system for safety resources will, on the one hand, provide accurate, timely and effective

information about the control of accident for users and help them make right decisions, on the other hand, make accounting develop with a new direction, the establishment of safety accounting system will accelerate the effective usage of the invested safety resources, and improve the productive situation and productive environment, in that way, the economic loss caused by production accident will be avoided, the economic benefit and social benefit will accordingly be improved, and in the end realize the sustainable development of society.

References

International Labor Office. (2005). Prevention: A global strategy. The ILO Report for World Day for Safety & Health at Work, Geneva.

Lai, Yining. (1984). E*conomics of education*. Beijing Publishing House.

Liu, Junhai. (1999). *Corporate Social Responsibility*. Law Press.

State Administration of Work Safety. (2006). National safety production situation from January 1st, 2006 to December 24th, 2006. [Online] Available: http://www.chinasafety.gov.cn.

Zhang, Lianying. (2006). *Occupational health and safety and environmental management*. Tianjin University Press.

Zhang, Shilian. (2005). *Management of construction safety*. China Architecture & Building Press.

The Forming Theory and the NC Machining for

The Rotary Burs with the Spectral Edge Distribution

Huran Liu

Department of Mechanical Engineering, Zhejiang University of Science and Technology

Hangzhou, c.y. chan, 310023, China

E-mail: lhrzust@126.com

Abstract

This paper researched the rotary burs with special cutting edges, which is the newest lay out of such tools, and represents the international direction of development and advanced level. So that improved the cutting condition of the cutter.

Keywords: Across edge, Rotary burs, NC machining

Introductions

For the ball ended or tipped rotary burs, the cutting edges must joint together at the tip, where the depth of the groove of cutting edge is zero in theory. In the vicinity of the tip, the grooves are very shadow, while the edges are very densely concentrated. So that the space is very limited, the cutting condition is very bed. In order to improve the cutting condition at the tip, the rotary burs with the spectral edge distribution is presented in this paper. In the vicinity of the tip, there are 2 kinds of cutting edges: one is called the main edge, it passing through the tip as the ordinary edge; another kind is called the branch edge, which did not passing through the tip. In the vicinity of the tip the main edges tack part into the cutting, while the branch edges did not tack part into the cutting, so that increased the space in the vicinity of the tip, and there for improved the cutting condition dramatically.

1. The special cutting edge

The ordinary cutting edge, is defined as the intersect curve of the inclined plane with the rotary surface of the cutter. The inclined angel of the plane is β_k. We have following relationship:

$$\sin \varphi = -\frac{L-x}{r} tg\beta_k \tag{1}$$

In the equation:

ϕ : The angel between the radiate line of any point on the edge and the *xoy* plane

L : The distance from the center of the ball to the intersect point of plane and the axis

r: The rotary radius of any point at the surface

β_k : The angel between the plane and the axis

The range of the x: $x \le L$.

The special cutting edges, however, is defined as a series of intersect curves of a series of inclined planes with the rotary surface of the cutter. The inclined angels of the plane are β_{ki}. We have following relationship:

$$\sin \varphi_i = -\frac{L_i-x}{r} tg\beta_k \text{ i} \tag{2}$$
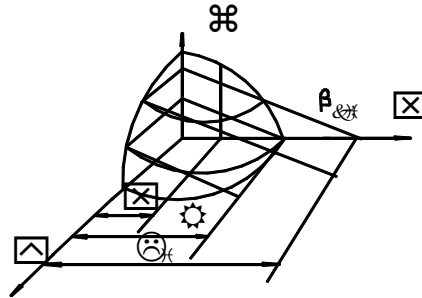
Figure 1. A series of intersect curves of a series of inclined planes with the rotary surface of the cutter

In the equation:

ϕ_i: The position angel

β_{ki}: The angel between the plane *i* and the axis.

L_i: The distance from the center of the ball to the intersect point of plane *i* and the axis.
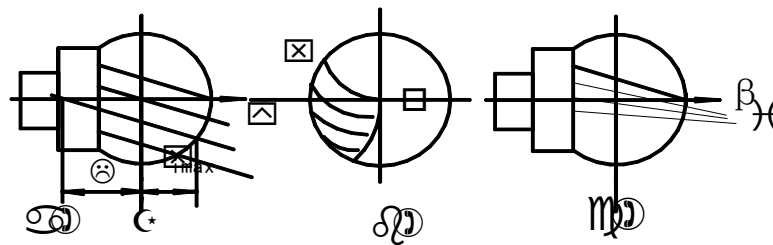
Figure 2.   Rotary burs with the spectral edge distribution

2. The composed cutting edge

For the composed cutting edge, at the connecting point of two kind edges($x = x_g$), the neighboring edges must have same position, and the two edges must satisfy the condition of smooth connection.   That mines the plans to cut the ball should not be parallel with each other. Let the angel between the planes *i* and the axis is β_i, than we have:

$$\sin\varphi_i = -\frac{L_i - x}{r}tg\beta_i \tag{1}$$

In the equation:

ϕ_i: The position angel

r: The radius of the ball.

β_i: The angel between the plane *i* and the axis.

L_i: The distance from the center of the ball to the intersect point of plane *i* and the axis.

$$\cos\varphi_i \frac{d\varphi_i}{dx} = \frac{r + (L_i - x)\frac{dr}{dx}}{r^2}tg\beta_i$$

$$\frac{d\varphi_i}{dx} = \frac{1}{r\cos\varphi_i}[tg\beta_i - \frac{dr}{dx}\sin\varphi_i]$$

$$tg\beta = \frac{r}{\sqrt{1+(\frac{dr}{dx})^2}}\frac{d\varphi_i}{dx} = \frac{tg\beta_i - \frac{dr}{dx}\sin\varphi_i}{\sqrt{1+(\frac{dr}{dx})^2}\cos\varphi_i} \tag{2}$$

β: The helical angel of the edge.

In order that, at the connecting point of two kind edges, the neighboring edges have the same helical angel, and equal to the given helical angel β_i, there must have the following equation:

$$tg\beta_i = tg\beta_o \sqrt{1+(\frac{dr_g}{dx})^2} \cos\varphi_{ig} + \frac{dr_g}{dx}\sin\varphi_{ig} \tag{3}$$

In the equation:

β_0 : The helical angel of the ordinary edge

r_g : The radius of the cutter at the point of connection

ϕ_{ig} : The position parameter of the edge at the point of connection

Tack the β_i into the equation (1), we can find L_i

$$L_i = -ctg\beta_i \sin\varphi_{ig}r_g + x_g \tag{4}$$

While the equation (4) can be rewritten into:

$$x_i^2(1+tg^2\beta_i) - 2L_i tg^2\beta_i x_i + (L_i^2 tg^2\beta_i - R^2) = 0 \tag{5}$$

3. The forming theory for the rotary burs with the spectral edge distribution
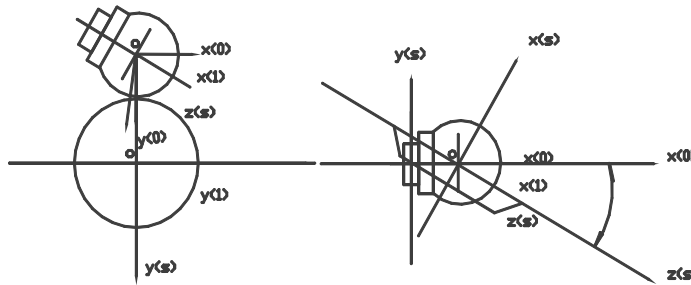
Figure 3. The coordinate system for the machining

The machining of the rotary burs with the spectral edge distribution is shown in fig.3. There are four systems:

(1)　the fixed system $S^{(0)}$:

In the system, the original point is at the center of the ball, the axes $x^{(0)}, y^{(0)}$ are along the longitudinal and transverse direction of the machine tool.

(2)　The system fixed to the Swinging base $S^{(1)}$:

　In the system, the original point $O^{(1)}$ coincides with the point $O^{(0)}$, the angel between $z^{(0)}$ and $z^{(1)}$ is τ.

(3)　The system fixed to the cutter $S^{(d)}$:

　In the system $x^{(d)}$ rotate an angel φ about $S^{(1)}$

(4)　The system fixed to the sand wheel $S^{(s)}$

In the system, the original point is at the center of the sand wheel, and moved with the sand wheel. $y^{(s)}$ and $y^{(0)}$ are parallel with each other. The angel between $y^{(0)}$ and $y^{(1)}$ is $\pi/Z-\sum$.

The transformation matrixes are as following:

$$M_{os} = \begin{bmatrix} \sin\sum & 0 & \cos\sum & x_c \\ 0 & 1 & 0 & y_c \\ -\cos\sum & 0 & -\sin\sum & z_c \\ 0 & 0 & 0 & 1 \end{bmatrix} \tag{6}$$

$$M_{o1} = \begin{bmatrix} \cos\tau & -\sin\tau & 0 & 0 \\ \sin\tau & \cos\tau & 0 & 0 \\ 0 & 0 & 1 & 0 \\ 0 & 0 & 0 & 1 \end{bmatrix}$$

(7)

Refer to the Figure 3, the coordinate of the any point at the surface of sand wheel M_B is:
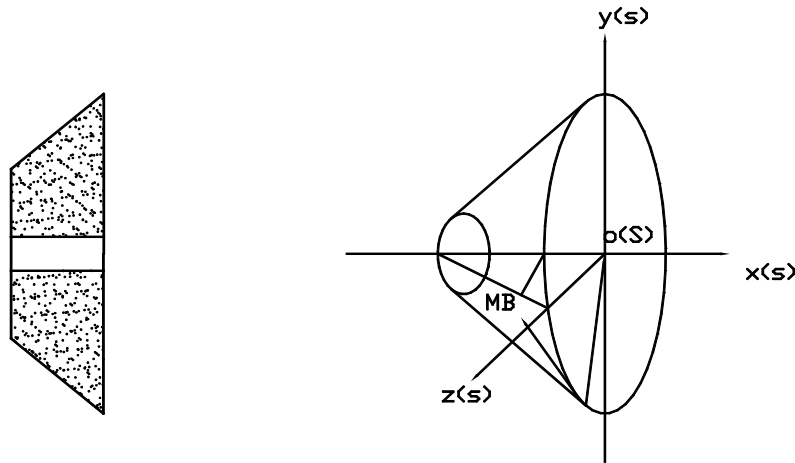
Figure 4. Sand wheel

$$x_{MB}^{(s)} = -(R - r_{mB}) tg\alpha_B$$

$$y_{MB}^{(s)} = -r_{mB}\cos\theta_B$$

(8)

$$z_{MB}^{(s)} = r_{mB}\sin\theta_B$$

In the equation,

R : The radius of the sand wheel.

r_{mb} : The radius of the f the any point at the surface of sand wheel M_B

θ_B : The angular position parameter of the any point at the surface of sand wheel M_B

α_B : The angel of the cone of the sand wheel

The normal vector of the any point at the surface of sand wheel M_B :

$$\overset{V}{n}{}_{MB}^{(s)} = (-\cos\alpha_B, -\sin\alpha_B\cos\theta_B, \sin\alpha_B\sin\theta_B)$$

(9)

When transformed into the fixed system:

$$x_{MB}^{(o)} = --(R - r_{mB}) tg\alpha_B\sin\sum + r_{mB}\sin\theta_B\cos\sum + x_c$$

$$y_{MB}^{(o)} = -r_{mB}\cos\theta_B + y_c$$

(10)

$$z_{MB}^{(o)} = (R - r_{mB}) tg\alpha_B\cos\sum + r_{mB}\sin\theta_B\sin\sum + z_c$$

(11)

$$\overset{V}{n}{}_{MB}^{(o)} = (-\cos\alpha_B\sin\sum + \sin\alpha_B\sin\theta_B\cos\sum, -\sin\alpha_B\cos\theta_B, \cos\alpha_B\cos\sum + \sin\alpha_B\sin\theta_B\sin\sum)$$

The coordinate of the any point at the bottom of sand wheel in the system $S^{(s)}$:

$$x_{MA}^{(s)} = 0 \qquad y_{MA}^{(s)} = -r_{mA}\cos\theta_A \qquad z_{MA}^{(s)} = r_{mA}\sin\theta_A$$

(12)

And the normal vector:

$$\overset{V}{n}{}_{MA}^{(s)} = (1, 0, 0)$$

(13)

When transformed into the fixed system:

$$x_{MA}^{(o)} = r_{mA}\sin\theta_A\cos\sum + x_c \qquad y_{MA}^{(o)} = -r_{mA}\sin\theta_A + y_c \quad z_{MA}^{(o)} = r_{mA}\sin\theta_A\sin\sum + z_c$$

(14)

$$\overset{V}{n}{}_{MA}^{(o)} = (\sin\sum, 0, \cos\sum)$$

(15)

The movement in manufacture:

The swinging angel of the Swinging base: $tg\tau = -\dfrac{dr}{dx}$

The rotation of the work: $\varphi = -\varphi_i$

The coordination of the center of the sand wheel:

$x_c = x_{p(i+1)}^{(0)} + (R - r_{mB})tg\alpha_B \sin\sum - r_{mB} \sin\theta_B \cos\sum$

$y_c = y_{p(i+1)}^{(0)} + r_{mB} \cos\theta_B$

$z_c = z_{p(i+1)}^{(0)} - (R - r_{mB})tg\chi_B \cos\sum - r_{mB} \sin\theta_B \cos\sum$

4. Examples

A ball end rotary burs with the spectral edge distribution, the basic parameters are as following:

The diameter of the ball: d = 13mm

The length of the cutter: l=10mm

The helical angel: β= 20°

The number of the tooth: z= 24

When divided into 6 districts, one district contains 4edges.

The radius of the sand wheel: D= 100mm

The angel of the cone of the sand wheel: α_B = 50 ^{o}

The machined rotary burs with the spectral edge distribution is as shown in Fig.5
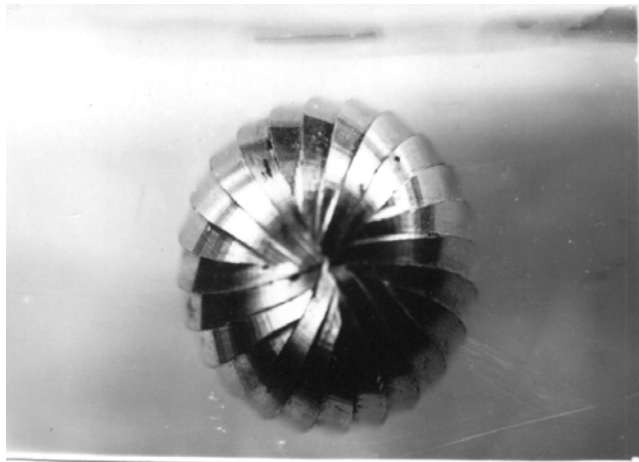
Figure 5. The rotary burs with the spectral edge distribution

References

Liu, Huran. (1994).The cutting edge of the rotary tool with complex surface. *Journal of Cutting Tool.* 8

Liu, Huran. (1998). The Forming Theory and the NC Machining for the Rotary Burs on the 5-axis NC machine tool. *Journal of Machine tool and manufactureing*. 1

Zhou, Ji. (2002). The moldering and design of the transitional cutting edges. *Journal of Chinese Mechanical Engineering* .No(5)

Oxovanadium (IV) Dipicolinate: Structure

Nucleolytic and Anticancer Property

Teoh Siang Guan (Corresponding author)

School of Chemical Science, Universiti Sains Malaysia, 11800 Minden,

Penang, Malaysia

Tel : +6016- 4510177   E-mail: ppsk1@yahoo.com or sgteoh@usm.my

Ng Chew Hee

Faculty of Engineering and Science, Universiti Tunku Abdul Rahman, 53100 Kuala Lumpur, Malaysia

Tel : 603-41079802   E-mail: ngch@mail.utar.edu.my

Tarn Fang Lai

Faculty of Engineering and Science, Universiti Tunku Abdul Rahman, 53100 Kuala Lumpur, Malaysia

Lim Eng Khoon

School of Chemical Science, Universiti Sains Malaysia, 11800 Minden,

Penang, Malaysia

Tel : +6016-4164478   E-mail: chemistlim@yahoo.com

Sharif Mahsufi Mansor

Centre for Drug Research, 11800 Penang, Universiti Sains Malaysia;

Pauline Balraj

Molecular Pathology Unit, Institute for Medical Research, 50588 Kuala Lumpur, Malaysia

Tai Lin Chu

Molecular Pathology Unit, Institute for Medical Research, 50588 Kuala Lumpur, Malaysia

Bohari M. Yamin

School of Chemical Science and Food Technology, Universiti Kebangsaan Malaysia, 43600 Bangi, Selangor, Malaysia

Tel : +6016-6587435   E-mail: bohari_nor@yahoo.com.my

Seik Weng Ng

Department of Chemistry, University of Malaya, 50603 Kuala Lumpur, Malaysia

Abstract

Diaqua(dipicolinato)oxovanadium (IV) ethanol solvate crystallizes in the triclinic space group $P1$. The complex was characterized by FTIR, elemental analysis, thermal gravimetric analysis, and solution visible spectral analysis. The complex alone cleaved DNA in the absence of hydrogen peroxide and its nucleolytic efficiency is greater than that of $VOSO_4$. Its nucleolytic efficiency is affected by the choice of buffer used and pH. DNA cleavage can be inhibited by DMSO, NaN_3 and catalase, implying involvement of ROS. An MTT assay, involving the lung cancer cell line PC9, gave IC_{50} values of 9.5 μM and 16 μM for the complex and $VOSO_4$ respectively. For breast cancer cell line MCF-7, this complex is less cytotoxic, with an IC_{50} of 16 μM.

Keywords: Oxovanadium(IV) complex, Dipicolinic acid, Crystal structure, DNA cleavage, Anticancer

1. Introduction

Vanadium(IV) and vanadium(V) inorganic salts and complexes have generated widespread interest due its insulin-mimetic property [Crans, *et al*., 2000, Sakurai, *et al*., 2002, Shechter, *et al*., 2003]. In the search for a better and less toxic oral substitute for insulin in the treatment of both Type I and Type II diabetes, vanadium complexes of newer

organic ligands have been synthesized. Among them, the vanadium (IV) and vanadium (V) complexes of dipicolinic acid and derivatives have been found to be insulin-mimetic [Crans, *et al*., 2000, 2003]. Besides this insulin-mimetic property, some vanadium salts and complexes have been investigated for their antitumor behaviour and their possible development into a new class of non-platinum antitumor agents [Evangelou, 2002]. Here, Evangelou reported that DNA cleavage *in vivo* and *in vitro* was shown to be among one of the different modes of action of these antitumor vanadium compounds. This paper presents the crystal structure of a di*aqua* (dipicolinato)oxovanadium(IV) ethanol solvate, abbreviated as VO(dipic), and both its nucleolytic and anticancer properties.

2. Experimental

2.1 Reagents, methods and instrumentation

All chemicals purchased were of reagent grade and were used without further purification. Ethanol, concentrated hydrochloric acid, sodium azide, dimethyl sulfoxide (DMSO) and catalase were used as received. Supercoiled plasmid pBR322 was purchased from BioSynTech (Fermentas). Elemental analysis was performed using a Perkin Elmer 2400 CHN/O analyzer series-11. Infrared spectra (KBr pellets) were recorded using a Perkin-Elmer 2000 Infrared Spectrometer. The UV-visible was obtained from a Hitachi U-2000 spectrophotometer. The electrophoresis experiments were performed on a horizontal gel   electrophoresis system.

2.2 Synthesis of VO(dipic)

A mixture of V_2O_5 (1.00g, 5.50 mmol), ethanol, concentrated hydrochloric acid and distilled water in a total volume of 20 ml was heated until all V_2O_5 dissolved. A solution prepared from dipicolinic acid (also called pyridine-2,6-dicarboxylic; 1.01g, 6.05 mmol) and NaOH (0.24 g, 6.05 mmol) in a small volume of water was then added to the vanadium solution. The mixture was heated for another 3 hours. The pH of the resultant mixture was adjusted to 2.5-2.7 with Na_2CO_3 solution. The dark green solution was then allowed to cool down to room temperature. Green crystals were obtained on cooling the solution overnight. Yield 0.91g (28.4 % based on V). Elemental analysis: found C, 32.71; H, 3.68; N, 4.38 %. Calculated for $[VO(C_7H_3NO_4)(H_2O)_2]$. 0.5 CH_3CH_2OH: C, 33.00; H, 3.46; N, 4.81 %. IR (KBr): 3160vs, 1670vs, 1598s, 1434m, 1350vs, 1258m, 1177s, 1141m, 1095w, 1071s, 1048s, 1033m, 972vs, 924m, 855w, 831w, 772s, 750s, 683s, 591w, 490w, 459s cm-1.

2.3 Crystal structure determination

Diffraction data was collected on a Bruker APEX CCD area-detector diffractometer at 295 K on a crystal of size 0.50 x 0.46 x 0.26 mm using the ω-scan technique over the range $2.0 < \theta < 25.0^o$ equipped with Mo Kα radiation ($\lambda = 0.71073$ Å). The intensity data was collected over the range $\theta = 2.0 – 25.0^o$ for 3676 reflections. Lorentz-polarization and absorption corrections were applied. Crystal structure data and refinement are tabulated in table 1. The structure was solved and refined by using SHELX system of programs [Sheldrick, 1997]. The final R ($F^2 > 2\sigma(F^2)$) and $Rw(F^2)$ values were 0.035 and 0.094. The water H atoms were located and refined. The ethanol molecule is disordered over two sites, and was refined with distance restraints. All non-hydrogen atoms were refined anisotropically. The hydrogen atoms were treated by a mixture of independent and constrained refinement. The weighting scheme was $w = 1/[\sigma^2(Fo^2) + (0.0548\ P)^2 + 0.5286\ P]$ where $P = (Fo^2 + 2Fc^2)/3$. The perspective view of the molecule was obtained using ORTEP [Johnson, 1976]. Selected bond distances and angles are listed in table 2. Detailed crystallographic data for the crystal structure analysis have been deposited with the Cambridge Crystallographic Data Center, CCDC No. 604153.

2.4 Electrophoresis

Agarose gel electrophoresis experiments were carried out on supercoiled plasmid DNA pBR322 (4.4 kb) using a horizontal gel system. For each experiment, a 20 μL mixture consisting of the appropriate volumes of stock solutions of DNA, complex dissolved in Tris-NaCl buffer pH 7 (100 mM Tris, 150 mM NaCl; abbreviated as TN buffer; Tris = Tris(hydroxymethyl)aminomethane; EDTA = disodium salt of ethylenediaminetetraacetic acid) buffer. The nucleolytic experiment was repeated in phosphate buffer at pH 7.5. The effect of ROS radical scavengers DMSO (.OH), catalase (peroxide species and superoxide radical anion) and sodium azide (singlet oxygen) on the nucleolytic activity of VO(dipic) was also investigated. Each 20 μL mixture in experiments involving scavengers was similarly prepared. All samples were incubated at 37 ^{o}C for 1 or 4 h, and then electrophoresed on 1% agarose gel for 2 - 3 h at 80V. Essentially, 0.0125 mg mL-1 DNA samples were incubated with the complex with or without the scavenger. The resultant DNA bands were stained with ethidium bromide before being photographed under UV light using a Syngene Bio Imaging system and the image was viewed with Gene Flash software.

2.5 MTT assay

The human lung adenocarcinoma cell line, PC9 used in this study was obtained from American Type Culture Collection. The cells were grown in RPMI 1640 supplemented with 10% FCS, 0.025 M Hepes, 0.024 M sodium bicarbonate, 50 units/ml penicillin G/streptomycin sulfate at 37 ^{0}C in 5% CO_2. All tissue culture reagents were obtained from Sigma and Life Technologies Inc., Gaitherburg, MD. Cell line was cultivated for a minimum of two passages after thawing prior to

experimentation. The oestrogen receptor positive human breast adenocarcinoma cell line MCF-7 was also similarly tested. MTT assay was used to test the antiproliferative property of VO(dipic) against both cell lines. Additionally for PC9, the precursor $VOSO_4$ was also evaluated to compare the effect of chelating the dipicolic acid to the oxovanadium(IV). Exponentially growing PC9 tumour cells were seeded into a 96-well plate at a density of 9×10^4 cells/well and incubated in a medium containing the vanadium compounds at concentration ranging from 1.6 – 240 µM for 72 h at 37 ^{0}C in humidified 5% CO_2 atmosphere. For the MCF-7 tumor cells, 0.25% trypsin EDTA solution was used to detach the cells from the surface, and the concentration of VO(dipic) used varies from 1.9 – 1000 µM. Every experiment was conducted on triplicate wells. Into each well 20 µl of MTT (5mg/ml) was added. The plates were then incubated at 37 ^{0}C for 4 h to allow MTT to form formazan crystals. The crystals were then solubilized using DMSO for a few minutes. The absorbance of each well was measured in a microplate reader Dynatech MRX at 570 nm with a reference wavelength of 630 nm. The percentage of cell viability was calculated with the formula: Average A570 value for live cell (test) / average A570 value for live cell (control) x 100. The IC_{50} values were obtained from the graphs drawn.

3. Results and discussion

3.1 Structure analysis

The ORTEP plot of the complex (Fig. 1) shows the structure of the complex together with the lattice ethanol molecule (which is disordered). The dipicolinate anion coordinates to the VO^{2+} cation as a tridentate ligand *via* two carboxylate oxygen atoms and its pyridyl nitrogen atom such that the carboxylate oxygen atoms are *trans* to each other while the pyridyl nitrogen atom is *trans* to the oxo atom of the VO^{2+} cation. The non-hydrogen atoms of both the dipicolinate and oxovanadium (IV) moieties are coplanar. The coordinated water molecules are *trans* to each other; they are roughly perpendicular to the 'dipicolinate-V=O' plane and have the appearance of the two wings of a spaceship as they are slightly bent inwards towards the pyridyl nitrogen atom. Thus, the vanadium atom has a distorted octahedral geometry. The structure of the present diaqua(dipicolinato)oxovanadium(IV) complex is the same as that of previously determined dihydrate and tetrahydrate species [Yong, *et al*., 2004, Chatterjee, *et al*., 1999 and Bersted *et al*. 1968]. The only difference is that our complex has ethanol molecules instead of water molecules in the crystal lattice, and this leads to a slight difference in the hydrogen bonding network. The ethanol molecule is disordered over two sites in a 1:1 ratio but the two moieties share a common hydroxyl group. Two adjacent diaqua(dipicolinato)oxovanadium(IV) molecules in the same unit cell are hydrogen-bonded to each other *via* bonding between coordinated O2w atom (proton donor) of one complex molecule to the carboxylate oxygen atom O3 (proton acceptor) of the other complex molecule; there are thus two such intermolecular hydrogen bonds. Hydrogen bonds involving coordinated water molecules (O2w, O1w), carbonyl and carboxylate oxygen atoms (O1, O2, O3, O4) and the ethanol oxygen atom (O6) link the diaqua(dipicolinato)oxovanadium(IV) and ethanol molecules in the crystal lattice into a three-dimensional network (Fig. 2). The difference in V-O (carboxylate oxygen atom) bond length observed (V1-O1 = 2.031; V1-O3 = 2.053 Å) may be ascribed to difference in the proton donors (O1···H-O6 of ethanol molecule) and (O3···H-O2w of coordinated water molecule). The above H-bonding network is reflected in the higher temperature for the onset of the first stage of the thermal degradation of the complex. The first stage occurs over the range 125.0 - 270.0 ^{0}C, and this corresponds to the loss of coordinated water and ethanol molecules. The total weight loss is 30.0 % which is in close agreement with the calculated value of 28.2 %. However, the DTG spectrum seems to be able to distinguish the loss of these molecules as there are three endothermic peaks at 157.1 ^{o}C, 167.6 ^{o}C and 195.1 ^{o}C. The second stage of the degradation occurs over the range of 360.0 - 620.0 ^{o}C and it has an endothermic peak (DTG signal) at 474.2 ^{o}C. This may be ascribed to partial decomposition of dipicolinate ligand as the weight loss is only 24.0 %. A black residue is obtained at 800 ^{o}C. As this paper presents the biomedical property of VO (dipic) solution, the electronic spectral data of its solution was also obtained. The solution of the present complex in Tris-NaCl (TN) buffer pH 7 has a λmax of 830 nm (ϵ, 28 M^{-1} cm^{-1}) in the visible region and this is slightly different from that value (~11.2 kK, ~880 nm) which was previously obtained for the VO(dipic) tetrahydrate in Nujol mull [Bersted *et al*. 1968]. There is also a shoulder at 620 nm (ϵ, 21 M^{-1} cm^{-1}). Dissolving the complex in water shows no appreciable change in its λmax value which is 844 nm (ϵ, 34 M-1 cm^{-1}) and a shoulder at 626 nm (ϵ, 17 M^{-1} cm^{-1}), suggesting no change in coordination sphere of the complex in both media. In contrast, the spectrum of $VOSO_4$ in TN buffer has a λmax of 763 nm (ϵ, 15 M^{-1} cm^{-1}) and a shoulder at 610 nm (ϵ, 12 M^{-1} cm^{-1}). The spectrum of $VOSO_4$ in water also shows no appreciable change in the corresponding λmax values, viz. 765 nm (ϵ, 13 M^{-1} cm^{-1}) and 610 nm (ϵ, 5 M^{-1} cm^{-1}). When the complex was dissolved in phosphate buffer pH 7 instead of TN buffer pH 7, the position of the two observed bands in the visible region seems unchanged. However, the intensity of these bands is about ten times higher in phosphate buffer. The increase in intensity was even more pronounced when the pH of the buffer was increased to pH 7.5 (Table 3). Similar trends are observed for the charge transfer bands for the complex dissolved in TN and phosphate buffers.

3.2 DNA cleavage and MTT assay

3.2.1 DNA cleavage by VO(dipic)

Agarose gel electrophoresis was used to study the cleavage of supercoiled plasmid DNA pBR322 (4361 bp) by the complex. The complex, at 50 µM, is able to induce small amount of single strand cleavage of the DNA in TN buffer at pH

7 (Fig. 3, lane 4). DNA cleavage increases with increasing concentration of the complex. At about 3 mM, a linear band of DNA is observed, and this arises due to double-strand cleavage. Although double-strand break is dangerous due to possible apoptosis, direct inactivation of key genes, or consequential serious chromosomal aberrations [Barzilai *et al*, 2004], such cellular concentration level may not be normally reached. When the DNA is incubated with 6 mM of complex, almost complete conversion of supercoiled pBR322 to both nicked and linear DNA occurs. In contrast, the starting material $VOSO_4$ does not seemed to cleave the DNA at 6mM (Fig. 3, lane 11). Complexation of dipicolinic acid to the VO^{2+} enhances its nucleolytic property. This result contrasts with previous studies of DNA cleavage by other oxovanadium(IV) complexes where hydrogen peroxide is needed and reactive ˙OH radicals are involved [Evangelou, 2002, Sakurai *et al*., 1995, 1994]. The above cleavage may be due to the reaction of the VO (dipic) complex with molecular oxygen to yield oxygen-derived radical species. A previous report mentioned that vanadium (IV) could generate O_2˙ and subsequently produced peroxovanadyl [V(IV)-OO˙] and vanadyl hydroperoxide [V(IV)-OH˙] radicals [Valko *et al*., 2006]. Binding of molecular oxygen to a vanadium (IV) complex and subsequent one electron transfer was postulated to yield a very reactive V(V)-OO˙ radical species [Kotchevar *et al*., 2001]. Similar radical species may be involved in the DNA cleavage by VO (dipic) as no attempt was made to exclude dissolved oxygen. When the buffer was changed to phosphate pH 7.5, the VO dipic) can nicked the DNA at a lower concentration, i.e. 10 μM (Fig. 4, lane 3) and shorter incubation time (1h). While 6 mM of the complex in TN buffer pH 7 was needed to convert most of the supercoiled DNA to both nicked and linear DNA, 1 mM of the complex in phosphate buffer at pH 7.5 could completely convert the supercoiled DNA to nicked and linear DNA (Fig. 4, lane 5). The increased nucleolytic efficiency may be partly attributed to relative quenching of ROS since it was previously found that Tris buffer could more efficiently scavenged ˙OH radical than phosphate buffer [Hicks et al., 1986]. The poorer scavenging effect of the phosphate buffer for the ROS produced in our experiment could help to explain the enhanced cleavage of DNA. Another contributing factor may be due to apparent increase in VO (dipic) species in phosphate buffer at pH 7.5 than those in TN buffer at pH 7. The λmax of the UV-visible spectral bands of the complex in both TN and phosphate buffers at pH 7 and pH 7.5 are practically the same (Table 3). The higher molar absorptivity, ε, of each band of the complex in phosphate buffer at pH 7.5 than the corresponding one in TN buffer at pH 7 suggests higher concentration of VO (dipic) species. Interestingly, increasing the concentration of the complex in the phosphate buffer from 1 mM to 6 mM did not cause increase in the extent of DNA cleavage. Inhibition of DNA cleavage by VO (dipic) was tested with various scavengers which are commonly used to quench the corresponding targeted radicals (Fig. 5). The results show that sodium azide (singlet oxygen scavenger), catalase (peroxide species scavenger) and DMSO (hydroxyl radical scavenger) can inhibit the DNA cleavage. Collectively, these results suggest the role of ROS in the DNA cleavage by VO(dipic). The cleavage mechanism is thus oxidative.

3.2.2 Cell viability assay

As some anticancer drugs act by targeting and degrading the DNA of the cancer cells, we have used MTT assay to screen the anticancer property of the VO (dipic) on two cancer cell lines. For the lung cancer cell line PC9, IC_{50} of the complex is 9.5 μM while that for $VOSO_4$ is 16 μM (Fig. 6). Coordination of the dipicolinate ligand to the oxovanadium (IV) ion seems to enhance its anticancer property. Our results differ from a recent investigation into the cytotoxicity of three vanadium (III, IV, V)-dipicolinate complexes on Caco-2 cells gave their IC_{50} values at 1.8 mM [V^{III}-dipic], 1.9 mM [V^{IV}dipic= VO (dipic) reported in this paper] and 1.7 mM [V^V-dipic] respectively [Zhang, *et al.*, 2006]. These values could not be correlated with the order of decreasing redox potential or of decreasing capacity to produce reactive oxygen and nitrogen species (RONS). Of relevant to our findings is that the [$V^{IV}O$ (dipic)($H_2O)_2$].$2H_2O$ used generated the least amount of RONS amongst the three vanadium-dipicolinate complexes and yet all these three complexes exhibited similar level of cytotoxicity. Our finding, in contrast, shows higher cytotoxicity using the same MTT assay. However, it is noted that the type of cells used is different. The VO (dipic) used may have a lower cytotoxicity to Caco-2 cells (which are originally derived from a human colorectal adenocarcinoma and are developed into a suitable model for the evaluation of intestinal absorption of drugs). Of relevance here is the fact that the IC_{50} values of these three vanadium-dipic complexes is similar to those obtained for *bis*(maltonato)oxovanadium(IV), vanadyl acetylacetonate, and other vanadium (IV, V) complexes [Yang , *et al.* 2004, Rehder, *et al.* 2002]. It also seems reasonable to exclude the presence of ethanol solvate (some concentration as complex, i.e. 9.5 μM) as a factor in the higher toxicity of the present VO (dipic) complex towards PC9 cells as mM concentrations of ethanol have been found to promote cell growth of breast cancer cell line MCF-7 [DeCupis *et al*., 1998, Przylipiak, *et al*., 1996, Izevbigie, *et al*. 2002]. When VO (dipic) was screened on the MCF-7 cancer cell line, its IC_{50} was slightly higher, at 16 μM. Thus, this complex is very cytotoxic towards PC9 and MCF-7 cancer cells. Our nucleolytic experiments suggest that cell death may be due to cleavage or fragmentation of DNA of these cancer cells and that the active species responsible for this are ROS which resulted from the *in vitro* reaction of VO (dipic). However, this is not the only mechanism whereby vanadium compounds induce cell death [Ray, *et al*. 2006].

References

Barzilai, A.& Yamamoto, K-I. (2004). DNA Repair, 3, pp.1109.

Bersted, B. H., Belford, R. L. & Paul, I. C. (1968). *Inorg. Chem.* 7, pp.1557.

Chatterjee, M. & Ghosh, S. (1999). *Transition Met. Chem.* 24, pp183

Crans, D. C. (2000). *J. Inorg. Biochem.*, 80, pp. 123.

Crans, D.C., Mohroof-Tahir, M., Johnson, M. D., Wilkins, P. C., Yang, L., Robbins, K., Johnson, A., Alfano, J. A., Godzala, M. E., Austin, L. T. & Willsky, G. R. (2003). *Inorg. Chim. Acta,* 356, pp 365.

DeCupis, A., Pirani, P., Fazzuoli, L.& Favoni, R. E. (1998). *In Vitro Cell Dev. Biol.* 34 pp. 836.

Evangelou, A. M. (2002). *Critical Rev. Oncology/Hematology*, 42, pp. 249.

Hicks, M. & Gebiski, J. M.(1986). FEBS Letters, 199, pp. 3563.

Izevbigie, E. B., Ekunwe, S. I., Jordan, J. & Howard, C. B. (2002). *Exp. Biol. Med.* 227, pp. 260.

Johnson, C. K., (1976). *ORTEP*-II, Report ORNL-5138 (Oak Ridge National Laboratory, Oak Ridge, Tennessee, USA, 1976).

Kotchevar, A. T., Ghosh, P., DuMex, D. D. & Uekun, F. M. (2001). *J. Inorg. Biochem*. 83**,** pp. 51.

Przylipiak, A., Rabe, T., Hafner, J., Przylipiak, M. & Runnehaum, M. (1996). *Arch. GynecolObstet.* 258, pp.137.

Ray, R. S., Rana, B., Swami, B., Venu, V.& Chatterjee, M. (2006). *Chemico-Biological Interactions*, 163, pp. 239.

Rehder, D., Costa Pessoa, J., Geraldes, C. F., Castro, M. C., Kabanos, T., Kiss, T., Meier, B., Micera, G., Pettersson, L., Rangel, M., Salifoglo, A., Turel, I. & Wang, D.(2002). *Inorg. Chem.* **7,** pp**.** 384.

Sakurai, H. (1994). *Envi. Health Perspect.* 3 pp. 35.

Sakurai, H., Kojima, Y., Yoshikawa, Y., Kawabe, K. & Yasui, H. (2002). *Coord. Chem. Rev.*, 226, pp 187.

Sakurai, H., Tamura, H. & Okatani, K. (1995). *Biochem. Biophys. Res. Commun*. 206, pp. 133

Shechter, Y.,Goldwaser, I., Mironchik, M., Fridkin, M. & Gefel, D. (2003). *Coord. Chem. Rev.*, 237, pp. 3.

Sheldrick, G. M. (1997). *SHELX*-97, Programs for Crystal Structure Analysis (Release

97-2):(Göttingen University: Germany, 1997).

Valko, M., Rhodes, C. J., Moncol, J., Izakovic, M. & Mazur, M. (2006) *Chemico-Biological Interactions* 160, pp 1.

Yong, H. X., Katsuyuki, A. & Feng, Y. B. (2004). *J. Coord. Chem.* 57, pp157

Yang, X. G., Yang, X. D., Yuan, L. , Wang, K.& Crans, D. C. (2004) *Pharm. Res*. 21, pp.1026.

Zhang, Y., Yang, X-D., Wang, K. and Crans, D. C. (2006). *J. Inorg. Biochem*., 100, pp. 80.

Table 1. Crystal data and structure refinement

Formula	$C_9H_{13}NO_8V$	a (Å)	6.7041(4)
Formula weight	314.14	b (Å)	9.2664(5)
Crystal system	Triclinic	c (Å)	11.0221(7)
Space group	$P1$	α(°)	112.9610(10)
V (Å^3)	608.42(6)	β (°)	102.3640(10)
D_c (g cm^{-3})	1.715	γ (°)	93.1950(10)
F(000)	322	T (K)	303(2)
μ (mm^{-1})	0.852	Z	2
Index ranges	$-7 \leq h \leq 6$; $-10 \leq k \leq 10$; $-12 \leq l \leq 13$	λ (Å)	0.71073
R [$F^2 > 2\sigma(F^2)$]	0.034	θ range (°)	2.0, 25.0
R_w [$F^2 > 2\sigma(F^2)$]	0.094	Reflections refined	2010
R (all data)	0.035	Goodness-of-fit on F^2	1.05
R_w (all data)	0.094	S	1.05

Table 2. Selected geometric parameters

Bond lengths and angles (Å, °)			
V1 - O5	1.592(2)	O5-V1- O1w	99.20(10)
V1 - O1w	2.015(2)	O5-V1- O1	110.13(9)
V1 - O1	2.031(2)	O1w- V1- O1	86.27(7)
V1 - O3	2.053(2)	O5 - V1- O3	102.90(9)
V1 - O2w	2.080(2)	O1w -V1- O3	89.27(7)
V1 - N1	2.157(2)	O1- V1- O3	146.97(7)
O1 - C1	1.296(3)	O5-V1- O2w	93.70(9)
O2 - C1	1.223(3)	O1w- V1- O2w	166.88(8)
O3 - C7	1.294(3)	O1- V1- O2w	87.10(7)
O4 - C7	1.224(3)	O3 - V1- O2w	90.13(7)
O6 - C8	1.529(8)	O5 - V1- N1	174.38(9)
O6 - C8'	1.430(8)	O1w - V1- N1	84.97(8)
		O1- V1- N1	73.75(7)
		O3 -V1- N1	73.26(6)
		O2w-V1-N1	82.32(7)
		C1- O1-V1	122.68(14)
		C7- O3-V1	122.52(14)

Table 3. Electronic spectral data of VO (dipic)

Type of buffer & pH	d-d transition λ (nm),ε (cm^{-1}M^{-1})	Charge transfer band λ (nm),ε (cm^{-1}M^{-1})
Phosphate pH 7.5	836, 26	268, 5494
	616 (sh), 16	207, 18575
TN pH 7.5	839, 25	267, 5081
	619 (sh), 12	214, 13516
Phosphate pH 7	839, 4	269, 70
	615 (sh), 2	202, 310
TN pH 7	840, 0.3	268, 72
	619 (sh), 0.2	209, 215
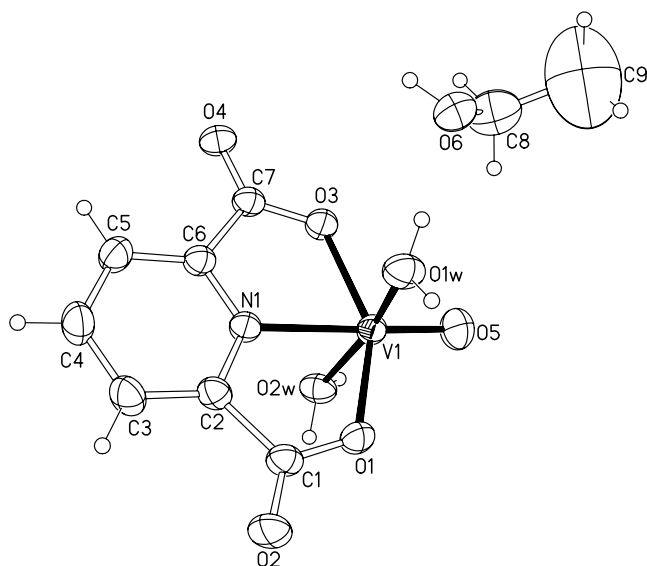
Figure 1. 50 % probability ORTEP plot of the VO (dipic)
complex showing the lattice ethanol molecule
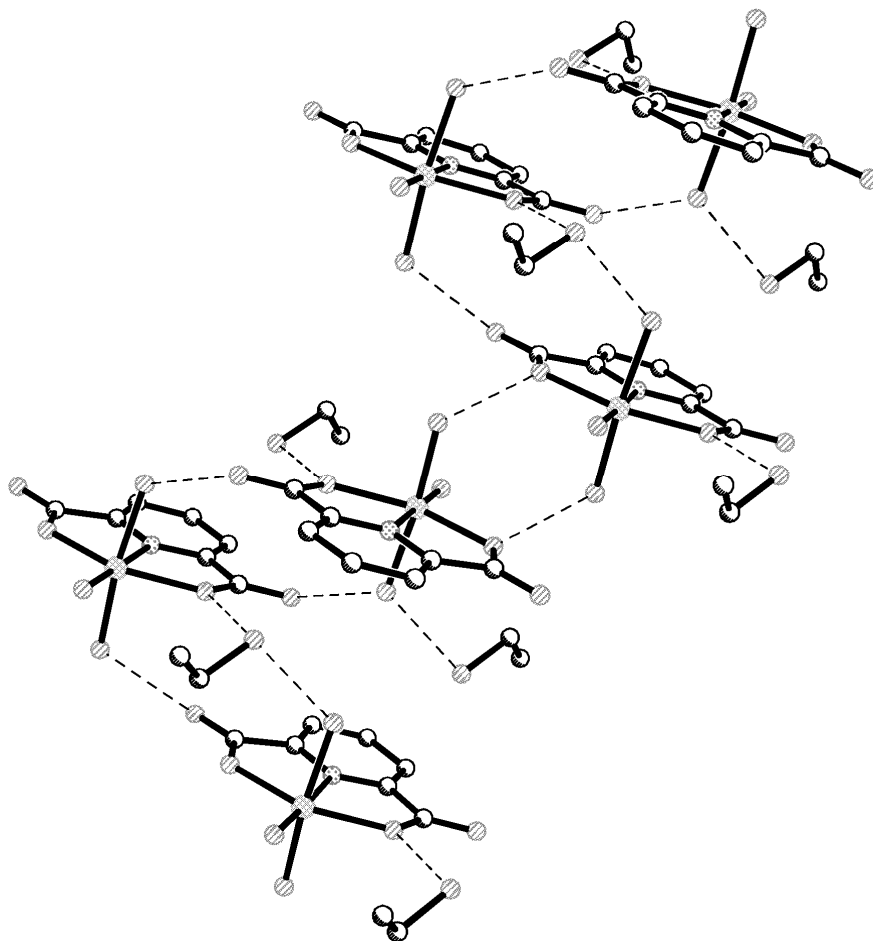
Figure 2. A view of the molecular packing of VO(dipic)
complex showing the hydrogen   Bonding interactions
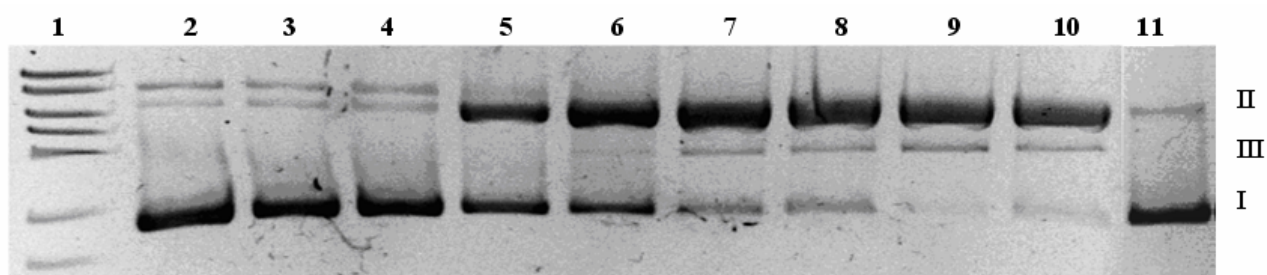
Figure 3. Cleavage of supercoiled pBR322 by VO(dipic) at different

concentrations in TN buffer pH 7 incubated at 4 h.

Note: Lane 1, DNA ladder; and Lane 2, DNA alone. Lanes 3-10 DNA with increasing concentration of VO(dipic): lane 3, 10 μM; lane 4, 50 μM; lane 5, 1 mM; lane 6, 3 mM; lane 7, 4 mM; lane 8, 5 mM; lane 9, 5.5 mM; lane 10, 6 mM. Lane 11, 6 mM $VOSO_4$ in TN buffer pH 7. Form I, supercoiled DNA; Form II, supercoiled nicked; Form III, linear DNA.
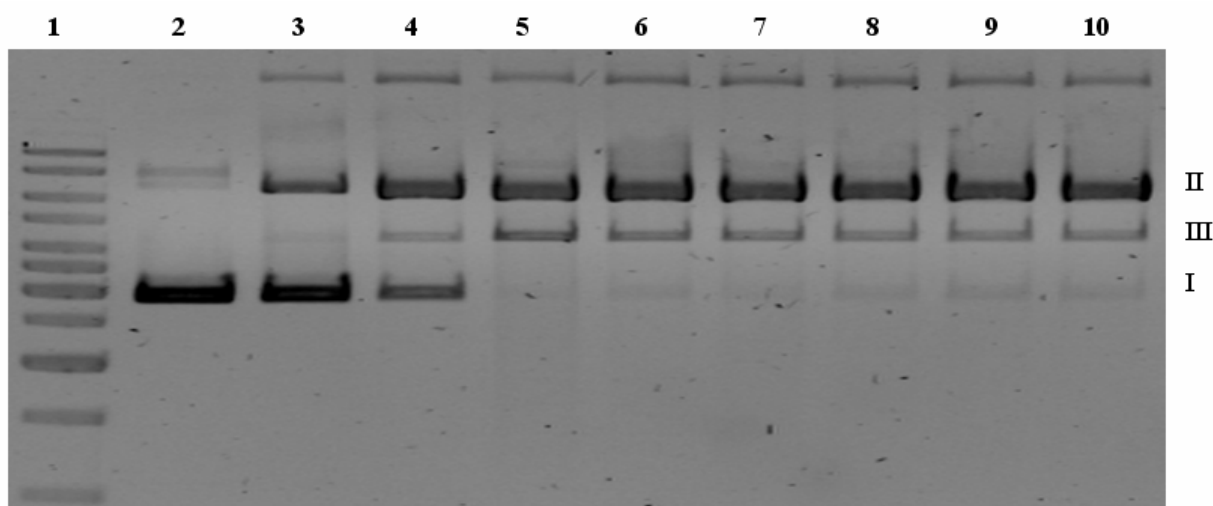
Figure 4. Cleavage of supercoiled pBR322 by VO(dipic) at different

concentrations in phosphate buffer pH 7.5 with 1 h incubation time.

Note: Lane 1, DNA ladder; and Lane 2, DNA alone. Lanes 3-10 DNA with increasing concentration of VO(dipic): lane 3, 10 μM; lane 4, 50 μM; lane 5, 1 mM; lane 6, 3 mM; lane 7, 4 mM; lane 8, 5 mM; lane 9, 5.5 mM; lane 10, 6 mM. Form I, supercoiled DNA; Form II, supercoiled nicked; Form III, linear DNA
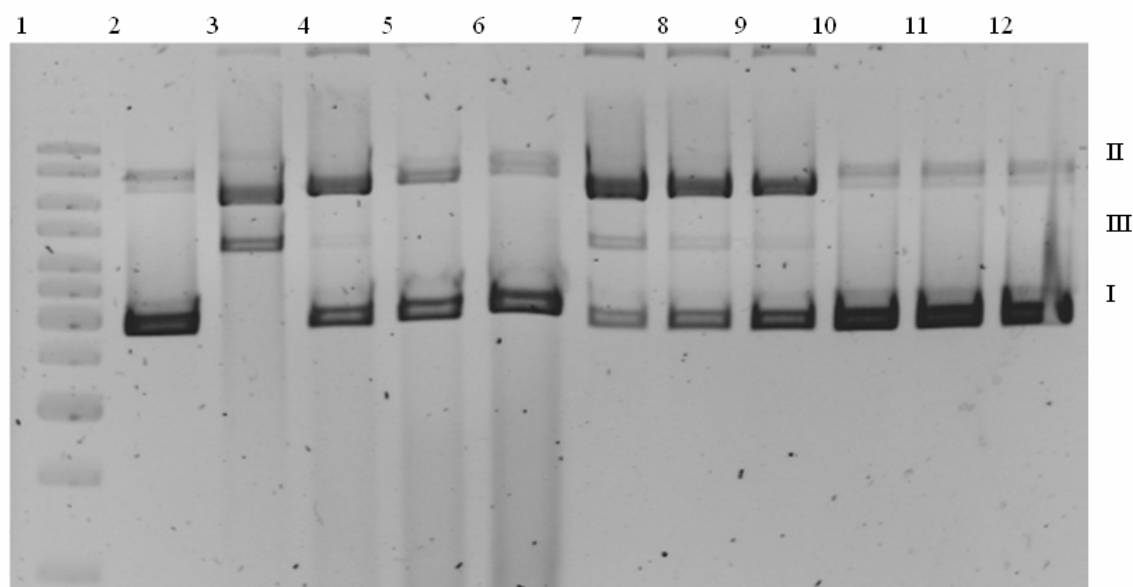
Figure 5. Effect of various scavengers on the cleavage of pBR322 (0.0125 mg mL-1) by

1 mM VO(dipic) in phosphate buffer pH 7.5 at 1 h incubation time.

Note: Lane 1, Gene Ruler 1 kb DNA ladder; lane 2, DNA alone; lane 3, DNA + 1 mM VO(dipic). Lanes 4 – 12 involves reaction of 1 mM complex with DNA in presence of various scavengers. Lanes 4 – 6: 1 μL, 2 μL, and 4 μL catalase; lanes 7 – 9: 1 mM, 2 mM and 4 mM NaN3; lanes 10 – 12: 1 μL, 2 μL, and 4 μL DMSO.
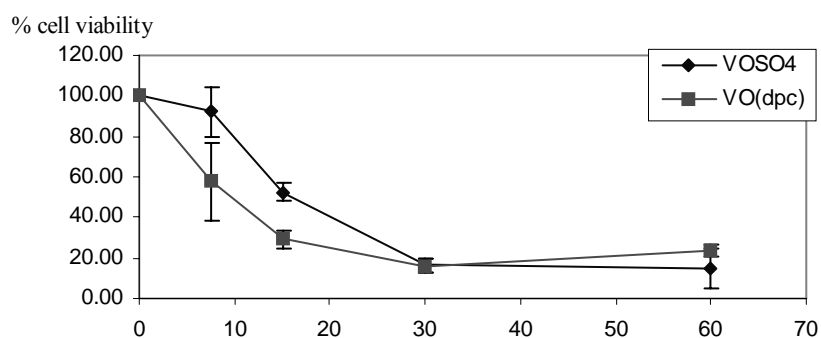
Figure 6. Cytotoxic activity of $VOSO_4$ and VO(dipic) against human lung adenocarcinoma PC9 cell line. Cancer cells were incubated at different concentration for 72 h in 96-well plates. Cell survival was determined using MTT assay. The average drug concentration needed to inhibit 50% of cell growth was obtained from pooled results from 3 different independent experiments.

% Cell viability
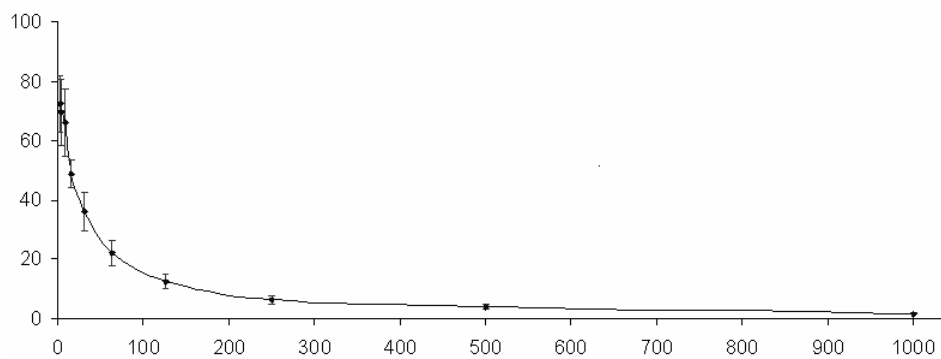
Figure 7. Cytotoxic activity of VO(dipic) against breast cancer MCF-7 cell line.
Cancer cells were incubated at different concentrations for 72 h in 96-well plates.

The Oscillation of Second-order Impulsive Delay

Difference Equations with Continuous Arguments

Ping Yu (Corresponding author)

Department of Science, Yanshan University, Qin Huangdao 066004, China

E-mail: swift0910@163.com

Xiaozhu Zhong, Ning Li, Wenxia Zhang, Shasha Zhang

Department of Science, Yanshan University, Qin Huangdao 066004, China

Abstract

In this paper, we considered the oscillation of second-order impulsive delay difference equation with continuous arguments, and the sufficient conditions are obtained for oscillation of all solutions and some results in the literatures are improved.

Keywords: Continuous arguments, Impulsive delay difference equation, Oscillation

1. Introduction

Recently, with the development of the medicine, biology mathematics and modern physics and so on, there have been many investigations into the study of delay difference equation. In particular, an extensive literature now exists on the oscillation theory for delay difference equation, and various applications have been found. But the study of the oscillation of impulsive delay difference equations with continuous arguments is very little, and this style of equations has very extensive application. Thus, to study the influence of impulsive to the system's stability has very important value applications. We refer to [1-6] and the references cited therein for more details.

In this paper, we consider the following second-order impulsive delay difference equations with continuous arguments

$$
\begin{cases}
\Delta_\tau^2 x(t) + \sum_{i=1}^{n} p_i(t)x(t-\sigma_i) = 0, & t \neq t_k, \\
x(t_k^+) - x(t_k) = b_k x(t_k), & t = t_k
\end{cases}
\tag{1}
$$

Where

$$\Delta_\tau x(t) = x(t) - x(t-\tau)；\quad \Delta_\tau^2 x(t) = \Delta_\tau(\Delta_\tau x(t)) = x(t) - 2x(t-\tau) + x(t-2\tau)$$

$\sigma_i > 0$，$i = 1,2,\Lambda$; τ is a nonnegative integer. The fixed moments of time t_k satisfy constants.

$0 \leq t_0 \leq t_1 \leq t_2 \leq \Lambda \leq t_k \leq \Lambda$ ，and $\lim_{k\to\infty} t_k = \infty$，$k = 1,2,\Lambda$ $b_k \neq -1$ $(k=1,2,\Lambda)$ are

For $\delta \geq 0$，we define $r_\delta = \min\{\delta - 2\tau, \delta - \sigma_i, i = 1,2,\Lambda, n\}$. For all $\varphi \in C([r_\delta, \delta], R)$,

we define the function $y : [r_\delta, \infty) \to R$ as the equation（1）satisfy

$$y(t) = \varphi(t)，\quad t \in [r_\delta, \delta] \tag{2}$$

If $y(t)$ is almost everywhere continuous in $[r_\delta, \infty)$, in $t_k(t > \delta)$ left continuous，$y(t_k^+)$ exist，for $t \in [\delta, \infty)$ satisfy (1),

for $t \in [r_\delta, \delta]$ satisfy initial condition (2)，then we easy to know that $\delta \geq 0$，

$\varphi \in C([r_\delta, \delta], R)$，(1) and (2) have the unique solution. The solution $x(t)$ of equation (1) is said to

be oscillatory if the terms x_n are neither eventually positive nor eventually negative. Otherwise, the solution is called non-oscillatory.

The assistant equation

$$y(t) - 2\prod_{t-\tau \leq t_k < t}(1+b_k)^{-1} y(t-\tau) + \prod_{t-2\tau \leq t_k < t}(1+b_k)^{-1} y(t-2\tau) + \sum_{i=1}^{n}\prod_{t-\sigma_i \leq t_k < t}(1+b_k)^{-1} p_i(t)y(t-\sigma_i) = 0 \tag{3}$$

the solution $y(t)$ of equation (3) satisfy initial condition (2) are almost everywhere continuous in $[r_\delta, \infty)$.

Lemma Suppose that $0 \le b < \dfrac{1}{4}$, and there exists $\{b_n\}$ satisfy $b_1 = \dfrac{b}{1-b}$ and $b_{n+1} = \dfrac{b}{1-b_n}$, for $n = 1,2,\Lambda$, then

$$\lim_{n \to \infty} b_n = \frac{1}{2}\left(1 - \sqrt{1-4b}\right)$$

2. Main results and proofs

Theorem 1 If $y(t)$ is the solution of equation(3), then $x(t) = \prod\limits_{\delta \le t_k < t}(1+b_k)y(t)$ is the solution of equation (1); If $x(t)$ is the

solution of equation(1), then $y(t) = \prod\limits_{\delta \le t_k < t}(1+b_k)^{-1}x(t)$ is the solution of equation(3).

Proof: Since $y(t)$ is the solution of equation (3), then $x(t) = \prod\limits_{\delta \le t_k < t}(1+b_k)y(t)$ is almost everywhere continuous in $[\delta, \infty)$.

Let $t \ne t_k$, then

$$\Delta_\tau^2 x(t) + \sum_{i=1}^{n} p_i(t)x(t-\sigma_i) = x(t) - 2x(t-\tau) + x(t-2\tau) + \sum_{i=1}^{n} p_i(t)x(t-\sigma_i)$$

$$= \prod_{\delta \le t_k < t}(1+b_k)y(t) - 2\prod_{\delta \le t_k < t-\tau}(1+b_k)y(t-\tau) + \prod_{\delta \le t_k < t-2\tau}(1+b_k)y(t-2\tau) + \sum_{i=1}^{n}\prod_{\delta \le t_k < t-\sigma_i}(1+b_k)p_i(t)y(t-\sigma_i)$$

$$= \prod_{\delta \le t_k < t}(1+b_k)\left[y(t) - 2\prod_{t-\tau \le t_k < t}(1+b_k)^{-1}y(t-\tau) + \prod_{t-2\tau \le t_k < t}(1+b_k)^{-1}y(t-2\tau) + \sum_{i=1}^{n}\prod_{t-\sigma_i \le t_k < t}(1+b_k)^{-1}p_i(t)y(t-\sigma_i)\right] = 0$$

Let $t = t_k > \delta$, because $x(t)$ is right continuous, then

$$x(t_k^+) = \prod_{\delta \le t_i < t_k^+}(1+b_i)y(t_k^+) = (1+b_k)\prod_{\delta \le t_i < t_k}(1+b_i)y(t_k) = (1+b_k)x(t_k)$$

we obtain that $x(t)$ is the solution of equation(1).

Since $x(t)$ is the solution of equation (1), then $y(t) = \prod\limits_{\delta \le t_k < t}(1+b_k)^{-1}x(t)$ is almost everywhere continuous in $[\delta, \infty)$. We

easy to proof that it satisfy equation （3）. When it equal to point t_k, then

$$x(t_k^+) = \prod_{\delta \le t_i < t_k^+}(1+b_i)^{-1}y(t_k^+) = \prod_{\delta \le t_i < t_k}(1+b_i)y(t_k) = x(t_k)$$

i.e. $x(t)$ is right continuous in point t_k. Then we obtain that $y(t)$ is the solution of equation (3), and the proof is completed.

Corollary Assume that $b_k > -1$, then all solutions of equation (1) oscillate are equals to all solutions of equation (3) oscillate.

Proof: By the results of theorem 1, we can proof the corollary. Then the proof is completed.

Theorem 2 Assume that $0 < 2\tau \le \sigma_1 \le \sigma_2 \le \Lambda \le \sigma_n$ and $p_i(t) \in C(R^+, R^+)$, for all of $t > 0$ and $i = 1,2,\Lambda, n$, then $p_i(t) > 0$; for all $k = 1,2,\Lambda$, then $b_k \ge 0$, $1 - 2\prod\limits_{t-\tau \le t_k < t}(1+b_k)^{-1} > 0$, such that

$$\liminf_{t \to \infty} \sum_{i=1}^{n+2} \gamma_i(t) = \alpha < \frac{1}{4} \tag{4}$$

$$\limsup_{t \to \infty} \sum_{i=1}^{n+2} \gamma_i(t) > 1 - \frac{1}{2}\left(1 - \sqrt{1-4\alpha}\right) \tag{5}$$

Where

$$\gamma_i(t) = \inf\left\{1 - 2\prod_{t-\tau \le t_k < t}(1+b_k)^{-1}; \prod_{t-2\tau \le t_k < t}(1+b_k)^{-1}; \prod_{s-\sigma_i \le t_k < s}(1+b_k)^{-1}p_i(s), s \in [t-\tau, t]\right\}$$

Then every solution of equation (1) oscillates.

Proof: Firstly, the assistant equation （3） of equation (1) can derived to be

$$y(t) - y(t-\tau) + \left(1 - 2\prod_{t-\tau \le t_k < t}(1+b_k)^{-1}\right)y(t-\tau) + \prod_{t-2\tau \le t_k < t}(1+b_k)^{-1}y(t-2\tau)$$

$$+ \sum_{i=1}^{n} \prod_{t-\sigma_i \le t_k < t} (1+b_k)^{-1} p_i(t) y(t-\sigma_i) = 0 \tag{6}$$

for $1 - 2 \prod_{t-\tau \le t_k < t} (1+b_k)^{-1} > 0$ and $p_i(t) \in C(R^+, R^+)$, equation（6）can derived to be

$$y(t) - y(t-\tau) + \sum_{i=1}^{n+2} \gamma_i(t) y(t-\tau_i) = 0 \tag{7}$$

Where

$$\tau_1 = \tau, \tau_2 = 2\tau, \tau_3 = \sigma_1, \tau_4 = \sigma_2, \Lambda, \tau_{n+2} = \sigma_n.$$

Secondly, by the front conclude, if every solution of equation (7) oscillates, then every solution of equation (3) oscillates.

Next , we proof that every solution of equation (7) oscillates. Assume the contrary. Then equation（7）may have an eventually positive solution $y(t)$, then exist $t_1^* > 0$, let $t > t_1^*$, such that $y(t) > 0$, $y(t-\tau_i) > 0$, for all $\varepsilon \in [0,\alpha)$ by（4）,exist $t^* > t_1^* + \sigma_n$, when $t > t^*$, then

$$\sum_{i=1}^{n+2} \gamma_i(t) > \alpha - \varepsilon \tag{8}$$

let $t_2^* = \max_{1 \le i \le n+2} \{t^* + \tau_i, t_1^*\}$, integral from $t-\tau$ to t for equation (7), by the integral midst value theorem, then

$$0 = \int_{t-\tau}^{t} y(s)ds - \int_{t-\tau}^{t} y(s-\tau)ds + \sum_{i=1}^{n+2} \int_{t-\tau}^{t} \gamma_i(s) y(s-\tau_i)ds$$

$$= \int_{t-\tau}^{t} y(s)ds - \int_{t-\tau}^{t} y(s-\tau)ds + \sum_{i=1}^{n+2} \gamma_i(\xi_{it}) \int_{t-\tau}^{t} y(s-\tau_i)ds \tag{9}$$

where $t > t_2^*$, $t-\tau \le \xi_{it} < t$, $i = 1,2,\Lambda, n+2$.

Let $z(t) = \int_{t-\tau}^{t} y(s)ds$, then $z(t)$ is continuous and almost everywhere derivate in (t^*, ∞) ,then

$$z'(t) = y(t) - y(t-\tau) = -\sum_{i=1}^{n+2} \gamma_i(t) y(t-\tau_i) < 0，\quad t > t_2^*$$

for $z(t) > 0$, then $z(t)$ is gradually reduce，and then

$$z(t-\tau) \le z(t-2\tau) \le z(t-\tau_i)，\quad t > t_2^*，\quad i = 1,2,\Lambda, n+2 \tag{10}$$

by (9), we have

$$z(t-\tau) = z(t) + \sum_{i=1}^{n+2} \gamma_i(\xi_{it}) z(t-\tau_i) \tag{11}$$

by（8）,(10)and (11),we have

$$z(t-\tau) > \sum_{i=1}^{n+2} \gamma_i(\xi_{it}) z(t-\tau_i) > \sum_{i=1}^{n+2} \gamma_i(\xi_{it}) z(t-2\tau) > (\alpha - \varepsilon) z(t-2\tau)$$

$$t > t_2^*，\quad t-\tau \le \xi_{it} < t，\quad i = 1,2,\Lambda\ n+2$$

i.e.

$$z(t) > (\alpha - \varepsilon) z(t-\tau)，\quad t > t_2^* + \tau \tag{12}$$

by (11) and (12), we have

$$z(t-\tau) > (\alpha - \varepsilon) z(t-\tau) + \sum_{i=1}^{n+2} \gamma_i(\xi_{it}) z(t-\tau_i) > (\alpha - \varepsilon) z(t-\tau) + (\alpha - \varepsilon) z(t-2\tau)$$

then $z(t-\tau) > \dfrac{\alpha - \varepsilon}{1 - (\alpha - \varepsilon)} z(t-2\tau)$, i.e

$$z(t) > \frac{\alpha - \varepsilon}{1 - (\alpha - \varepsilon)} z(t-\tau)，\quad t > t_2^* + 2\tau \tag{13}$$

by (11) and (13),we have

$$z(t-\tau) > \frac{\alpha-\varepsilon}{1-(\alpha-\varepsilon)}z(t-\tau) + \sum_{i=1}^{n+2}\gamma_i(\xi_{it})z(t-\tau_i) > \frac{\alpha-\varepsilon}{1-(\alpha-\varepsilon)}z(t-\tau) + (\alpha-\varepsilon)z(t-2\tau)$$

Thus, we have

$$z(t-\tau) > \frac{\alpha-\varepsilon}{1-\dfrac{\alpha-\varepsilon}{1-(\alpha-\varepsilon)}}z(t-2\tau)$$

Let $b_1 = \dfrac{\alpha-\varepsilon}{1-(\alpha-\varepsilon)}$, $b_2 = \dfrac{\alpha-\varepsilon}{1-b_1}$, then

$$z(t-\tau) > \frac{\alpha-\varepsilon}{1-b_1}z(t-2\tau), \quad t > t_2^* + 3\tau$$

by simple induction, in the end we have

$$z(t) > \frac{\alpha-\varepsilon}{1-b_{m-1}}z(t-\tau), \quad b_{m-1} = \frac{\alpha-\varepsilon}{1-b_{m-2}}, \quad m = 2,3,\Lambda ; \tag{14}$$

by (11) and (14) ,we have

$$z(t-\tau) > \frac{\alpha-\varepsilon}{1-b_{m-1}}z(t-\tau) + \sum_{i=1}^{n+2}\gamma_i(\xi_{it})z(t-\tau_i)$$

$$\geq b_m z(t-\tau) + \sum_{i=1}^{n+2}\gamma_i(\xi_{it})z(t-\tau_i) > b_m z(t-\tau) + \sum_{i=1}^{n+2}\gamma_i(\xi_{it})z(t-\tau)$$

and

$$\sum_{i=1}^{n+2}\gamma_i(\xi_{it}) \leq 1-b_m \tag{15}$$

As we all know，if $t \to \infty$, then $m \to \infty$, by the define of ε ,we know if $t \to \infty$ then $\varepsilon \to 0$. Thus, by the lemma and （15）,we have

$$\limsup_{t\to\infty}\sum_{i=1}^{n}\gamma_i(t) \leq \lim_{t\to\infty}(1-b_m) = \lim_{m\to\infty}(1-b_m) = 1 - \frac{1}{2}\left(1-\sqrt{1-4\alpha}\right)$$

This contradicts (5), then we prove that the positive solution of equation (7) doesn't exist. Similarly, we can proof that the negative solution of equation (7) doesn't exist. i.e. the every solution of equation (7) oscillates. Thus, the every solution of equation (3) oscillates. By the corollary, the every solution of equation (1) oscillates.

Then the proof is completed.

3. Conclusion

In this paper, by study the method of the oscillation first-order linear impulsive difference equation with continuous arguments, we study the second-order impulsive delay difference equations with continuous arguments. The sufficient conditions are obtained for oscillation of all solutions and some results in the literatures are improved.

References

Yang Y H. (2003). Oscillation of impulsive difference equations with continuous variables. *Journal of north china electric power university*. 30, 97-99.

Zhang.Y.S, & Yu.J.S. (2000). Oscillation of linear delay difference equations with continuous arguments. Appl. Math .J. Chinese Univ.Ser.A, 15, 25-33.

Zhou Y. (1996). Oscillation for delay difference equations with continuous arguments. *Mathematics*. in economics. 13, 86-89.

Effect of Blending Temperature on the

Characteristics of Modified Polyacrylonitrie Homopolymer

Ahmad Fauzi Ismail[a] (corresponding author), Azeman Mustafa[a]

[a] Faculty of Chemical and Natural Resources Engineering,

Membrane Research Unit,

Universiti Teknologi Malaysia,

81310 Skudai   Johor, Malaysia

Tel: +607-553 5592   E-mail address. afauzi@utm.my

Muhammad Syukri Abd. Rahaman[a,b]

[b] Faculty of Engineering,

Department of Chemical and Process Engineering,

Universiti Kebangsaan Malaysia,

43600 UKM Bangi, Selangor, Malaysia

Abstract

This paper examines the modification of polyacrylonitrile (PAN) homopolymer by a blending technique. The discussion on this modified PAN fiber involves the comparison a new concept of comonomer attachment compared to the conventional method. The PAN homopolymer and comonomers (i.e. itaconic acid (IA) and methylacrylate (MA)) were dissolved in dimethylformamide (DMF) at two different temperatures; 70°C (Type 1) and ambient temperature (Type 2). These fibers were fabricated using a simple the dry/wet spinning process before subjected to a stabilization process. FTIR result shows that the peaks (around $1600cm^{-1}$) indicated that the comonomers in Type 1 fiber were attached to the PAN homopolymer backbone during the dope preparation step. However for Type 2 fibers, the comonomers were only attached to the PAN homopolymer backbone during the stabilization process. Type 1 fibers also have higher weight loss and faster stabilization compared to Type 2 fibers. Therefore, the blending process at heat temperature of 70ºC is claimed as the technique that can modify the PAN homopolymer and make the stabilization process of PAN fibers faster.

Keywords: Polyacrylonitrile, Comonomers, Stabilization, Cross-section, TGA, Infrared

1. Introduction

Polyacrylonitrile (PAN) is a polymer with carbon chain connected to one another. Polyacrylonitrile is hard, horny, relatively insoluble, and a high-melting material (Schwartz, 2002). The main characteristic of the PAN molecule is its bulky nitrile (CN) side groups which characterized by high dipole moment, the lone pair orbital of nitrogen atoms, and the electrons in the p orbital of the nitrile triple bond. Based on previous works (Bahl and Manocha, 1974; Wangxi et al., 2003; Wiles, 2003), PAN is the main precursor material for manufacturing carbon fibers as it can produce carbon fiber with a high carbon yield of up to 50% are thermally stable and extremely oriented molecular structure when subjected to low temperature treatment. Hence, manufacturing of PAB fibers with high tensile and high modulus is of significant interest

In terms of processing path, Liu *et al.* (1994) has listed three main steps in converting PAN based fibers to carbon fibers. They are:

(1) Oxidative stabilization, which form ladder structures to enable them to undergo processing at higher temperatures;

(2) High temperature carbonization, (i.e. up to 1600 ° C) to evolve non-carbon atoms and yield a turbostatic structure;

(3) Further heating, up to 2000 °C to improve the orientation of the basal planes and the stiffness of fibers, which is also known as graphitization.

Among these three steps, the stabilization process is the most important one. It plays a significant role in converting PAN fibers into an infusible stable ladder polymer. Through process triple bonds (C≡N groups) transformed into double bonds (C=N groups) and consequently develop cross-links between the molecules of PAN fiber (David and Ismail, 2002).

Comonomers are also normally used to accelerate the stabilization process and improving the thermal behavior of PAN. There are various types of comonomers such as itaconic acid, acrylic acid, methacrylic acid, methyl acrylate (MA), etc. (Edie and Diefendorf, 1993). Grassie and McGuchan (1972) observed that acrylate and methacrylate comonomers have diluent effect on the exothermic reactions occurring during heat treatment of PAN, while acidic comonomers by having of electrophilic groups could initiate stabilization reactions at a lower temperature. At least 15% of regular PAN textiles are comonomers (Chand, 2000) and most of PAN fiber contains at least 1-1.1% of itaconic acid (IA). Other researchers (Tsai and Wu, 1993) stated that PAN precursors with a few percent of acrylate comonomers also have more preferred orientations, and as a result, the resulting carbon fibers possessed the best mechanical properties. Hence, the objective of this study is to characterize the modified polyacrylonitrile (PAN) homopolymer through blending with comonomers such as itaconic acid and methylacrylate with regards to fiber properties.

2. Experimental

2.1 Dope Preparation

Polyacrylonitrile homopolymer have a glass transition temperature of 120°C. Thus, at ambient temperature the polymer is in a glassy phase. This state can interrupt the spinning process by reducing the draw ability of the polymer solution. The presence of comonomers in this experiment can reduce this problem which improves the solubility and draw ability in the spinning process. As mentioned before, most researchers have been focusing their study by investigating the minimum amount of methyl acrylate (MA) and itaconic acid (IA) in order to improve the properties of carbon fiber.

In this study, the modification of PAN homopolymers was carried out by blending PAN and its comonomers (i.e MA and IA) using two different techniques. The first technique (Type 1) involved reaction of comonomers and PAN polymer at 70°C, while in the other technique (Type 2), the comonomers were mixed with PAN at ambient temperature. The blending and mixing of the PAN polymers lasts at least 7-9 hours to ensure that a completely homogenous solution can be produced.

2.2 Spinning technique

In this research, the dry/wet spinning method was used to fabricate PAN fiber. The spinning solution was extruded through a spinneret through a 2 cm air gap before entering the coagulation bath. The fiber then immersed into the nonsolvent (water) coagulation bath for wet separation and then to the washing treatment bath. The coagulation bath temperature was controlled at 10°C by a refrigeration/heating unit to ensure rapid solidification, while the washing bath was kept at ambient temperature. The resulting fiber with a diameter of 50μm, was subjected to solvent exchange for 1 day before drying at ambient condition. The specification of spinning conditions is listed in Table 1.

2.3 Stabilization Process

Stabilization process influences the processing sequence that is used to convert PAN precursors to carbon fibers and will determine whether the final carbon fibers will have desirable properties. In this study, PAN fiber bundles were inserted into a quartz tube and wrapped with stainless steel wires of type 304 (outer diameter 3 mm) at both end. The quartz tube was inserted into a Carbolite wire wound tube furnace (Model CTF 12/65/550) that can be set to a maximum temperature of 1200°C.

The PAN chain was cross-linked by conducting a slow heating treatment on the PAN fibers. As a result, a new structure of PAN fiber was formed which could withstand high temperature during the carbonization process. The heating rate used was as low as 1ºC/min, in order to avoid shrinkages (Chen and Harrison, 2002). For the final heating process, the temperature was varied from 200-300°C with an increment of 10°C for 1hour soaking time. This stabilization process was conducted with air flow and without air flow. Figure 1 illustrates the stabilization system used in the present work.

2.4 Thermogravimetry Analysis (TGA)

The weight loss of the sample caused by the heating process was studied by TGA using a Mettler Toledo TGA model (TGA/SDTA851^{e}). The sample size was about 40 mg and the analysis was performed under an inert atmosphere (nitrogen gas) at a heating rate of 20°C/min until the temperature reached 1000ºC. The residue after the heating process was analyzed using Mettler STARe software.

2.5 Fourier Transform Infrared Spectroscopy (FTIR) of PAN fiber.

Analysis of the existence and information on the organic structure of PAN fibers before and after heating treatment was due by infra-red spectroscopy using the potassium bromide (KBr) disk method. In order to mix the polymer with KBr thoroughly we used an agate grinder. The stabilized fibers were grinded into small particle and mixed thoroughly with KBr. The mixture was pressed to form a thin layer, and then the sample was subjected to FTIR analysis.

3. Results and Discussion

3.1 Effect of Different Dope Preparation temperature on Polyacrylonitrile Properties

Polyacrylonitrile was modified with copolymers through a blending technique. As stated before, dimethylformamide (DMF) is suitable to dissolve any polar polymers and usually recommended for the copolymerization of acrylonitrile. By dissolving polyacrylonitrile and its comonomers in DMF, carbanion condition can exist. Carbanion is a condition which the carbon atom bears a negative charge which help to initiate the reaction of comonomers and polyacrylonitrile (Wade, 1999). In this case, two types of polymer solutions have been prepared which produced Type 1 and Type 2 fibers.

The existence of the functional groups of these PAN fiber was determined by using infrared (IR) spectra. Generally the PAN fiber shows peaks in the range of 3000-2850 cm^{-1} (–CH stretch), 2260-2240 cm^{-1} (C≡N stretch) and 1465 cm^{-1} (–CH_2 band). Figure 2 shows the spectrum of the Type 1 fibers before the fiber was stabilized. The first method caused the comonomers to be fully ionized and could attach the polyacrylonitrile during the preparation of the dope. Thus, peaks similar to those found by Dalton et al. can be observed (Dalton et al., 1999). In Figure 2, there are four important peaks that can be seen. A very sharp and strong peak representing nitrile band is observed at 2245 cm^{-1} and this is due to the dominant functional groups in the polyacrylonitrile structure. The second peak is at 1701.5 cm^{-1} which represents to carbonyl stretching. In conjunction with the peaks at 1072.9 (most likely due to C-O-C bend), the carbonyl peak seems to confirm the presence of methecrylate ($H_2C=C(CH_3)CO_2R$) as a comonomer. In addition, through the combination of the broad adsorption around 3600-3300 cm^{-1} (due to OH stretch) and the peak in the 1300-1000 cm^{-1} range (due to the C-O stretch and the C-C stretch), the carbonyl peak also confirms the likely presence of an acid comonomer (itaconic acid) ($HO_2CCH_2C(=CH_2)CO_2H$). There are also bands in the regions with 2941.4, 1454.7, 1353.0 and 1270–1220 cm^{-1} wavenumbers which represent the aliphatic CH group vibrations of different modes of CH, CH_2 and CH_3. However, the essential requirement of the comonomer was proven when the cyclization reaction became faster in stabilization process. This topic is discussed in section 3.2.

In the second technique, the comonomers could not fully react with the PAN polymer because the PAN powder might have already been dispersed in the solvent. Therefore, the comonomers might only have been dispersed in acrylonitrile as additives. The comonomers which were dispersed in the PAN matrix were attached to the PAN structure when heat was supplied especially in the stabilization process. Based on Figure 3, the important peak (~1700cm^{-1}) which represents attached comonomers is nearly non-existent. The peak at 1700 cm^{-1} is shifted to around 1660 cm^{-1} and this could be evidence that comonomers were dispersed in the PAN matrix. It is because the resonances that form at this peak reduced the stretching frequency of the carbonyl group in both comonomers (Wade, 1999). The resonance reaction is illustrated in Figure 4. The resonance phenomenon could have inhibited the initiation of the cyclization reaction during the heat treatment. As a result, initial observation showed that, there was no significant change in the PAN fiber colour although the temperatures reached 200°C in contrast to the PAN fiber of Type 1.

It was reported that copolymerization with itaconic acid could initiate the cyclization reaction. Beltz and Gustafson (Beltz and Gustafson, 1996) stated that PAN homopolymer cyclizes slower than any of the co-polymers, resulting in a lower extent of cyclization for the homopolymer than the acidic co-polymers at all reaction times. In addition, with short reaction time, the initial cyclization rate is faster for co-polymers with larger itaconic acid concentrations. However, as stated by Tsai and Lin (1990), in the presence of itaconic acid as additive, the cyclization of PAN precursors can also initiated at a lower temperature thus reducing stabilization time.

3.2 Cross Section of the PAN Fiber

Figure 5 shows the morphology of a PAN fiber produce through a dry-wet spinning process. It is clearly seen that the fiber was free from void. However, flaws can be seen at the surface of the PAN fiber. This flaw might be due to the free solvent system that was applied in the spinning process. The systems caused the mass transfer within the fiber surface and coagulation bath inconsistent and thus produce a bad fiber shape.

Meanwhile, the evenness of the cross-section or fineness of PAN precursors was largely influenced by the flow conditions in the spinneret, and the design of the roller for drawing. Referring to Figure 5, the cross sectional shape of the fiber seems to be slightly kidney bean or round shaped. The formation of the shape is dependent on the center of the fiber, whether it has solidified or not during fiber collection. Rigid fiber skin can also form in the spinning process before the center of the fiber has solidified, and as a result yields the kidney bean shape.

As a comparison, fibers diameter were also measured by scanning electron microscopy (SEM). The diameter of the fibers were in the range of 50-55μm which depended on the size of the spinneret. The fibers of Type 1 were 7% bigger in diameter compared to Type 2 because the Type 1 solution had the highest viscosity due to heating process during dope preparation. Typically a jet stretch of 2.0 is applied during the fabrication process. However, the high value of the jet stretch will cause the PAN fiber from the Type 1 solution tend to break during the spinning process. Therefore, it is

recommended that the jet stretch value is maintained at 1.0 for the fabrication of PAN fibers of Type 1. However, the diameter of fibers is examined to be bigger with a jet stretch of 1.0 under SEM.

3.3 Effect of thermal degradation temperature

The thermal behavior of the samples was investigated by thermogravimetric analysis (TGA) under a nitrogen (N_2) atmosphere until the temperature reached up to 1000ºC. When polyacrylonitrile was heated in the TGA instrument under an inert atmosphere, degradation occurred and the mass decreased as the temperature increased. Typical thermograms of various polyacrylonitrile samples are presented in Figure 6. These thermograms of the PAN powder and PAN fiber (Type 1 and Type 2 PAN fibers) were obtained without stabilization.

From Figure 6, it can be seen that at the beginning of the heating process (below 300°C) there was no weight loss observed in the PAN powder and only a little weight change occurred in the PAN fiber (Type 2). This occurred because the PAN powder did not contain comonomers that initiated the cyclization reaction. A cyclization reaction of the nitrile groups was believed to be the cause of loss of polyacrylonitrile weight during heating. In addition, Devasia *et al.* (2003) also stated that the cyclization of nitrile groups would initiate an exothermic reaction which is then followed by a loss of the polyacrylonitrile weight. However, PAN fibers with side chain comonomers had a larger weight loss because chain scission occurred in the fiber during the cyclization reaction.

Based on Figure 6, significant weight loss occurred around 300-350°C for the PAN powder and PAN fiber of Type 2 (i.e., PAN powder at 313.19°C; Type 2 PAN fibers at 320.2ºC). Meanwhile, for PAN fibers with the comonomers attached to the PAN structure (Type 1), the onset of the thermal decomposition took place at two temperature regions (i.e. 265.63ºC and 376.47ºC). The reason was possibly due to the glassy temperature of polyacrylonitrile at 317°C. This decomposition trend was also discovered by David and Ismail (2002). However in the region at 350-750°C TGA temperatures of the loss of Type 1 PAN fibers were slower. This indicated that the comonomers which attached to the PAN structure (Type 1 PAN fibers) could cyclize the structure faster than others and then stabilized the PAN structure. However, because of the chain scission of the comonomers, the overall weight loss of this fiber is on average the greatest. As shown in Figure 6, the PAN powder has degraded to 66.99% of the total mass, Type 2 PAN fibers lost 61.18% of their weight and Type 1 PAN fibers were left with only about 14.35% of their original weight.

From the percentage loss, the total weight loss of PAN fibers prepared by method 2 is less. It is also shown in Figure 6 that after about 50% weight loss the rate of loss was slow. It is postulated that the molecular crosslinking that occurred in the PAN structure inhibited the weight loss of PAN fibers. It is believed that a cross-linked polymer is more thermally stable than the corresponding thermoplastic polymer. The molecular crosslink in the PAN polymer could crystallize the PAN structure. Zhu *et al.* (2002) discovered that PAN in a crystal structure would decelerate the weight loss in order to produce high carbon yield.

3.4 Effect of stabilization process

For comparison, the fibers that were produced from both methods (method 1 and method 2) were stabilized at the same condition. Figures 7 and 8 show the shifting of the spectrum of PAN samples after heating in air (without air flow) at different temperatures around 200-300°C for 1 hour, in order to develop hydronaphthiridine rings. During stabilization process, thermal heating played an important role to initiate the cyclization reaction. Heat was produced by the cyclization of pendant CN groups of PAN fibers, although they were heated under a nitrogen atmosphere (exothermic reaction). Thus, more heat evolution occurred which caused a lot of CN groups undergo cyclization and form hydronaphthiridine rings. The presence of hydronaphthiridine rings was proved by Memetea *et al.*(1995) and the new bands within 1600-1620 cm^{-1} which were attributed to C=N vibrations appeared. In addition, it is apparent that the carbonyl peak intensities at (~1700cm^{-1}) of PAN fibers (Figures 7 and 8), was shifted to the intensity of the band at 1600 cm^{-1}.

Meanwhile, the intensity of the 2240 cm^{-1} wavenumber in these figures (Figures 7 and 8), which associated to a stretching vibration of C≡N bonds and the strong band around 2930 cm^{-1} representing the CH_2 groups in the polymer chain were hardly changed or reduced. These could result in alterations in molecular structure of polyacrylonitrile. The changes in the PAN intensities also depend on the concentration of comonomers that are used in an experiment. According to Wangxi et al (2003), an increase in the amount of comonomers will cause a reduction in cyclization temperature. Hence, a lower cyclization temperature will avoid the unstable cyclization that occurs in pure PAN and leads to chain-breaking. However, as the content of itaconic acid increased slightly, the conversion of acrylonitrile decreased greatly. This phenomenon had been explained by Tsai and Lin (1991).

From the IR result, it showed that the Type 1 fiber started the cyclization reaction at a lower temperature compared to Type 2 fiber. The intensity of the nitrile peak for the Type 1 fiber (Figure 7) reduced faster than Type 2 fibers (Figure 8). This is because the preparation of dope by method 2, the comonomers were only reacting as additives to the fiber during stabilization process. Whereas the Type 1, the comonomers were attached to the PAN polymer during dope preparation. The additive reactions in the PAN structure were confirmed by Tsai and Lin (1990), whereas the additives could also

reduce the initial cyclization temperature of modified PAN fibers than PAN homopolymer. The mechanism of the reaction as additives is illustrated in Figure 9. In addition, in the stabilization process, the colour of fibers of Type 1 also became yellow at a lower temperature compared to fibers of Type 2 which started to be yellow at a higher temperature.

Typically, in stabilizing the PAN fiber in air, the other main reaction namely oxidation process will also occur. The oxidation process takes place by means of dehydrogenation and crosslinking. The hydrogen moles continue to decrease with progressive oxidation as a result of in dehydrogenation reaction. Wang, (1998) also discovered the same phenomenon in this dehydrogenation reaction which could assist in stabilizing the PAN structure. Subsequently, these reactions helped in increasing the peak around at 1600 cm^{-1} which is represented as a double bond. This unsaturated bond caused by cyclization and the dehydrogenation reaction improved the stability of PAN fibers and reduced chain scission when the fibers were subjected to high temperature processing. The cyclization and dehydrogenation reactions are concluded from Figure 10.

4. Conclusion

Modified polyacrylonitrile (PAN) homopolymer was spun using dry/wet spinning process. Based on the results presented and discussed, this section summarizes the important conclusions from each of the major portions of this work.

(1) PAN homopolymers have been successfully modified by reacting them with comonomers. The heat applied during dope preparation (Type 1) caused an interaction between comonomers and PAN homopolymer. Subsequently, a peak around 1660-1700cm^{-1} was observed.

(2) The modification of PAN homopolymers at the temperature of 70ºC underwent the stabilization process faster than modification at ambient temperature because this can attach to the PAN structure at the heated temperature.

(3) High weight loss of the fibers is likely to be by the large fiber diameter which can cause inconsistent heat treatment. Moreover, with attached comonomers (Type 1 fibers) the weight loss could be increased.

References

Bahl, O. P. and Manocha, L. M. (1974). Characterization of Oxidized PAN Fibers. *Carbon.* 12(4): 417-423.

Beltz, L. A. and Gustafson, R. R. (1996). Cyclization Kinetics of Polyacrylonitrile. *Carbon.* 34(5): 561-566.

Chand, S. (2000). Carbon Fiber for Composites. *Mater. Sci.* 35(6): 1303-1313.

Dalton, S., Heatley, F. and Budd, P. M. (1999).Thermal Stabilization of Polyacrylonitrile Fibers. *Polymer.* 40(20): 5531–5543.

David, L. I. B. and Ismail, A. F. (2002). Influence of the Thermastabilization Process And Soak Time During Pyrolysis Process on the Polyacrylonitrile Carbon Membranes For O_2/N_2 Separation. *Mem. Sci.* 213(1-2): 285–291.

Devasia, R., Reghunadhan Nair, C. P. and Ninan, K. N. (2003). Copolymerization of Acrylonitrile with Itaconic Acid in Dimethylformamide: Effect of Triethylamine. *Eur. Polym. J.* 39(3): 537-544.

Edie, D. D. and Diefendorf, R. J. (1993). Carbon fiber manufacturing. In: Buckley, J. D. and Edie, D. D. eds. *Carbon-Carbon Materials and Composites*. Park Ridge: Noyes Publications. 19-37.

Fitzer, E., Frohs, W. and Heine, M. (1986). Optimization of Stabilization and Carbonization of PAN Fibers and Structural Characterization of the Resulting Carbon Fibers. *Carbon.* 24(4): 387-395.

Grassie, N. and McGuchan, R. (1972). Crystallizable Trans-Tactic Copolyalkenamers. *Eur. Polym. J.* 8(3): 257-260.

Liu, J., Wang, P. H. and Li, R. Y. (1994). Continuous Carbonization of Polyacrylonitrile Based Oxidized Fibers: Aspects on Mechanical Properties and Morphological Structure. *Appl. Polym. Sci.* 52(7): 945-950.

Memetea, L. T., Billingham, N. C. and Then, E. T. H. (1995). Hydroperoxides in Polyacrylonitrile and Their Role In Carbon-Fiber Formation. *Polym. Deg. and Stab.* 41(2): 189-201.

Schwartz, M. (2002). *Encyclopedia of Materials, Parts, and Finishes*. 2nd ed. Boca Raton, Florida: CRC Press p. 545.

Tsai, J. S. and Lin, C. H. (1990). Polyacrylonitrile Precursors by Copolymer and Additive with Itaconic Acid. *Mater. Sci. Let.* 9(8): 869-871.

Tsai, J. S. and Lin, C. H. (1991a). Effect of Comonomer Composition on the Properties of Polyacrylonitrile Precursor and Resulting Carbon Fiber. *Appl. Polym. Sci.* 43(4): 679-685.

Tsai, J. S. and Wu, C. J. (1993). Effect of Cross-Section Evenness for Polyacrylonitrile Precursor on the Properties of Carbon Fiber. *Mater. Sci. Let.* 12(6): 411-413.

Wade, L. G. Jr. (1999). *Organic chemistry. 4th ed*. Upper Saddle River, N. J.: Printice-Hall, Inc.

Wang, P. H. (1998). Aspects on Prestretching of PAN Precursor: Shrinkage and Thermal Behavior. *Appl. Polym. Sci.* 67(7): 1185–1190.

Wangxi, Z., Jie, L. and Gang, W. (2003). Evolution of Structure and Properties of PAN Precursors during Their Conversion to Carbon Fibers. *Carbon.* 41(14): 2805–2812.

Wiles, K. B. (2002). *Determination of Reactivity Ratios For Acrylonitrile/ Methyl Acrylate Radical Copolymerization Via Nonlinear Methodologies Using Real Time FTIR.* Faculty of the Virginia Polytechnic Institute and State University: MSc Thesis.

Zhu, D., Xu, C., Nakura, N. and Matsuo, M. (2002a). Study of Carbon Films From PAN/ VGCF Composites By Gelation / Crystallization From Solution. *Carbon.* 40(3): 363–373.

Table 1. Specification of spinning conditions

Specifications	Conditions
Spinning dope composition	20 wt.% polymer
	80 wt.% Dimethylformamide
Spinning dope temperature	Ambient temperature (27ºC)
Air distance	10 cm
Spinneret dimensions	Hole diameter 200 μm
Force convection gas	Nitrogen
External bath composition	Tap Water
External bath temperature	10 ºC
Jet stretch	1.0 to 2.0
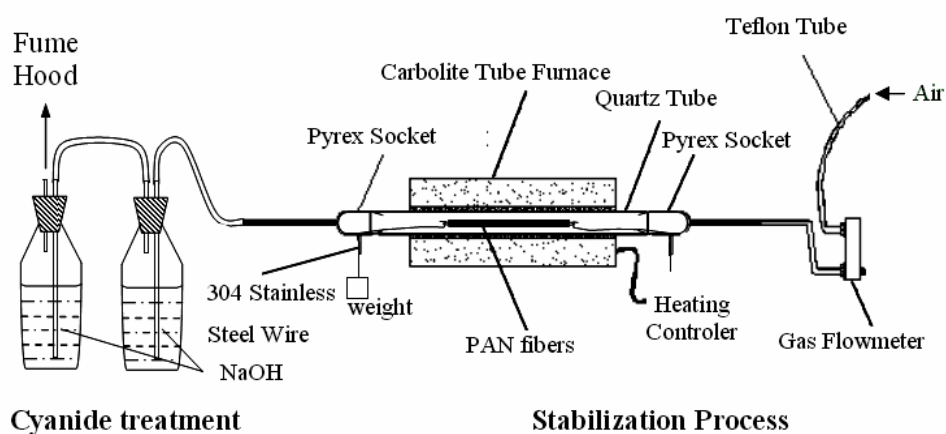
Figure 1. Stabilization heating system.
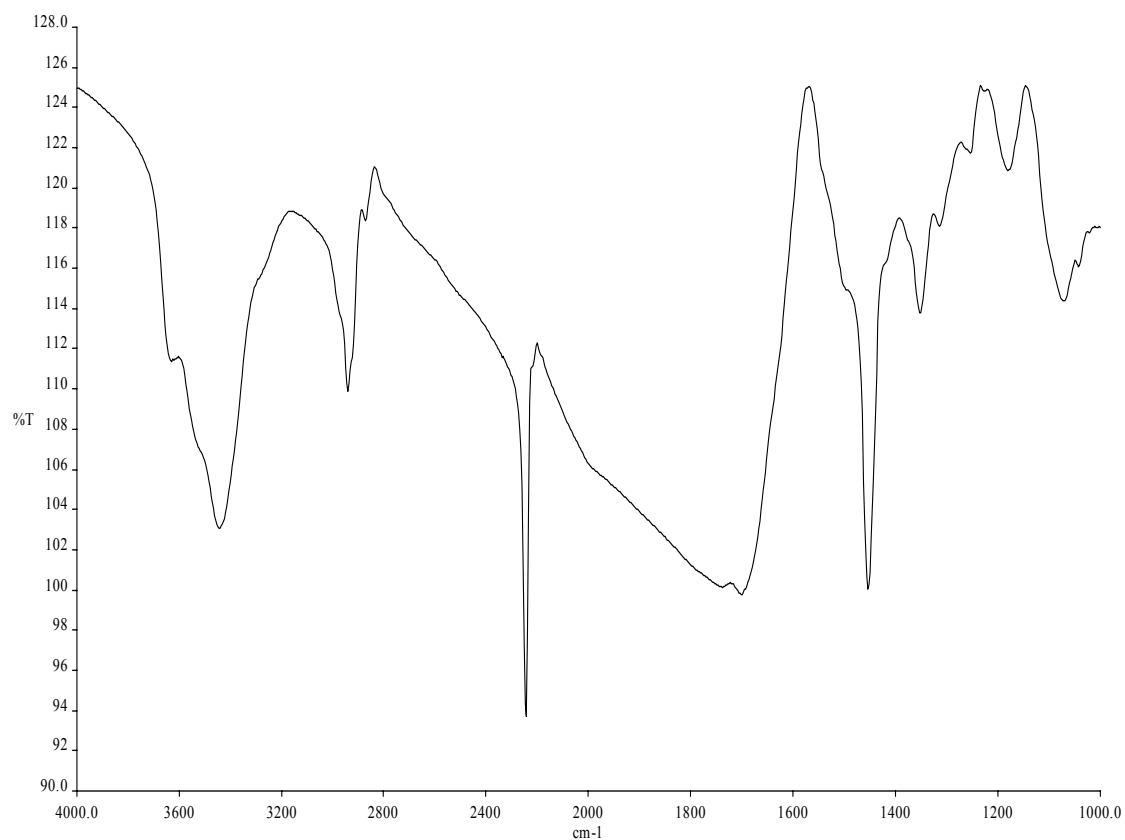
Figure 2. Infrared transmission for PAN fiber (Type 1).
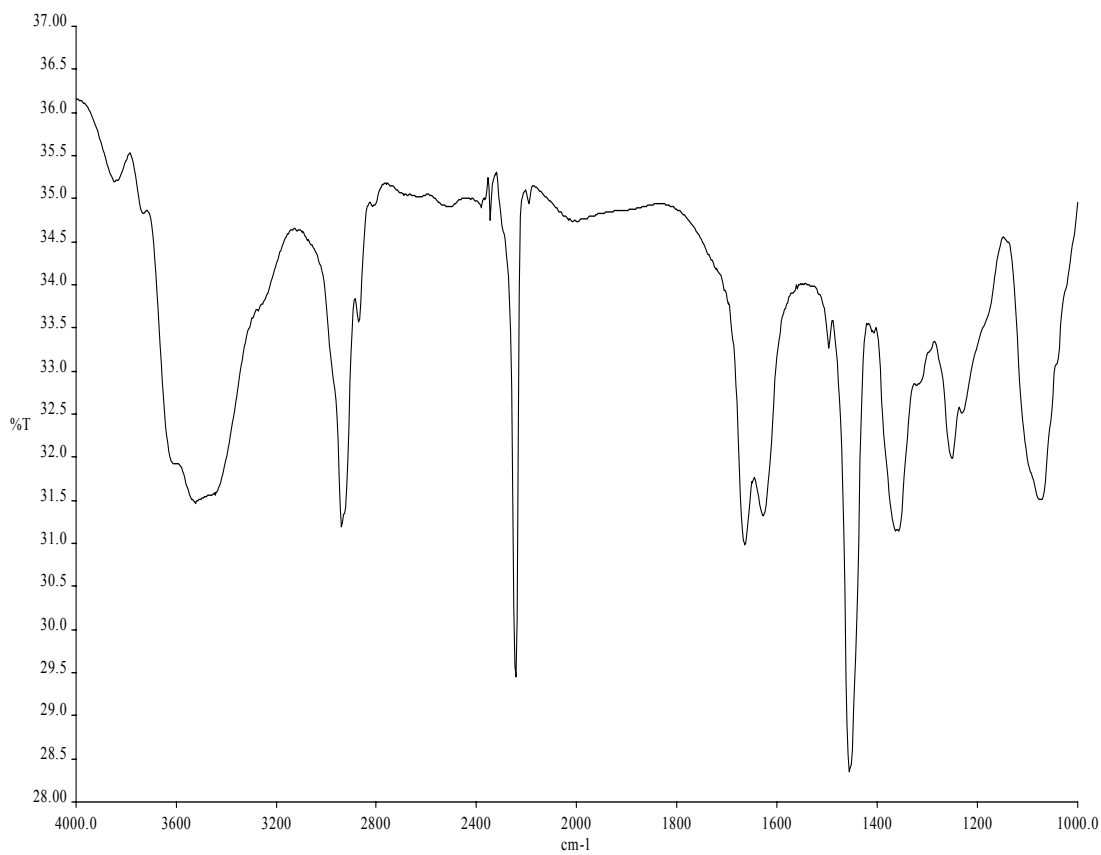
Figure 3. Infrared transmission for PAN fiber (Type 2).

(1) Methylacrylate

(2) Itaconic acid
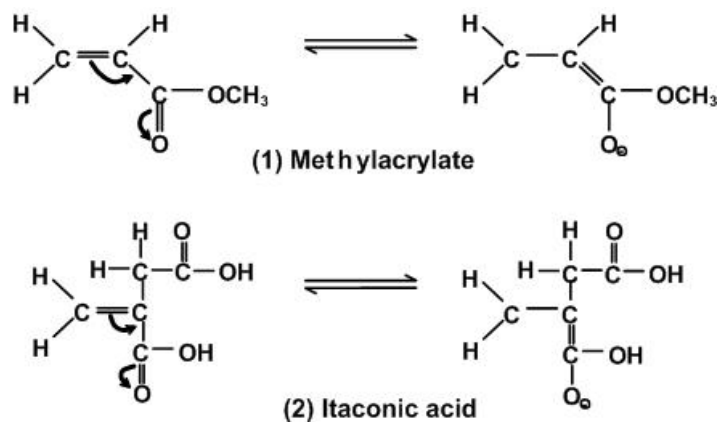
Figure 4. Resonance or conjugation phenomenon occurs in comonomers.
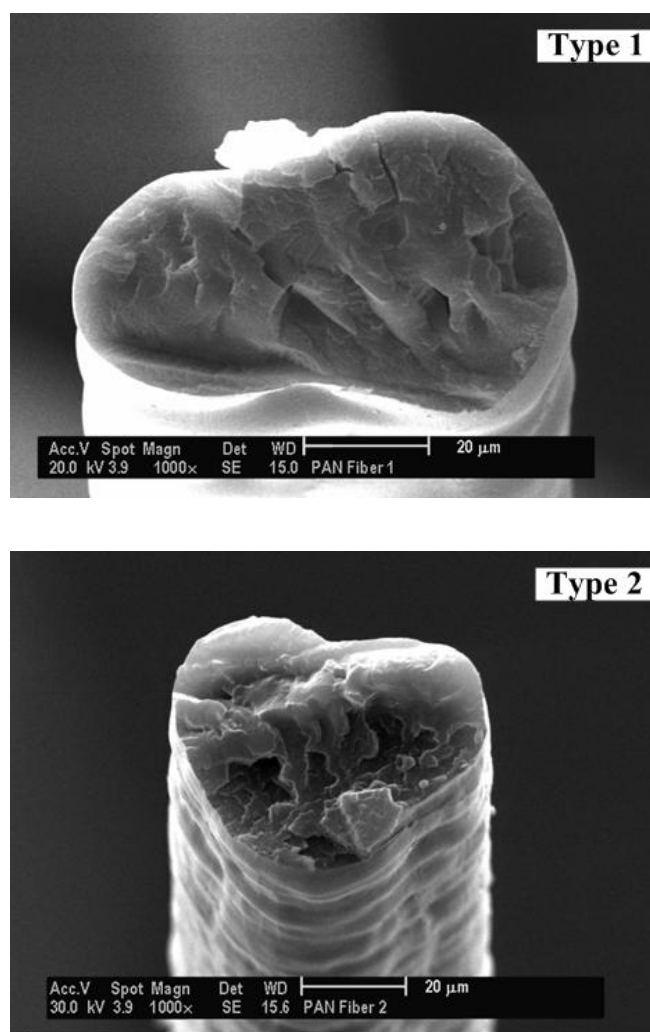
Figure 5. The cross section of PAN Fiber with different types of
dope preparation: (a) for Type 1 and (b)for Type 2 (Magnification: 1000×)
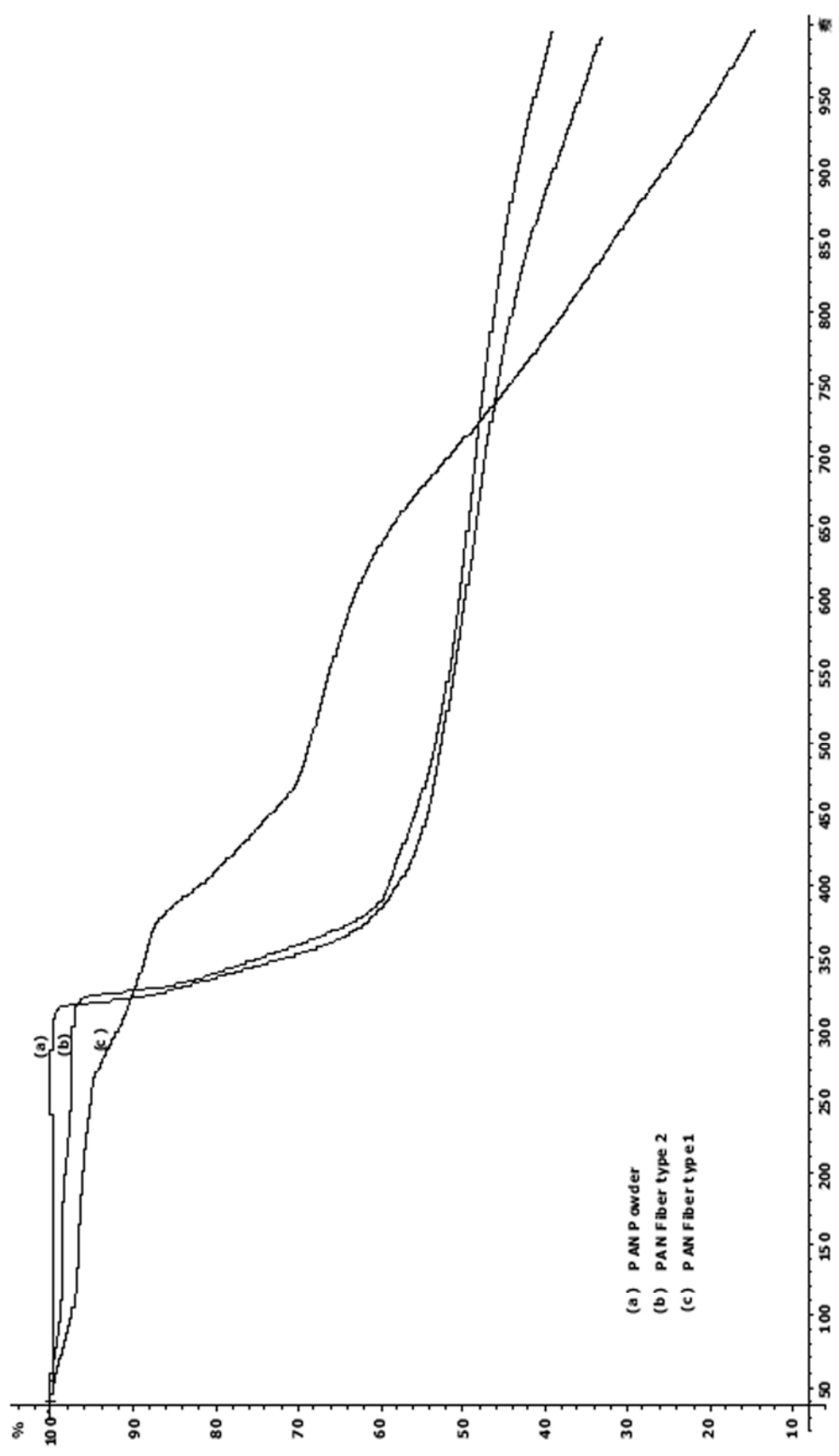
Figure 6. TGA curves of PAN powder and PAN fiber with different dope preparation
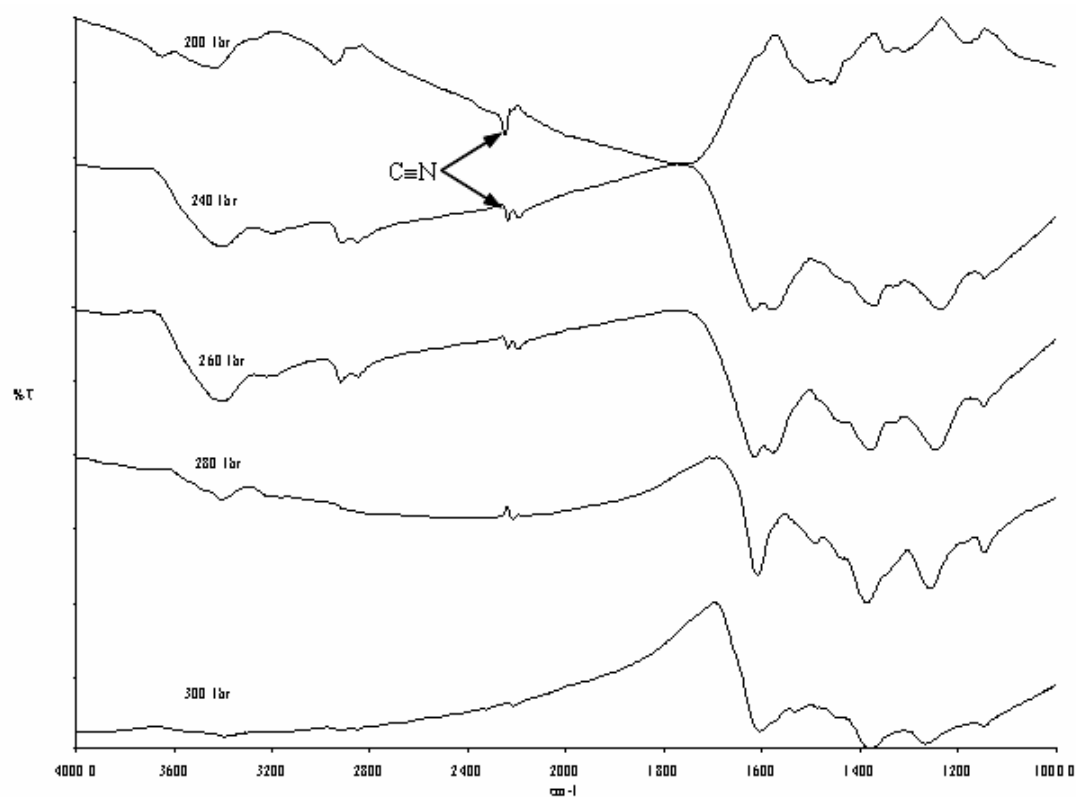
Figure 7. IR spectrum of stabilized PAN fiber (Type 1) in air.
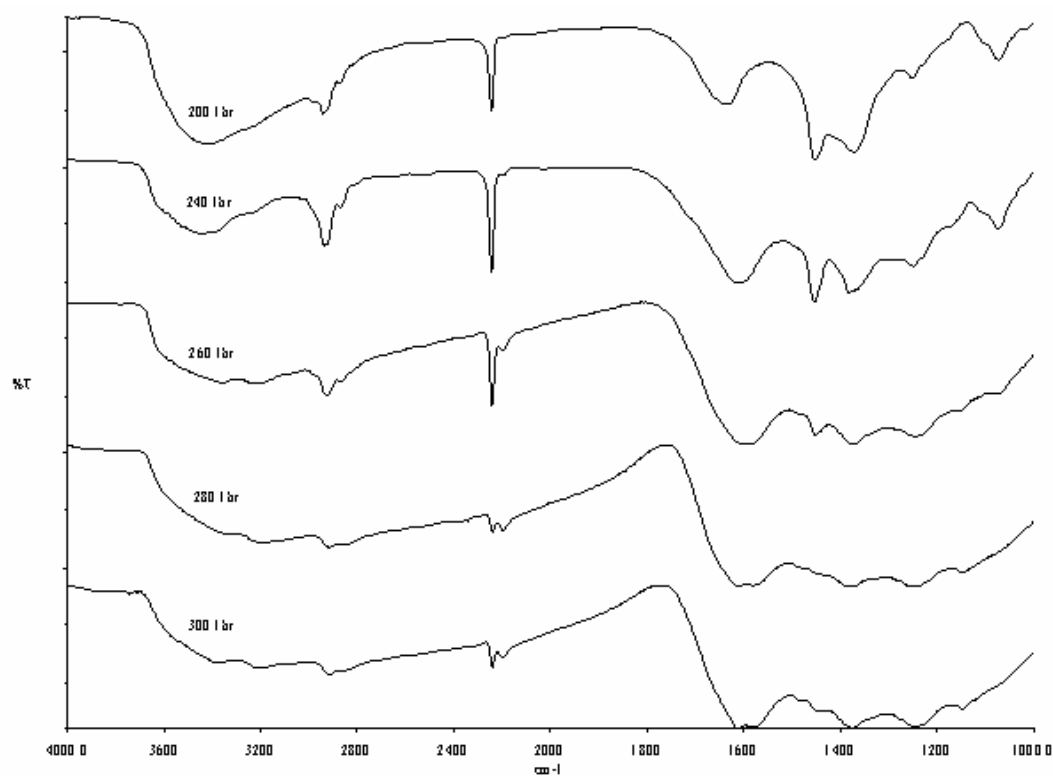
Figure 8. IR spectrum of stabilized PAN fiber (Type 2) in air.
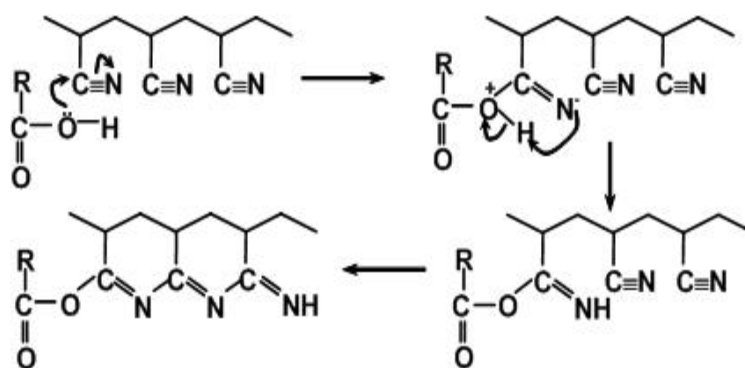
Figure 9. Comonomers react as an additive to initiate cyclization reaction (Tsai and Lin, 1990).
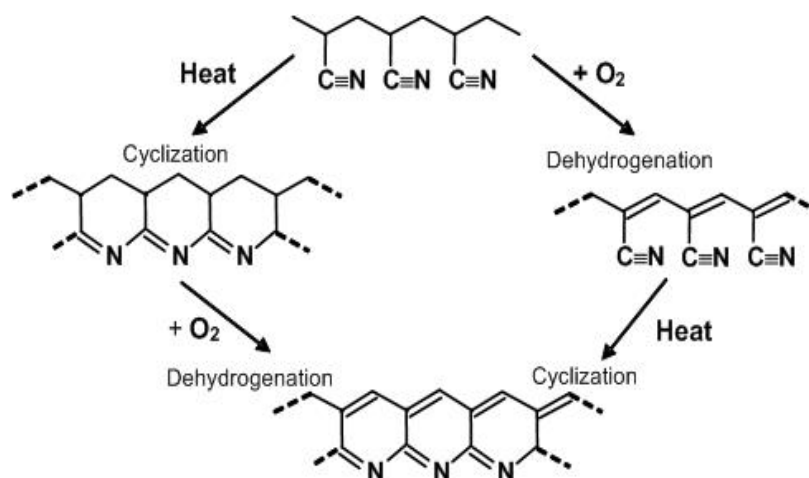
Figure 10. Cyclization and dehydrogenation reaction during stabilization process.

A New Variant of ARFIMA[1] Process and Its Predictive Ability

Yip Chee Yin (Corresponding author)

Faculty of Quantitative Sciences

Universiti Utara Malaysia

Sintok, Kedah Darul Aman

Malaysia

Tel: 60-125150462   E-mail: yip@uum.edu.my

Quah Soon Hoe

School of Mathematical Sciences

Universiti Sains Malaysia

Penang

Malaysia

Tel: 60-125693341   E-mail: shquah@gmail.com

Abstract

ARFIMA models generated an enormous amount of interest in the literature about three decades ago. However, this interest vaned after Granger (1999) showed that an ARFIMA process might have stochastic properties that do not mimic the properties of the data at all. The empirical results of our research in which we used exchange rate data for the analysis, show that a variant of an ARFIMA process indeed can beat the ARFIMA, the Random Walk and the ARMA process of the order one in out of sample forecasting. This indirectly indicates that our variant of the ARFIMA process can be considered as the data generating process for the long memory time series.

Keywords: Forecast evaluation, A new variant of ARFIMA process

1. Introduction

The search for a model which can outperform random walk in out of sample forecasting was started about two decades ago in two important areas of study: volatility modelling and purchasing power parity (PPP) hypothesis. In volatility modelling, it has been recognized that the simple random walk can outperform many sophisticated volatility models in out of sample forecasting, while in purchasing power parity research, the existence of mean reverting behaviour in exchange rates has not been established convincingly yet. In research on mean reversion behaviour, the most significant negative results were obtained by Meese and Rogoff (1983a, b). They evaluated the predictive ability of a series of linear structural exchange rate models and found that none was able to consistently outperform a simple random walk for all the known exchange rates and horizons.   This seemingly robust result was then put into dispute when Mark and Sul (2002) , Rapach and Wohar (2002), and Faust, Rogers and Wright(2003) obtained some evidence of linear structural models outperforming random walk models. Recent work done by Taylor, Sarno, Clarida and Valente (2003) using nonlinear models show the promising positive result that there are structural models which can outperform random walk models in out of sample forecasting, or to put it differently, there is mean reverting behaviour in exchange rate.

In this paper, we offer another structural model based on a long memory process, which can outperform the random walk soundly. Our approach is by adding an explanatory variable into the ARFIMA long memory model. This explanatory variable is chosen based on the research finding of Taylor, Sarno, Clarida and Valente (2003) that there is nonlinearity in exchange rates. Our dependent variable is made up of two components: the intrinsic y component and its logarithmic counterpart. By using this transformation, we are able to use this compound dependent variable to capture the nonlinear behaviour of the exchange rate. This is because ln y is a nonlinear function. Equivalently, we can view the ln y component as an explanatory variable just as the first lag of y is acting as an explanatory variable in a first order autoregressive model.

The rest of the paper is organized as follows. In section 2, we briefly review ARFIMA processes and outline the empirical estimation methodology used in the rest of the paper. Section 3 describes how we construct our YQ-ARFIMA model. Section 4 discusses three predictive accuracy techniques, while in section 5, we outline the predictive model selection procedures used in the research. In section 6, we present the empirical analysis. Section 7 presents one application of our model and we conclude this paper in section 8.

2. The ARFIMA Long Memory Process

There are basically two experimental evidence, which show that a long memory process is very useful in long horizon forecasting. However, there is also one experimental finding that a long memory process is not suitable for forecasting. The two experimental evidences are as follows:

Going back to the 1960s, experience of nonparametric spectral estimation for many economic time series has suggested very marked peakedness around the zero frequency. This essentially suggests that the maximum likelihood of events happening will be at a low frequency. Moreover, a low frequency component is closely related to the long run dynamics of the process. However, at frequency $\lambda = 0$, we can have two conditions: one, the spectral density function is bounded and the other one is unbounded. In a long memory process, an ARFIMA model would have its spectral density function unbounded at frequency $\lambda = 0$, making it more suitable for long horizon forecasting. In terms of autocorrelation, ARFIMA models show characteristics of hyperbolic autocorrelation decay patterns when modelling economic and financial time series. Despite these positive evidences, one piece of negative evidence has emerged around 1999, when Granger acknowledges that an ARFIMA model might have stochastic properties that essentially do not mimic the properties of the data at all. With this experimental evidence in mind, we shall now present the prototypical ARFIMA model examined in the literature.

The standard ARFIMA model is shown below,

$$B(L)(1-L)^d y_t = A(L)u_t \tag{1}$$

where $B(L) = 1 - B_1 L - ... - B_p L^p$ and $A(L) = 1 + A_1 L + ... + A_q L^q$, d is the fractional differencing parameter or rather the memory parameter, and u_t is the white noise. This process is covariance stationary if -0.5 < d < 0.5, with mean reversion when d < 1. The lag polynomials shown in equation (1) can be easily expanded to reveal the importance of the hyperbolic decay property of ARFIMA. This is shown in equation (2)

$$(1-L)^d = 1 - dL + \frac{d(d-1)}{2!}L^2 - \frac{d(d-1)(d-2)}{3!}L^3 + ... = \sum_{j=0}^{\infty} g_j(d) \tag{2}$$

2.1 Long Memory Model Estimation

Long memory model estimation essentially boils down to the estimation of the memory parameter *d*, which describes the characteristics of the autocorrelation of the series. There are a few estimation techniques for the value of *d*, notably the semi-parametric estimation procedure of Geweke and Porter-Hudak(1983), and Robinson(1995), modified rescaled range estimator of Lo(1991), and the exact local Whittle estimator of Shimotsu and Phillips (2004). We focus only on the GPH estimator (Geweke and Porter-Hudak) since its computation is easier and its range of errors is acceptable when it is used for comparison purposes.

The GPH estimation is basically a two step procedure. It begins with the estimation of *d*, which is based on the log-periodogram regression. It is given by equation (3)

$$\ln[I(\lambda_j)] = \beta_0 + \beta_1 \ln\left[4\sin^2\left(\frac{\lambda_j}{2}\right)\right] + u_j \tag{3}$$

where $\lambda_j = \frac{2\pi j}{T}$, $j = 1,2..,m$ and λ_j represents the $m = \sqrt{T}$ Fourier frequencies.

$I(\lambda_j)$ which denotes the sample periodogram is defined as follows:

$$I(\lambda_j) = \frac{1}{2\pi T}\left|\sum_{T=1}^{T} y_t e^{\lambda_j t}\right|^2 \tag{4}$$

The critical assumption for this GPH estimator is that the spectrum of the ARFIMA(p,d,q) process is the same as that of an ARFIMA(0,d,0) process. Robinson (1995a) shows the following asymptotic result,

$$\left(\frac{\pi^2}{24m}\right)^{-1/2}\left(\hat{d}_{GPH} - d\right) \to N(0,1) \tag{5}$$

for -0.5 < d < 0.5 and $j = 1,..,m$ in the equation for λ_j above. Equation (5) is due to Robinson, and essentially

implies that for *d* between -0.5 and 0.5, the long memory process is stationary and invertible. If the value of *d* is outside this range, Robinson suggested that we difference the series until *d* is within the specified range for stationarity and invertibility.

3. YQ (Note 2)-ARFIMA Model

Recently, intense interest has been growing in nonlinear modelling especially in modelling exchange rates. This is largely due to the positive result obtained through nonlinear modelling; for example, a research finding by Taylor, Sarno, Clarida and Valente (2003), shows that exchange rate has nonlinear characteristics. By constructing a three regime switching intercept heteroskedatic VECM model, they are able to show that their model can beat the random walk. We follow the direction used by this piece of research, that is, we try to capture the nonlinearity of the exchange rate by incorporating another component into the dependent variable of the standard ARFIMA model which is given by equation (1). We assume that exchange rate is constructed by an additive method with a linear component added to a nonlinear component. The nonlinear component is generated by a nonlinear transformation of the linear component. Thus, we have the YQ-ARFIMA model given by

$$B(L)(1-L)^d z_t = A(L)u_t, \qquad u_t \sim iid(0, \sigma_t^2) \tag{6}$$

$$z_t = y_t - \Phi(L)\ln y_t \tag{7}$$

$$B(L)(1-L)^d \Phi(L) = c \tag{8}$$

where $B(z) = 0$ has roots inside the lag polynomials and c is a constant.

3.1 Theoretical Analysis of the YQ-ARFIMA Model

We are interested in two special cases of the general model set up as in equations (6), (7) and (8). They are:

Combining equation (6), (7) and (8), and after recognizing that $B(L)$ has an inverse, we obtain the following equation

$$B(L)(1-L)^d y_t = A(L)u_t + c\ln y_t \tag{9}$$

When $\Phi(L) = 1$, equation (6) would become

$$B(L)(1-L)^d (y_t - \ln y_t) = A(L)u_t, \tag{10}$$

$$y_t = \ln y_t + [B(L)(1-L)^d]^{-1} A(L)u_t \tag{11}$$

For the first case, we use mainly equation (9) for empirical analysis. Notice that in equation (9), we can treat $\ln y_t$ as an explanatory variable for the standard ARFIMA. We can use Hermite polynomials to verify equation (10).

A special mention must be made of equation (11), which reveals very clearly that the forecast values are accurate because this equation (11) essentially means regressing y_t on $\ln y_t$. We know that $y_t \approx \ln y_t$ when y_t is small after expanding it using the Taylor expansion. This simply means that the R squared value is close to unity, which in turn implies that it is a very good forecasting model.

4. Predictive Ability Evaluation Techniques

We shall use three evaluation techniques for evaluating the predictive ability of YQ-ARFIMA, ARFIMA, RW and ARMA. The first one is by using root mean square error (RMSE). It is essentially similar to mean square prediction error (MSPE). The difference is that we do not assume the loss function to be quadratic in nature.

4.1 Ratio G of RMSE Measure

We compare the predictive ability of two models by defining the ratio of their respective RMSE measure, where the RMSE measure of the benchmark model 0 is the denominator and the RMSE of the model 1 is the numerator. Thus, we define the following:

$$G = \frac{RMSE\ \text{Model 1}}{RMSE\ \text{Model 0}} \tag{12}$$

If the ratio *G* > 1, this means that model 0 is a better forecasting model than model 1 by *G* times. On the other hand, if *G* < 1, then model 1 is a better forecasting model than model 0. One word of caution, this ratio *G* can be taken as a rough guide only because we have not established its distributional properties yet. To fulfil this deficiency, we shall present a simple but accepted to be good enough model evaluation technique for non-nested models in the next subsection.

4.2 The Diebold & Mariano (DM) Statistic (1995)

We use the simple version of the DM statistical test, that is, the Sign Test. This simple test is used because we have obtained an affirmative result from the ratio of RMSE test, and by this test, we have extended the result from the ratio of RMSE test for the sample to that of the population.

Define the loss differential *d* as follows:

$$d_t = [g(e_{it}) - g(e_{jt})] \tag{13}$$

We have made the assumption that the loss function is a direct function of the forecast error and that the absolute value of the forecast error is a direct function of the forecast error itself. Thus, we have the simple case where

$$g(e_{it}) = |e_{it}|$$
$$g(e_{jt}) = |e_{jt}| \tag{14}$$

We further assume that the loss differentials are iid, which simply means that the models must be non-nested, and that the number of positive loss differential observations in a sample of size T has the binomial distribution with parameters T and 0.5 under the null hypothesis that the two models have similar forecasting abilities against the alternative hypothesis that the two models have different forecasting abilities. With that, we have the following results:

For small samples, we have the sign-test statistic as given by

$$S_a = \sum_{t=1}^{T} I_+(d_t) \tag{15}$$

where

$$I_+(d_t) = 1 \quad \text{if} \quad d_t > 0$$
$$= 0 \quad \text{otherwise} \tag{16}$$

Using a table of the cumulative binomial distribution, we may obtain and assess the significance of the test. However, if the sample size is large, we use the studentized *t* test to approximate the distribution. The studentized statistic is given by

$$S_b = \frac{S_a - 0.5T}{\sqrt{0.25T}} \sim N(0,1) \tag{17}$$

One word of caution: because we have assumed that the loss differential series is iid, the above test can only be applied to non-nested models. Otherwise, the limiting distribution will be non standard. However, if we use a Newey-West (1987) type estimator for the DM test, then the tabulated critical values are quite close to those for the *N*(0,1). Moreover, the non-standard limit distribution is reasonably approximated by a standard normal in many contexts (see McCracken (1999) for tabulated critical values). Furthermore, this DM test is suitable for evaluating the predictive ability of non-nested models only.

4.3 The Clark and McCracken Encompassing Test (CM statistic)(2001)

This CM statistic is designed for comparing nested models. This CM test is conducted for the purpose of further confirming the empirical results obtained by using the ratio of RMSE measure and the DM test, as the latter two tests have not eliminated the chances that the two models concerned may be nested. This test has the same null hypotheses as the DM test, except that the alternative is model 1 can outperform model 0. Thus, CM statistics is given by:

$$CMt = \sqrt{(P-1)} \frac{\bar{u}}{[P^{-1}\sum_{t=R}^{T-1}(u_{t+h} - \bar{u})]^{1/2}} \tag{18}$$

where $u_{t+h} = e_{0,t+h}(e_{0,t+h} - e_{1,t+h})$ and $\bar{u} = P^{-1}\sum_{t=R}^{T-1} u_{t+1}$, and *P* is the prediction period. The limiting distribution for $h > 1$ is non-standard, but if we use the Newey-West type estimator the tabulated critical values are quite close to those for the N (0,1).

5. Predictive Model Selection

We use forecast horizons of 5 steps, 20 steps, 60 steps and 240 steps to correspond to 1 week, 1 month, 3 months and 1 year, respectively. We first split the sample of size T into two equal halves. The first half is used to produce 0.25T recursive (and rolling) predictions. The other 0.25T observations are used as the initial sample for estimating the parameters for the next step of the predictions. To put it differently, parameters are updated before each new prediction is constructed. These predictions are then used to obtain the best YQ-ARFIMA, ARFIMA, RW and ARMA by comparing the out of sample root mean square forecast errors.

After selecting the best YQ-ARFIMA, ARFIMA, RW and ARMA models, we fix the respective specifications for the ratio of RMSE test, DM test and CM test for the evaluation of predictive ability. Table 1 shows the respective specifications selected for the various best models. (See Table 1)

6. The Empirical Analysis

In this empirical analysis, we have conducted two experiments: one, we determined the values of the RMSE measure for 15 exchange rates around the globe and two, we determine the RMSE measure, the DM statistics and the CM statistics for 6 exchange rates specially selected to represent different parts of the globe. For the first experiment, we conducted only point forecasts. However, for the second experiment, we performed point forecasts as well as interval forecasts. The results of the first experiment are recorded in Table 2 and the results from the second experiment are recorded in Table 3 to Table 13.

6.1 Analysis of the first experimental results

This first experiment was aimed at testing the robustness of the YQ-ARFIMA with regard to different exchange rates around the globe. In this experiment, we performed only the recursive forecasts and the forecast horizon is 8 periods only. Moreover, the sample size is fixed at 1000.   Column 6 of Table 2 shows that there are 6 exchange rates and 9 exchange rates where the YQ-ARFIMA model is better than RW in out of sample forecasting on the average about 49 times and 5 times, respectively. As for the YQ-ARFIMA model   versus ARFIMA model, the former is about 45 times and 6 times better than the latter for same 6 exchange rates, and for the other 9 exchange rates, the YQ-ARFIMA model is better about 6 times. With regard to RW model versus ARFIMA model, the former is better than the later for 9 out of the 15 exchange rates.

Thus, on the whole, the YQ-ARFIMA model can outperform the RW model and ARFIMA model in out of sample forecasting soundly. In addition RW model can outperform ARFIMA model in 9 out of the 15 exchange rates. However, we have used the ratio of the RMSE measure for comparison which is accurate for the samples concerned. These spectacular results may not be valid for population in general as we have not accounted for the distributional properties of the ratio of the RMSE measure. (See Table 2)

6.2 Analysis of the second experimental results

In this experiment, we have conducted three investigations: one, we determined the robustness of the first experimental results with regard to variation in sample sizes and forecast horizons, two, we tested these results by using the Diebold and Mariano statistical test and three, we tested   the results again by using the Clark and McCracken test. This last test is necessary in order to ensure that the nestedness of the two models will not affect our final results.

6.2.1 Comparison of the ratio of RMSE measures

With respect to sample size, in column 3 of Tables 3, 4, 5 and 6, the YQ-ARFIMA model beat random walk soundly for sample sizes 500, 1000, 2000 and 5000, except that in the case of the recursive scheme for sample size 1000, it lost to the RW model for the case of the British pound at a forecast horizon of 20 periods only, and for sample size 2000 for case of the Euro dollar also at a forecast horizon 20 periods. However, for the case of rolling scheme, the YQ-ARFIMA model performs much better. It lost to RW only for one case, i.e., the British pound at forecast horizon 240 periods. In general, the YQ-ARFIMA performs better at the short horizons of 5 periods and 20 periods, both for the recursive and the rolling schemes of forecast.

For the case of the YQ-ARFIMA model versus the ARFIMA model as in column 4 of Tables 3, 4, 5 and 6, a similar situation arises, where the ARFIMA model beat the YQ-ARFIMA model only for case of the British pound, sample size 1000 at a forecast horizon of 60 periods, and for case of the Singapore dollar, sample size 2000 at a forecast horizon of 240 periods.

For the case of the YQ-ARFIMA model versus the ARMA model as shown in column 5 of Tables 3, 4, 5, and 6, the former is better than the latter on the average by more than 10 times. Only at three instances for the case of recursive forecast, was the ARMA model is better than the YQ-ARFIMA model that is, for the British pound with sample size 500 at a forecast horizon of 20 periods; with sample size 2000 at a forecast horizon of 240periods, and for the Euro dollar with sample size 2000 at a forecast horizon of 240 periods. For the case of rolling forecast, there are two instances where the ARMA model is better than the YQ-ARFIMA model, that is, for the British pound with sample size 2000 at a forecast horizon of 240 periods, and for the Malaysian ringgit with sample size 2000 at a forecast horizon of 5 periods.

As for the RW model versus the ARFIMA model, the former can still beat the latter marginally. However, for sample size 2000, the two models are equal on the average for recursive forecast but for rolling forecast, the RW model lose to the   ARFIMA model. (See Table 3, 4, 5 and 6)

6.2.2 Evaluation of predictive ability- DM statistic

For the YQ-ARFIMA model versus the RW model, the DM statistics are all negative with absolute values more than 2 for sample sizes 500, 1000, 2000 and 5000, and for horizons 5 periods, 20 periods, 60 periods and 240 periods. This simply means that the null hypothesis of equal models is rejected and that the loss differential for the YQ-ARFIMA

model is smaller than the RW model, which implies that the YQ-ARFIMA is a better forecasting model than the RW model in out of sample forecasting.

As for the YQ-ARFIMA model versus the ARFIMA model, we obtain a similar result except that with sample size 5000 at a forecast horizon 20 periods, the null hypothesis is accepted. As for the ARFIMA model versus the ARMA model, we find that the ARMA model is better than the ARFIMA model for about 26 instances, whereas the ARFIMA model is better the ARMA model for about 32 instances. (See Table 7, 8, 9, and 10)

6.2.3 Evaluation of predictive ability- CM statistic

It must be noted that the DM statistic is intended to be applied to non-nested models. What if the two models are nested? In that case, we have to use the Clark and McCracken statistic (CM statistic). As the main objective of this paper is to prove that the YQ-ARFIMA model can beat the random walk model, we shall conduct this CM test only for the YQ-ARFIMA model versus the RW model for the selected 6 exchange rates for sample sizes 500, 1000, 2000, 5000 and at forecast horizons 5 periods, 20 periods, 60 periods and 240 periods. The results are recorded in Table 11, which shows that the YQ-ARFIMA model beat the random walk (RW) model rather convincingly. (See Table 11)

7. One application of the YQ-ARFIMA model

Since our model can outperform many other existing models in out of sample forecasting, there would be many uses for the YQ-ARFIMA model. In this section, we shall present one application of the YQ-ARFIMA model. For the past two decades, many research papers have been investigating the mean reversion behaviour of exchange rates. Until now, this controversy still remains to be settled convincingly, especially with regard to the exchange rate after the breakdown of the Bretton Woods System in 1973. Many tools for testing the mean reverting behaviour have used the notably more powerful unit root test, panel data analysis and fractional cointegration. However, no consensus has been reached on the mean reversion property of exchange rates. Since our model can beat the random walk model soundly, it can be used to show this mean reverting behaviour. The idea is as follows: If the YQ-ARFIMA model can beat the random walk model for one particular exchange rate, then this exchange rate cannot show 100 % persistency since the random walk is not the data generating process of the exchange rate. If not fully persistent, this implies that the exchange rate has some degree of stationarity, or to put it differently, there is mean reverting behaviour for this set of data. We test this idea by using the exchange rate British pound per unit US dollar (UKEX)

UKEX has been shown to exhibit mean reverting behaviour by using two centuries of exchange rate data (see Lothian, James and M. Taylor, 1996). We shall show the same result by using data after the breakdown of the Bretton Woods System. We test whether the YQ- ARFIMA model can beat the random walk model in out of sample forecasting by using the said data set. If a positive result is obtained, we shall conclude that indeed, the British pound per unit US dollar exhibits mean reverting behaviour.

Table 13(a) and Table 13(b) show the experimental results. We select randomly five samples from the UKEX exchange rate series for testing. These five samples are of sizes 259, 530, 780, 1038 and 1230. It is very clear from the experimental figures shown in Table 13(a) and Tale 13(b), that the YQ-ARFIMA model outperforms the random walk model soundly. Thus, indeed, UKEX exhibits mean reverting behaviour.   (SeeTables 12(a) and (b))

8. Conclusion

We have shown convincingly that the YQ-ARFIMA model can beat the random walk model in out of sample forecasting. We have used the ratio of RMSE measure, DM test and CM test to verify the above result. However, we have not used a Newey and West type of estimator for the variance used in these two tests. We think that it is not necessary because the ratio of RMSE measure is very large indeed for it to be invalid in statistical testing.

As for the uses for our model, we have shown how to use it to test the mean reverting behaviour of exchange rates. With this new tool, we hope to put to rest the controversy of mean reversion and its existing testing tools. With this accurate model, we can devise more accurate volatility models with a long memory or a short memory data generating process. We also can use the YQ-ARFIMA model to devise an early warning system for currency attack.

References

Clark, T.E. & McCracken, M.W.   (2001). Tests of equal forecast accuracy and encompassing for nested models. *Journal of Econometrics* 105: 85-110.

Cheung, Y. & Lai K. (1998).   Parity reversion in real exchange rates during the post-Bretton Woods period. *Journal of International Money and Finance* 17: 597 – 614.

Cheung, Y., Chinn M. D. &   Antonio G. P. (2003): Empirical Exchange Rate Models of the nineties: Are Any Fit to Survive? Working Paper: University of California, Santa Cruz.

Clarida, R.H., Sarno, L. Taylor, M.P. and Valente, G. (2003). The out of sample success of term structure models as exchange rate predictors. A step beyond. *Journal of International Economics* 60: 61-83.

Diebold, F.X., & Mariano R.S. (1995). Comparing predictive accuracy. *Journal of Business & Economic Statistics* July 1995, Vol. 13, No.3: 253-263.

Faust, J., Rogers J. and Wright, J. (2003). Exchange rate forecasting: The errors we've made. *Journal of International Economics*, 60: 35-59.

Fox, R. and Taqqu, M. S. (1986): Large sample properties of parameter estimates for strongly dependent stationary Gaussian time series. *Annals of Statistics* 14, 517-32.

Geweke J. & s. Porter – Hudak S. (1983). The estimation and application of long memory time series models. *Journal of Time Series Analysis* 4: 221 – 238

Granger C.W.J. & Hyung, N. (1998). Occasional Structural Breaks and Long Memory Working Paper 99: UCSD.

Lothian, J. R. and Taylor, M. P. (1996). Real exchange rate behavior: The recent float from perspective of the last two centuries. *Journal of Political Economy* 104: 488-509.

Lo A.W. (1988). Maximum Likelihood Estimation of Generalized Ito Process with Discretely Sampled Data. *Econometric Theory*, 41: 231-247.

Lo, A. W. (1991): Long term memory in Stock Market. *Econometrica* 59 : 1279 – 1313

McCracken, M.W. & Sapp, S (2004). Evaluating the Predictability of Exchange Rates using Long Horizon Regressions: Mind Your p's and q's. Working Paper. University of Western Ontario.

Meese, R.A. & Rodoff, K (1983). Empirical exchange rate models of the seventies: do they fit out of sample? *Journal of International Economics*, 14: 3-24.

Newey, W.K. and K.D. West. (1987). A simple, positive semi-definite, heteroskedasticity and autocorrelation consistent covariance matrix. *Econometrica*, 55: 703-08.

Rapach, D. and Wohar M. (2002). Testing the monetary model of exchange rate determination.:New evidence from a century of data. *Journal of International Economics,* 58: 359-385.

Robinson, P.M & Henry, M. (1999). Long and short memory conditional Heteroskedasticity in estimating the memory parameter in levels. *Econometric Theory* 15:   299 – 336.

Robinson, P.M. (1995). Gaussian semiparametric   estimation of long range dependence. *Annals of Statistics* 23: 1630 – 1661.

Shimotsu, K. & Phillips P.C.B., (2004): Exact local Whittle estimation of fractional integration. Working paper: University of Essex.

White, H. (1980). A Heteroskedastic- Consistent Covariance Matrix and a Direct Test for Heteroskedasticity. *Econometrica*   48: 421-448.

Notes

Note 1. ARFIMA stands for autoregressive fractional integrated moving average process

Note 2. YQ-ARFIMA stands for the new variant of ARFIMA. Y denotes Yip and Q denotes Quah

Note 3. The 15 sets of exchange rate data are obtained from the Federal Reserve Bank of US.

Table 1. Best specifications for YQ-ARFIMA, ARFIMA, RW and ARMA with respect to the AUSD, UKPD, CAND, SIND, MALR and EURO

Models	AUSD (Australian Dollar)	UKPD (British Pound)	CAN (Candian Dollar)	SIND (Singapore Dollar)	MALR (Malaysian Ringgit)	EURO (Euro Dollar)
YQ ARFIMA	2,[-0.070],1	2,[0.208],1	2,[-0.053],1	1,[0.094],1	1,[0.493],0	2,[-0.112],1
ARFIMA	1,[0.065],1	1,[0.035],1	1,[0.473],1	2,[0.209],1	1,[0.111],1	1,[0.039],0
RW	0,1,0	0,1,0	0,1,0	0,1,0	0,1,0	0,1,0
ARMA	1,0,1	1,0,1	1,0,1	1,0,1	1,0,1	1,0,1

Note: The first, second and third values in each cell denote autoregressive parameter, difference parameter and

moving average parameter. RW denotes random walk while ARMA is the autoregressive moving average process.

Table 2. Comparing the 8 periods forecasting ability of ARFIMA, YQ-ARFIMA and Random Walk (RW) in terms of RMSE values for all the 15 exchange rate series.

Name of the exchange rate (Note 1)	ARFIMA (P)	YQ-ARFIMA (Q)	R.W (R)	R/P	R/Q	P/Q
Aus dollar	0.0031	0.00006	0.0032	1.05	48.53	46.17
Mal ringgit	0.0016	0.00005	0.0027	1.67	51.61	30.91
Thai bath	0.2946	0.00293	0.2923	0.99	99.75	100.52
Sin dollar	0.0085	0.00034	0.0082	0.98	24.07	24.58
Jap yen	0.3792	0.02358	0.4016	1.06	17.03	16.08
UK pound	0.0048	0.00089	0.0037	0.78	4.14	5.32
Euro Eur	0.0062	0.00113	0.0071	1.13	6.24	5.50
China yuan	0.0112	0.00133	0.0107	0.95	7.96	8.38
HK dollar	0.0231	0.00307	0.0186	0.81	6.07	7.51
S.Afri Rand	0.1628	0.03376	0.1638	1.01	4.85	4.82
Den Kronor	0.0689	0.02062	0.0487	0.71	2.36	3.35
Swiss Franc	0.0125	0.00193	0.0085	0.68	4.43	6.46
Can dollar	0.0092	0.00017	0.0094	1.02	56.37	55.38
Mexi Pesos	0.1620	0.01831	0.1473	0.91	8.05	8.85
Brazil Real	0.1209	0.01302	0.0586	0.48	4.49	9.28

Note: RMSE denotes root mean square error, Aus-Australia, Mal- Malaysia, Thai-Thailand, Sin-Singapore, Jap-Japan, UK-United Kingdom, Eur-Europe, HK-Hong Kong, S.Afri-South Africa, Den-Denmark,Can-Canadian,

And Mexi-Mexico

Note 1. These 15 exchange rate data are obtained from Federal Reserve Bank of US.

Table 3.   Comparison ratio of RMSE measure for sample size 500 with recursive forecast, and rolling forecast in bracket

Exrate	h	R/Q	F/Q	M/Q	F/R	M/R
AUSD	5	16.9(13.3)	21.5(16.4)	22.1(16.8)	1.28(1.23)	1.31(1.27)
(Australian	20	22.7(11.5)	34.4(16.6)	34.8(17.3)	1.51(1.44)	1.53(1.51)
Dollar)	60	108(9.49)	53.4(16.3)	52.7(17.1)	0.49(1.72)	0.48(1.79)
	240	33.6(90.3)	30.7(107)	30.6(108)	0.91(1.18)	0.91(1.19)
CAND	5	28.1(32.2)	31.4(27.1)	23.7(26.5)	1.11(0.84)	0.84(0.82)
(Canadian	20	22.1(19.2)	31.9(25.5)	32.7(26.8)	1.44(1.32)	1.48(1.39)
Dollar)	60	30.0(21.7)	55.9(34.3)	74.2(49.2)	1.47(1.58)	1.95(2.26)
	240	31.0(18.1)	61.0(26.6)	2.08(31.4)	1.961.46)	2.08(1.73)
UKPD	5	4.42(5.16)	4.59(7.19)	4.25(5.59)	1.04(1.38)	0.96(1.08)
(British	20	6.32(6.51)	1.03(2.23)	0.93(2.37)	0.16(0.34)	0.15(0.36)
Pound)	60	7.11(5.91)	7.80(5.53)	1.19(7.12)	1.09(0.94)	1.19(1.20)
	240	1.65(0.70)	22.9(10.4)	22.6(10.4)	13.9(15.1)	13.7(14.8)
SIND	5	9.06(13.4)	8.22(9.51)	11.3(23.5)	0.91(0.71)	1.25(1.76)
(Singapore	20	6.27(19.5)	7.51(10.6)	1.86(28.4)	1.19(0.54)	0.30(1.45)
Dollar)	60	7.37(16.8)	5.13(16.6)	11.3(16.5)	0.69(0.98)	1.54(0.98)
	240	9.83(8.81)	1.13(6.85)	7.69(6.89)	0.11(0.78)	0.78(0.79)
MALR	5	51.1(60.6)	45.0(98.0)	152(87.0)	0.88(1.61)	2.97(1.43)
(Malaysian	20	185(66.2)	407(254)	276(48.1)	2.20(3.84)	1.49(0.73)
Ringgit)	60	61.3(60.4)	127(232)	123(240)	2.08(3.84)	2.00(3.98)
	240	224(173)	176(124)	125(130)	0.79(0.71)	0.56(0.75)
EURO	5	17.2(12.0)	19.8(14.1)	18.6(10.6)	1.15(1.17)	1.08(0.88)
(Euro	20	14.4(26.7)	11.7(18.0)	11.4(18.0)	0.81(0.67)	0.79(0.67)
Dollar)	60	67.5(19.3)	83.4(22.4)	79.1(21.8)	1.23(1.16)	1.17(1.13)
	240	8.13(211)	15.6(47.5)	14.5(239)	1.91(0.23)	1.78(1.13)

R = RMSE for random walk; Q = RMSE for YQ-ARFIMA; F = RMSE for ARFIMA; M = RMSE for ARMA,
Exrate = Exchange rate, h = Forecast horizon

Table 4.   Comparison ratio of RMSE measure for sample size 1000 with recursive forecast and rolling forecast in bracket

Exrate	h	R/Q	F/Q	M/Q	F/R	M/R
AUSD	5	50.2(11.6)	58.5(10.5)	58.7(15.6)	1.16(0.91)	1.17(1.35)
(Australian	20	13.5(12.3)	18.5(10.4)	16.3(9.5)	1.37(0.85)	1.21(0.77)
Dollar)	60	20.1(16.3)	16.0(13.4)	23.2(13.4)	0.79(0.82)	1.15(0.80)
	240	20.9(158)	11.2(61.2)	11.3(140)	0.54(0.39)	0.54(0.89)
CAND	5	7.53(10.8)	13.8(1.15)	12.3(12.1)	1.83(1/83)	1.64(1.11)
(Canadian	20	20.0(39.0)	25.2(1.15)	1.63(1.15)	11.8(1.26)	1.64(1.11)
Dollar)	60	43.9(37.9)	50.1(20.0)	52.2(21.3)	1.14(0.53)	1.18(55.4)
	240	19.5(39.3)	39.3(60.0)	39.7(62.2)	2.01(0.80)	2.03(0.83)
UKPD	5	3.17(2.48)	10.7(0.75)	3.20(2.47)	3.29(0.30)	1.00(0.97)
(British	20	0.59(2.76)	1.59(1.18)	2.81(2.38)	2.49(0.43)	4.71(0.86)
Pound)	60	1.65(2.85)	0.98(1.87)	2.97(1.87)	0.35(0.66)	1.06(1.07)
	240	3.07(4.15)	3.55(2.10)	3.65(3.82)	1.15(0.51)	1.18(0.92)
SIND	5	10.4(12.6)	9.67(11.5)	10.3(12.4)	0.93(0.91)	0.99(0.98)
(Singapore	20	8.81(13.7)	8.58(10.1)	8.22(12.8)	0.93(0.73)	0.93(0.93)
Dollar)	60	10.2(14.4)	11.5(45.5)	11.6(36.0)	1.12(3.16)	1.14(2.50)
	240	17.2(5.15)	22.9(6.45)	20.1(5.59)	1.32(1.25)	1.16(1.08)
MALR	5	11.9(7.92)	173(3.99)	177(3.99)	14.5(0.50)	14.8(0.50)
(Malaysian	20	22.4(5.33)	25.18.04)	25.6(8.04)	1.12(1.51)	1.14(1.51)
Ringgit)	60	39.5(9.07)	45.5(1.20)	45.0(10.6)	1.15(1.20)	1.13(1.16)
	240	61.4(13.7)	62.1(0.15)	63.7(19.5)	1.01(0.15)	1.04(1.41)
EURO	5	8.08(7.87)	10.1(15.0)	10.1(6.02)	1.25(1.90)	1.25(0.76)
(Euro	20	8.71(15.6)	8.16(15.0)	8.11(6.02)	0.94(0.96)	0.93(0.38)
Dollar)	60	6.25(5.03)	7.54(5.65)	7.56(5.63)	1.21(1.12)	1.21(1.12)
	240	26.8(4.29)	21.8(6.14)	22.5(5.83)	0.81(1.43)	0.84(1.36)

R = RMSE for random walk; Q = RMSE for YQ-ARFIMA; F = RMSE for ARFIMA; M = RMSE for ARMA, Exrate = Exchange rate, h = Forecast horizon

Table 5.   Comparison ratio of RMSE measure for sample size 2000 with recursive forecast and rolling forecast in bracket

Exrate	h	R/Q	F/Q	M/Q	F/R	M/R
AUSD	5	7.09(5.74)	6.25(5.99)	6.58(5.84)	0.88(1.04)	0.93(1.02)
(Australian	20	7.97(6.73)	8.60(6.04)	8.60(6.18)	1.08(0.89)	1.07(0.92)
Dollar)	60	6.65(7.04)	6.42(4.86)	6.12(5.03)	0.96(0.69)	0.92(0.71)
	240	5.27(15.9)	4.80(13.7)	4.85(13.7)	0.91(0.86)	0.92(0.84)
CAND	5	17.9(24.6)	17.4(1.04)	17.6(1.02)	0.97(1.04)	0.98(1.02)
(Canadian	20	16.5(21.9)	16.3(22.8)	16.2(22.4)	0.99(1.04)	0.98(1.02)
Dollar)	60	12.7(18.5)	12.6(19.2)	12.9(18.8)	0.99(1.04)	1.01(1.02)
	240	52.3(13.9)	46.6(15.1)	47.6(14.7)	0.89(1.08)	0.91(1.05)
UKPD	5	12.4(12.2)	12.2(9.38)	12.2(9.38)	0.98(0.76)	0.98(0.98)
(British	20	12.5(14.5)	13.1(12.8)	13.1(16.4)	1.04(0.88)	1.04(1.13)
Pound)	60	8.98(9.48)	9.15(9.12)	9.06(9.12)	1.02(0.96)	1.01(0.96)
	240	10.5(7.18)	9.87(0.99)	0.94(0.99)	0.93(0.99)	0.94(0.99)
SIND	5	15.4(19.4)	16.9(19.6)	15.7(19.6)	1.09(1.01)	1.02(1.01)
(Singapore	20	20.2(19.8)	17.4(12.5)	28.9(12.5)	0.86(0.63)	1.43(1.77)
Dollar)	60	15.9(8.58)	33.9(25.7)	16.5(35.1)	2.13(2.99)	1.04(4.09)
	240	18.9(10.9)	0.73(11.8)	16.4(11.3)	0.73(1.07)	0.86(1.03)
SIND	5	15.4(19.4)	16.9(19.6)	15.7(19.6)	1.09(1.01)	1.02(1.01)
(Singapore	20	20.2(19.8)	17.4(12.5)	28.9(12.5)	0.86(0.63)	1.43(1.77)
Dollar)	60	15.9(8.58)	33.9(25.7)	16.5(35.1)	2.13(2.99)	1.04(4.09)
	240	18.9(10.9)	0.73(11.8)	16.4(11.3)	0.73(1.07)	0.86(1.03)
MALR	5	72.1(36.4)	83.1(26.6)	85.4(0.73)	1.15(0.73)	1.18(0.72)
(Malaysian	20	121(25.0)	149(17.0)	147(16.7)	1.23(0.68)	1.21(0.67)
Ringgit)	60	48.6(13.4)	61.6(25.7)	53.7(25.7)	1.27(1.92)	1.10(1.35)
	240	15.6(20.7)	23.9(38.8)	23.6(37.3)	1.53(1.87)	1.51(1.80)
EURO	5	4.67(4.97)	4.64(4.66)	4.83(5.06)	0.99(0.94)	1.03(1.02)
(Euro	20	0.45(7.59)	4.56(3.71)	4.89(3.36)	10.2(0.49)	10.9(0.44)
Dollar)	60	3.79(1.42)	4.42(1.32)	4.43(1.19)	1.16(0.93)	1.16(0.84)
[1200]	240	4.43(4.37)	6.03(4.03)	0.58(3.80)	1.36(0.92)	0.13(0.87)

R = RMSE for random walk; Q = RMSE for YQ-ARFIMA; F = RMSE for ARFIMA;   M = RMSE for ARMA, Exrate = Exchange rate, h = Forecast horizon

Table 6. Comparison ratio of RMSE measure for sample size 5000 with recursive forecast and rolling forecast in bracket

Exrate	h	R/Q	F/Q	M/Q	F/R	M/R
AUSD	5	3.93(7.00)	4.62(7.22)	4.00(6.00)	1.17(1.03)	1.01(0.86)
(Australian	20	3.79(3.45)	3.96(3.98)	3.85(3.96)	1.04(1.15)	1.01(1.15)
Dollar)	60	4.11(3.63)	4.80(3.86)	4.55(3.79)	1.16(1.06)	1.11(1.04)
	240	4.86(3.78)	6.22(3.21)	5.58(3.42)	1.28(3.21)	1.15(0.91)
CAND	5	11.8(12.3)	13.3(12.3)	11.6(12.3)	1.12(1.00)	0.98(1.03)
(Canadian	20	12.5(11.6)	12.9(11.9)	1.08(1.04)	1.03(1.02)	1.08(1.05)
Dollar)	60	11.9(10.8)	10.8(11.3)	10.7(11.7)	0.91(1.05)	0.89(1.08)
	240	12.5(3.33)	10.1(11.5)	9.53(21.7)	0.80(3.46)	0.76(3.65)
UKPD	5	95.0(62.6)	100(58.8)	98.3(1.01)	1.06(0.94)	1.03(1.01)
(British	20	72.3(36.4)	73.5(35.9)	57.1(38.8)	1.02(0.99)	0.79(1.06)
Pound)	60	27.4(34.5)	30.5(36.4)	59.3(37.1)	1.11(1.05)	2.16(1.07)
	240	6.54(50.7)	6.98(54.6)	7.04(55.5)	1.06(1.08)	1.07(1.09)
SIND.	5	62.2(3.67)	20.9(7.62)	76.6(7.62)	1.24(2.07)	76.6(2.06)
(Singapore	20	78.2(6.74)	56.1(8.38)	50.6(8.93)	0.72(1.24)	0.65(1.32)
Dollar)	60	85.0(5.79)	127(6.95)	122(7.38)	1.49(1.19)	1.43(1.27)
[3000]	240	16.7(13.7)	24.0(7, 51)	13.5(7.12)	1.44(0.55)	0.81(0.52)
MALR	5	124(80.6)	114(96.6)	124(65.6)	0.92(1.19)	1.00(0.81)
(Malaysian	20	104(55.9)	99.7(59.6)	101(50.0)	0.96(1.07)	0.97(0.89)
Ringgit)	60	44.5(25.6)	41.9(26.8)	42.3(24.2)	0.94(1.05)	0.95(0.94)
[3500]	240	62.1(37.7)	66.4(32.5)	65.2(31.3)	1.07(0.86)	1.05(0.83)

R = RMSE for random walk; Q = RMSE for YQ-ARFIMA; F = RMSE for ARFIMA; M = RMSE for ARMA, Exrate = Exchange rate, h = Forecast horizon

Table 7. DM test statistics (YQ-ARFIMA versus RANDOM WALK)

Exrate	h	Sample size			
		500	1000	2000	5000
AUSD	5	-2.24[0.00]	-2.24[0.00]	-2.24[0.00]	-2.24[0.00]
(Australian	20	-4.47[0.00]	-4.47[0.00]	-4.47[0.00]	0.00[0.58]
Dollar)	60	-7.74	-7.74	-7.23	-7.74
	240	-48.9	-15.4	-15.1	-15.4
UKPD	5	-2.24[0.00]	-2.24[0.00]	-2.24[0.00]	-2.24[0.00]
(British	20	-4.47[0.00]	-4.47[0.00]	-4.47[0.00]	-4.47[0.00]
Pound)	60	-7.74	-7.48	-7.48	-7.48
	240	-15.4	-15.4	-15.4	-12.0
CAND	5	-2.24[0.00]	-2.24[0.00]	-2.24[0.00]	-2.24[0.00]
(Canadian	20	-4.47[0.00]	-4.47[0.00]	-4.02[0.00]	-4.47[0.00]
Dollar)	60	-7.74	-7.74	-7.48	-7.74
	240	-15.4	-15.4	-15.4	-15.2
SIND.	5	-2.24[0.00]	-2.24[0.00]	-1.34[0.18]	-2.24[0.00]
(Singapore	20	-4.47[0.00]	-4.47[0.00]	-4.02[0.00]	-4.47[0.00]
Dollar)	60	-7.74	-7.74	-7.74	-7.48
	240	-15.4	-15.4	-13.1	-13.9
					(3500)
MALR	5	-2.24[0.00]	-2.24[0.00]	-2.24[0.00]	-2.24[0.00]
(Malaysian	20	-4.47[0.00]	-4.47[0.00]	-4.47[0.00]	-4.47[0.00]
Ringgit)	60	-7.74	-7.74	-7.48	-7.74
	240	-15.4	-15.4	-15.2	-15.2
				(1200)	
EURO	5	-2.24[0.00]	-2.24[0.00]	-2.24[0.00]	-
(Euro	20	-4.47[0.00]	-4.47[0.00]	-4.47[0.00]	-
Dollar)	60	-7.74	-7.74	-7.23	-
	240	-14.5	-15.4	-14.3	-

H_0: Model 0 = Model 1 H_1: Model 0 $\neq$ Model 1   Reject H_0 when DM statistic > 2

When DM statistics < 0, Model 0 performs better than Model 1. When DM statistics > 0, Model 1 performs better than Model 0. Exrate = Exchange rate Exrate = Exchange rate

DM statistics = Diebold and Mariano Statistics

[   ] = Binomial probability of accepting   null hypothesis   ( )= sample size
          Model 0 =YQ-ARFIMA, and   Model 1 = RANDOM WALK are equal.

Table 8. DM test statistics (YQ-ARFIMA versus ARFIMA)

Exrate = Exchange rate

| Exrate | h | Sample size | | | |
		500	1000	2000	5000
AUSD	5	-2.24[0.00]	-2.24[0.00]	-2.24[0.00]	-2.24[0.00]
(Australian	20	-4.47[0.00]	-4.47[0.00]	-4.47[0.00]	0.00[0.58]
Dollar)	60	-7.48	-7.48	-7.74	-7.74
	240	-15.1	-15.3	-14.1	-15.4
UKPD	5	-2.24[0.00]	-1.34[0.18]	-2.24[0.00]	-2.24[0.00]
(British	20	-4.47[0.00]	-4.47[0.00]	-4.47[0.00]	-4.47[0.00]
Pound)	60	-7.74	-7.48	-7.48	-7.74
	240	-15.4	-15.3	-15.4	-13.5
CAND	5	-2.24[0.00]	-2.24[0.00]	-2.24[0.00]	-2.24[0.00]
(Canadian	20	-4.47[0.00]	-4.47[0.00]	-4.47[0.00]	-4.47[0.00]
Dollar)	60	-7.74	-7.74	-7.74	-7.74
	240	-15.4	-15.4	-15.1	-15.1
SIND.	5	-2.24[0.00]	-2.24[0.00]	-2.24[0.00]	-2.24[0.00]
(Singapore	20	-4.47[0.00]	-4.47[0.00]	-4.47[0.00]	-4.02[0.00]
Dollar)	60	-7.48	-7.48	-7.74	-7.74
	240	-15.4	-14.8	-13.4	-15.4
					(3500)
MALR	5	-2.24[0.00]	-2.24[0.00]	-2.24[0.00]	-2.24[0.00]
(Malaysian	20	-4.47[0.00]	-4.47[0.00]	-4.47[0.00]	-4.47[0.00]
Ringgit)	60	-7.74	-7.74	-7.74	-7.74
	240	-15.4	-15.1	-15.4	-15.2
				(1200)	
EURO	5	-2.24[0.00]	-2.24[0.00]	-2.24[0.00]	-
(Euro	20	-4.47[0.00]	-4.47[0.00]	-4.47[0.00]	-
Dollar)	60	-7.74	-7.48	-7.74	-
	240	-15.4	-15.4	-15.1	-

H_0: Model 0 = Model 1 H_1: Model 0 $\neq$ Model 1   Reject H_0 when DM statistic > 2

When DM statistics < 0, Model 0 performs better than Model 1. When DM statistics > 0, Model 1 performs better than Model 0.

DM statistics = Diebold and Mariano Statistics

[   ] = Binomial probability of accepting   null hypothesis   ( )= sample size

        Model 0 =YQ-ARFIMA and   Model 1 = ARFIMA are equal.

Table 9. DM test statistics (RW versus ARFIMA)

Exrate = Exchange rate

		Sample size			
Exrate	h	500	1000	2000	5000
AUSD	5	-2.24[0.00]	-2.24[0.00]	2.24[0.00]	-2.24[0.00]
(Australian	20	-3.57[0.0002]	-3.13[0.0013]	-2.68[0.50]	-3.13[0.0013]
Dollar)	60	-5.93	5.93	2.84	-0.26
	240	9.29	15.2	-4.64	-14.9
UKPD	5	-1.34[0.31]	-2.24[0.00]	2.24[0.00]	-2.24[0.00]
(British	20	1.78[0.98]	2.24[0.00]	-3.13[0.0013]	-0.89[0.25]
Pound)	60	-7.23	4.46	-7.74	-2.84
	240	-14.9	-4.91	15.1	-4.00
CAND	5	-2.24[0.00]	0.44[0.81]	2.24[0.00]	-2.24[0.00]
(Canadian	20	-3.13[0.0013]	-4.47[0.00]	4.02[0.00]	-4.02[0.00]
Dollar)	60	-6.71	-6.19	1.29	6.45
	240	-9.03	-7.10	10.8	14.5
SIND.	5	1.34[0.97]	0.44[0.81]	-0.44[0.5]	-0.44[0.5]
(Singapore	20	-3.57[0.0002]	3.13[0.0002]	1.78[0.97]	0.44[0.5]
Dollar)	60	7.74	-2.32	-1.29	-1.03
	240	-15.3	-8.00	-2.32	-1.29
					(3500)
MALR	5	0.44[0.81]	-1.34[0.97]	-1.34[0.97]	-2.24[0.00]
(Malaysian	20	-8.49[0.000]	-4.47[0.00]	-4.46[0.00]	-4.47[0.00]
Ringgit)	60	-7.74	-3.61	-6.97	6.19
	240	14.7	1.67	-8.13	-5.81
				(1200)	
EURO	5	-0.45[0.81]	-1.34[0.0.97]	2.24[0.00]	-
(Euro	20	3.13[0.98]	0.89[1.00]	-0.44[0.5]	-
Dollar)	60	-7.74	-7.23	-2.58	-
	240	-12.0	14.9	-13.4	-

H_0: Model 0 = Model 1 H_1: Model 0 $\neq$ Model 1   Reject H_0 when DM statistic > 2

When DM statistics < 0 , Model 0 performs better than Model 1. When DM statistics > 0 , Model 1 performs better than Model 0.

DM statistics = Diebold and Mariano Statistics

[   ] = Binomial probability of accepting null hypothesis   ( )= sample size

Model 0 =RW and Model 1 = ARFIMA are equal.

Table 10. DM test statistics (ARFIMA versus ARMA)

Exrate = Exchange rate

Exrate	h	Sample size			
		500	1000	2000	5000
AUSD	5	0.44[0.81]	0.44[0.81]	-2.24[0.00]	2.24[0.00]
(Australian	20	-4.47[0.02]	4.02[0.0013]	-3.13[0.0013]	4.47[0.02]
Dollar)	60	0.00	-5.93	5.42	0.52
	240	-14.1	-4.51	-8.13	12.9
UKPD	5	1.34[0.31]	2.24[0.00]	2.24[0.00]	-2.24[0.00]
(British	20	-3.57[0.002]	-2.23[0.02]	-3.57[0.002]	0.89[0.25]
Pound)	60	-7.48	-4.91	7.74	0.00
	240	4.38	17.2	-12.1	-5.55
CAND	5	2.24[0.00]	0.44[0.81]	-2.24[0.00]	2.24[0.00]
(Canadian	20	-3.13[0.0013]	-3.57[0.0002]	4.47[0.00]	-4.02[0.00]
Dollar)	60	-7.48	0.26	-4.13	3.09
	240	-9.94	-7.74	-9.81	14.2
SIND.	5	-1.34[0.97]	1.34[0.97]	1.34[0.97]	-0.44[0.00]
(Singapore	20	2.68[0.005]	0.89[0.99]	1.34[0.97]	3.57[0.002]
Dollar)	60	-7.22	-3.09	5.42	7.22
	240	5.93	8.77	-9.94	8.00
					(3500)
MALR	5	-1.34[0.31]	2.24[0.00]	-0.44[0.81]	2.24[0.00]
(Malaysian	20	3.57[0.002]	-4.47[0.00]	2.23[0.02]	-4.47[0.00]
Ringgit)	60	1.29	4.46	6.45	-5.42
	240	8.13	-7.23	7.87	-0.75
				(1200)	
EURO	5	-0.44[0.81]	-1.34[0.97]	-2.24[0.00]	-
(Euro	20	2.68[0.005]	0.89[0.99]	-3.57[0.00]	-
Dollar)	60	7.74	-2.06	-0.77	-
	240	15.4	-14.9	13.7	-

H_0: Model 0 = Model 1 H_1: Model 0 ≠ Model 1   Reject H_0 when DM statistic > 2

When DM statistics < 0, Model 0 performs better than Model 1. When DM statistics > 0, Model 1 performs better than Model 0.

DM statistics = Diebold and Mariano Statistics

[   ] = Binomial probability of accepting null hypothesis   ( )= sample size

Model 0 = ARFIMA and Model 1 = ARMA are equal.

Table 11. CM test statistics (YQ-ARFIMA versus RW)

Exrate = Exchange rate

		Sample size			
Exrate	h	500	1000	2000	5000
AUSD	5	-2.82	-3.17	-2.37	-2.72
(Australian	20	4.97	-6.26	-5.37	0.04
Dollar)	60	-9.42	-12.8	-11.2	-8.92
	240	-16.1	-19.3	-17.5	-25.5
UKPD	5	-2.51	-2.09	-2.97	-2.37
(British	20	-6.22	8.04	-6.52	-5.63
Pound)	60	-6.57	-9.39	-19.4	-9.23
	240	-18.3	-14.6	-20.3	-15.6
CAND	5	-3.18	-1.85	-4.23	-3.27
(Canadian	20	-4.06	-6.38	-8.67	-4.99
Dollar)	60	-12.0	-7.38	-11.1	-14.5
	240	-13.9	-15.0	-14.7	-24.6
SIND.	5	-2.64	-1.48	-2.53	-3.15
(Singapore	20	-4.48	-3.43	-4.26	-4.31
Dollar)	60	-11.1	-14.4	-10.4	-0.06
	240	-16.8	-13.8	-19.9	-15.4
MALR	5	-2.25	-2.55	-2.79	-2.57
(Malaysian	20	-4.89	-9.16	-6.34	-23.8
Ringgit)	60	-8.21	-6.26	-12.5	-7.76
	240	-27.2	-12.8	-19.5	-14.7
EURO	5	-2.04	3.69	-3.23	-
(Euro	20	-5.85	5.56	-5.20	-
Dollar)	60	-10.3	8.37	-7.05	-
	240	-14.7	14.4	18.1	-

H_0: Model 0 = Model 1 H_1: Model 0 > Model 1   Reject H_0 when CM statistic > absolute 2

When CM statistics < absolute 2, Model 0 performs better than Model 1.

CM statistics = Clark and McCracken Statistics

Null hypothesis: The two competing models are equal

Alternate hypothesis: Model 1 is a better forecasting model than model 0

Model 0 = YQ-ARFIMA and Model 1 = RW are equal.

Table 12. (a)– Comparison of the RMSE values for the case of   British pound per unit US dollar by using the YQ-ARFIMA model and   the Random Walk.

Sample size	Model Specifications		
	ARFIMA(2, d, 1) (*M*)	Random Walk (*W*)	*W/M*
Euro			
259	0.0013225	0.026926	20.4
530	0.0025324	0.013686	5.40
780	0.0057584	0.021163	3.68
1038	0.0054069	0.015672	2.89
1240	0.0094798	0.078815	8.31

Table 12. (b) – Comparison of the MAPE   values for the case of   British pound per unit US dollar by using the YQ-ARFIMA model and   the Random Walk.

Sample size	Model Specifications		
	ARFIMA(2, d, 1) (*M*)	Random Walk (*W*)	*W/M*
Euro			
259	0.065827	1.3474	20.5
530	0.104560	0.5556	5.31
780	0.374140	1.3611	3.64
1038	0.398240	1.1654	2.93
1241	0.609850	5.3464	8.77

Selenium and Body Health

Yuan Chen

Key National Sscientific Metastable Material Preparation Technology Laboratory, Yanshan University

Qinhuangdao 066004, China

Supervision Bureau of Health Enforcement in Haigang district, Qinhuangdao 066000, China

Qingshan Li

Key National Sscientific Metastable Material Preparation Technology Laboratory, Yanshan University

Qinhuangdao 066004, China

Abstract

Selenium is one of body micronutrients, which has a very close relationship with body health. Selenium is blessed with many important functions on biology, to certain category, such as protecting cells complete, keeping cells functions of physiology and biochemistry normal, improving the synthesis of cell DNA and RNA, participating the synthesis of ubiquinone and improving antibody developing, and effecting endocrine function in body. Selenium is closely connected with many diseases, mainly cancer, kashin-beck disease and keshan disease with deep study. Here, the relationship of selenium and body health is being reviewed.

Keywords: Selenium, Microbe, Body health, Disease, Control

It had been thought that selenide was toxic by old chemistry, but after 1970's, the fact that selenium could provide body with essential trace nutrients was found. After that, the study on selenium was paid more attention. Nutrition and toxicity of selenium mainly depends on its category of biological concentration. The experiments proved that selenium within 0.1 ppm can do well to body, while beyond 10 ppm may be bring about carcinogenesis. For taking selenium, at least 2-4PPm can result in death once. Normal body must reserve 14-21 mg selenium within, but about 0.5 mg selenium is expelled out of body in a single day. Therefore, human body is badly in need of selenium supplementation. Otherwise, disease will be brought about easily.

Yangguangyin laboratory of National Preventive Medicine Science College got the safety limit of selenium for body-needing by more investigations and body experiments, and it was proposed in the fourth international selenium symposium held in Xide on July in 1988 that the selenium intake for meal is 50-250ug in a single day, the safe intake is 500ug in a single day, and toxic intake is 750ug in a single day.

Suitable Concentration Category: Selenium within human body is of many important functions of biology, which has a close relationship with body health.

1. Biological Functions of Selenium

In recently years, the study on biological functions of selenium has been developed much further, and the below aspect is concluded:

1.1 to protect the completeness of cell membrane

The experiments proved that the lack of human erythrocyte and selenium content will result in the decrease of Na/k ---ATP enzyme activity and membrane fluidity, and the two functions will be enhanced if adding up trace sodium selenate. Obviously, selenium can affect the structure and function of red cell membrane to protect the completeness of cell membrane.

1.2 to keep normal physiological and biochemical function of cell

Selenium is the essential component of GSHPx. Peroxide reaction of GSHPx catalytic tanimitsu peptide; superoxide dismutase and catalase cleanse O2 and H2O2 in course of cell respiratory metabolism together to prevent forming hydroxyl radical and peroxide, so as to make cells keeping normal physiological and biochemical functions.

1.3 to promote the synthesis of cell DNA and RNA

Selenium can promote the synthesis of cell DNA and RNA, regulating nucleic acid and protein metabolism. Selenium lack will make GSHPx activity and its mRNA decreased. Selenium supplementation can increase GSHPX---mRNA to make GSHPx activity upper, which can prove that selenium, plays an important role against GSHPx gene rotor degradation. Selenium is also two kinds of RNA's specific component of glutamate and lysine accepted by colibacillus.

RNA with selenium is in some mammalian body, and they can improve mRNA's playing function in acylation.

1.4 participating composition of ubiquinone

Selenium can improve formation of anti-body, and also can adjust the absorption of vitamin A, C, E and K and consume biosynthesis of ubiquinone. Coenzyme Q is the key one in living creature, which is not only capture agent of excessing free radical, but also can keep normal cellular respiration and promote immune. Coenzyme Q10 is blessed with abilities of anti-infectious disease, cancer, heart disease, periodic disease and hypertension, whose functions are evident.

Selenium can stimulate formation of immunoglobulin and anti-body, so as to affect body's immune function. Selenium's influence on immune system and GSHPx's metabolism participated nut olefine acid can affect synthesis of prostaglandin and leukotriene.

1.5 affected endocrine function

Thyroxine5---deiodinase (T45---D) found lately is a kind of selenium-contained enzyme. T45---D can catalysis thyroxine (T4) to triiodothyronine (T3) of more biological activity, so as to affect physiological function of thyroid hormone.

In addition, result of hormone test showed that selenium lack could result in decrease of rat testis ketone secretion, and selenium of toxic dose would disturb secretion of prostaglandin, leading to damage of kidney function possibly. Selenium lack also results in increase of rat plasma thyroid hormone. Adding selenium into high fat diet of rabbit can increase thyroid hormone, insulin and cortisone in plasma.

1.6 other functions

Selenide is capture agent, which brings about too much biochemical matter to lead to carcinogenesis and free radical of too much senility, so as to play an important function in courses of cancer prevention and anti-aging. Selenium can also keep sperm activity functional and pancreas function to ensure lipid absorption. Selenium controls parts of ion in cell membrane flowing out to perfect keratin, avoiding hyperkeratosis and formation of cataract. Selenium is blessed with functions of antagonizing physiological antagonize and so on by adaptability of affected brown adipose tissue to bring about heat, so as to affect anti-cold ability of body.

2. Selenium and Certain Diseases

It was confirmed by great more studies that selenium is blessed with wide biological function. Selenium lack can result in a series of such diseases as cancer, AIDS, liver and pancreas disease, hypertension, diabetes mellitus, anemia, keshan disease, infertility, cataract, depression, asthma, arthritis, many kinds of dysarthrosis and so on. What is paid more attention is the prevention of selenium and diseases below.

2.1 selenium and cancer

In recently years, the study of selenium and cancer was developed constantly and showed that selenium lack was connected with cancer. Meanwhile, VA and VE lack can lead to disease of some degree. If selenium and VE are lacked in body, H2O2 and ROOH will appear and lead to degradation and variation.

In 1998, according to his study, Xiangboge proposed a great deal of cancer and death in sub-selenium districts once. According to the survey in Qidong town, high risk area of liver cancer of Jiangsu province, the death of liver cancer had a close relationship with blood selenium. Serum selenium of patients suffering from nasopharyngeal carcinoma is lower than that of healthy people obviously in Sihui town in Guangdong province. Zhuyajun reported that blood selenium of lung cancer patients is lower than that of healthy people obviously. Study team of medical college in Arizona University investigated and studied selenium englobement's influence on cancer among patients in sub-selenium districts in America. During four years and a half, one group of patients was intaken 200ug selenium every day, while another was given control agent. It lasted six years for tracking follow-up. That selenium englobement decreased kinds of cancer incidence obviously was reported, among which prostate cancer incidence decreased 60%, lung cancer 46%, colon rectal cancer 58% on December in 2001, and the death of selenium englobement group suffering from kinds of cancers decreased 50%.

Selenium's anti-cancer theory is that it can decrease certain hydroxylase activating carcinogenesis sources and the activity of aryl hydrocarbon hydroxylase to improve the system of detoxifying enzymes, such as glucose aldehyde group can move the activity of enzyme and take effect in early stage carcinogenesis, possibly related to the activity effecting DNA polymerase and nucleoside kinase, or to repair DNA function by mutagenicity decreased.

2.2 selenium and kashin-beck disease

Kashin-beck disease is a kind of endemic osteoarthrosis with main pathology of endostosis disorder. Many researchers thought that the fundamental reason is disproportionality among elements, while sub-selenium is the essential factor. Practice showed that to control kashin-beck disease with selenium can do a good job. Selenium plays an important role in cartilage histocyte development, and can prevent deterioration of epiphysis end lesion to repair to prevent bone

atrophy, degeneration, and retrogradation and so on. Therefore, selenium can prevent kashin-beck disease. Moreover, selenium can also inhibit toxicity of organic compound humic acid to prevent kashin-beck disease, avoiding damage to chondrocyte.

In 1996, it was reported that selenium had a close relationship with rheumatism arthritis. Within serum, mercapto lack is the main feature of arthritis, while selenium can develop disulfide bond to mercapto in protein synthesis, which can become more along with VE increase. Therefore, selenium supplementation along with VE supplementation plays an important role against rheumatoid arthritis.

2.3 selenium and cardiovascular disease

Selenium lack is connected with keshan disease, hypertension, coronary heart disease and cardiovascular disease. Selenium supplementation in drinking water or oral sodium selenite can make a remarkable effect against keshan disease. Keshan disease is a kind of endemic disease, chiefly myocardial lesions. Selenium lack is one of the reasons leading to diseases. According to multi-year study, it was found by domestic experts that keshan disease never appeared in districts with selenium. Contrarily, keshan disease had great incidence rate in sub-selenium district. It had been surveyed and tested in China Academy of Preventive Medicine, Shenyan Medical University, Yunnan, Sichuan and Guizhou provinces successively. The results confirmed that selenium had a good function against preventing keshan disease.

The main principle of selenium supplementation against keshan disease is that selenium supplementation can increase activity of decomposing peroxide in vivo to prevent the damaging function to cell membrane system. Selenium is one of the components of human cell pigment C protein, which plays an important role in course of cell biological oxidation. Selenium can improve biosynthesis of coenzyme A, and physiological function of coenzyme A to heart maintenance is essential. Selenium can enhance immunologic function, so as to decrease invasion of keshan disease virus. Therefore, selenium supplementation increased protecting function to myocardial cells.

Selenium can also prevent hypertension and thrombus. Clinically, selenium is used to prevent angina pectoris and myocardial infarction, along with VE.

2.4 selenium and AIDS

Study on relationship of selenium and AIDS have newly developed further. AIDS is immune system by immune defecting virus invades body to lead to immune defect, secondarily infection appears to become AIDS syndrome and AIDS by chance. Serum selenium of asymptomatic HV infected people kept normal, while selenium of ARC and ADS patients decreased obviously. Selenium lack will increase along with getting worse disease.

Theory of selenium lack is thought that due to damaging immune function, kinds of virus are infected very easily to lead to gastrointestinal dysfunction. Thus, exogenous selenium will be malabsorpted and endogenous selenium will be lost. Meanwhile, related kidney function will be damaged to make selenium expelled from urine, in addition to insufficient uptake of diet will lead to failure of selenium food gradually. Along with gradually worse disease, selenium lack will be severe, but sub-selenium will lead to decrease of immune function of T cell and decrease of oxidation defensive system will make AIDS worse and immune function lower to form vicious circle. Selenium supplementation food can promote serum selenium content and improve disease syndrome, which has an important meaning in AIDS adjuvant therapy.

2.5 selenium and thyroid disease

In recently years, the relationship of selenium and thyroid disease was found and it was reported that selenium lack had a close relationship with myxedema-typed cretinism. Cretinism is a kind of disease with severe iodine lack. Iodine lack makes thyroid hormone within body decreased. If selenium is lacked, it will result in decrease of T3 content further and accelerate forming endemic goiter and cretinism. In certain district, such case was still existed after iodine supplementation, possibly which is connected with selenium lack. If at the time of iodine supplementation with meanwhile selenium supplementation, T45---D activity will be enhanced, which can do work to promotion of thyroid hormone and its prevention and treatment.

Besides the above deeper study on relationship of selenium and diseases, selenium lack is also connected with liver disease, skin disease, cataract, acne vulgaris, rheumatoid arthritis and so on. Theory of selenium lack's influence on diseases is under deep clinical experiment with selenium against disease.

References

Liang, Runmei & Deng, Yun. (2000). Trace Element Selenium and Study on Health. *Taiyuan Normal University Newspaper*. 8 (4): 13-14.

Lin, Panping, Wang, Baojun, Chen, Chunrong and so on. (2002). Latest Development of Study on Selenium Nutrition. *Chinese Medical Magazine*. 24 (2): 45-51.

Lin, Qiuhua & Wang, Yuangliang. (2003). Trace Element Selenium and Body Disease. *Qiannan People University Newspaper*. 15 (4): 4-5.

Lu, Tong, Wang, Yun & You, Li. (2004). Influence of Trace Element Selenium on Experimental Porridge-Shaped Arteriosclerosis Regression. *Nutrition Newspaper.* 15 (2): 15-1.

Wang, Wei. (2004). New Way of Healthy Food of Selenium. *Chinese Food Magazine.* 12: 3-4.

Xiao, Xushen & Huang, Kelong. (2006). *Application of Biological Material in the Field of Medicine   Biology and Technology Newspaper*. 3 (6): 11-12.

Zhang, Ming, Ren, Qichang & Liu, Xiaoqing. (2005). Biological Selenium Preparation and Function of Anti-Cancer. *Nutrition Newspape*. 22 (1): 8-9.

Modern Applied Science